DEVELOPMENT OF CHEMICAL TOOLS FOR DELIVERY OF HYDROGEN SELENIDE TO BIOLOGICAL ENVIRONMENTS

by

TURNER D. NEWTON

A DISSERTATION

Presented to the Department of Chemistry and Biochemistry
and the Division of Graduate Studies of the University of Oregon
in partial fulfillment of the requirements
for the degree of
Doctor of Philosophy

September 2022

DISSERTATION APPROVAL PAGE

Student: Turner D. Newton

Title: Development of Chemical Tools for the Delivery of Hydrogen Selenide to Biological Environments

This dissertation has been accepted and approved in partial fulfillment of the requirements for the Doctor of Philosophy degree in the Department of Chemistry and Biochemistry by:

Dr. Michael M. Haley	Chairperson
Dr. Michael D. Pluth	Advisor
Dr. Darren W. Johnson	Core Member
Dr. Thomas Giachetti	Institutional Representative

and

Krista Chronister	Vice Provost for Graduate Studies

Original approval signatures are on file with the University of Oregon Division of Graduate Studies.

Degree awarded September 2022.

DISSERTATION ABSTRACT

Turner D. Newton

Doctor of Philosophy

Department of Chemistry and Biochemistry

September 2022

Title: Development of Chemical Tools for the Delivery of Hydrogen Selenide to Biological Environments

Hydrogen selenide (H_2Se) is the central species in the selenium metabolic cycle, sitting at the crossroads of protein-synthetic and excretory pathways. Despite its importance in biology and potential for therapeutic applications, this species has received limited attention from researchers in the past. Commonly used methods for studying H_2Se in biology are confined to solutions of H_2Se/HSe^- prepared through hydrolysis of selenide salts or reduction of elemental selenium, but significant drawbacks are presented with these techniques that prevent comprehensive investigation. It is necessary for researchers to develop tools that will facilitate investigations into the roles and fates of H_2Se in biology, and inspiration can be taken from the closely related field of research on hydrogen sulfide (H_2S), the third gasotransmitter. The research presented in this dissertation is aimed at adapting previously established strategies for studying H_2S in biology to the heavier chalcogenide H_2Se.

Fully understanding the motivations behind H_2Se research requires a familiarity with the necessity of selenium in the mammalian diet, specifically its inclusion in the family of selenoproteins, which play key roles in the maintenance of redox status and thyroid hormone modulation among many others. This material is covered in Chapter I along with more detailed analysis of the challenges currently facing H_2Se research. The development of the first well-characterized H_2Se donor, modeled after the most widely-studied H_2S donor, is covered in Chapter II and sets the stage for future research in this area. Chapter III details an expansion upon the technology discussed in the previous chapter with efforts to produce H_2Se donors with tunable hydrolysis rates. Additionally, experiments on the viability of these compounds in biology are discussed in Chapter III

through performing cell permeability and antioxidant capacity experiments in HeLa cells. Current work is detailed in Chapter IV, revealing the use of selenocarbamates as H_2Se donors with the goal of developing donors with diverse triggering mechanisms and amine-based payloads that facilitate investigations into the chemical and biological behavior of H_2Se. Finally, Chapter V summarizes this work, the current state of the field, and provides avenues for further advancement of H_2Se donor technology.

This dissertation includes previously published and unpublished co-authored materials.

CURRICULUM VITAE

NAME OF AUTHOR: Turner D. Newton

GRADUATE AND UNDERGRADUATE SCHOOLS ATTENDED:

University of Oregon, Eugene
Worcester Polytechnic Institute, Massachusetts

DEGREES AWARDED:

Doctor of Philosophy, Chemistry, 2022, University of Oregon
Master of Science, Chemistry, 2020, University of Oregon
Bachelor of Science, Chemistry, 2015, Worcester Polytechnic Institute

PROFESSIONAL EXPERIENCE:

Teaching assistant, Department of Chemistry and Biochemistry, University of Oregon, Eugene, 2017-2022

Research scientist, Crop Enhancement, Cambridge, Massachusetts, 2016-2017

Senior R&D technician, GCP Applied Technologies, Cambridge, Massachusetts, 2015-2016

GRANTS, AWARDS, AND HONORS:

High Distinction, Worcester Polytechnic Institute, 2015

Order of Omega Award for Academic Excellence, Worcester Polytechnic Institute Interfraternal Council, 2013

Charles O. Thompson Scholar, Worcester Polytechnic Institute, 2012

PUBLICATIONS:

Gilbert, A.K.*; Newton, T.D.*; Hettiaratchi, M.H.; Pluth, M.D. Reactive sulfur and selenium species in the regulation of bone homeostasis, *Free Radic. Biol. Med.* **2022**, *190*, 148-157.

Newton, T.D.; Bolton, S.G.; Garcia, A.C.; Chouinard, J.E.; Golledge, S.L.; Zakharov, L.N.; Pluth, M.D. Hydrolysis-based small-molecule hydrogen selenide (H_2Se) donors for intracellular H_2Se delivery, *J. Am. Chem. Soc.* **2021**, *143*, 19542-19550.

Newton, T.D.; Pluth, M.D. Development of a hydrolysis-based small-molecule hydrogen selenide (H_2Se) donor, *Chem. Sci.* **2019**, *10*, 10723-10727.

Cerda, M.M.; Newton, T.D.; Zhao, Y.; Collins, B.K.; Hendon, C.H.; Pluth, M.D. Dithioesters: simple, tunable, cysteine-selective H_2S donors, *Chem. Sci.* **2019**, *10*, 1773-1779.

ACKNOWLEDGMENTS

I would like to start by thanking my family. There are no words for how meaningful your love and support have been throughout this process and the last several years in general. To my parents, Todd and Kim, I thank you every day for teaching me to read at a young age and encouraging my curiosity about the world around me; I can trace much of my success directly back to my love of books and my desire to know the answers. To my sister, Madison, who, as a National Champion, is a constant inspiration and model of hard work, perseverance, and glowing success. To my future brother-in-law, Jack, we are lucky to have you joining our ranks. To my grandparents, Wayne, Bobbye, Mary, Jim, and Cliff, I wish you could see me today, and I know you would be so proud. To my unofficial family members, too numerous to name, who have helped shape me as a person and who I thank in advance for listening to me describe what I did in graduate school.

I would like to thank Professor Mike Pluth for giving me the green light on moving down the periodic table to research H_2Se; it has been far from easy, but our effort has been greatly rewarded, and this field will continue to blossom because of it. I could not ask for a better leader and mentor. His continuous support and inspiration throughout my time in his lab in addition to his patience and understanding in regards to the challenges that both research and life have presented in recent years has made all the difference. I would also like to thank my committee, Professors Michael M. Haley, Darren W. Johnson, and Thomas Giachetti for encouraging me and always showing genuine interest and excitement in the research I presented.

Additionally, I would like to thank all of the teachers who came before this journey, too numerous to name. To my high school chemistry teacher, Mr. Blaine Goguen, it all started in your classroom, and I certainly would not be writing this without the solid foundation you gave me. To my undergraduate advisor, Dr. Marion H. Emmert, you gave me the opportunity to pursue chemical research in your lab, and there I developed the tools to succeed as a scientist.

Of course, none of this would have been possible without the friends I gained along the way. To the squad – Grace, Michael, Rachael, Zack, Rebecca, Steph, and

Taylor – nobody floats a river as proficiently as we do. To my labmates past and present – Dr. Annie Gilbert, Dr. Toby Sherbow, Dr. Matt Cerda, Dr. Carolyn Levinn, Dr. Nathan Lau, Dr. Sarah Bolton, Arman Garcia, Kaylin Fosnacht, Andy Davis, Haley Smith, Olivia Apicella, Dr. Hazel Fargher, Dr. Dan Seidenkranz, Dr. Yu Zhao, and Dr. Andrea Steiger – there is no Pluth Lab without all of you, and you have all pushed me to become the best scientist I can be. To the Hansen Lab, my second home at UO. A special thanks to Dr. Matt Cerda, Dr. Jeremy Bard, and Dr. Ngoc-Minh Phan, who guided me through my rotations and taught me what to expect and how to succeed in graduate school.

Most of all I would like to thank Grace Waddell, my better half. Your love and support has been instrumental to my perseverance in this program, and I most definitely would not have endured without you. The reminder that there is a whole beautiful world to explore outside of the fume hood helps keep life in perspective. And of course I must thank Kitty-Baby for being such a good cat and getting us through the last few years.

Lastly, I would like to thank the University of Oregon for accepting me and the National Science Foundation (CHE-2004150) for funding the projects that are covered in this dissertation. I would also like to thank our collaborators Dr. Stephen L. Golledge, Julie E. Chouinard, and Dr. Lev N. Zakharov for assisting in these investigations.

For my family, who has believed in me every step of the way.

TABLE OF CONTENTS

LIST OF FIGURES

LIST OF SCHEMES

CHAPTER I

SELENIUM AND HYDROGEN SELENIDE IN BIOLOGY

Selenium, among many other elements on the periodic table, is crucial to the proper function of mammalian biological systems.[1-3] Illustrating the necessity of selenium in the human diet are a number of debilitating physiological conditions seen primarily in selenium-deficient soil regions of the world, such as Keshan and Kashin-Beck Disease.[4-6] Keshan Disease occurs as a result of selenium deficiency in combination with a mutated strain of Coxsackievirus and leads to congestive cardiomyopathy that is often fatal.[5] Kashin-Beck Disease occurs as a result of selenium and iodine deficiency during developmental stages of life and leads to deformities in the joints and bones that can be detrimental to mobility and dexterity.[4, 7] In modern society, instances of these conditions have become much rarer, which can be attributed to the increase in outsourced farming, where crops are grown in more nutrient-rich soils.[2, 6] Additionally, Se supplementation in Se-deficient regions has been shown to mitigate the effects of endemic Se deficiency in soil.[2-3]

While Se supplementation and consumption of more Se-rich foods can combat deficiencies, there is a narrow window between nutritional and toxic levels of selenium in humans. This range is between 50 and 400 μg daily, with the ideal dosage being around 100 μg for adults, though this is heavily dependent upon the Se speciation and many physiological factors present in a person.[6] Despite this narrow window, humans are generally well-equipped to deal with acutely high Se levels in the diet, which result in an upregulation of the excretory pathways in the Se metabolic cycle (Figure 1.1a; for a more detailed scheme, see Figure 2.1) but cannot be sustained over a long period of time.[8-9] Chronic overconsumption of Se-rich foods, the Brazil Nut for example, is the primary cause of Se poisoning (selenosis) in humans, evidenced by abnormalities in the nailbeds, foul breath, alopecia, and in extreme cases neurological dysfunction.[9-11] In light of this delicate balance between deficiency and toxicity, it is crucial that researchers develop a deeper understanding of the machinations and fates of Se-species in biology.

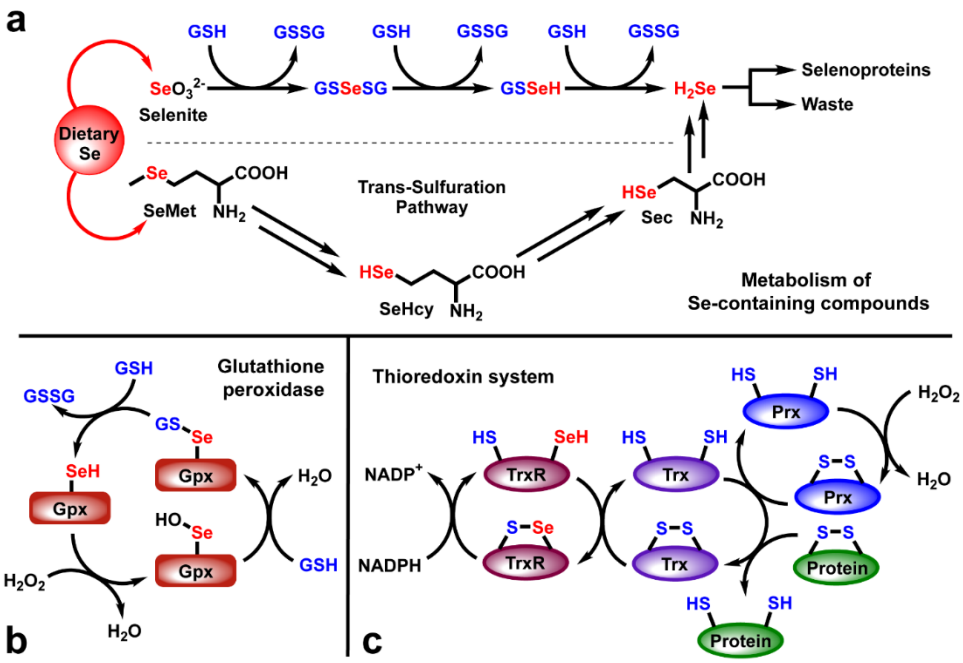

Figure 1.1 (a) Simplified metabolic pathways of selenium-containing compounds. (b) Selenium contribution to glutathione peroxidase function. (c) Selenium and sulfur interplay in the regulation of the thioredoxin system.

The active form of Se in living organisms is a selenocysteine (Sec) residue appended to a protein, giving rise to the term "selenoproteins" that applies to all proteins containing a Sec residue. Sec is considered the 21st amino acid, but its incorporation into proteins differs from other amino acids. Selenoprotein mRNA contains a stop codon UGA in the open reading frame followed by a stem-loop structure called the selenocysteine insertion sequence (SECIS) that signals a Sec insertion site rather than a stop to translation. Sec synthase then uses selenophosphate to convert a phosphoserine residue in the growing tRNA to Sec, which remains intact after the selenoprotein is constructed.[8] Selenomethionine (SeMet) is also incorporated into the human proteome where methionine (Met) residues would normally exist; however, the methylation of the Se atom inhibits the reactivity of this amino acid and removes SeMet-containing proteins from the pool of selenoproteins.[9] Chiefly important are the selenoproteins glutathione peroxidase (Gpx) and thioredoxin reductase (TrxR), which play key roles in the body's antioxidant system (Figure 1.1b,c).[12-14] Additionally, iodothyronine deiodinases (DIO) regulate production of thyroid hormones like thyroxine (T4), which are crucial to human physiology.[15-16] Interestingly, selenoprotein P (SepP) is the only known selenoprotein of

the 25 in humans that contains more than one Sec residue; the purpose of this increased Sec concentration is to transport Se from the liver, where it is initially processed, to other sites in the body that require Se.[17-18] During times of Se deficiency, the body's production of SepP naturally diminishes, but expression of the receptors apoER2 and megalin are upregulated in systems, such as the skeletal system, that are vital for maintaining physiological function so that Se can be delivered preferentially.[19] Considering the important and diverse roles that selenoproteins play in the body, researchers have made efforts to harness their power and apply it to disease states in search of new therapeutics.[20]

One way that researchers have approached the study of selenoproteins is to develop molecules that mimic the activity of selenoproteins. The most widely-studied of these selenoprotein mimics is called Ebselen, which is a Gpx mimic and serves to reduce ROS *in vivo* in a catalytic fashion (Scheme 1.1a).[21-23] The therapeutic effects of this compound and its derivatives, ranging from X to Y, have been so beneficial that the molecule is currently in clinical trials.[23] Gpx is the most frequently mimicked selenoprotein, and while Ebselen is king among them, additional examples can be found in the literature, such as α-methylselenocysteine (α-MeSec). The methyl group of this modified amino acid confers a resistance to β-syn elimination when exposed to peroxides (Scheme 1.1b) and causes the molecule to instead undergo reduction and return to its starting form, completing a short catalytic cycle.[24] In addition to Gpx, DIO has been mimicked with naphthalenes bearing chalcogens at the 1 and 8 positions (Scheme 1.1c).[25] Researchers here showed that increased chalcogen size led to increased activity of the mimics with respect to the modulation of thyroid hormone concentrations in addition to demonstrating that the fundamental concepts of non-covalent halogen and chalcogen bonding were involved in the mimic activity.[25] Aside from mimicking selenoprotein behavior, researchers have sought to use other Se-containing technology, such as selenite-doped nanoparticles, to assess the utility of Se-based therapeutics for cancer and other physiological ailments. One notable example of this technology is selenite-doped hydroxyapatite nanoparticles (SeHANs) that have been developed to combat bone cancer.[26] Hydroxyapatite is the principal inorganic component in bones, and the basis of this research was hydroxyapatite nanoparticles (HANs) designed to fill the voids left by

bone tumor excision and accelerate bone repair. Researchers have included selenite in these compounds to act as a potent anti-cancer agent[27] and decrease the chances of cancer resurgence with even more promising results obtained by including other substances in SeHANs, such as catechins.[28] The potential for Se-based cancer therapies is high, and not just in relation to bone cancer. It is pertinent for researchers concerned with Se in biology to dig deeper in understanding the full landscape of effects on biological systems when Se-containing compounds are applied, and a large part of this mission revolves around studying Se metabolites more effectively.

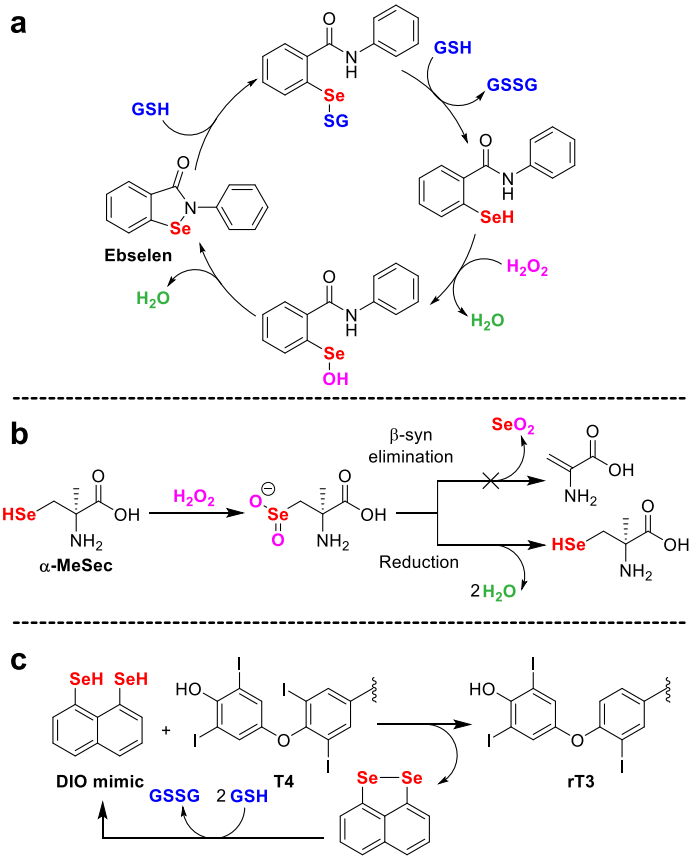

Scheme 1.1 Actions of selenoprotein mimics, pictured are (a) Ebselen as a Gpx mimic in tandem with GSH, (b) α-MeSec also as a Gpx mimic but without requiring GSH, and (c) 1,8-naphthalenediselenol as a DIO mimic with GSH.

Taking a closer look at the metabolism of dietary Se-containing compounds, it is clear that both protein-synthetic and excretory pathways proceed through the common intermediate of hydrogen selenide (H_2Se).[29] With the last two decades providing an

influx of research on hydrogen sulfide (H_2S) in biology, one would expect there to also be a blooming body of research on its heavier congener H_2Se, especially given the marked similarities in chemical and physical properties of sulfur and selenium.[29] This, however, is not the case, and there remain deep chasms in the knowledge surrounding H_2Se in biology along with its potential in therapeutic applications. Historically, most studies on the biological activity of Se species have been conducted with sodium selenite[27] (+IV oxidation state) or Se-supplemented (selenized) yeast,[30] both of which have inherent shortcomings. The former strategy provides a viable dietary source of Se but does not provide a discrete active Se species, making it difficult to precisely assess which Se metabolite is causing the observed effects. The latter strategy provides even more nebulous information as selenized yeast contains a mixture of the oxidized inorganic forms of Se along with SeMet that has been non-discriminately incorporated into the yeast proteome.[31] Biological effects specifically attributed to H_2Se are even more difficult to assess, as this species is exceptionally reactive in both nucleophilicity and susceptibility to oxidation and, as a result, can be severely toxic in elevated concentrations. Further complicating investigations are the infinitesimally (and immeasurably) low concentrations of H_2Se *in vivo* along with a myriad of biological reactive sulfur species (RSS) that are also potent nucleophiles and steadfast reductants.[29]

Detection and sensing of H_2Se is primarily accomplished through fluorescent probes with reducible motifs (Scheme 1.1a),[32-34] though recently a successfully selective probe based on the nucleophilic attack of H_2Se (Scheme 1.1b) was developed.[35] A number of materials-based methods for detecting H_2Se are also available, such as gold nanoclusters, but these strategies are not very applicable to biological investigations as they are designed for detecting gaseous H_2Se.[36-37] It is, therefore, more feasible to pursue the study of H_2Se through its application and subsequent observation of downstream effects.

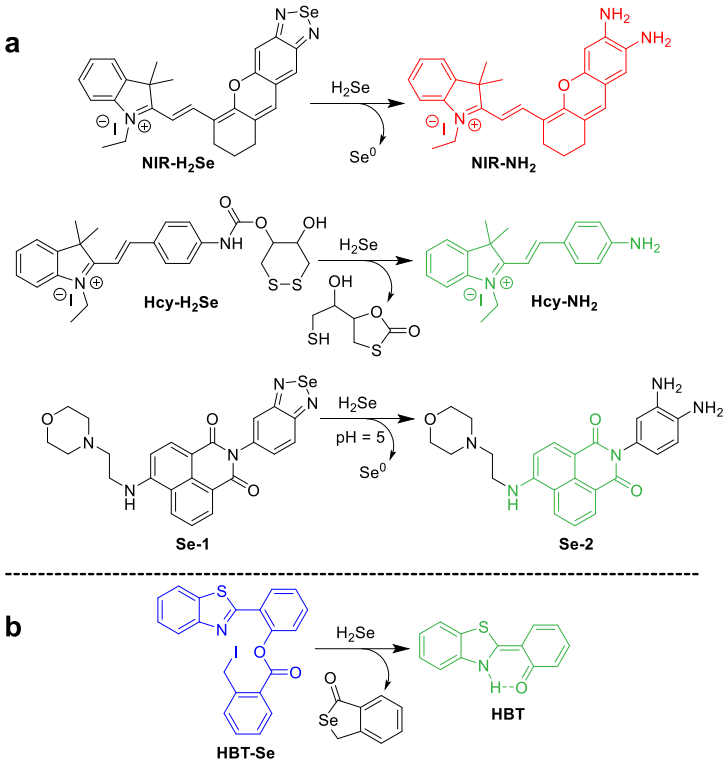

Scheme 1.2 Fluorescent H_2Se probes based on (a) reduction and (b) nucleophilic attack.

Until 2019, the standard method of delivering H_2Se was the administration of a freshly prepared solution of H_2Se/HSe^-. This feat is commonly accomplished through the reduction of Se with sodium borohydride, affording a solution of sodium hydroselenide (NaHSe),[38-39] or through the hydrolysis of inorganic selenide salts, like aluminum or lithium selenide.[33] Major issues with this method include the potential for oxidation of H_2Se back to its elemental form and the toxicity of H_2Se, which can be problematic if the concentration is not well-controlled and spikes suddenly. Sharing both of these issues is the delivery of gaseous H_2Se in air for inhalation, which has been used effectively in previous studies on the inhibition of mitochondrial complex IV and suspended animation.[38] Recently, several small-molecule sources of H_2Se have emerged from our lab[40-41] and others[42-43] that have adopted prior H_2S donor technology to produce H_2Se instead. During the last several years in the Pluth Lab, my efforts have focused on developing these small molecule H_2Se donors, studying their mechanisms of action, and applying them to biological samples to discern their effects and set the stage for further research in this field.

CHAPTER II

DEVELOPMENT OF A HYDROLYSIS-BASED HYDROGEN SELENIDE (H_2Se) DONOR

This chapter includes previously published and co-authored material from Newton, T.D.; Pluth, M.D. Development of a hyrolysis-based hydrogen selenide (H_2Se) donor. *Chem. Sci*. **2019**, *10*, 10723-10727. This manuscript was written by Turner D. Newton with editorial assistance by Professor Michael D. Pluth. The project in this chapter was conceived of by Turner D. Newton and Professor Michael D. Pluth. The experimental work was performed by Turner D. Newton. Crystal structure determination was performed by Dr. Samantha N. MacMillan at Cornell University.

2.1 Introduction

Selenium is often regarded as a toxic metalloid, but it is also an essential bioinorganic dietary micronutrient.[44-46] For example, geographic regions with selenium-deficient soil display unusually high occurrences of conditions including Keshan and Kashin-Beck diseases in the population, which are both tied to a dietary scarcity of selenium.[5, 47] Dietary sources of selenium are typically selenomethionine (SeMet) and selenate salts (SeO_4^{2-}), which must pass through complex metabolic pathways prior to incorporation into selenium-containing biomolecules.[48] In the body, selenium exerts function primarily as selenocysteine, often referred to as the 21st amino acid, which is incorporated into and gives rise to the often unique reactivity of selenoproteins.[1]

Twenty-five selenoproteins have been identified in humans and fall into several main categories. These categories include glutathione peroxidases (Gpx), which scavenge harmful peroxide species, thioredoxin reductases (TrxR), which regulate thiol-disulfide redox homeostasis, iodothyronine deiodinases (DIOs), which regulate thyroid hormone equilibria, and specialized selenoproteins that exhibit alternative functions, such as protein folding and selenium transport.[46] Selenium-deficient environments often result in the preferential expression of these proteins, whereas selenium-rich environments result in the upregulation of selenium excretion pathways to reduce selenium toxicity.[8] Many of these pathways are hypothesized to proceed through the intermediate formation of

hydrogen selenide (H_2Se/HSe^-), which is an important yet elusive small biomolecule of interest (Figure 2.1).[29]

A common approach to increase the bioavailability of selenium is to use exogenous synthetic selenium-containing small molecules. For example, the organoselenium compound Ebselen mimics the behavior of glutathione peroxidase and exhibits cytoprotective, anti-inflammatory, and antioxidant effects.[49-50] Similarly, the glutathione-mediated reduction of selenite (SeO_3^{2-}) to elemental selenium is thought to proceed through a selenodiglutathione (GS-Se-SG) intermediate en-route to a selenopersulfide (GS-Se$^-$), which subsequently decomposes to either GSH and Se^0 or is converted to H_2Se through both enzymatic and non-enzymatic pathways.[51-52] More recently, the hydrolysis of phthalic selenoanhydride was used for generating reactive selenium species to examine the differential synergies of these compounds with H_2S and GSH in radical scavenging.[53] In this investigation, H_2Se release was proposed during hydrolysis but was not observed directly in the experiments.

Interest in developing chemical tools for investigating H_2Se has grown in the last few years, with new investigations into the molecular recognition of HSe^- in synthetic host-guest systems[54] and with the advent of first-generation fluorescent probes for H_2Se detection.[32-33] In part, these investigations are motivated by potential roles of selenides in treating conditions ranging from arsenic poisoning, in which toxic arsenic species can react with H_2Se to form readily-excreted products,[55-56] to cancer, in which H_2Se can induce oxidative stress under normoxic conditions or reductive stress under hypoxic conditions in HepG2 cells, resulting in HMGB1 protein damage and ultimately apoptosis.[57] At physiological pH, almost all H_2Se exists as HSe^- due to the acidity of the diprotic form of H_2Se ($pK_a = 3.9$). The high redox activity and high nucleophilicity of H_2Se/HSe^-, when coupled with the relatively low biological selenium content (~0.2 mg/kg in humans), make investigations into the biological roles of H_2Se difficult.[58] Building from these past results and increased interest in biorelevant small reactive selenium species, we viewed that well-characterized, synthetic small molecules that release H_2Se directly and under controlled conditions would provide a much-needed chemical tool for expanding research related to the chemical biology of selenium. Here we report the development and characterization of a hydrolysis-based small-molecule

H_2Se donor and provide insights into the reaction mechanism and methods for direct H_2Se trapping.

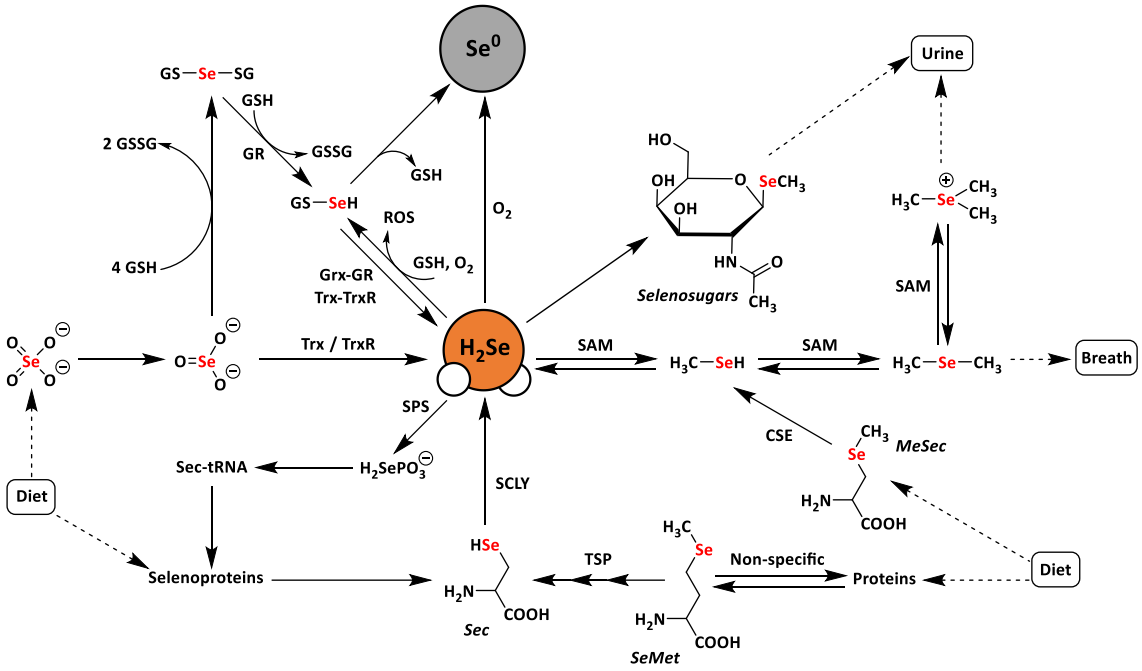

Figure 2.1 Schematic representation of metabolic pathways of dietary selenium compounds including various reactive selenium species. Selenate (SeO_4^{2-}), selenite (SeO_3^{2-}), selenophosphate ($H_2SePO_3^-$), selenocysteine (Sec), selenomethionine (SeMet), methylselenocysteine (MeSec), thioredoxin (Trx), thioredoxin reductase (TrxR), glutaredoxin (Grx), glutathione reductase (GR), glutathione (GSH), diglutathione (GSSG), selenodiglutathione (GSSeSG), glutathioselenol (GSSeH), selenophosphate synthetase (SPS), selenocysteine lyase (SCLY), *S*-adenosylmethionine (SAM), transsulfuration pathway (TSP), elemental selenium (Se^0), and reactive oxygen species (ROS).

2.2 Results and Discussion

2.2.1 Synthesis and Characterization of TDN1042

Drawing parallels to biological organosulfur chemistry, the last decade has witnessed a surge in research related to hydrogen sulfide (H_2S/HS^-) as an important reactive sulfur species and gasotransmitter.[59] Substantial efforts have focused on the development of small-molecule H_2S donors for delivery to biological environments.[60-62] Although the structure and complexity of such systems have evolved significantly, an early and broadly-used example of such donors is the hydrolysis-activated donor GYY4137, which relies on the hydrolytic cleavage of P=S bonds to generate H_2S.[63]

GYY4137 has been used in >200 publications to date (Web of Science) and exhibits anti-inflammatory, vasorelaxant, and anti-cancer as well as other effects in different biological models[63-65] with diverse applications ranging from medicinal to agricultural science.[66-67] Motivated by the broad utility of this approach to access H_2S donor motifs, we sought to use similar chemistry to generate well-defined H_2Se donors that are activated by P=Se bond hydrolysis. To prepare such a donor, we treated Woollins' Reagent with an excess of morpholine to generate TDN1042 in moderate yield (Figure 2.2a). The resultant product was characterized by ^{1}H, $^{13}C\{^{1}H\}$, ^{31}P, and ^{77}Se NMR spectroscopy (Figure S2.1-S2.4). Single crystals suitable for X-ray diffraction were grown by layering hexane onto a solution of TDN1042 in CH_2Cl_2, which confirmed the molecular structure (Figure 2.2b).

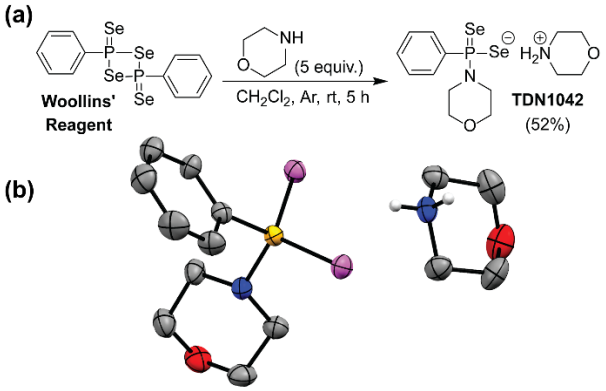

Figure 2.2 (a) Synthesis of TDN1042 from Woollins' reagent. (b) ORTEP diagram (50% ellipsoids) of TDN1042. Hydrogen atoms, except those on the morpholinium nitrogen, are omitted for clarity.

2.2.2 Hydrolysis Studies on TDN1042

With TDN1042 in hand, we next evaluated its reaction chemistry by NMR spectroscopy. Initial studies using ^{31}P NMR spectroscopy in wet DMSO-d^6 revealed the clean conversion of TDN1042 to phenylphosphonic acid (PPA) as expected (Figure 2.3a). We next monitored the hydrolysis in buffered aqueous solutions using quantitative ^{31}P NMR spectroscopy with triethylphosphate (TEP) as an internal integration standard. In these experiments, we also observed clean conversion of TDN1042 ($\delta(^{31}P)$ = 61 ppm) to the expected PPA hydrolysis product ($\delta(^{31}P)$ = 12 ppm). To determine the effect of pH on this reaction, we measured the rate of hydrolysis of TDN1042 (10 mM) in citrate

buffer (50 mM) ranging from pH 3.0 to pH 6.0 in flame-sealed NMR tubes at ambient temperature (Figure 2.3b). The resulting hydrolysis data (Figure 2.3c) revealed an increase in rate at more acidic pH values, which is consistent with the expected hydrolysis mechanism. A similar pH dependence was observed for GYY4137 in previous reports,[63] suggesting that the TDN1042 donor motif could also find utility in different biological contexts.

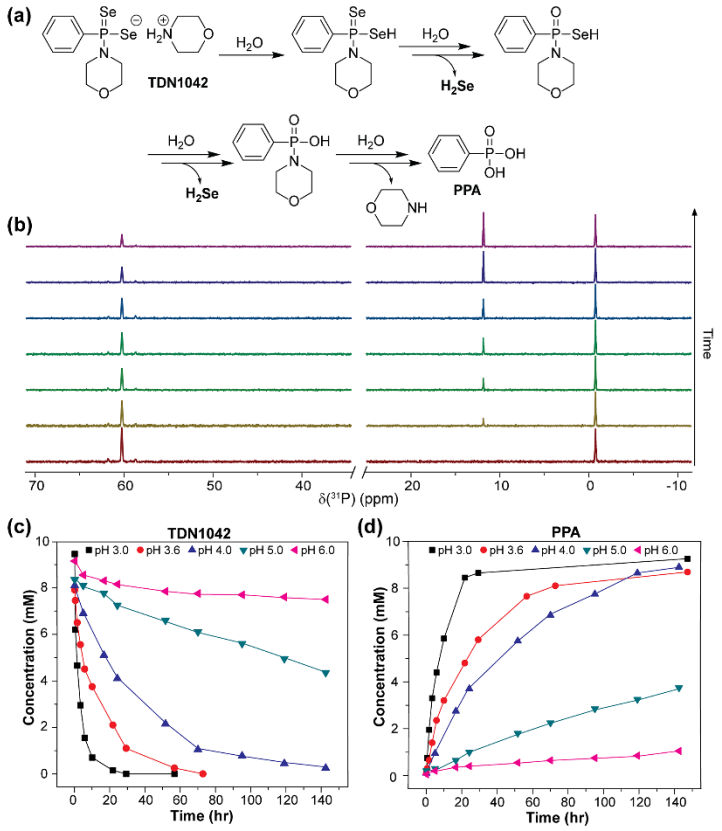

Figure 2.3 (a) Proposed hydrolysis mechanism of TDN1042 resulting in H_2Se release. (b) ^{31}P NMR spectra during the hydrolysis of TDN1042 showing the consumption of TDN1042 (61 ppm) and generation of PPA (12 ppm). (c) pH dependence of TDN1042 during the hydrolysis experiments. (d) pH dependence of PPA formation during the hydrolysis experiments. General conditions: 10 mM TDN1042 in 50 mM citrate buffer ranging from pH 3.0 to pH 6.0 at room temperature.

2.2.3 Mechanistic Studies on TDN1042

Having established that the hydrolysis of TDN1042 results in PPA formation, we next sought to confirm H_2Se release directly. To monitor H_2Se release, our goal was to trap H_2Se directly rather than use fluorogenic probes in case a reactive intermediate en-

route to H_2Se release resulted in the activation of such systems. To accomplish this labeling, we used benzyl bromide (BnBr) as an electrophilic trapping agent for TDN1042 and monitored the reaction by ^{31}P and ^{77}Se NMR spectroscopy (Figure 2.4a). On the basis of the proposed release mechanism of H_2Se from TDN1042, we expected that, akin to initial protonation, BnBr would initially alkylate the P=Se moiety, which would activate TDN1042 toward hydrolysis to release benzyl selenol (BnSeH) with subsequent alkylation by BnBr to generate dibenzyl selenide (Bn_2Se). By monitoring the reaction by both ^{31}P and ^{77}Se NMR spectroscopy, we observed immediate formation of an intermediate (1) upon addition of BnBr and H_2O to a solution of TDN1042 in DMSO-d^6 (Figure 2.4b, c). Intermediate **1** exhibited a singlet in the ^{31}P spectrum (δ = 69 ppm) with two sets of selenium satellites with different coupling constants ($J_{P\text{-}Se}$ = 786 Hz, $J_{P\text{-}Se}$ = 401 Hz). This coupling pattern is consistent with inequivalent selenium environments in **1** and is in contrast to the single set of selenium satellites seen in TDN1042 ($\delta(^{31}P)$ = 61 ppm,$^1J_{P\text{-}Se}$ = 671 Hz). Furthermore, the ^{77}Se NMR spectrum of **1** revealed both a doublet (δ= -129 ppm, $^1J_{P\text{-}Se}$ = 786 Hz) and a doublet of triplets (δ= 354 ppm, $^1J_{P\text{-}Se}$ = 401 Hz, $^2J_{Se\text{-}H}$ = 11 Hz), which correspond to the P=Se and P-SeCH_2Ph moieties, respectively (Figure 2.4e). As the reaction proceeded, the intensity of the δ = -129 and 354 ppm peaks decreased, with concomitant formation of PPA ($\delta(^{31}P)$ = 12 ppm) in the ^{31}P NMR spectrum. The ^{77}Se NMR spectrum revealed two Se-containing products, with a triplet at $\delta(^{77}Se)$ = 394 ppm and a pentet at $\delta(^{77}Se)$ = 330 ppm. The 330 ppm resonance corresponds to Bn_2Se, in which the selenium signal is split by two sets of benzylic protons. The 394 ppm resonance corresponds to dibenzyl diselenide (Bn_2Se_2), which was confirmed by comparison with an authentic Bn_2Se_2 sample (Figure A13). Formation of the diselenide is likely due to the auto-oxidation of BnSeH, which as has been observed previously.[68] Taken together, these alkylation experiments support the mechanism of H_2Se release and provide mechanistic insights into the hydrolysis mechanism.

To definitively establish H_2Se release, we next performed experiments in which the electrophilic trapping agent was separate from the donor. For this investigation, we used 2,4-dinitrofluorobenzene (FDNB) as an electrophilic labeling reagent to trap the H_2Se released and volatilized into the headspace of the reaction apparatus.[69-70] In these experiments, a vial containing an aqueous solution of TDN1042 was acidified with HCl

and sparged with N_2 to help volatilize any H_2Se into the headspace, which subsequently bubbled through a trapping solution containing a large excess of FDNB (Figure 2.5a). A final solution containing $AgNO_3$ was used to scavenge any unreacted H_2Se. Using HPLC, we observed formation of both di(2,4-dinitrophenyl) selenide ($(DNP)_2Se$) and the corresponding diselenide ($(DNP)_2Se_2$) in the trapping solution (Figure 2.5b, Figure A14), which is consistent with directly trapping H_2Se as well as the auto-oxidation process. The identity of the observed products was confirmed by comparison to authentic samples of $(DNP)_2Se$ and $(DNP)_2Se_2$ synthesized according to published procedures (Figure A18).[71] Taken together, these results confirm that TDN1042 releases H_2Se directly.

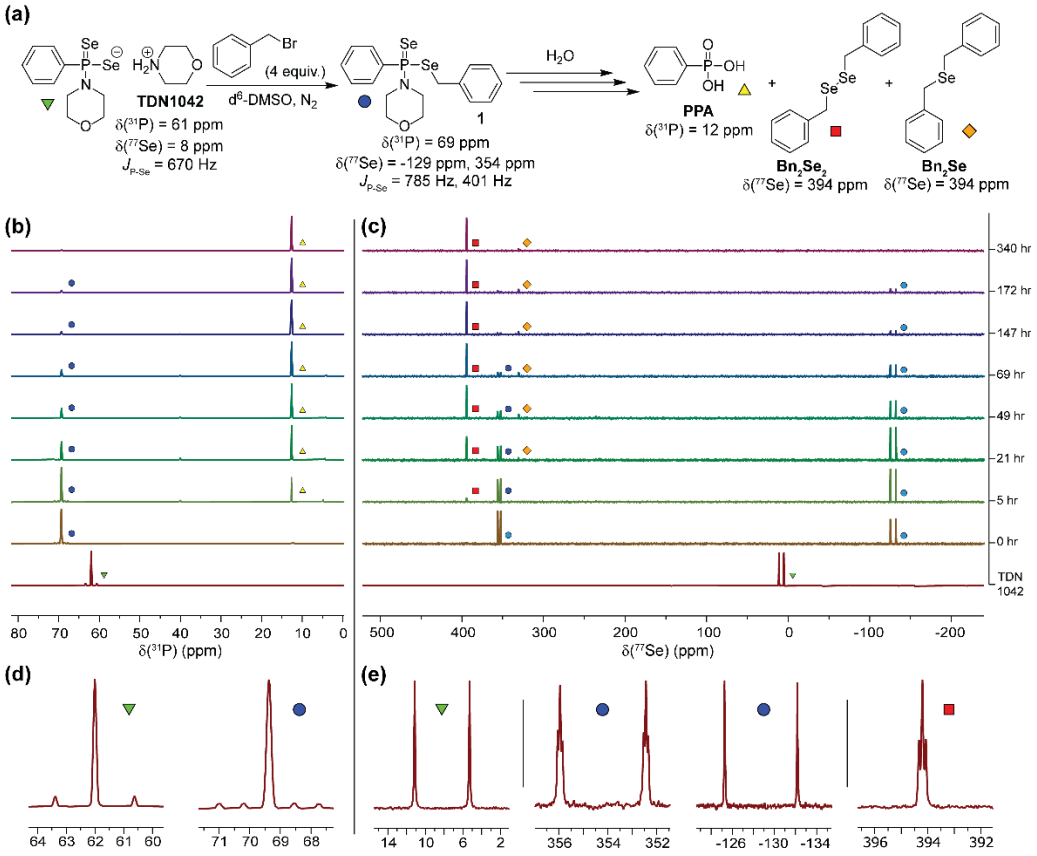

Figure 2.4 (a) Proposed hydrolysis and trapping pathways. See Scheme A3 for a more detailed mechanism. (b) ^{31}P NMR spectra during alkylation and hydrolysis. (c) ^{77}Se NMR spectra during alkylation and hydrolysis. (d and e) Expanded regions of the ^{31}P and ^{77}Se NMR spectra highlight the observed coupling patterns.

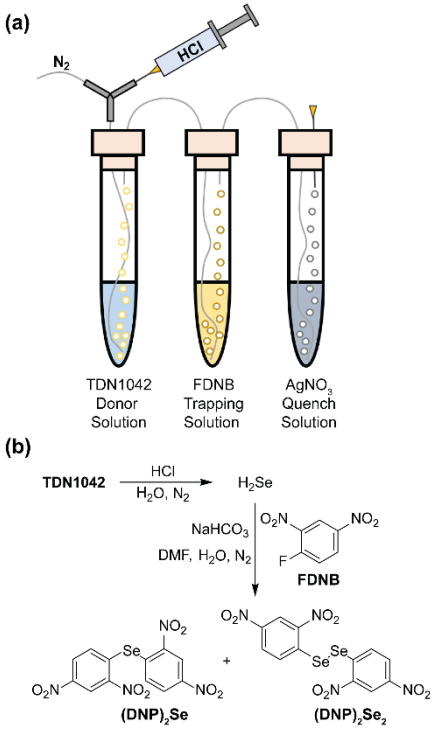

Figure 2.5 (a) Experimental setup for volatilization and trapping of H_2Se with FDNB. (b) General reaction pathways for $(DNP)_2Se$ and $(DNP)_2Se_2$ formation.

2.3 Conclusions

Here we report the development and characterization of the hydrolysis-based H_2Se donor TDN1042. Using multinuclear NMR experiments, we monitored the reaction pathway for H_2Se release and confirmed H_2Se generation using different electrophilic trapping methods. We anticipate that this well-characterized H_2Se donor will find utility in biological investigations into the roles of H_2Se and related reactive selenium species in the future and will facilitate the development of chemical tools for further investigating H_2Se in chemical biology.

CHAPTER III

HYDROLYSIS-BASED SMALL MOLECULE HYDROGEN SELENIDE (H_2Se) DONORS FOR INTRACELLULAR H_2Se DELIVERY

This chapter includes previously published and co-authored material from Newton, T.D.; Bolton, S.G.; Garcia, A.C.; Chouinard, J.E.; Golledge, S.L.; Zakharov, L.N.; Pluth, M.D. Hydrolysis-Based Small Molecule Hydrogen Selenide (H_2Se) Donors for Intracellular H_2Se Delivery. *J. Am. Chem Soc.* **2021**, *143*, 19542-19550. This manuscript was written by Turner D. Newton and Dr. Sarah G. Bolton with editorial assistance from Professor Michael D. Pluth. The project in this chapter was conceived of by Turner D. Newton and Professor Michael D. Pluth. The experimental work was performed by Turner D. Newton, Dr. Sarah G. Bolton, Arman C. Garcia. TOFSIMS experiments were performed by Julie E. Chouinard and Dr. Stephen L. Golledge. Crystal structure determination was performed by Dr. Lev N. Zakharov.

3.1 Introduction

Selenium is a trace nutrient that is required in the human diet for proper physiological function.[1, 44, 72-73] The biological concentration window for selenium is narrow, and dietary selenium deficiency or excess can lead to detrimental conditions including Keshan's Disease[5] and selenosis.[10] Primary dietary sources of selenium include organoselenium compounds and inorganic salts,[74] both of which can be incorporated into selenoproteins through different transformations or excreted to prevent toxic accumulation.[8, 46] One commonality between these major metabolic pathways is that they are thought to proceed through the intermediate formation of hydrogen selenide (H_2Se) (Figure 3.1). Drawing parallels to its lighter congener H_2S, H_2Se is highly reactive and toxic but also crucial for selenium homeostasis, proper function of endogenous antioxidant systems, and thyroid function.[29] Despite the importance of H_2Se and related reactive selenium species (RSeS), few chemical tools allow for direct delivery of these species to biological environments. For example, most investigations focused on the therapeutic benefits of selenium, especially in relation to various cancers, have used oxidized selenium sources, such as sodium selenite (Na_2SeO_3), as the selenium source.[75-

[76] Significant evidence, however, suggests that reduced RSeS, such as selenium-glutathione adducts, organoselenium species, or H_2Se, rather than oxidized Se species are responsible for observed *in vivo* activities.[77] For example, in a recent study by the Tang group, H_2Se was reported to be the active selenium metabolite responsible for cell death in HepG2 cells that were initially treated with Na_2SeO_3, which is commonly used as a source of selenium in biological studies.[57] Similarly, Roth and co-workers found that direct administration of H_2Se, but not Na_2SeO_3, reduced heart damage in mouse models of myocardial ischemia reperfusion injury suggesting that reduced RSeS exert different physiological effects than the more commonly-used oxidized selenium sources.[38]

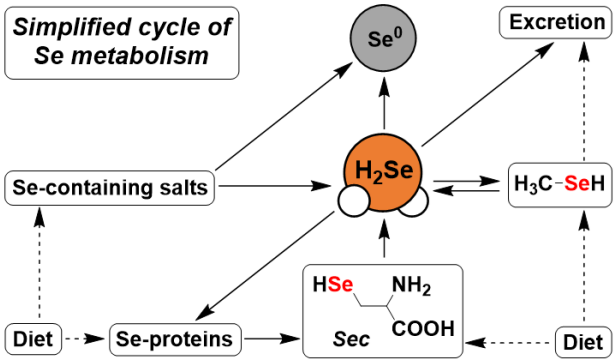

Figure 3.1 A simplified view of the selenium metabolic cycle highlighting the role of H_2Se in both protein synthesis and excretory pathways from dietary sources.

The blossoming interest in studying the chemical biology of H_2Se is reminiscent of the beginnings of contemporary research on biological H_2S. H_2S was classically recognized as a toxin but was later found to play essential roles in key many mammalian processes, including angiogenesis.[78] Sulfur and selenium are the most similar main group elements on the periodic table, and researchers are already proposing that H_2Se may be a fourth biological gasotransmitter, adding to the more commonly-accepted H_2S, NO, and CO. Already meeting many of the criteria to be classified as a gasotransmitter, H_2Se is produced endogenously, is a gas in its diprotic state, is membrane permeable, and can exert unique biological effects although specific molecular targets in signaling pathways have not yet been identified.[59, 79] When administered exogenously to mice through either inhalation (0-5 ppm in air) or injection (solution of NaSeH, 0.05-24.9 mg/kg), H_2Se modulates aerobic respiration in mice by inhibition of mitochondrial complex IV, again

drawing striking parallels to observed H_2S activities in similar systems.[38] A significant limitation to advancing our understanding of the potential roles of H_2Se in biology, however, is the lack of suitable methods for studying H_2Se directly in living systems, although new approaches for both donor and probe technology are beginning to emerge.[32-33, 53, 80]

To expand our basic understanding of differences in the bio(in)organic chemistry between reactive sulfur and selenium species, we recently reported a hydrolysis-based H_2Se donor based on the P=Se motif. By modifying the widely-used P=S containing H_2S donor GYY4137, we prepared the analogous P=Se containing compound TDN1042 and demonstrated that it releases H_2Se upon hydrolysis by ^{31}P and ^{77}Se NMR spectroscopy as well as H_2Se trapping experiments.[80] Building from this work, here we report second-generation H_2Se donors that allow for modified H_2Se release rates. To further bridge the gap to using these H_2Se releasing compounds in biological settings, we use TOF-SIMS (Time of Flight Secondary Ion Mass Spectroscopy) to demonstrate that these donors are cell permeable and result in a dose-dependent increase in intracellular selenium levels. Moreover, we demonstrate that exogenous treatment with the H_2Se donors reduces ROS levels in live cells, which is consistent with antioxidant activity. We anticipate that these results will not only broaden the available chemistry of H_2Se releasing compounds, but will also enable future investigations into direct administration of H_2Se in different biological contexts.

3.2 Results and Discussion

3.2.1 Design and Synthesis of Cyclic H_2Se Donors

Although sulfur and selenium are similar main group elements, the inherent reaction chemistry of these elements if often dissimilar. Demonstrating that design approaches for hydrolysis-based H_2S donors can be translated to develop H_2Se donors provides an important step toward advancing and expanding investigations into H_2Se and RSeS in biology. One limitation of the initial TDN1042 system was that H_2Se release was quite slow. To improve on this system and expand the palette of P=Se based H_2Se donors, we diversified the P=Se platform to investigate how structural modifications impact H_2Se release rates and to compare how these modifications align with known

structure-function activities in P=S based systems.[81] We modified TDN1042 by incorporating *ortho*-substituted phenols that coordinate in a bidentate fashion to the phosphorus center and result in a donor with a single P=Se motif. These donors were prepared by treating Woollins' reagent ($P_2Se_4Ph_2$) with catechol- and 2-aminophenol-based reagents.[82-83] Briefly, refluxing Woollins' reagent with 3 equiv. of the desired phenol under N_2 results in formation of the corresponding malodorous cyclized products that can then be purified by silica gel chromatography to afford Cat-PSe (catechol), 2AP-PSe (2-aminophenol), and NMe2AP-PSe (*N*-methyl-2-aminophenol) in low to moderate yields (Figure 3.2). Each compound was characterized by ^{1}H, ^{13}C, ^{31}P, and ^{77}Se NMR spectroscopy as well as mass spectrometry. The P=Se motif is readily identifiable as a doublet in the ^{77}Se NMR spectrum and as a singlet in the ^{31}P NMR spectrum with characteristic ^{77}Se satellites.

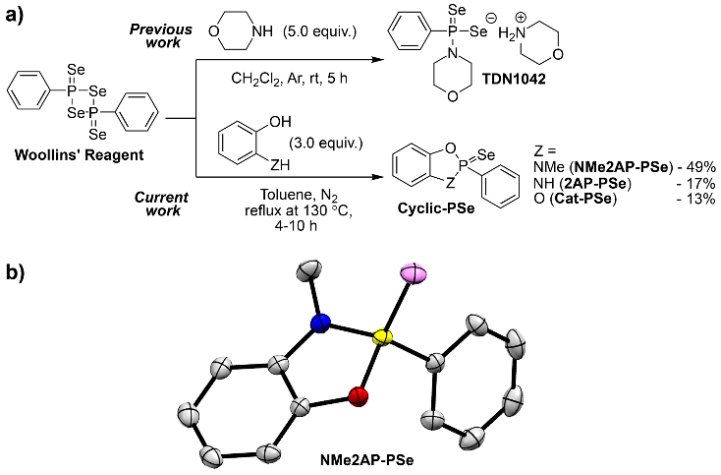

Figure 2.2 (a) Synthesis of TDN1042 and cyclic-PSe H_2Se donors. (b) ORTEP diagram of NMe2AP-PSe showing 50% probability ellipsoids. Hydrogen atoms are omitted for clarity.

3.2.2 P=Se Hydrolysis and H_2Se Release

With cyclized P=Se donor compounds in hand, we next used ^{31}P NMR spectroscopy to monitor donor hydrolysis in pH 7.4 PIPES buffer. Under these reaction conditions, H_2Se release is accompanied by generation of the corresponding phosphine oxide, which is ultimately hydrolyzed to generate phenylphosphonic acid (PPA). In the case of Cat-PSe, addition to aqueous buffer immediately resulted in the formation of an

intermediate that was shifted ~50 ppm upfield in the ^{31}P NMR spectrum (Figure 3.3, red square). We attribute this signal to a 5-coordinate phosphorus species with P-OH and P-Se^- motifs that is formed attack of water at the phosphorus center. Subsequent protonation of the anionic selenide leads to rapid extrusion of H_2Se/HSe^- (pK_a = 3.9) with concomitant P=O bond formation.

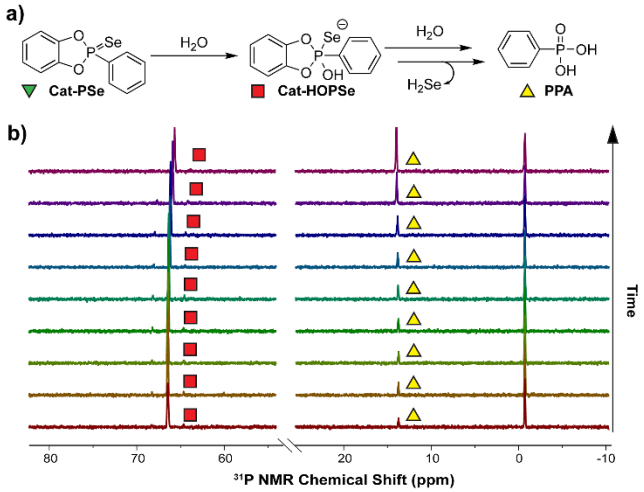

Figure 3.3 (a) Hydrolysis of Cat-PSe to release H_2Se. (b) Stacked ^{31}P NMR spectra of Cat-PSe (10 mM) hydrolysis in PIPES buffer (pH 7.4, 100 mM) over 450 h at 25 °C.

We also investigated the hydrolysis of 2AP-PSe and NMe2AP-PSe and compared the k_{obs} hydrolysis rates. Our initial hypothesis was that the rate of hydrolysis would depend primarily on the electronegativity of the atoms surrounding the phosphorus center, with a more electropositive phosphorus center leading to faster hydrolysis rates. This trend, however, was not observed, which suggests that electronic effects are not the primary contributor to donor hydrolysis (Figure 3.4). For example, we expected that the presence of two aryl P-O bonds in Cat-PSe would result in the most electrophilic phosphorus center, but Cat-PSe displays the slowest hydrolysis rate. The 2-aminophenol based donors, however, did follow the expected trend, with the *N*-methylated donor (NMe2AP-PSe) releasing H_2Se more slowly than 2AP-PSe. One contributing factor to the faster hydrolysis rates of the aminophenol-based donors is the differential bond strength between the weaker aryl P-O bond (141 kcal/mol) when compared to the stronger aryl P-N bond (148 kcal/mol). These small structural changes, when comparing the Cat-PSe and 2AP-PSe donors, result in almost an order of magnitude increase in the

rate of donor hydrolysis. Taken together, these data reflect the tunability of P=Se bond hydrolysis based on the structure of the H_2Se donor core.

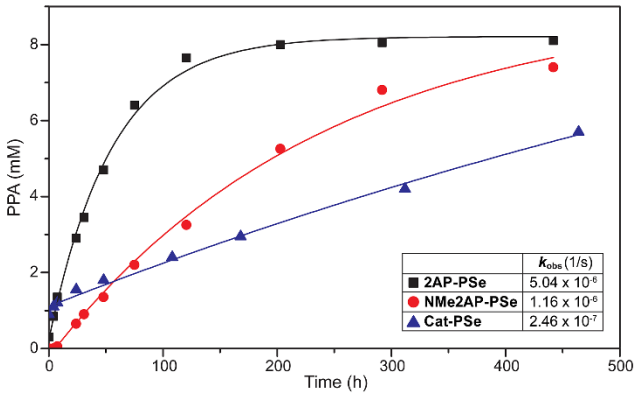

Figure 3.4 Plotted hydrolysis data (10 mM donor in PIPES 7.4, 100 mM buffer with 5 mM TEP standard at 25 °C) based on the concentration of PPA with tabulated observed rate constants.

3.2.3 Mechanistic Studies with ^{31}P and ^{77}Se NMR Spectroscopy

To further investigate the hydrolysis mechanism for the cyclic-PSe compounds and to confirm H_2Se release, we performed alkylative trapping experiments with benzyl bromide (BnBr). These experiments are useful for monitoring selenide release by generating stable, alkylated products, whereas direct H_2Se release often results in selenium auto-oxidation. Conveniently, these experiments can be followed by ^{1}H, ^{31}P, and ^{77}Se NMR spectroscopy, all of which help to inform on intermediate structures in solution based on the observed heteronuclear coupling constants and multiplicities. Representative NMR spectra for 2AP-PSe are shown in Figure 3.5, and similar results were observed for the other donors (See Appendix B, Figure B16 and B17 for Cat-PSe and NMe2AP-PSe, respectively).

To simplify the reaction conditions, we performed these experiments in THF-d_8 with 62 mM donor, 124 mM BnBr, and 2.33 M (35 equiv.) of water. Under these reaction conditions, attack by water on the phosphorus center breaks the 2-aminophenol chelate to form a 4-coordinate P-N intermediate (**1**). This step results in an upfield shift in both the ^{31}P and ^{77}Se NMR spectra and a decrease in the $J^{1}_{P\text{-}Se}$ from 899 Hz to 823 Hz. The identity of this intermediate is supported by the independent synthesis and isolation of the analogous methoxylated species, which showed similar spectroscopic properties

including ^{31}P and ^{77}Se chemical shifts of 72 ppm and -212 ppm, respectively, and a $J^{1}_{P\text{-}Se}$ value of 817 Hz (See Appendix B, Figure B18 for X-ray structure). In the absence of an electrophilic alkylating trap, intermediate **1** would be protonated prior to subsequent H_2Se release. Analogously, in the presence of BnBr, intermediate **1** is alkylated to form intermediate **2**, which is supported by the upfield shift of the ^{31}P NMR signal to 27 ppm and downfield shift of the ^{77}Se NMR signal to 300 ppm. Notably, the ^{77}Se signal appears as a doublet of triplets due to coupling to the phosphorus center and the benzyl CH_2 motif ($J^{1}_{P\text{-}Se}$ = 384 Hz, $J^{2}_{Se\text{-}H}$ = 7.1 Hz). Hydrolysis of **2** liberates benzyl selenol (BnSeH), as evidenced by the new resonance in the ^{77}Se spectrum at 78 ppm (dt, $J^{1}_{Se\text{-}H}$ = 42.4 Hz, $J^{2}_{Se\text{-}H}$ = 12.5 Hz). Selenol **2** is subsequently oxidized to form dibenzyl diselenide (Bn_2Se_2), which is characterized by a triplet at 400 ppm in the ^{77}Se NMR spectrum ($J^{2}_{Se\text{-}H}$ = 14.0 Hz). Under these reaction conditions, the auto-oxidized Bn_2Se_2 is the major product, but dibenzyl selenide (Bn_2Se) is also formed upon reaction of BnSeH with BnBr, which is characterized by a pentet at 330 ppm in the ^{77}Se NMR spectrum. The resultant phosphorus byproduct (**3**) does not accumulate in the reaction mixture and is rapidly hydrolyzed to PPA, which appears at 14 ppm in the ^{31}P NMR spectrum.

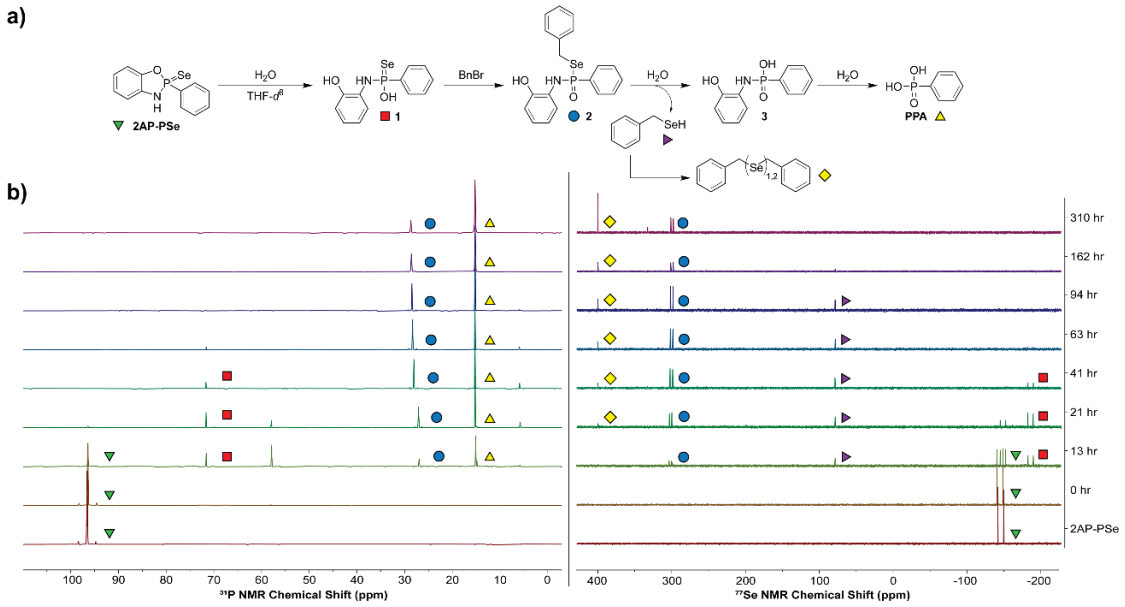

Figure 3.5 Results of alkylative trapping experiments with BnBr showing (a) the proposed reaction scheme and (b) the corresponding ^{31}P and ^{77}Se NMR data for this reaction (62 mM 2AP-PSe, 124 mM BnBr, and 2.33 M water in THF-d_8 at 25 °C).

3.2.4 Colorimetric H_2Se Detection

Although NMR spectroscopy provides useful information on the chemical environment and connectivity of the different species formed during H_2Se release, spectroscopic detection of H_2Se using optical methods would aid the future development of H_2Se donors and H_2Se detection. Drawing parallels to work on colorimetric systems commonly used for H_2S trapping, we investigated whether 4-chloro-7-nitrobenzofurazan (NBD-Cl) could be used for colorimetric H_2Se detection. Previously, we demonstrated that NBD-Cl reacts with H_2S to generate NBD-SH, which has a characteristic absorbance at 536 nm and allows for colorimetric H_2S detection.[84] NBD-based electrophiles have been used broadly by many groups to develop both colorimetric and fluorescent reporters for H_2S[85] as well as other small molecules.[86] Building from this basic chemistry, we expected that the electrophilic NBD-Cl would also react with H_2Se to produce a highly colored product that could aid H_2Se detection.

To test this chemistry directly, we first treated NBD-Cl with tetrabutylammonium hydroselenide (NBu_4SeH) in pH 7.4 PBS buffer (Figure 3.6a). When a sub-stoichiometric amount of HSe^- is present with respect to NBD-Cl, NBD_2Se (λ_{max} = 428 nm) is the primary product, which is formed by the intermediate generation of NBD-SeH and subsequent reaction with a second equivalent of NBD-Cl. If stoichiometric HSe^- with respect to NBD-Cl is present, then NBD-SeH (λ_{max} = 551 nm) is the primary product, which forms from either direct reaction of NBD-Cl with HSe^- or the cleavage of the NBD_2Se intermediate with HSe^-. This chemistry can be clearly demonstrated by titrating 0.1 equiv. aliquots of NBu_4SeH (10 mM in DMSO) into a solution of NBD-Cl. The intermediate formation of NBD_2Se is observed, which reaches a maximum at 2:1 NBD-Cl:HSe^- stoichiometry, with NBD-SeH being the primary species at a 1:1 NBD-Cl:HSe^- ratio (Figure 3.6b). The observed absorbance of NBD-SeH at 551 nm is red-shifted from the NDB-SH absorbance at 534 nm, which is consistent with substitution of a heaver chalcogenide. Based on these data, NBD-Cl provides a unique colorimetric response to H_2Se/HSe^- upon formation of the highly colored NBD-SeH product.

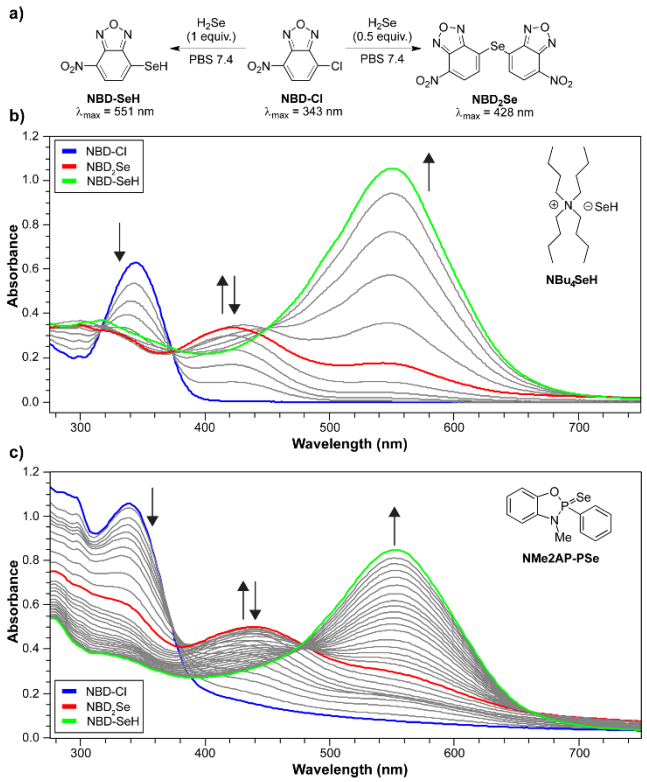

Figure 3.6 (a) Addition of 1.0 equiv. of H_2Se to NBD-Cl results in the direct formation of NBD-SeH. Addition of 0.5 equiv. of H_2Se to NBD-Cl results in the formation of NBD_2Se, which can react further with H_2Se to generate NBD-SeH. (b) Titration of NBD-Cl (66 μM in PBS 7.4 buffer) with NBu_4SeH (10 mM in DMSO) in 0.1 equiv increments at 25 °C. (c) Treatment of NBD-Cl (66 μM in PBS 7.4 buffer) with NMe2AP-PSe (1.5 equiv, 99 μM from a 10 mM solution in THF) at 25 °C forms NBD-SeH.

In prior unpublished work, we found that attempts to measure H_2Se release from TDN1042 with NBD-Cl resulted in the formation of an unidentified adduct rather than the expected NBD-SeH. This observation was consistent with analogous experiments done on GYY4137, which also formed an unidentified adduct. In addition, we found that this reaction was significantly faster than the hydrolysis of TDN1042 (Scheme 3.1) based on ^{31}P NMR experiments. Because the cyclic-PSe compounds hydrolyze faster than TDN1042, we wanted to further investigate this reactivity and determine whether NBD-Cl could be used to monitor H_2Se release. To test this system initially, we added Cat-PSe (1.0 equiv.) to a solution of NBD-Cl (66 μM in PBS 7.4 buffer) and observed the expected formation of NBD-SeH (λ = 551 nm), which is consistent with H_2Se generation (Figure 3.6c). When comparing this UV-vis data to ^{31}P NMR hydrolysis experiments, however, we noted a significant difference in rate, with complete hydrolysis occurring in

hours as opposed to days. This difference suggests that the presence of a strong electrophile, such as NBD-Cl, will result in a deviation from the assumed pathway of hydrolysis. Based on these rate differences, we propose that the cyclic-PSe compounds react directly with NBD-Cl to form an intermediate that facilitates the subsequent liberation of selenide and NBD-SeH formation. Although the NBD-Cl trapping system confirms that these donors are a source of labile reduced Se, we caution other researchers that NBD-Cl trapping experiments should be complemented with other measurements for RSeS releasing compounds.[87]

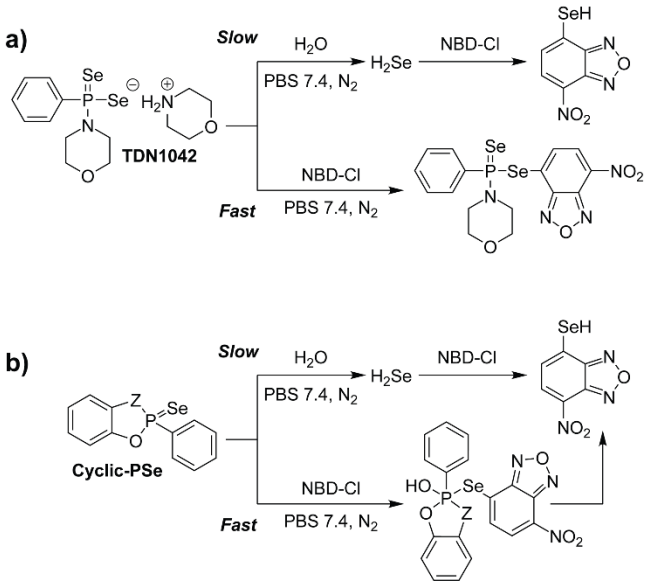

Scheme 3.1 Proposed Reaction Pathways for the Reaction of (a) TDN1042 and (b) Cyclic-PSe Compounds with NBD-Cl.

3.2.5 Cell Permeability Studies Using TOF-SIMS

Because H_2Se delivery strategies are only beginning to emerge, little is known about the biocompatibility of these RSeS donors. To help bridge the gap between H_2Se donor development and applications to biological systems, we first focused on determining whether the prepared donors are cell permeable. To achieve this goal, we used Time of Flight Secondary Ion Mass Spectrometry (TOF-SIMS) to measure the concentration of different elements in cells that were treated with donors. This method allows atomic identities to be mapped by monitoring characteristic elemental masses of ionized particles (e.g. Se^- for selenium, PO_3^- for phosphorus). Furthermore, ion beam

ablation of the exposed frozen cell surfaces allows for 3D elemental maps to be constructed. Similar approaches based on X-ray fluorescence (XRF) have been used previously to observe cellular localization of Ebselen, a Se-containing glutathione peroxidase (GPx) mimic.[50]

To determine whether H_2Se donors were cell permeable, HeLa cells were grown on silicon chips, incubated with different concentrations of H_2Se donors overnight, fixed with formaldehyde, and measured by TOF-SIMS in depth profiling mode. Cell bodies and peripheral boundaries were identified by mapping the PO_3^- peak. A high level of phosphorus is present throughout the cell and also in the cell membrane phospholipid bilayer (Figure 3.7ai, 3.7bi). To determine whether the H_2Se donors are cell permeable, we measured the total intracellular Se content as a function of H_2Se donor concentration. If the donors are cell permeable, we would expect to observe a dose-dependent increase in intracellular Se levels up on donor treatment. In the absence of H_2Se donors (DMSO vehicle), the HeLa cells showed only trace levels of intracellular Se (Figure 3.7aii). When treated with 2AP-PSe, significant Se accumulation was observed within the cell boundaries (Figure 3.7bii). Cell ablation in the z-axis allowed for 3-dimensional mapping of intracellular Se, which confirmed that the Se was not solely localized at the cell surface and had been internalized within the cells (Figure 3.7cii). To further support these conclusions, we also measured the total Se accumulation in HeLa cells with different concentrations of 2AP-PSe (Figure 3.7d). The Se^- peak intensity detected within the cell boundaries was normalized by the total ion intensity, which allowed us to verify a dose-dependent increase in intracellular Se from 0 - 25 μM, after which the cellular levels plateau. Taken together, the TOF-SIMS data support that these donors can be used to increase intracellular Se levels.

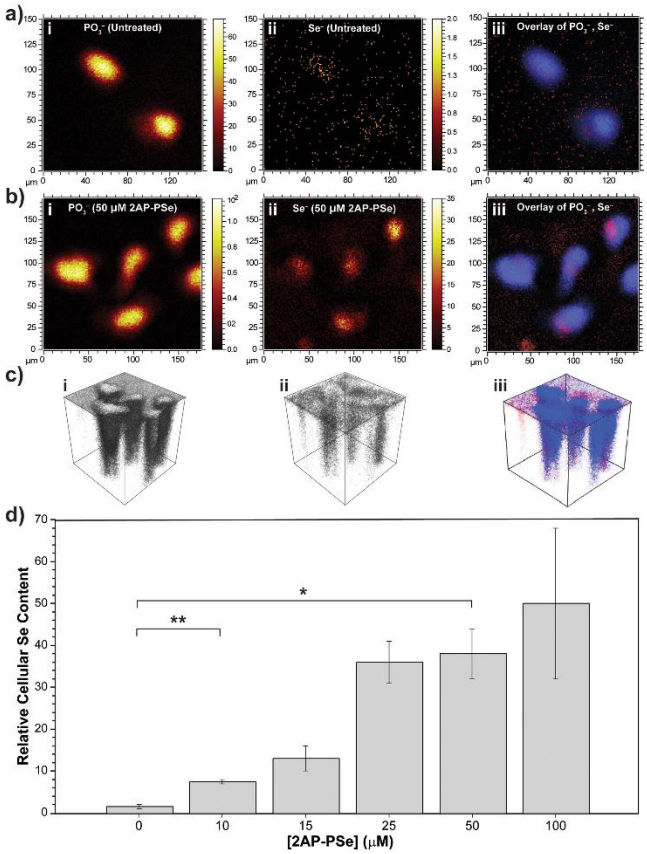

Figure 3.7 TOF-SIMS images of HeLa cells treated with (a) DMSO (vehicle) showing (i) P, (ii) Se, and (iii) element overlay; (b) 2AP-PSe (50 μM, 18 h) showing (i) P, (ii) Se, and (iii) element overlay. (c) 3D representations of elemental distributions from the data in (b), confirming intracellular localization. (d) Cellular Se content as a function of 2AP-PSe concentration. *$p < 0.05$; **$p < 0.01$ vs control group.

3.2.6 Antioxidant Activity of H_2Se Donors

Having demonstrated that 2AP-PSe can increase intracellular Se levels, we next sought to determine whether 2AP-PSe could exert antioxidant activities in live cells. To probe ROS levels, we used 2′,7′-dichlorofluorescin diacetate (DCFH-DA), a widely-used, cell-trappable, fluorescent ROS reporter.[88] Upon reaction with ROS such as peroxides, DCFH-DA is oxidized to the highly fluorescent 2′,7′-dichlorofluorescein (DCF, Figure 3.8a). Our expectation was that pre-treatment of cells with 2AP-PSe would provide greater antioxidant activity toward exogenous ROS, which could be monitored directly by DCFH-DA.

To test this antioxidant activity directly, HeLa cells were treated with 5 - 25 μM 2AP-PSe for 20 hours prior to treatment with 5 μM DCFH-DA for 30 minutes. Cells

were washed with buffer and subsequently treated with 500 μM of H_2O_2 for 30 minutes. When compared to background cellular autofluorescence, addition of DCFH-DA resulted in a small fluorescence increase due to endogenous ROS. Addition of 25 μM of 2AP-PSe, however, decreased DCF formation, which suggests that 2AP-PSe exerts antioxidant effects on cells. To determine whether 2AP-PSe could be used to provide protection against exogenous ROS, we treated HeLa cells with H_2O_2 and monitored to DCF fluorescence response. Treatment of cells with 500 μM H_2O_2 in the absence of 2AP-PSe resulted in a significant fluorescence response. As expected, pre-treatment of cells with 5, 10, or 25 μM 2AP-PSe significantly reduced DCF formation (Figure 3.8b). Representative images from these experiments clearly show the fluorescence turn-off effect caused by treatment with 2AP-PSe (Figure 3.8c). It is unlikely that these effects are the result of a buildup of H_2Se in the cells due to the high reactivity and toxicity of this species. The antioxidant effect, therefore, should be attributed to an increase in concentration of selenium-containing metabolites in the cells resulting from gradual H_2Se production. Further study is needed to elucidate the identities of these reducing metabolites. Taken together, these data show that 2AP-PSe exerts potent ROS scavenging activity, which is consistent with proposed antioxidant activity selenide-containing compounds in biology.

3.3 Conclusions

This work advances H_2Se donor technology by imparting rate tunability into the hydrolysis of P=Se motifs. Further ^{31}P and ^{77}Se NMR spectroscopic studies utilizing alkylative trapping experiments reveal a general mechanism of action, which is consistent with the proposed mechanism of action. Advancing the biological applications of H_2Se donors, we used TOF-SIMS to demonstrate that 2AP-PSe is cell permeable and increases intracellular Se levels in a dose-dependent manner. In addition, we show that 2AP-PSe can reduce ROS and H_2O_2 levels in live cells, which further supports the antioxidant activity of H_2Se. We anticipate that these as well as future H_2Se donors will significantly advance investigations into the roles of reduced RSeS, including H_2Se, in biological investigations.

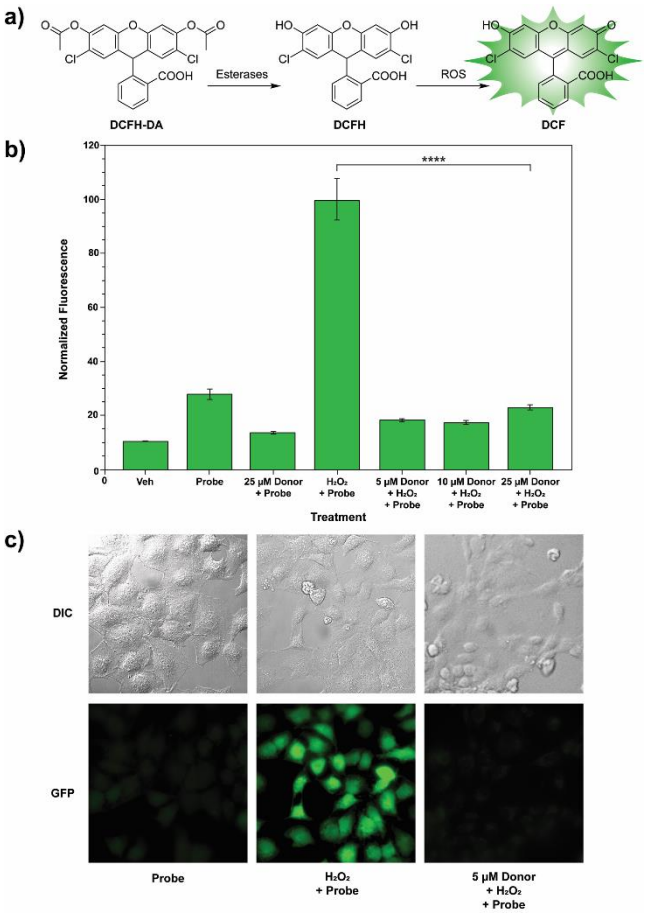

Figure 3.8 Demonstrated antioxidant activity of 2AP-PSe on HeLa cells as measured by (a) dichlorofluorescein diacetate (DCFH-DA) reacting with ROS, where a major decrease in fluorescence is detected in (b) when the H_2Se donor is applied; probe, DCFH-DA, 5 μM; donor, 2AP-PSe, 24 h incubation; H_2O_2, 500 μM, 30 min incubation; ****$p < 0.0001$ vs control group. (c) Images of cells under the listed treatment conditions on DIC and GFP channels.

3.4 Experimental Section

Materials and methods

Reagents were purchased from Sigma-Aldrich, Alfa Aesar, and TCI Chemicals and were used directly as received. Deuterated solvents were purchased from Cambridge Isotope Laboratories and used directly as received, except for THF-d_8, which was distilled over sodium and benzophenone prior to use. NBu_4SeH was prepared as described in the literature.[89] Cat-PSe and 2AP-PSe were prepared as described below, and spectroscopic data matches previously reported data.[82] ^{1}H, $^{13}C\{^{1}H\}$, ^{31}P, and ^{77}Se NMR spectra were recorded on Bruker 500 and 600 MHz instruments. Chemical shifts are

reported relative to residual protic solvent resonances for ^{1}H and $^{13}C\{^{1}H\}$ spectra. All air-free manipulations were performed in an inert atmosphere using standard Schlenk techniques or an Innovative Atmospheres N_2-filled glove box. Fluorescent images were taken on a Leica DMi8 widefield microscope. Images were analyzed and quantified in ImageJ.

General synthesis of cyclic-PSe compounds

Woollins' reagent (0.32 g, 0.60 mmol) and the desired *o*-substituted phenol (1.8 mmol) were added to a flask with anhydrous toluene (15 mL) in a glove box. The flask was then attached to a septum-sealed reflux condenser, removed from the glove box, attached to a N_2 line, and placed in an oil bath at 130 °C to reflux. The reaction was monitored by TLC (general reaction time 4 to 10 hours). Upon completion, the reaction mixture was concentrated *in vacuo* to afford a black crust, extracted with CH_2Cl_2, and purified via flash column chromatography (SiO_2, 25% EtOAc/hexanes). The identity of the product was verified by ^{1}H, $^{13}C\{^{1}H\}$, ^{31}P, and ^{77}Se-NMR. See SI for NMR spectra. *Cat-PSe*: Pink powder, 46 mg, 13%. ^{1}H NMR (600 MHz, $CDCl_3$) δ: 7.89 (m, 2H), 7.62 (td, 1H, $J^{5}_{P\text{-}H}$ = 1.7 Hz, $J^{3}_{H\text{-}H}$ = 7.5 Hz), 7.49 (td, 2H, $J^{4}_{P\text{-}H}$ = 4.3 Hz, $J^{3}_{H\text{-}H}$ = 7.8 Hz), 7.14-7.06 (m, 4H). $^{13}C\{^{1}H\}$ NMR (151 MHz, $CDCl_3$) δ: 145.8, 134.1, 133.3, 131.2, 128.7, 123.8, 112.8. ^{31}P NMR (241 MHz, $CDCl_3$) δ: 115.6 (t, $J^{1}_{P\text{-}Se}$ = 959 Hz, $J^{3}_{P\text{-}H}$ = 16.0 Hz). ^{77}Se NMR (115 MHz, $CDCl_3$) δ: -177.1 (d, $J^{1}_{P\text{-}Se}$ = 959 Hz).

2AP-PSe: Orange-pink powder, 60 mg, 17%. ^{1}H NMR (600 MHz, $CDCl_3$) δ: 7.96 (m, 2H), 7.57 (td, 1H, $J^{5}_{P\text{-}H}$ = 1.7 Hz, $J^{3}_{H\text{-}H}$ = 7.5 Hz), 7.47 (td, 2H, $J^{4}_{P\text{-}H}$ = 4.3 Hz, $J^{3}_{H\text{-}H}$ = 7.8 Hz), 7.05 (d, 1H, $J^{3}_{H\text{-}H}$ = 8.1 Hz), 6.98 (t, 1H, $J^{3}_{H\text{-}H}$ = 8.0 Hz), 6.89 (t, 2H, $J^{3}_{H\text{-}H}$ = 7.7 Hz), 5.24 (s, 1H). $^{13}C\{^{1}H\}$ NMR (151 MHz, $CDCl_3$) δ: 146.4, 133.6, 133.2, 131.1, 128.4, 112.7, 111.6. ^{31}P NMR (241 MHz, $CDCl_3$) δ: 97.1 (t, $J^{1}_{P\text{-}Se}$ = 894 Hz, $J^{3}_{P\text{-}H}$ = 16.1 Hz). ^{77}Se NMR (115 MHz, $CDCl_3$) δ: -134.3 (d, $J^{1}_{P\text{-}Se}$ = 894 Hz).

NMe2AP-PSe: Pink powder, 181 mg, 49%. ^{1}H NMR (600 MHz, $CDCl_3$) δ: 7.86 (m, 2H), 7.57 (td, 1H, $J^{5}_{P\text{-}H}$ = 1.7 Hz, $J^{3}_{H\text{-}H}$ = 7.5 Hz), 7.47 (td, 2H, $J^{4}_{P\text{-}H}$ = 4.3 Hz, $J^{3}_{H\text{-}H}$ = 7.8 Hz), 7.04 (m, 2H), 6.86 (t, 1H, $J^{3}_{H\text{-}H}$ = 7.90 Hz), 6.74 (d, 1H, $J^{3}_{H\text{-}H}$ = 7.8 Hz), 3.00 (d,

3H, $J^3_{P\text{-}H}$ = 11.8 Hz). $^{13}C\{^1H\}$ NMR (151 MHz, $CDCl_3$) δ: 146.3, 136.5, 135.2, 134.4, 133.3, 131.3, 128.5, 123.4, 120.1, 112.1, 108.6, 28.03. ^{31}P NMR (241 MHz, $CDCl_3$) δ: 103.5 (tq, $J^1_{P\text{-}Se}$ = 894 Hz, $J^3_{P\text{-}H}$ = 15.3 Hz, $J^3_{P\text{-}H}$ = 11.8 Hz). ^{77}Se NMR (115 MHz, $CDCl_3$) δ: -181.5 (d, $J^1_{P\text{-}Se}$ = 894 Hz). LRMS (ASAP) calc'd for $C_{13}H_{13}NOPSe^+$ $[M+H]^+$ 310.0, found 310.1.

2AP-PSe-OMe: The crude product was treated with methanol (5 mL), after which chromatographic purification according to the general procedure produced the title compound. White powder, 182 mg, 46%. ^1H NMR (600 MHz, $CDCl_3$) δ: 7.81 (m, 2H), 7.46 (td, 1H, $J^5_{P\text{-}H}$ = 1.7 Hz, $J^3_{H\text{-}H}$ = 7.5 Hz), 7.40 (td, 2H, $J^4_{P\text{-}H}$ = 4.3 Hz, $J^3_{H\text{-}H}$ = 7.8 Hz), 6.80 (m, 3H), 6.64 (m, 1H), 6.12 (s, 1H), 3.84 (d, 3H). $^{13}C\{^1H\}$ NMR (151 MHz, $CDCl_3$) δ: 145.3, 134.1, 133.2, 132.1, 130.6, 128.7, 127.9, 123.2, 121.1, 119.1, 115.4, 52.4. ^{31}P NMR (241 MHz, $CDCl_3$) δ: 71.9 (m, $J^1_{P\text{-}Se}$ = 817 Hz).^{77}Se NMR (115 MHz, $CDCl_3$) δ: -211.6 (d, $J^1_{P\text{-}Se}$ = 817 Hz).

Hydrolysis studies

Stock solutions of phosphine selenide complexes (60 mM) and triethylphosphate (30 mM) were prepared in THF in GC vials in a glovebox. Aliquots of 0.10 mL of each stock solution were added to 0.40 mL PIPES buffer solution (pH 7.4, 100 mM) in NMR tubes. These NMR tubes were removed from the glovebox with tape-sealed septum caps, and the samples were monitored via ^{31}P NMR spectroscopy with gradient shimming and elongated pulse/relaxation times.

Mechanistic studies with ^{31}P and ^{77}Se NMR spectroscopy

In a glovebox, the donor (0.035-0.040 mmol) was dissolved in THF-d_8 (0.50 mL) and charged to an NMR tube, which was then capped with a septum and sealed with electrical tape. Baseline ^{31}P and ^{77}Se NMR spectra of the donor solution were acquired prior to addition of a BnBr stock solution in THF-d_8 (0.10 mL, 2.0 equiv., also prepared in a glovebox) and degassed Millipore water (25 μL, 1.4 mmol) via argon-purged Hamilton syringes. This reaction mixture was shaken and monitored by ^{31}P and ^{77}Se NMR spectroscopy over the course of two weeks, revealing the formation and conversion

of various intermediates to the final products dibenzyl diselenide (Bn_2Se_2, major) and dibenzyl selenide (Bn_2Se, minor).

Hydrolysis monitoring with NBD-Cl

A stock solution of tetrabutylammonium hydroselenide (NBu_4SeH, 10 mM in DMSO) and NBD-Cl (10 mM in DMSO) were prepared in a glovebox in GC vials that were sealed with electrical tape. In a separate glovebox specifically for aqueous work, a quartz cuvette with septum cap was charged with PBS 7.4 buffer (3.0 mL, 10 mM). The solutions and cuvette were transported to a UV-vis spectrometer, and a baseline scan (250-750 nm) was taken before addition of NBD-Cl solution (20 μL for a 66 μM solution in the cuvette) and an additional scan to establish the NBD-Cl baseline. After this scan, NBu_4SeH was titrated into solution (2 μL injections, 0.1 equiv.) until spectral changes were no longer evident.

The previous procedure was modified slightly to monitor the hydrolysis of the H_2Se donors. Specifically, stock solutions were prepared in THF (10 mM), and the cuvette was equipped with a stirring flea. Baseline scans were taken as detailed above, but the donor was added as a single injection (30 μL, 1.5 equiv.), and the hydrolysis was monitored as the reaction stirred. Scans were taken at 2 nm intervals every 12 seconds for 30 minutes or until spectral changes were no longer evident.

Cell culture

HeLa cells (ATCC) were cultured in DMEM containing phenol red (Gibco) and supplemented with 10% fetal bovine serum (FBS) (VWR) and 1% penicillin-streptomycin (PS) (10,000 units/mL penicillin and 10,000 μg/mL streptomycin) (Gibco). Cells were maintained at 37°C under 5% CO_2.

Cellular proliferation assay

HeLa cells were seeded in Nunc 96 well Nunclon Delta plates at 10,000 cells/well under normal culturing conditions. The next day, media was aspirated off and replaced with FBS-free DMEM containing test compounds in 0.5% DMSO (vehicle). Cells were

with test compounds for 24 hours before treatment with Cell Counting Kit-8 (CCK-8, Dojindo Molecular Technologies). Data was normalized to vehicle and pooled.

Cell treatment with 2AP-PSe: TOF-SIMS depth profiling and imaging

HeLa cells were seeded in a 12-well plate containing p-doped (boron) polished wafers (<100> orientation, Czochralski-grown, resistivity around 0.012 Ohm/cm^2) and were grown overnight in 10% FBS DMEM. The following day, the media was removed, and the cells were washed (2x FBS-free DMEM), treated with 2AP-PSe (10-100 μM, 0.5% DMSO vehicle) in FBS-free DMEM, and incubated for 18 h. After incubation, media was aspirated off and wafers were rinsed 3x with pH 7.4 PBS, and fixed with freshly-prepared 3.7% paraformaldehyde (PFA) in Milli-Q water for 15 minutes at room temperature. After incubation, PFA was aspirated off and wafers were rinsed 3x with PBS, 0.1 M ammonium acetate, and Milli-Q water. TOF-SIMS spectra were acquired with a Model IV TOF-SIMS instrument manufactured by ION-TOF GmbH, Münster, Germany, using a 25kV Bi_3^+ primary ion beam and a 2kV Cs^+ sputter beam. Typically, three or four cells were in the field of view during the depth profile. The depth profile was acquired until all cellular material was ablated, as determined by following the PO_3^- peak intensity during the profile. Using software provided by the vendor we extracted the spectra from the cellular material and measured the Se^- peak area. The software provided the relevant measure of total ion intensity, which was used for normalization. This protocol allows one to compare relative Se content in the cells.

Cell treatment with 2AP-PSe: ROS assay with DCFH-DA

HeLa cells were plated in glass-bottom imaging dishes (MatTek) at a density of 100,000 cells per dish and were grown in DMEM under normal conditions overnight. The following day, the media was removed and the cells were washed (2x FBS-free DMEM). After rinsing, cells were incubated with 2AP-PSe (5-100 μM) for 20 h in FBS-free DMEM. After incubation the media containing 2AP-PSe was removed, and the cells were washed (2x FBS-free DMEM). Cells were then treated with DCFH-DA (5 μM, 45 min in serum-free DMEM for 30 minutes. After incubation, cells were rinsed 2x with

serum-free DMEM and then were incubated with H_2O_2 (500 μM, 30 min). Cells were then washed 2x with PBS and imaged in FluoroBrite DMEM (Gibco).

CHAPTER IV

SELENOCARBAMATES AS H_2Se DONORS

This chapter includes unpublished and co-authored material. The manuscript in Chapter 4 was written by Turner D. Newton with editorial assistance by Professor Michael D. Pluth. The project in this chapter was conceived of by Turner D. Newton and Professor Michael D. Pluth. The experimental work in this chapter was performed by Turner D. Newton.

4.1 Introduction

Selenium (Se) is an essential micronutrient in human physiology.[6, 72] Dietary deficiency of this element can result in debilitating conditions such as Keshan Disease, which presents as congestive cardiomyopathy and is often fatal.[5] Additionally, chronic overconsumption of Se-rich foods such as the Brazil Nut can induce Se poisoning, called selenosis, which presents as foul breath, loss of hair and nails, and neurodegeneration in extreme cases.[10-11] Various forms of Se consumed in the human diet are either converted to selenoproteins, the active form of Se in the body, or are excreted as waste products to prevent toxic buildup.[8]

At the crossroads of the metabolic pathways of Se is the highly reactive and toxic species hydrogen selenide (H_2Se), which is vital to the production of selenophosphate before incorporation into selenoproteins.[29] Despite being central in Se metabolism and crucial to the production of selenoproteins, H_2Se has received limited attention from researchers, leaving gaps in the knowledge surrounding its involvement in other biological processes and potential for use as a therapeutic agent. Recent years have seen the advent of a number of small molecule chemical tools for studying the roles and effects of H_2Se in biological settings.[40-43] These tools are activated by water or the presence of thiols, such as cysteine, to release H_2Se in a controlled and gradual fashion. The simplicity of these H_2Se donors has given researchers a solid foothold to use for studying H_2Se, but moving forward, we seek to impart elements of complexity to the field of H_2Se donors, such as broadening the palette of stimuli and installing fluorescent payloads to facilitate biological investigations.

Recent advances in the field of hydrogen sulfide (H_2S) research have shown that thiocarbamates (TCMs) can function as indirect sources of H_2S. Upon reaction of the triggering group, they generate carbonyl sulfide (COS), which undergoes assisted hydrolysis in the presence of the ubiquitous mammalian enzyme carbonic anhydrase (CA) to produce H_2S (Scheme 4.1a),[90-91] Following this chemistry, we wanted to determine whether similar approaches could be adapted to construct a series of selenocarbamates (SeCMs) that would release carbonyl selenide (COSe) as an indirect source of H_2Se in the presence of CA (Scheme 4.1b). In addition to advancing the fundamental chemistry of reactive selenium species (RSeS), if such donors were to release COSe/H_2Se, they would significantly increase the versatility of triggering and release approaches for H_2Se delivery. This approach could be expanded to design SeCMs that respond to light,[92] cysteine,[93] reactive oxygen species (ROS),[94] and esterases,[95] among other stimuli, drawing inspiration from similar approaches for COS/H_2S delivery. Additionally, further improvement from previous H_2Se donors would also allow for diversification of the amine-based payload coupled to the SeCM motif. Development of these donors will expand the capabilities of H_2Se donor technology and shed light on the fundamental chemistry and biological utility of another elusive RSeS in COSe.

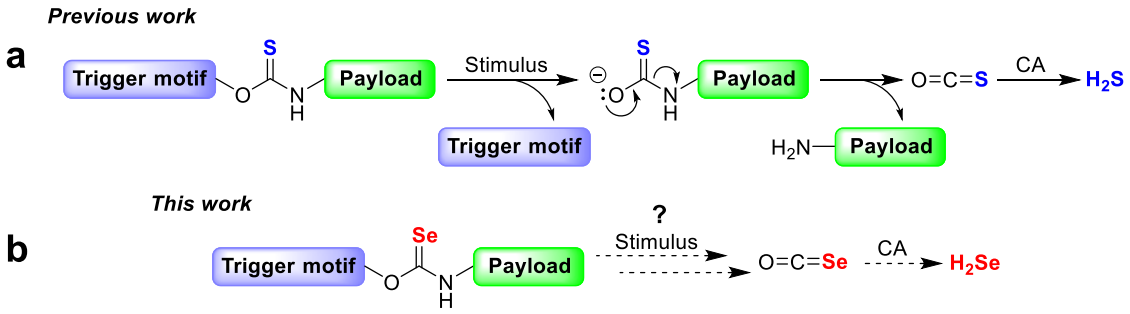

Figure 4.1 (a) Previous work on thiocarbamates as COS/H_2S donors in the presence of carbonic anhydrase (CA) and (b) the proposed design of selenocarbamate COSe/H_2Se donors with diverse triggers and amine-based payloads.

4.2 Results and Discussion

4.2.1 Photoactive Selenocarbamates

Our initial approach to developing SeCMs centered around using a photoactive 2-nitrobenzyl group that would initiate the self-immolative cascade in response to light,[92]

and this trigger was chosen for two main reasons. The first reason is that the synthesis of the TCM analogs is straightforward compared to others in the literature, and benzyl alcohol could easily be used as a model unreactive trigger to refine synthetic procedures if the SeCMs proved difficult. The second reason is that using light as an external stimulus should prevent side reactivity associated with introducing chemical stimuli directly to the SeCMs, which could severely hinder mechanistic investigations that are crucial for new technology. Thus, following the published procedures from our lab on photoactivatable thiocarbamates (Photo-TCMs) as COS donors,[92] we were able to prepare the Se-containing analog (Scheme 4.1). The easily synthesized phenyl and 4-fluorophenyl isoselenocyanates were made according to the literature,[96] and the synthesis of these compounds was both functional group tolerant, high yielding, and scalable. The appropriate isoselenocyanate (1.1 equiv.) was then dissolved in THF and added slowly to an ice-cooled solution of 2-nitrobenzyl alcohol (1.0 equiv.) in THF that had been treated with sodium hydride (2.5 equiv.) and was protected from light. The reaction was brought to room temperature and allowed to proceed for 1 h before quenching in brine and extraction in EtOAc. NMR analysis of the crude mixture showed almost exclusively the *O*-alkyl selenocarbamate (**1**), and upon chromatographic purification, the *Se*-alkyl (**3**) isomer was obtained, suggesting a Newman-Kwart rearrangement[97] promoted by silica gel. The fluorinated analog (**2**) required no further purification after workup, and later chromatographic purification of the sample, which had degraded over several months, also afforded only the *Se*-alkyl isomer (**4**). The ^{1}H NMR spectra of these compounds revealed similarities between the Photo-SeCMs and Photo-TCMs, specifically that the amine proton has a characteristic shift around $\delta(^{1}H) = 12$ ppm for the *O*-alkyl isomers and around $\delta(^{1}H) = 10$ ppm for the *Se*-alkyl isomers. Additionally, the ^{77}Se NMR spectra revealed singlet peaks in the $\delta(^{77}Se) = 250\text{-}300$ ppm range for the *O*-alkyl isomers and triplet peaks in the $\delta(^{77}Se) = 400\text{-}450$ ppm range for the *Se*-alkyl isomers, which was in agreement with similar compounds in the literature.[97] Finally, the ^{19}F NMR spectrum of **2** showed a peak at $\delta(^{19}F) = -116$ ppm, a valuable spectroscopic handle for monitoring the expected photochemical reaction.

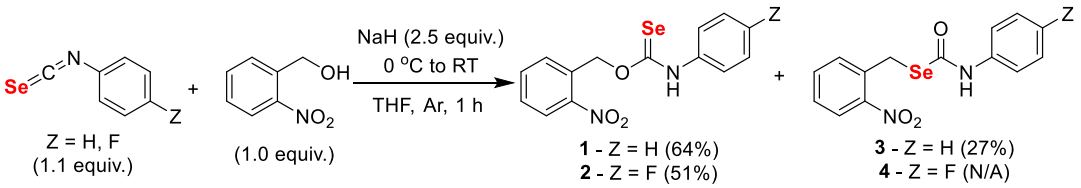

Scheme 4.1 Synthesis of Photo-SeCMs from isoselenocyanates. The yield for **4** is unavailable because it was obtained through purification of a degraded sample of **2**.

With these compounds in hand, we next examined their behavior, specifically the fluorinated analog, in response to photoactivation. Upon irradiation of a 50 mM sample of **2** at 365 nm in THF, conversion from the pF-PhotoSeCM to form products with further upfield shifts in the ^{19}F NMR spectrum was observed (Figure 4.2b). Our initial hypothesis was that the photoactivation of **2** would generate COSe and 4-fluoroaniline in addition to 2-nitrosobenzaldehyde (Figure 4.2ai), but this turned out to not be the case. An authentic sample of 4-fluoroaniline appears at $\delta(^{19}F)$ = -130 ppm, but the main peak observed post-irradiation appeared at $\delta(^{19}F)$ = -122 ppm, which means that 4-fluoroaniline is not the primary reaction product. Reevaluation of the mechanism based on the observed chemical shifts in the NMR spectra led us to the conclusion that the main fluorine-containing product 4-fluorophenyl isocyanate, which was confirmed by comparison to an authentic sample. Based on this mechanism, HSe^-/H_2Se should be released directly as the Se-containing product rather than COSe. This observed reactivity is fundamentally different from the established chemistry of thiocarbamates, and direct release of H_2Se actually facilitates future studies on SeCMs since no probes or other methods of detection have previously been developed for COSe. Overall, PhotoSeCMs have shown promise as H_2Se donors and have informed us of important mechanistic differences between TCMs and SeCMs. We will use this understanding to develop a new class of H_2Se donors based on the SeCM motif and bolster the growing toolbox of H_2Se donor technology.

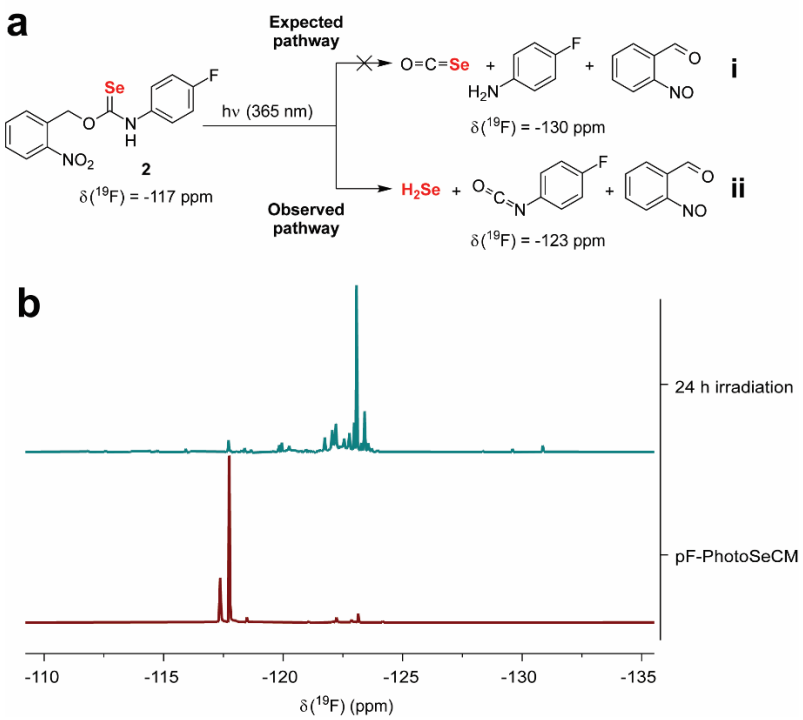

Figure 4.2 Photoactivation of **2** at 365 nm for 24 h with (ai) the expected reaction pathway to generate COSe and 4-fluoroaniline, (aii) the observed pathway showing generation of 4-fluorophenyl isocyanate supported by (b) the ^{19}F NMR spectroscopic data.

4.2.2 Hydrolysis-active Selenocarbamates

Knowledge gained from the PhotoSeCMs informed us that the SeCM systems are more complex and sensitive than TCM systems, so we decided to simplify our system by eliminating the photoactivation trigger. This would theoretically allow us to avoid any irradiation-induced degradation of carbon- and Se-based species involved in the reaction and monitor more well-defined products from a direct H_2Se-releasing platform. Previous work in our lab led us to adapt γ-ketothiocarbamates (GKTCMs), which are COS/H_2S donors that are activated by hydrolysis. Under hydrolytic-conditions, deprotonation at the 3-position of the GKTCM initiates a self-immolative cascade to generate COS/H_2S and an amine-based payload (similar to Figure 4.3a) with reaction rates increasing with increasing basicity.[98] Our goal was to expand the range of amine-based payloads available and instill more biological utility in this set of SeCMs. Initial efforts were directed at preparing simple GKSeCMs with the colorimetric payload of 4-nitroaniline to facilitate hydrolysis monitoring. We began by attempting to synthesize the parent

GKSeCM (**5**) by treating 4-nitrophenyl isoselenocyanate (PNA-NCSe) dissolved in THF with an excess of 4-hydroxybutanone (10.0 equiv.) and stirring this mixture for several days, analogous to the published synthesis of thiocarbamates (Scheme 4.2a).[98] Despite our efforts and modifications, **5** was only ever prepared in an NMR tube and was unable to be isolated from the reaction mixture, likely due to the decreased stability when compared to the TCM analog. We then focused on preparing the less reactive methylated GKSeCM (**6**) and unreactive dimethylated GKSeCM (**7**), which were made by treating a solution of 3-methyl-4-hydroxy-2-butanone (or 3,3-dimethylated analog) and PNA-NCSe in THF with a sub-stoichiometric amount of DBU (Scheme 4.2b). These GKSeCMs were isolated in meager yield after chromatographic purification that fortunately did not induce isomerization as was observed with the PhotoSeCMs.

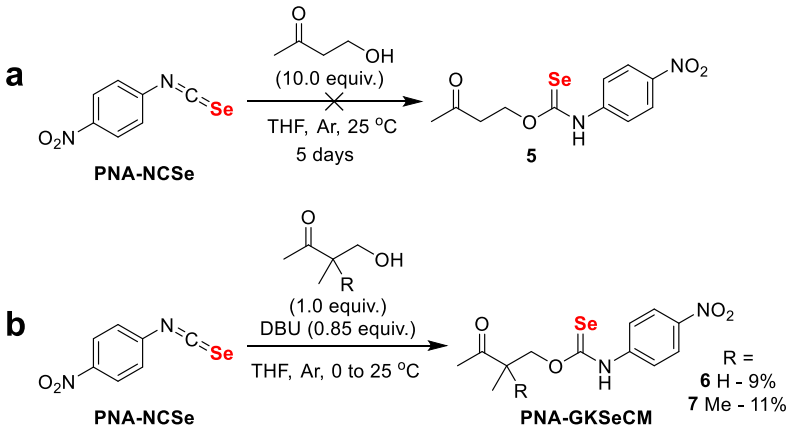

Scheme 4.2 Synthesis of hydrolysis-active GKSeCMs from 4-nitrophenyl isoselenocyanate (PNA-NCSe) with colorimetric payloads. (a) Unsuccessful synthesis of **5** led to (b) our pursuit of the methylated analogs, which were successfully synthesized.

With these compounds in hand, we proceeded to evaluate their hydrolytic behavior and gather kinetic data based on production of the colorimetric payload. These hydrolysis experiments (Figure 4.3) were conducted in PBS buffer at different pH values. We observed conversion of **6** (λ_{max} = 335 nm) to PNA (λ_{max} = 381 nm), while the dimethyl version **7** exhibited no reactivity, as expected. Because 4-nitrophenyl isocyanate is poorly soluble in water, we proposed that the generated isocyanate would rapidly undergo further hydrolysis to the 4-nitroaniline with carbon dioxide (CO_2) as a byproduct. As expected, the production of PNA occurred more rapidly under basic

conditions, and relative rate constants were obtained from these experiments, showing a steep drop off of reaction rate in the most acidic sample. The well-defined hydrolysis profile of **6** at physiological pH is bodes well for future biological studies on hydrolysis-active GKSeCMs.

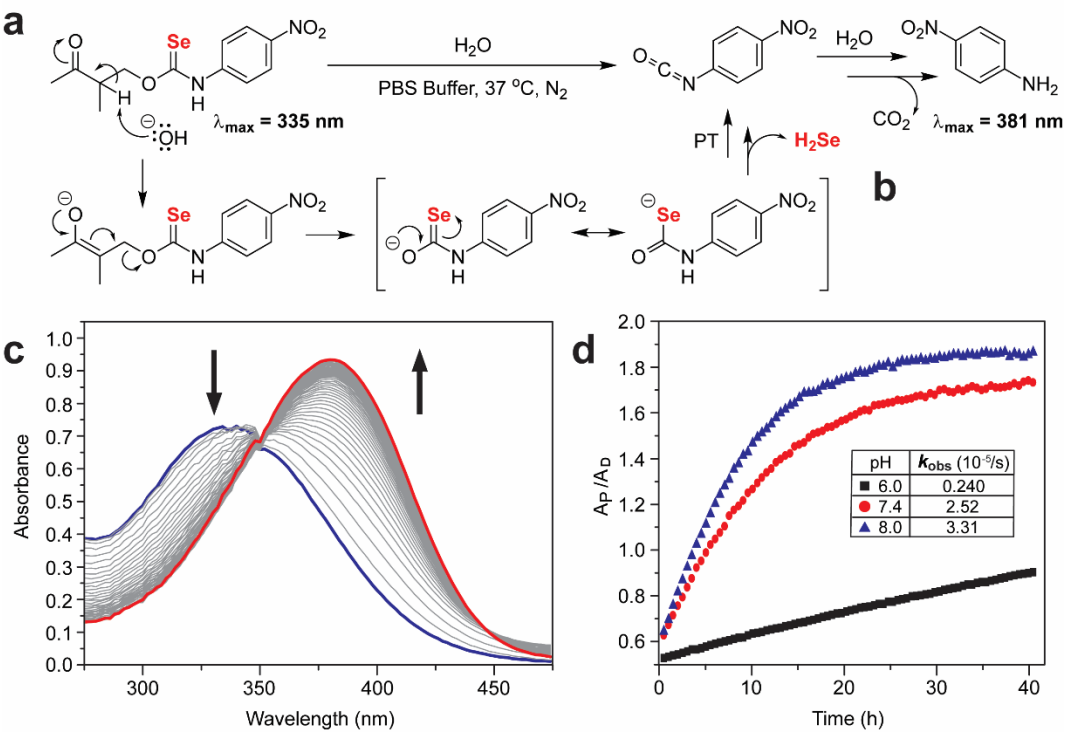

Figure 4.3 Hydrolysis experiment results showing (a) the proposed reaction mechanism producing PNA, (b) cuvettes before (left) and after (right) hydrolysis monitoring, (c) the absorbance spectrum of a sample of **6** in PBS (pH 7.4, 10 mM) at 37 °C and under N_2, and (d) plotted pH dependent formation of PNA with tabulated observed rate constants (A_P = PNA absorbance (381 nm); A_D = **6** absorbance (335 nm)).

Having established the hydrolysis profile of **6**, we then sought to investigate the mechanism of hydrolysis via ^{77}Se NMR spectroscopy using benzyl bromide (BnBr) as an alkylating agent. BnBr aids in monitoring the Se-atoms in the starting material, intermediates, and products. After initial baseline analysis, an air-free sample of **6** in DMSO-d_6 (50 mM) received BnBr (2.5 equiv.) and basic water (pH 10.0, 25 µL) before being reanalyzed periodically over 24 h. The resulting ^{77}Se NMR spectra supported our mechanistic hypothesis (Scheme 4.3). After injecting BnBr and water into the NMR tube, the initial scans showed the emergence of a triplet at $\delta(^{77}Se)$ = 415 ppm, which was

assigned to intermediate **6i**, the shift range and splitting being characteristic of alkylated selenide species.[40] Subsequent scans show the full consumption of **6**, an increase in the intensity of **6i**, and the emergence of a small pentet peak at $\delta(^{77}Se)$ = 330 ppm that signifies production of dibenzyl selenide (Bn_2Se). Further analysis of the sample revealed the degradation of Bn_2Se, full consumption of **6i**, and the emergence of a small triplet peak at $\delta(^{77}Se)$ = 394 ppm, which signifies the production of dibenzyl diselenide (Bn_2Se_2), another expected product of this reaction. The fleeting intermediate **6ii** is not observable via NMR spectroscopy but must exist along this reaction pathway.

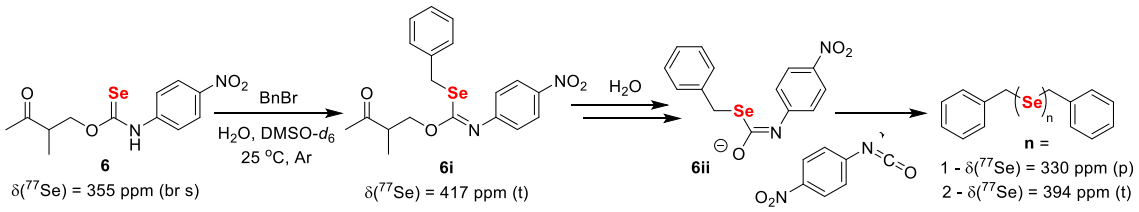

Scheme 4.3 ^{77}Se NMR study on the mechanism of hydrolysis of **6** under basic conditions with BnBr used as an alkylating agent to trap and visualize released selenide species. (NMR data is crude yet informative and needs to be repeated to achieve publication quality spectra and will then be included in this figure, which is a scheme for now.)

To further support our hypothesized reaction mechanism, a fluorinated analog of **6** was prepared to confirm the production of isocyanate, which will be apparent in the resulting ^{19}F NMR spectra. Initial attempts at synthesizing this analog used 4-fluorophenyl isoselenocyanate as the starting material, but the desired product could not be isolated from the reaction mixture, so 4-(trifluoromethyl)phenyl isoselenocyanate (PTFM-NCSe) was used instead. The trifluoromethyl moiety possesses a σ-value more similar to the nitro moiety, so the resulting GKSeCM should more closely mimic the behavior of **6** under hydrolysis conditions.[99] (This work is currently in progress; further discussion will follow completion of these experiments.)

4.2.3 Diversification of Amine-based Payload

After investigation of the hydrolysis behavior and mechanism of action of the GKSeCM compounds with simple payloads, we sought to diversify the available payloads to include biologically-applicable fluorescent reporters. Our first pursuit was a

GKSeCM bearing 7-amino-4-methylcoumarin (AMC-GKSeCM) as the payload, which was synthesized analogously to the previously discussed GKSeCMs. Unfortunately, evaluation of the hydrolysis showed no conversion of the starting material even at pH 8.0. We then moved on to a GKSeCM bearing 4-amino-1,8-naphthalimide (AmNap-GKSeCM) as the payload, a fluorophore that has been used previously in biological studies. (The synthesis of this GKSeCM is still underway; further discussion will follow experiment completion.)

4.3 Conclusions

The growing field of research on H_2Se and its roles in biology has led to the development of a number of small molecule H_2Se donors akin to previously produced H_2S donor technology. Current examples in the literature highlight the potential for these compounds in deepening our understanding of H_2Se in biology, but thus far the technology has been quite simple, and the published donors are either activated by water or thiols. With the goal of expanding the palette of H_2Se donor capability, we have pursued SeCMs, initially postulated to be indirect sources of H_2Se via hydrolysis of COSe in the presence of CA, a well-established reactivity for TCMs as COS/H_2S donors. Investigations on the photoactivatable SeCMs revealed that the reactivity of SeCMs deviates significantly from that of TCMs, and SeCMs are now understood to be direct sources of H_2Se that do not produce COSe. This fundamental difference between the TCM and SeCM motifs led us to simplify our system by eliminating the need for photoactivation, which can degrade species that may be vital to understanding the reactivity mechanisms of SeCMs. Hydrolysis-activated GKSeCMs were then studied as H_2Se donors with colorimetric payloads for facile reaction monitoring via UV-vis spectrometry. The resulting data followed the trends previously observed with the GKTCMs, where the reaction rate is increased in more basic environments. Subsequent ^{77}Se NMR studies on hydrolysis of GKSeCMs in the presence of an alkylating agent supported our mechanistic hypothesis on the direct release of H_2Se from SeCMs. Diversification of the amine-based payload to include fluorescent reporters was successful synthetically, but the prepared GKSeCMs did not exhibit analogous hydrolytic activity, so further investigations are required to determine the feasibility of appending

amine-based fluorophores to the SeCM motif. Though many questions have been raised by this work, overall it marks a significant expansion upon H_2Se donor technology as well as sets the stage for future work on SeCM scaffolds. We now have the capacity to include diverse triggering groups and amine-based payloads in H_2Se donors to facilitate studying this elusive chalcogenide species in biology.

CHAPTER V

CONCLUSIONS

The field of research on the roles and fates of Se-containing species in biology has taken an exciting leap in the last several years. While a slew of organoselenium compounds have been studied in this light, many were designed as mimics of selenoproteins, and it was not until 2019 that we began to accumulate tools for studying the central metabolite in the biological Se cycle, H_2Se. Initially, a phthalic selenoanhydride was developed and described as a radical scavenger and source of H_2Se, but this donor was poorly characterized with scant evidence of H_2Se production. The Pluth Lab staked the claim to the first well-characterized H_2Se donor with the publication of the hydrolysis-active TDN1042, the direct Se-analog of the most widely-studied H_2S donor GYY4137. The unfaltering use of GYY4137 in biological studies despite the wide array of tools available for studying H_2S in biology suggests that TDN1042 will be a staple compound in the field for years to come. Its familiar structure provides a comfortable platform for biological researchers to take steps into studying H_2Se. Previously they would have needed to prepare solutions of H_2Se from either selenide salts or the reduction of elemental selenium, both of which present significant drawbacks and complications that could deter investigators from pursuing this research. To improve the utility of TDN1042, we are currently working on preparing the sodium salt analog, which will remove one of the potentially bioactive morpholine units from the structure of this compound and facilitate the assessment of the biological effects of H_2Se even further.

With the establishment of TDN1042, we then wanted to expand the toolbox of available H_2Se donors, and the progression of donors followed closely to that of hydrolysis-active H_2S donors also based on a central phosphorus atom. This work culminated in the development of the cyclic-PSe compounds, which exhibit hydrolysis rates that are far greater than that of TDN1042. The advancements in chemistry witnessed in the cyclic-PSe work were significant, but the crowning achievement with these compounds was their application to HeLa cells for the assessment of their cell permeability, cytotoxicity, and antioxidant activity. The use of TOF-SIMS to determine

cell permeability and map the areas of Se content in cells was an unusual technique that was inspired by previous XAS/XFM studies on cellular Se localization, and we expect to see these techniques refined in coming years to facilitate subcellular localization studies. Antioxidant activity of H_2Se produced from these donors was expected, as it is a strong reductant, but we were pleased to see that major antioxidant effects occur at concentrations (5 μM) lower than those that begin to exhibit cytotoxicity (10 μM). While some biological effects of H_2Se have been previously established through selenide solution administration, this work has set the stage for future studies on the biological effects of H_2Se produced from small molecule donors.

As of 2022, the first H_2Se donors from outside of our lab were published as cysteine-active selenoamides. This work marks both a significant expansion of H_2Se donor technology and a vote of confidence from other researchers in the field for the work that we have done to facilitate the investigation of H_2Se in biology. Turning our eyes to further expansion of H_2Se donor technology, we have recently been developing SeCMs as H_2Se donors. Attractive elements of this technology are the capability for installing diverse triggering groups and useful amine-based payloads to facilitate chemical and biological investigations The initial idea of using these compounds as COSe donors and indirect sources of H_2Se in analogy to TCMs as COS/H_2S donors was sound, but we discovered a deviation in reactivity from TCMs to SeCMs. Rather than releasing COSe and an amine payload, the SeCMs release H_2Se directly with an isocyanate payload. Our initial efforts on the SeCM front saw us preparing photoactivatable SeCMs based on the photoactivation of the 2-nitrobenzyl motif, and installation of a fluorine-containing payload led us to conclude that the isocyanate is produced rather than the amine. We have additionally prepared hydrolysis-active SeCMs based on the deprotonation at the 3 position of the γ-ketoselenocarbamate, leading to self-immolation and expulsion of a colorimetric payload along with H_2Se. Work still remains to be done on this front, but we ultimately hope to develop a comprehensive toolbox of SeCMs with diverse triggering mechanisms and payloads. The future of SeCMs is bright and will bring deeper understanding to the roles and effects of H_2Se in biology. The work discussed in this dissertation marks my contributions to the field of H_2Se research, and I

am both honored to have had the opportunity to make such contributions and excited to see where future investigations take us.

APPENDIX A

SUPPLEMENTARY INFORMATION FOR CHAPTER II

Appendix A is the supplementary information for Chapter 2 of this dissertation. It includes experimental procedures, spectra, and data relevant to the content of Chapter 2.

Materials and Methods

Reagents were purchased from Sigma-Aldrich, Alfa Aesar, and TCI Chemicals and were and used directly as received. Deuterated solvents were purchased from Cambridge Isotope Laboratories and used directly as received. ^{1}H, $^{13}C\{^{1}H\}$, ^{31}P, and ^{77}Se NMR spectra were recorded on Bruker 500 and 600 MHz instruments. Chemical shifts are reported relative to residual protic solvent resonances for ^{1}H and $^{13}C\{^{1}H\}$ spectra. All air-free manipulations were performed in an inert atmosphere using standard Schlenk techniques or an Innovative Atmospheres N_2-filled glove box.

Synthesis of TDN1042

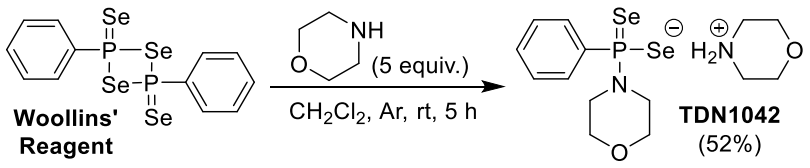

Scheme A1. Synthesis of TDN1042 from Woollins' Reagent

Morpholinium morpholinophenylphosphinodiselenoate (TDN1042). Woollins' reagent (0.54 g, 1.0 mmol) was added to anhydrous CH_2Cl_2 (10 mL) in a flame-dried round bottom flask under argon. Morpholine (0.44 mL, 5.1 mmol) was added using an air-tight syringe, and the resultant reaction mixture was allowed to stir for 5 h at room temperature. The reaction mixture was then filtered, leaving behind a black precipitate. The resultant golden-yellow filtrate was concentrated under reduced pressure to approximately 10% of the initial volume and cooled to 0 °C to promote crystallization. The resulting precipitate was isolated via filtration, washed with CH_2Cl_2 (3.0 mL), and dried overnight under

reduced pressure to afford a white, microcrystalline solid (0.46 g, 52% yield). The identity of the product was verified by ^{1}H, ^{13}C{^{1}H}, ^{31}P, and ^{77}Se-NMR. Crystals suitable for structural determination were obtained by slow layering of hexane into a dilute solution of the product and CH_2Cl_2. ^{1}H NMR (600 MHz, DMSO-d^{6}) δ: 8.67 (s, 2H), 8.08 (dt, 1H, $^{3}J_{P\text{-}H}$ = 2 Hz), 8.07(dt, 1H, $^{3}J_{P\text{-}H}$ = 1 Hz), 7.30 (m, 3H), 3.76 (m, 4H), 3.50 (t, 4H), 3.11 (m, 4H), 2.75 (m, 4H). ^{13}C{^{1}H} NMR (151 MHz, DMSO-d^{6}) δ: 142.97, 141.95, 130.78, 128.68, 126.57, 66.21, 63.34, 45.45, 42.93. ^{31}P NMR (241 MHz, DMSO-d^{6}) δ: 62.10 (s, $^{1}J_{P\text{-}Se}$ = 671 Hz). ^{77}Se NMR (115 MHz, DMSO-d^{6}) δ: 8.22 (d, ^{1}J = 671 Hz). TOF MS (ES^{-}) (*m*/*z*): [M + H]$^{+}$ calc'd for $C_{10}H_{13}NOPSe_2$ 353.9065; found 353.9064.

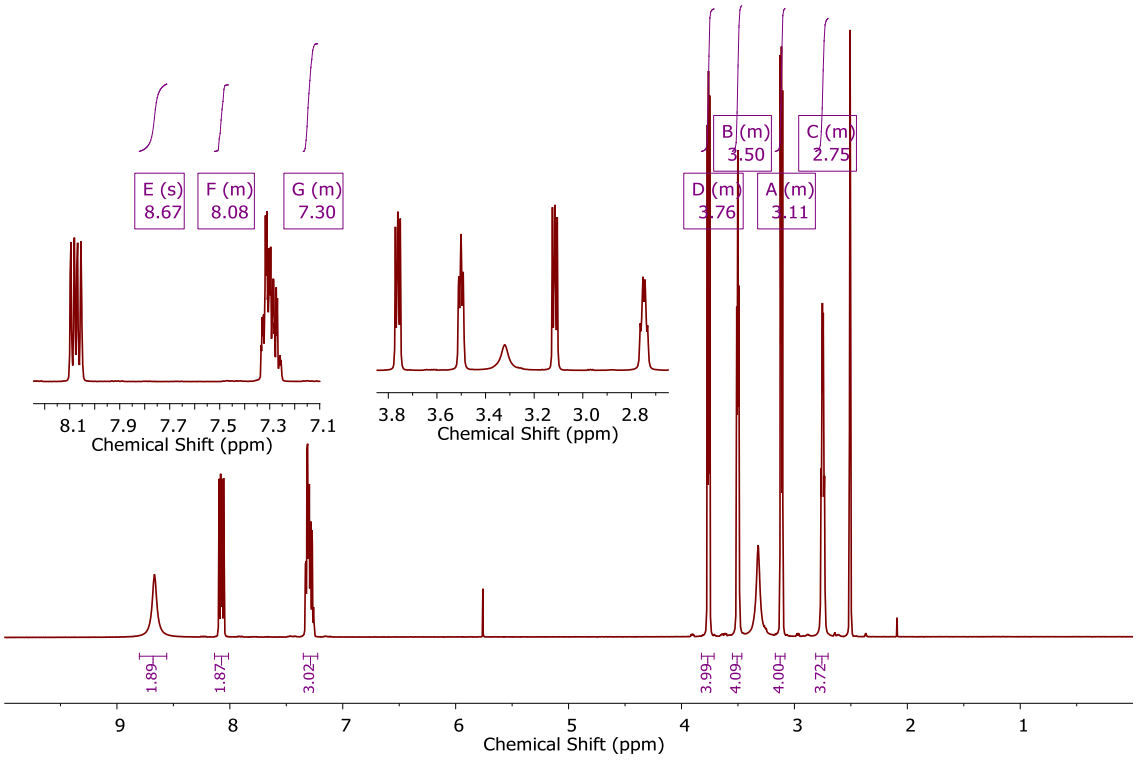

Figure A1. ^{1}H NMR (600 MHz, DMSO-d^{6}) spectrum of TDN1042.

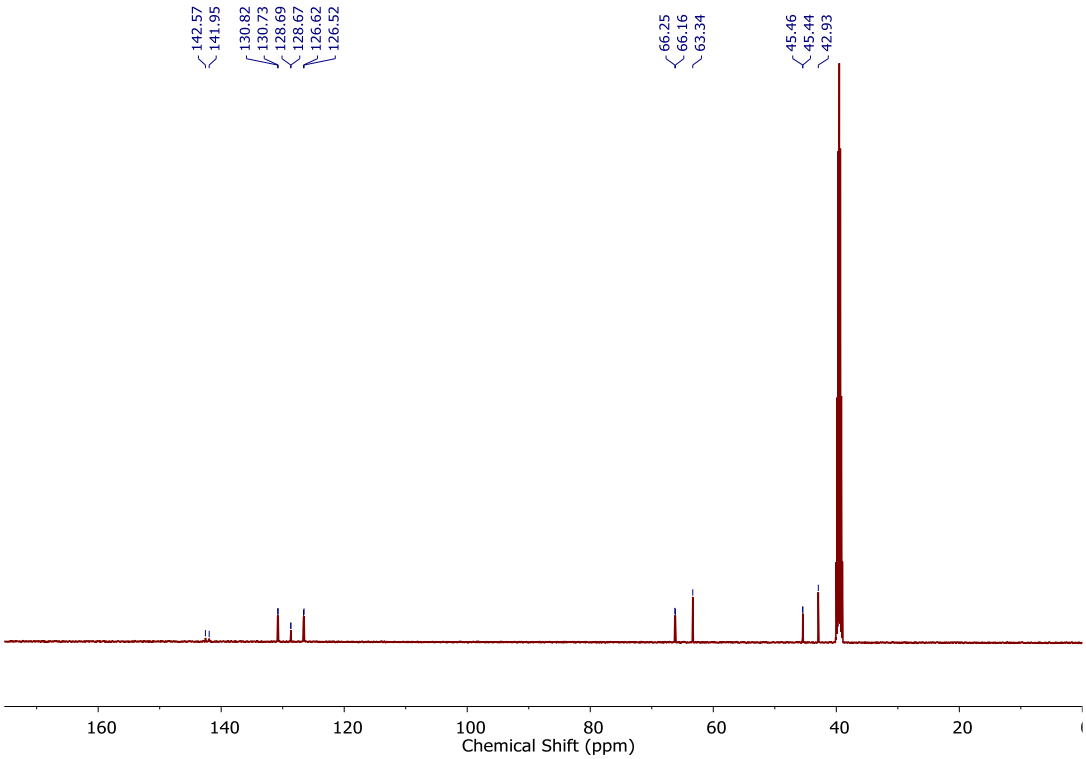

Figure A2. $^{13}C\{^{1}H\}$ NMR (151 MHz, DMSO-d^6) spectrum of TDN1042.

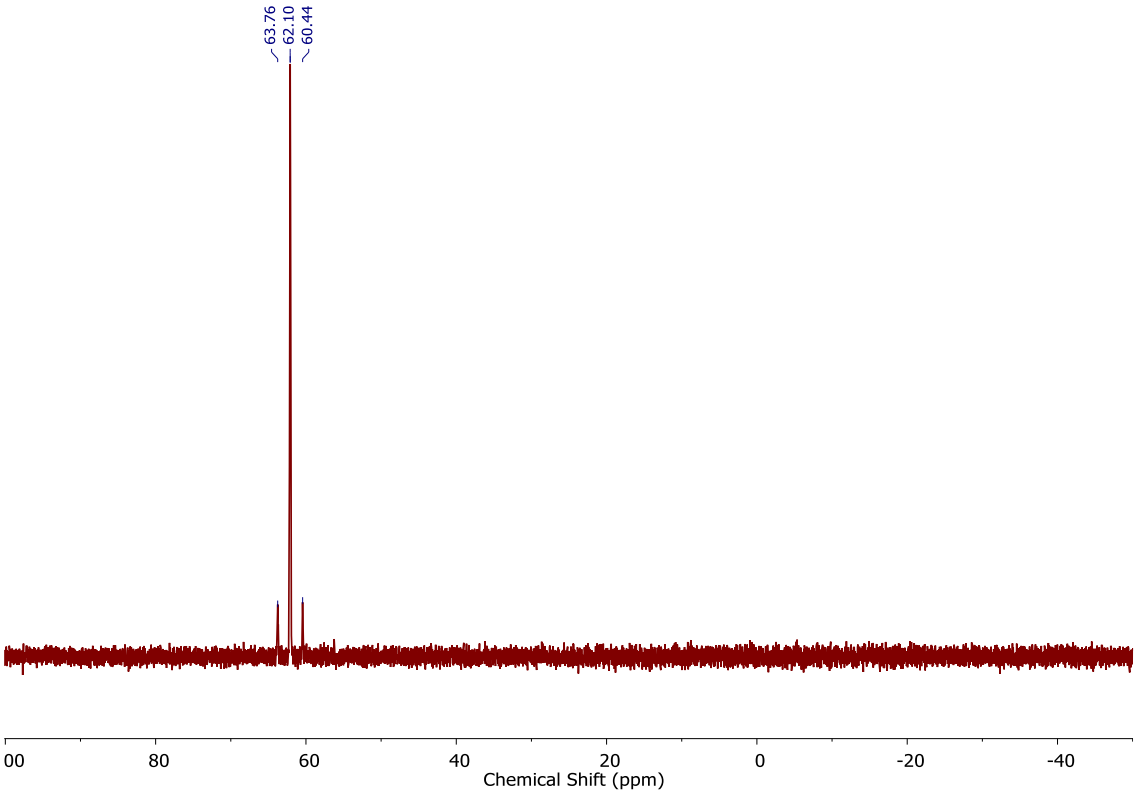

Figure A3. ^{31}P NMR (241 MHz, DMSO-d^6) spectrum of TDN1042.

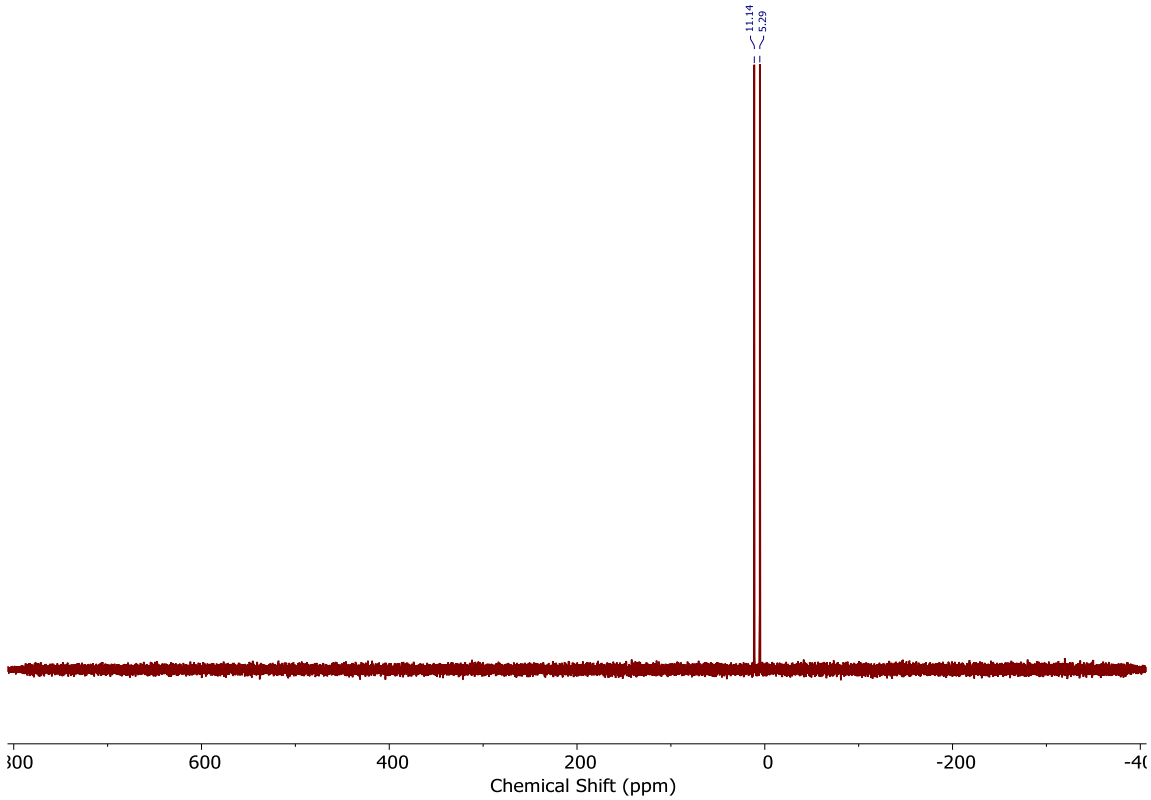

Figure A4. ^{77}Se NMR (115 MHz, DMSO-d^6) spectrum of TDN1042.

Hydrolysis Studies

Stock solutions of TDN1042 (70 mM) and triethylphosphate (35 mM) were prepared in DMSO-d^6 in GC vials in a glovebox. Aliquots of 0.10 mL of each stock solution were added to 0.50 mL citrate or HEPES buffers (pH 3.0-7.4, 50 mM) in NMR tubes. These NMR tubes were removed from the glovebox and flame sealed under vacuum.

Recorded spectra:

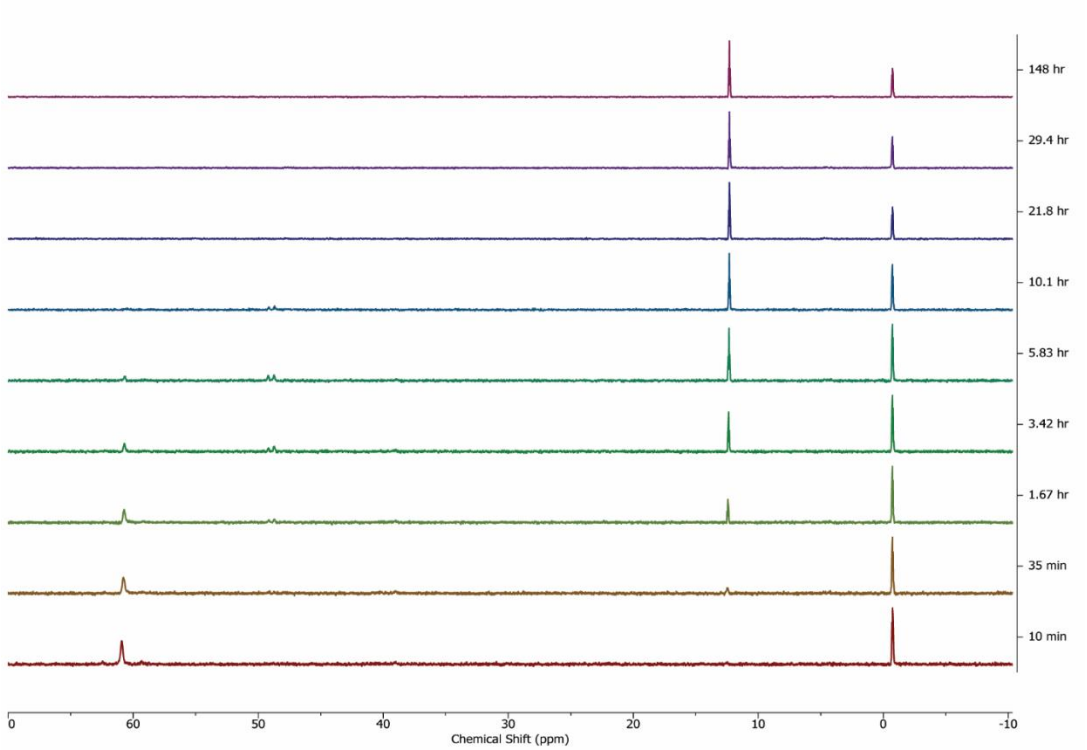

Figure A5. ^{31}P NMR (202 MHz, DMSO-d^{6}) spectra of TDN1042 hydrolysis at pH 3.0.

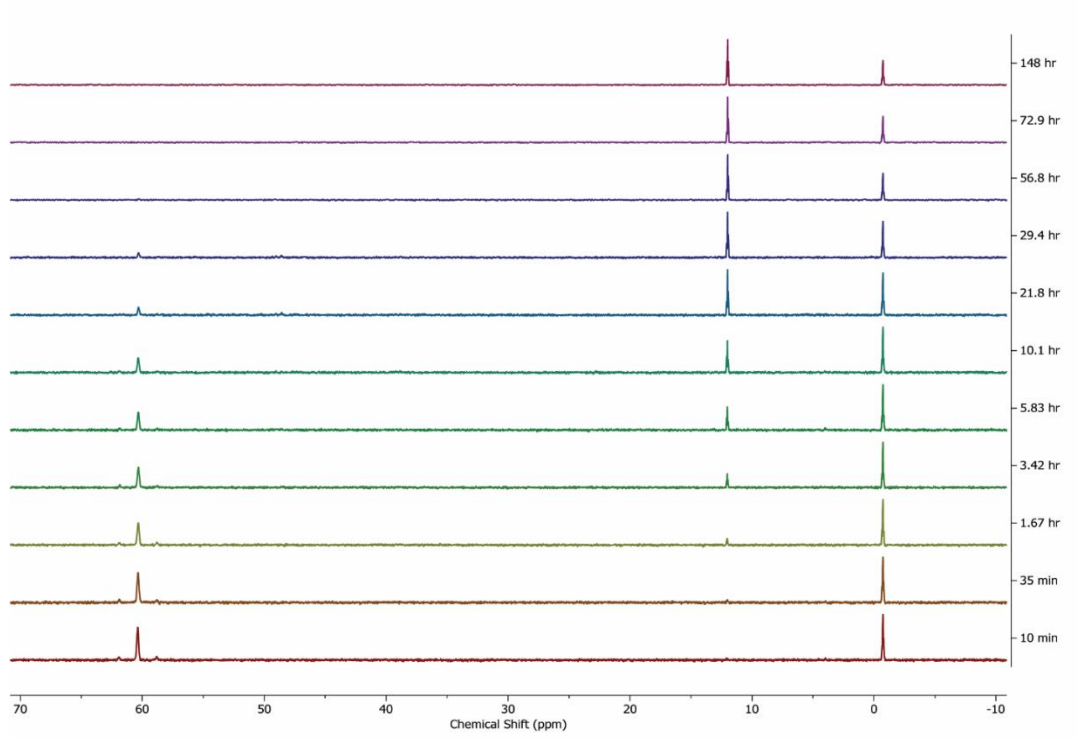

Figure A6. ^{31}P NMR (202 MHz, DMSO-d^{6}) spectra of TDN1042 hydrolysis at pH 3.6.

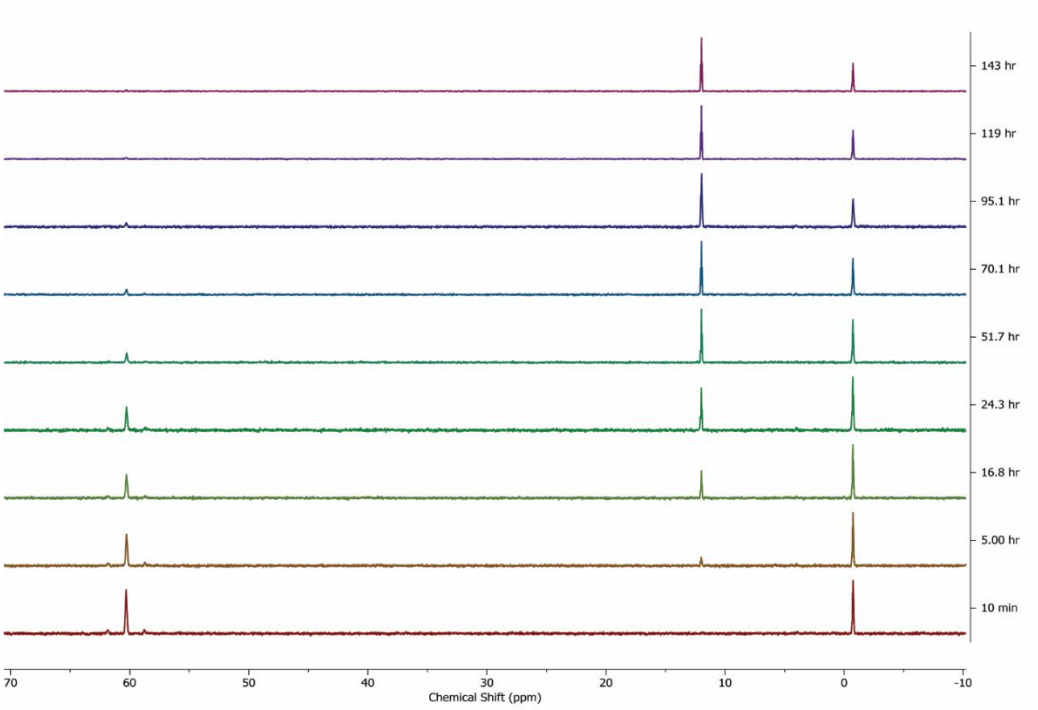

Figure A7. ^{31}P NMR (202 MHz, DMSO-d^{6}) spectra of TDN1042 hydrolysis at pH 4.0.

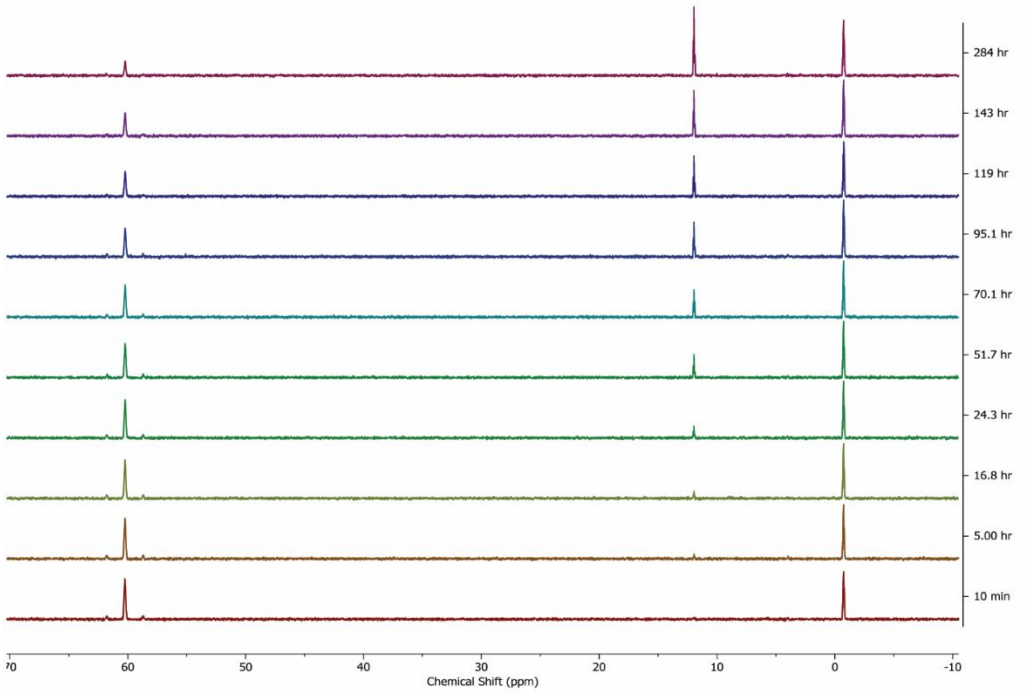

Figure A8. ^{31}P NMR (202 MHz, DMSO-d^{6}) spectra of TDN1042 hydrolysis at pH 5.0.

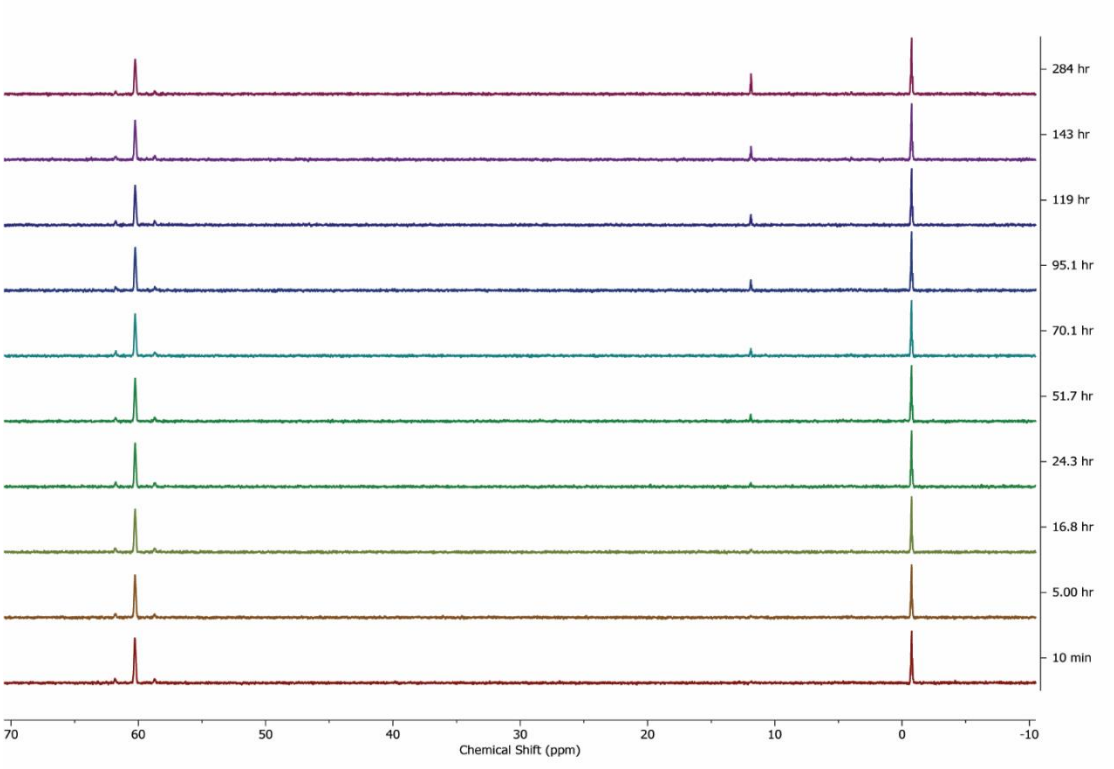

Figure A9. ^{31}P NMR (202 MHz, DMSO-d^6) spectra of TDN1042 hydrolysis at pH 6.0.

H_2Se Trapping Experiments

Trapping Experiments with BnBr.

In a glovebox, TDN1042 (20 mg, 0.045 mmol) was dissolved in DMSO-d^6 (0.50 mL) in an NMR tube, capped with a septum, and sealed with electrical tape. Benzyl bromide (BnBr, 44 μL) was dissolved in DMSO-d^6 (0.20 mL) in a septum-capped vial in a glovebox. Baseline ^{1}H, ^{13}C{^{1}H}, ^{31}P, and ^{77}Se NMR spectra of the TDN1042 solution were acquired prior to addition of the BnBr stock solution (0.10 mL, 0.18 mmol) and degassed Millipore water (25 μL, 1.4 mmol) were injected by syringe. This reaction was monitored by NMR spectroscopy over the course of two weeks. Analysis revealed the formation of an alkylated intermediate (**1**) (δ(^{31}P) = 69 ppm; δ(^{77}Se) = 354 ppm, -129 ppm) and the generation of both the Bn_2Se (δ(^{77}Se) = 330 ppm) and Bn_2Se_2 product (δ(^{77}Se) = 394 ppm), the latter of which is generated through auto-oxidation.

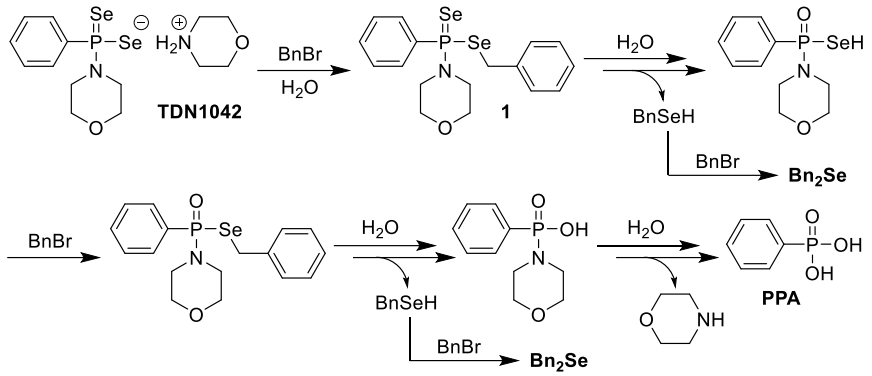

Scheme A3. Proposed pathway for the hydrolysis of TDN1042 in the presence of BnBr, leading to an alkylated intermediate (1) with further hydrolysis affording a trapped selenide product Bn_2Se (auto-oxidation pathway to Bn_2Se_2 is not included here).

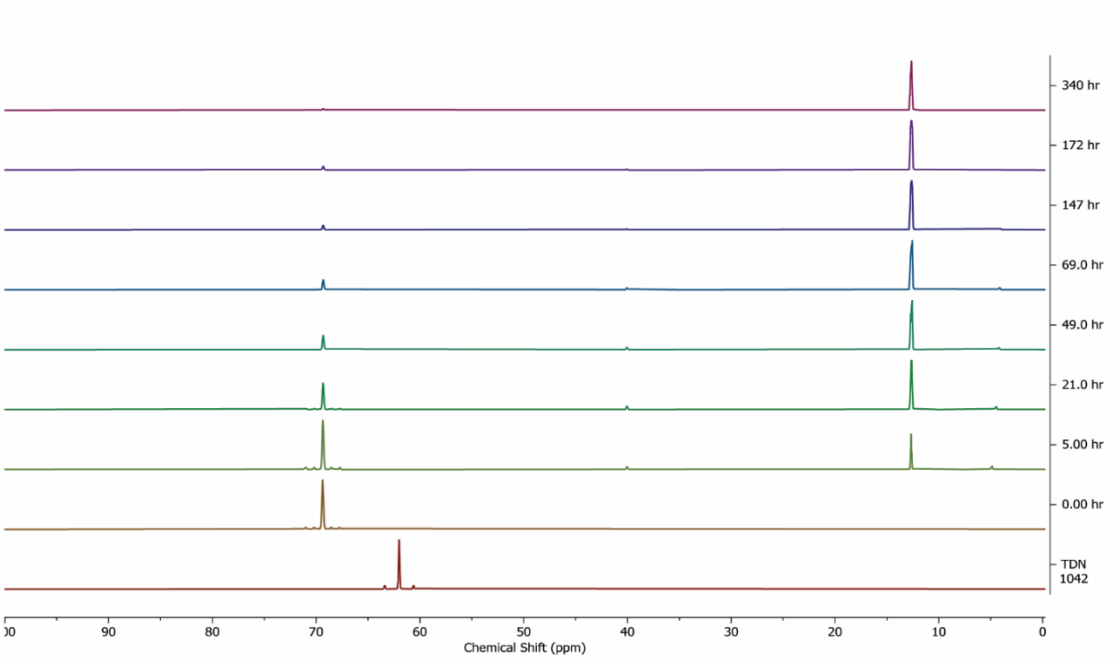

Figure A11. ^{31}P NMR (242 MHz, DMSO-d^6) spectra of TDN1042 hydrolysis in the presence of BnBr.

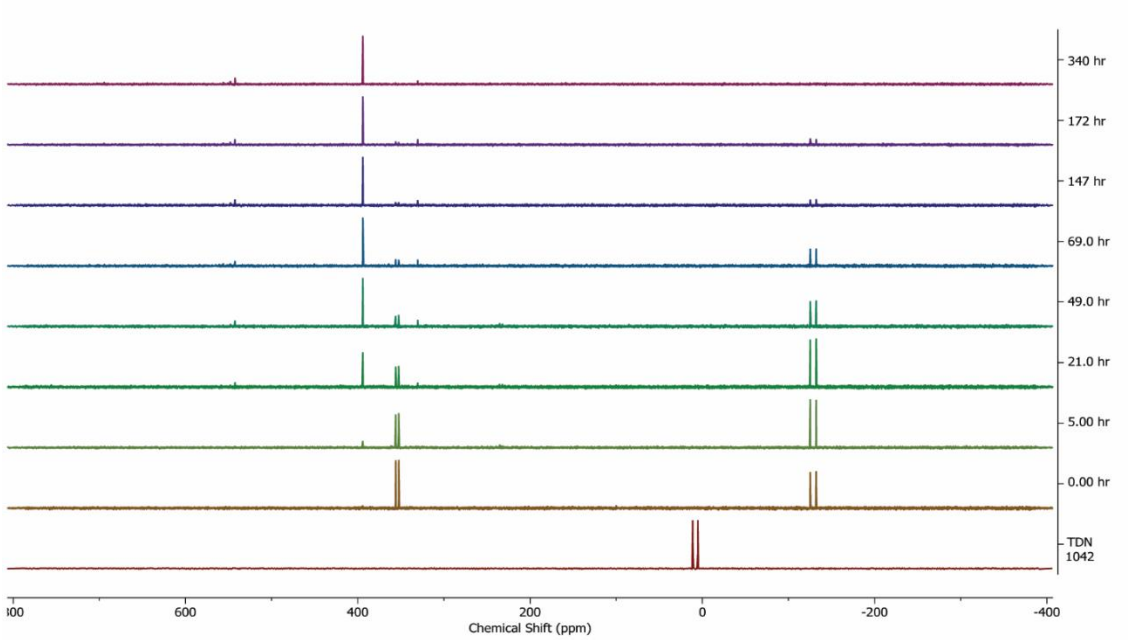

Figure A12. ^{77}Se NMR (115 MHz, DMSO-d^6) spectra of TDN1042 hydrolysis in the presence of BnBr.

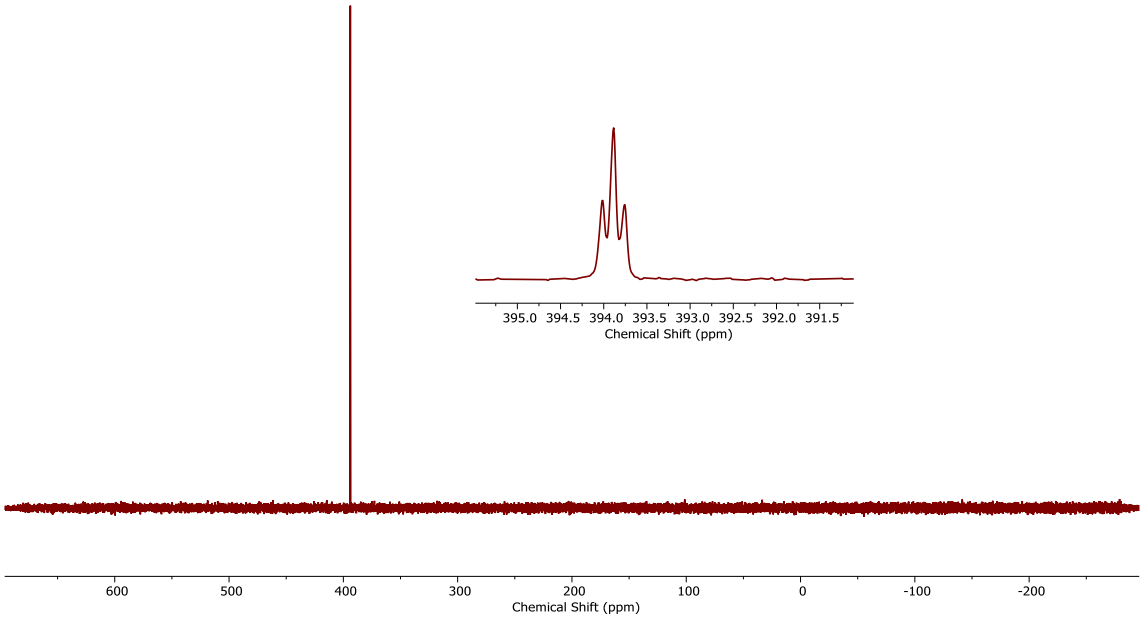

Figure A13. ^{77}Se NMR (115 MHz, DMSO-d^6) spectrum of an authentic sample of Bn_2Se_2.

Trapping Experiments with FDNB.

Volatilization and trapping apparatus can be seen in the main text (Figure 5a). The sample vial (centrifuge tube, 15 mL) contained H_2O (2.0 mL, 0.11 mol), TDN1042 (30 mg, 0.068 mmol), and *n*-octanol (2 drops) was connected with PE tubing to the trapping vial (15 mL glass tube). This trapping vial contained FDNB (15 µL, 0.12 mmol) and $NaHCO_3$ (15 mg, 0.18 mmol) in *N*,*N*-dimethylformamide (DMF, 1.6 mL) and H_2O (0.40 mL), and it was connected to the second trapping vial (15 mL glass tube) that contained a solution of $AgNO_3$ (3.0 mL, 0.10 M in H_2O, 0.30 mmol) meant for sequestering any excess H_2Se. Then, a N_2 line was connected to the Y-adapter, the Y-adapter's other side was sealed, and the Y-adapter was connected to the sample tube. The apparatus was purged with N_2 for 15 minutes, then concentrated HCl (3.0 mL, 36 mmol) was quickly injected through the sealed side of the Y-tube, and the reaction was allowed to proceed for 30 minutes. After this time, the FDNB-containing vial was extracted with benzene (3 x 10 mL), and this extract was dried over $MgSO_4$ and filtered before being concentrated *in vacuo*. The resulting oil was dissolved in DMSO and subjected to HPLC analysis.

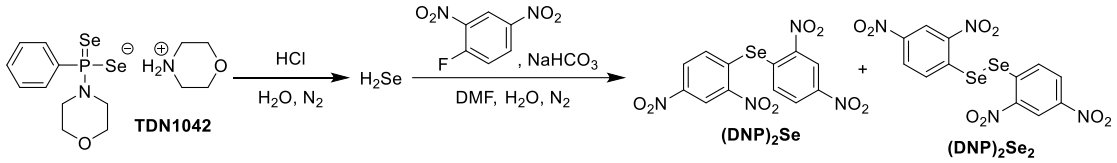

Scheme A4. Pathway for the volatilization of H_2Se from TDN1042 and trapping with FDNB.

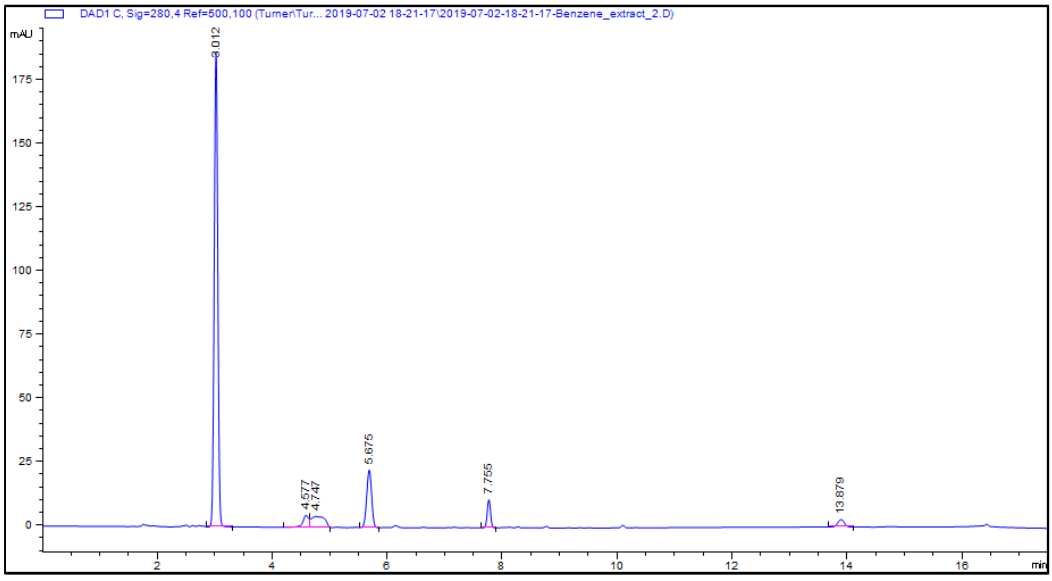

Figure A14. HPLC trace of volatilization-trapping reaction mixture (H_2O(5% MeOH):CH_3CN = 35:65, 280 nm) revealing the presence of FDNB (3.0 min), $(DNP)_2Se$ (5.7 min), and $(DNP)_2Se_2$ (7.8 min).

Authentic samples of $(DNP)_2Se$, $(DNP)_2Se_2$, and FDNB were used to verify retention times for HPLC experiments. $(DNP)_2Se$ and $(DNP)_2Se_2$ were prepared as described in the literature[71] and recrystallized from hot nitrobenzene layered with EtOH to afford yellow needles (152 mg, 20%). This preparation afforded a mixture of the monoselenide and diselenide, which is consistent with the reported reaction products.

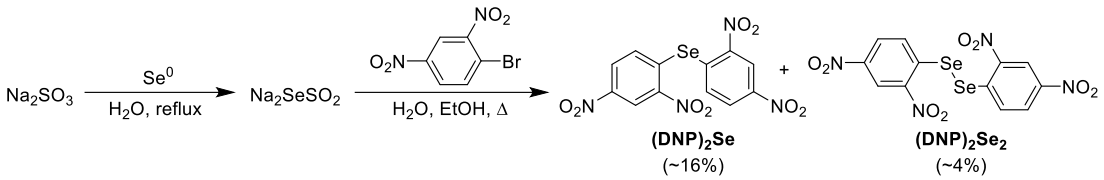

Scheme A5. Synthesis of $(DNP)_2Se$ and $(DNP)_2Se_2$.

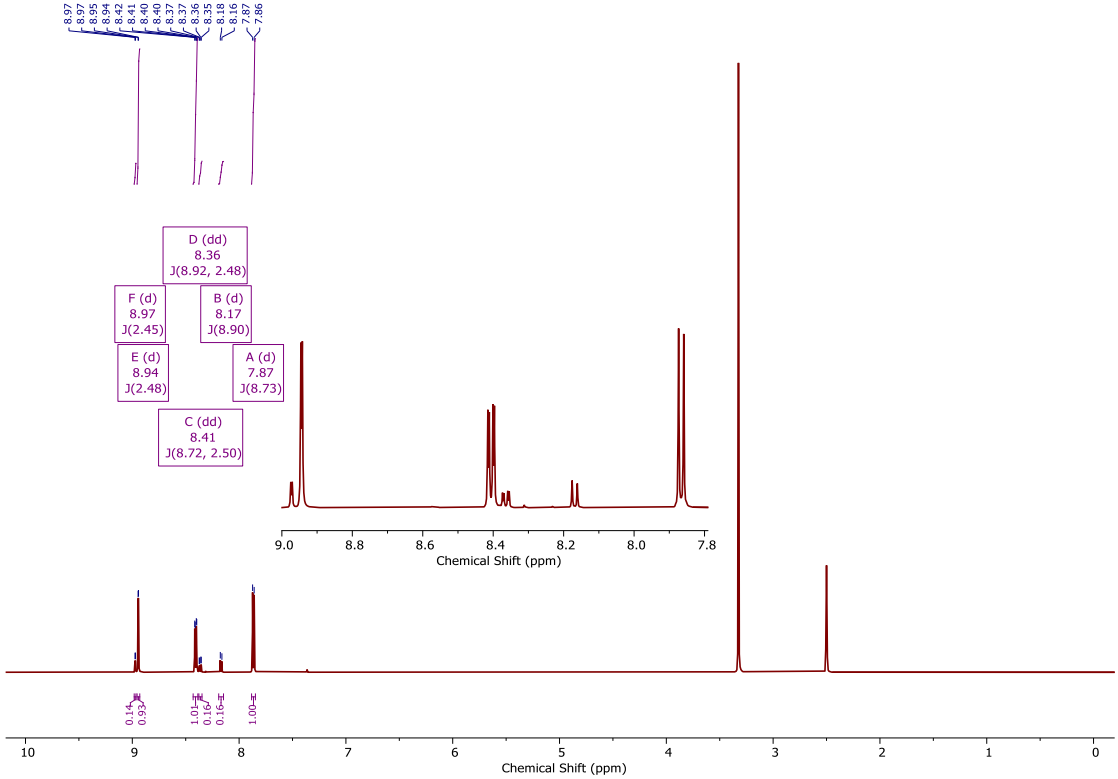

Figure A15. ^1H NMR (600 MHz, DMSO-d^6) spectrum of $(DNP)_2Se$ and $(DNP)_2Se_2$ mixture.

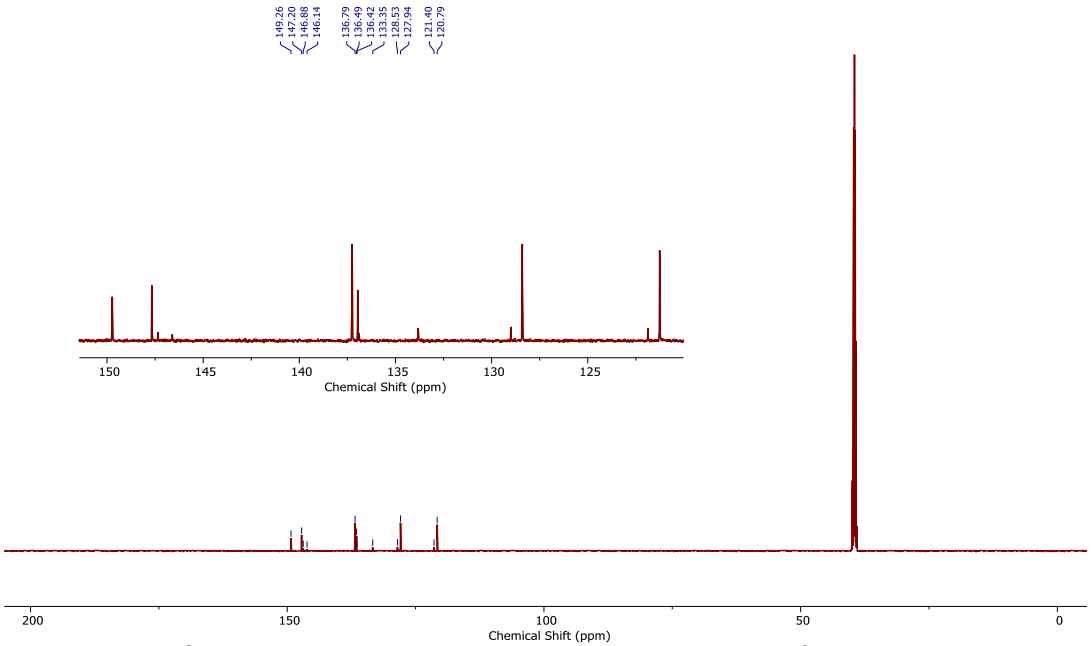

Figure A16. $^{13}C\{^{1}H\}$ NMR (151 MHz {600 MHz}, DMSO-d^6) spectrum of $(DNP)_2Se$ and $(DNP)_2Se_2$ mixture.

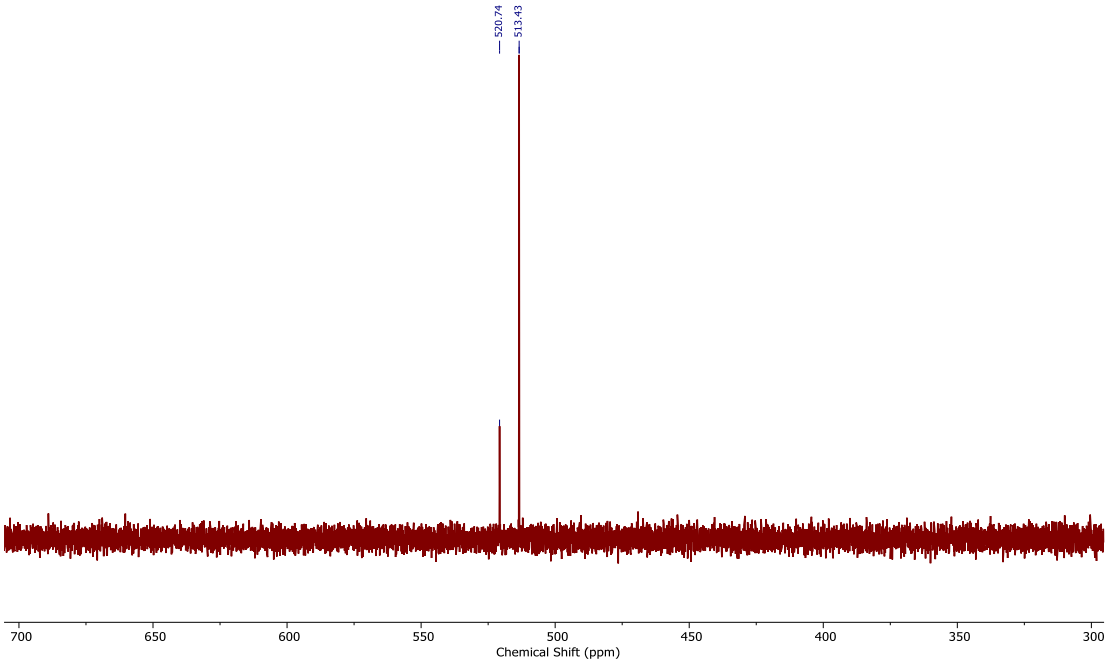

Figure A17. ^{77}Se NMR (115 MHz, DMSO-d^6) spectrum of $(DNP)_2Se$ and $(DNP)_2Se_2$ mixture.

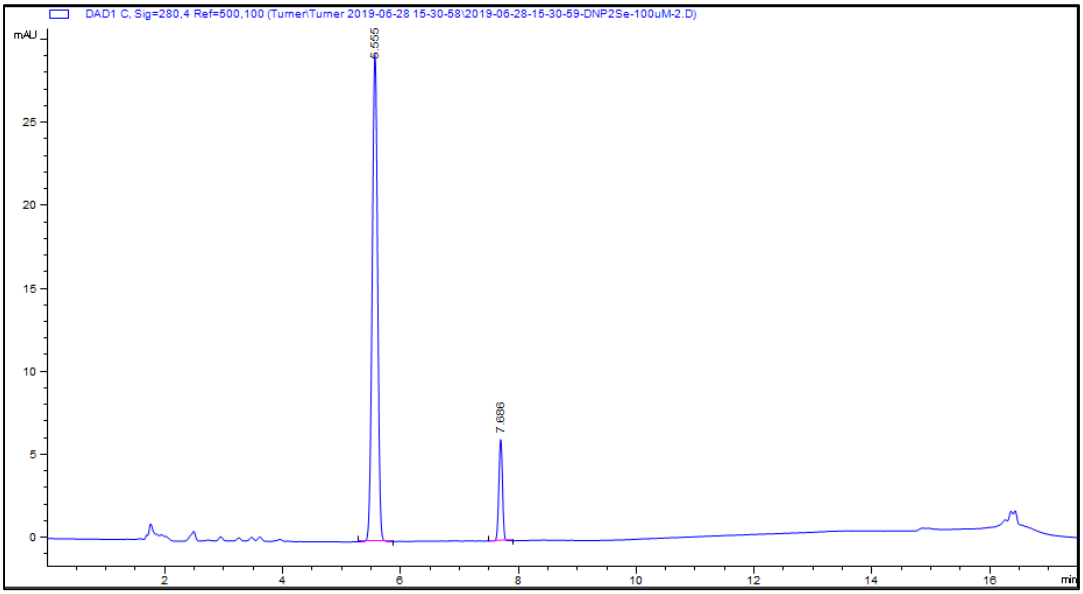

Figure A18. HPLC trace (H_2O(5% MeOH):CH_3CN = 35:65, 280 nm) of $(DNP)_2Se$ (5.6 min) and $(DNP)_2Se_2$ (7.7 min) mixture.

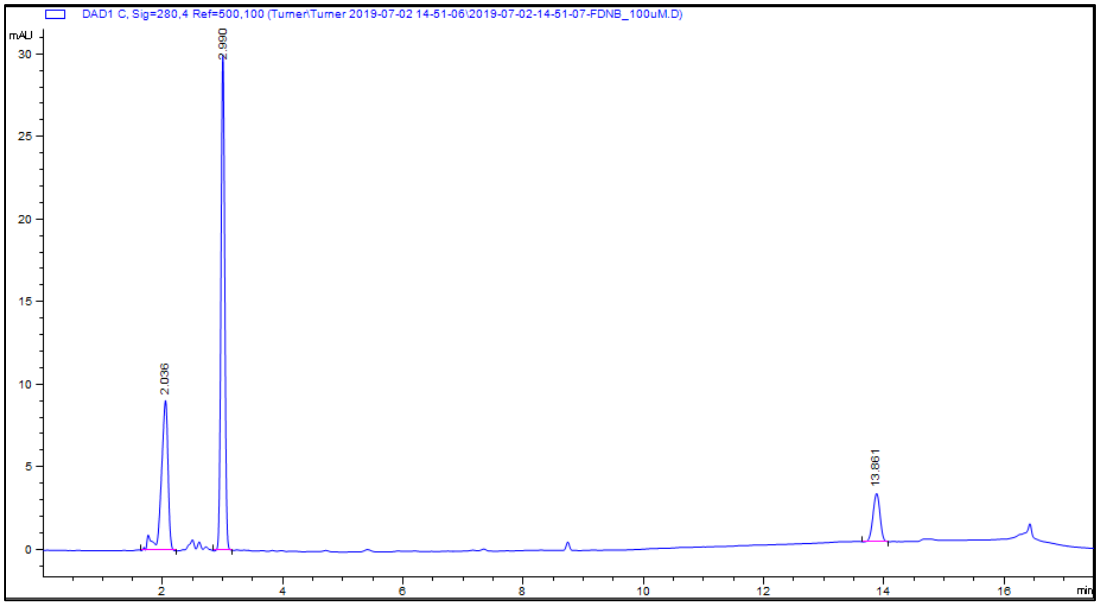

Figure A19. HPLC trace (H_2O(5% MeOH):CH_3CN = 35:65, 280 nm) of FDNB (3.0 min).

APPENDIX B

SUPPLEMENTARY INFORMATION FOR CHAPTER III

Appendix B is the supplementary information for Chapter 3 of this dissertation. It includes spectra and data relevant to the content of Chapter 3.

NMR spectra of phosphine selenide compounds

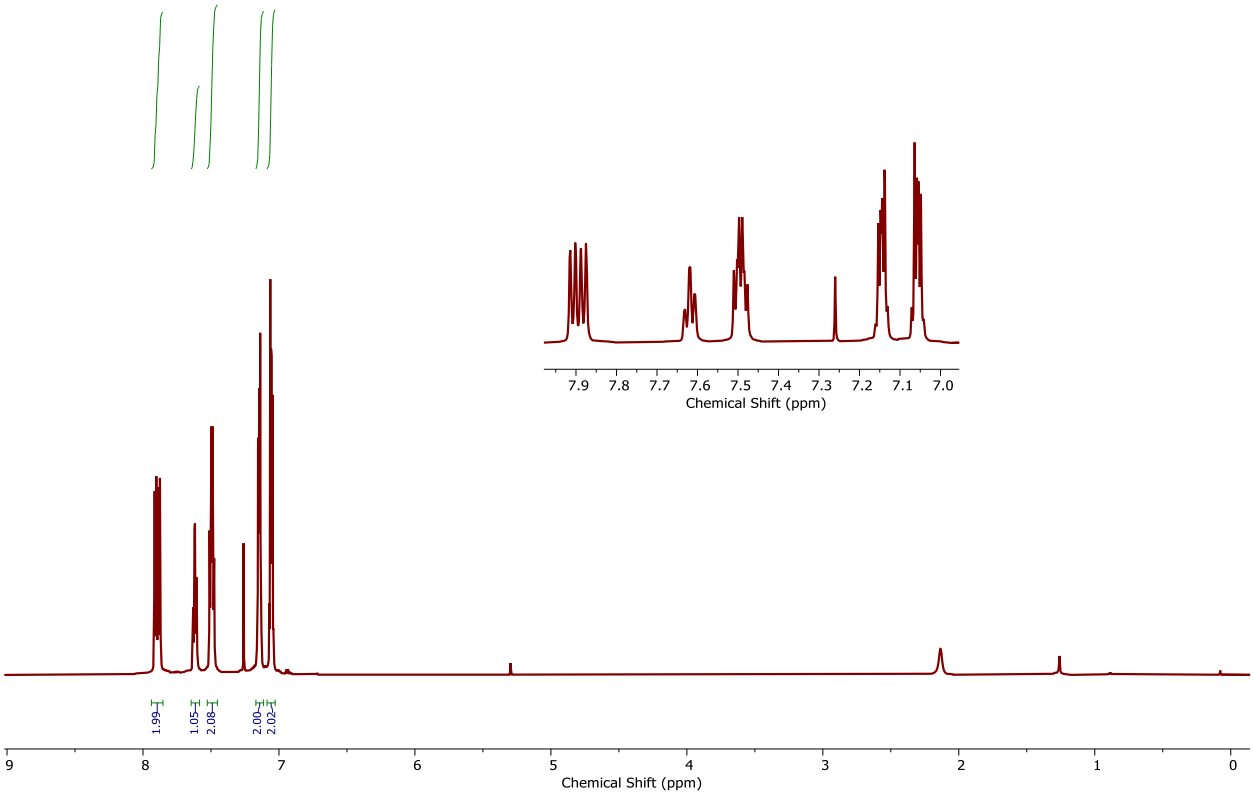

Figure B1. ^{1}H NMR (600 MHz, $CDCl_3$) spectrum of Cat-PSe.

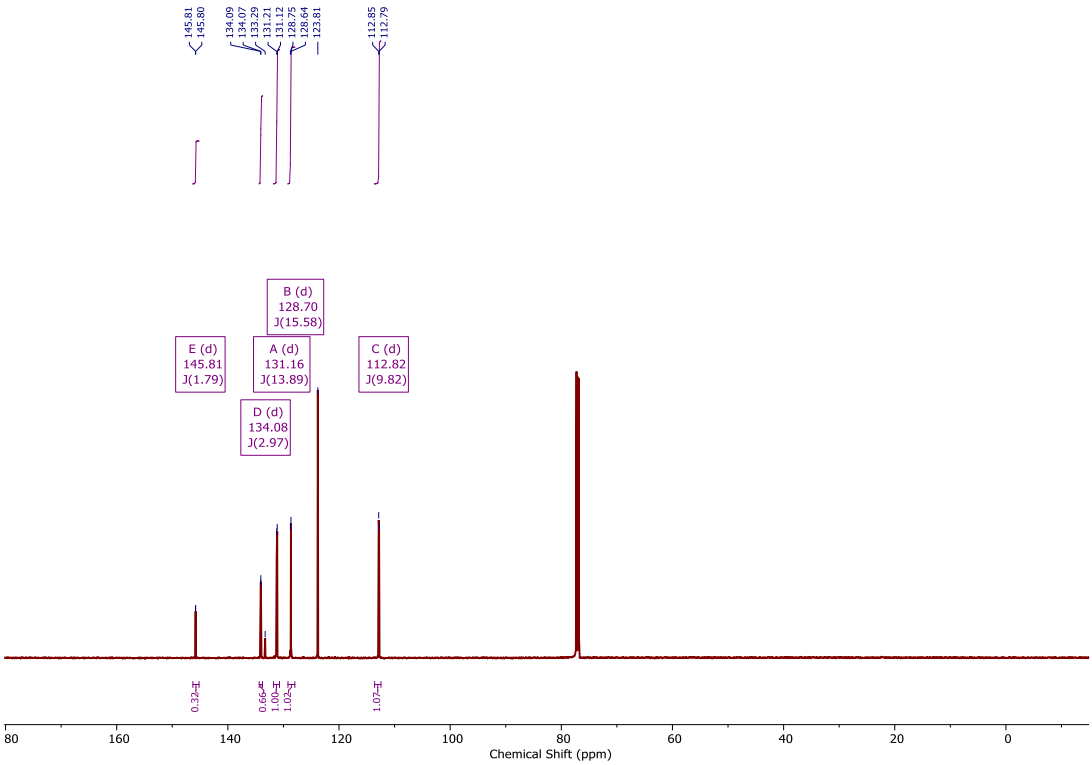

Figure B2. $^{13}C\{^{1}H\}$ NMR (151 MHz, $CDCl_3$) spectrum of Cat-PSe.

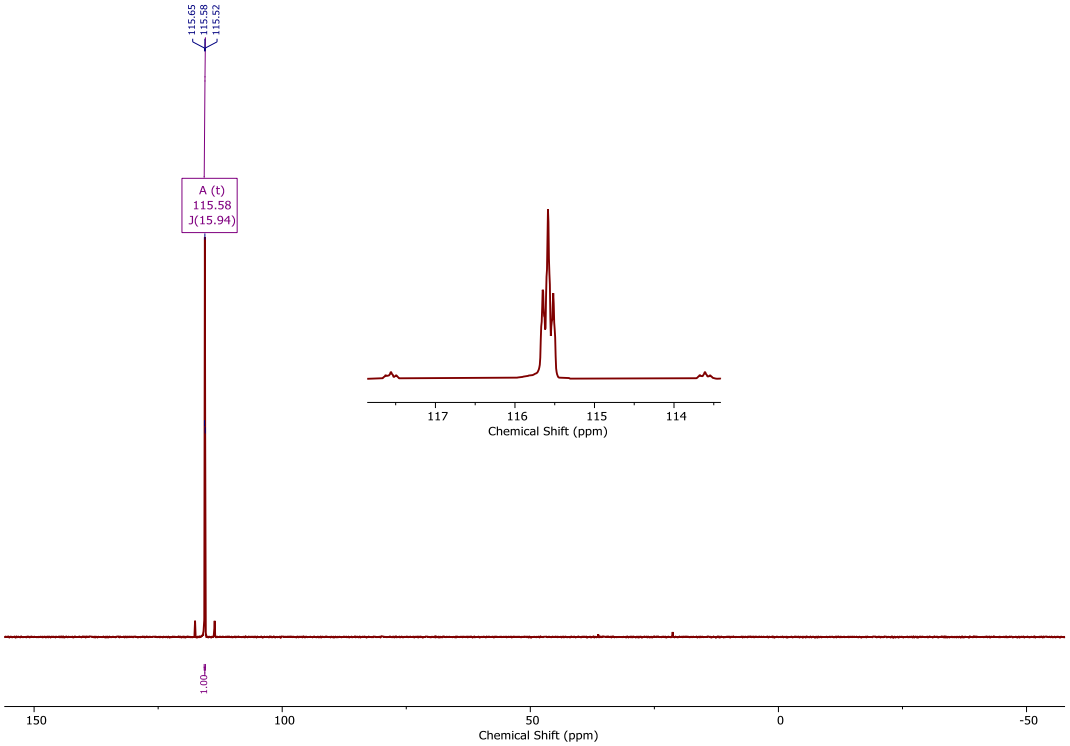

Figure B3. ^{31}P NMR (241 MHz, $CDCl_3$) spectrum of Cat-PSe.

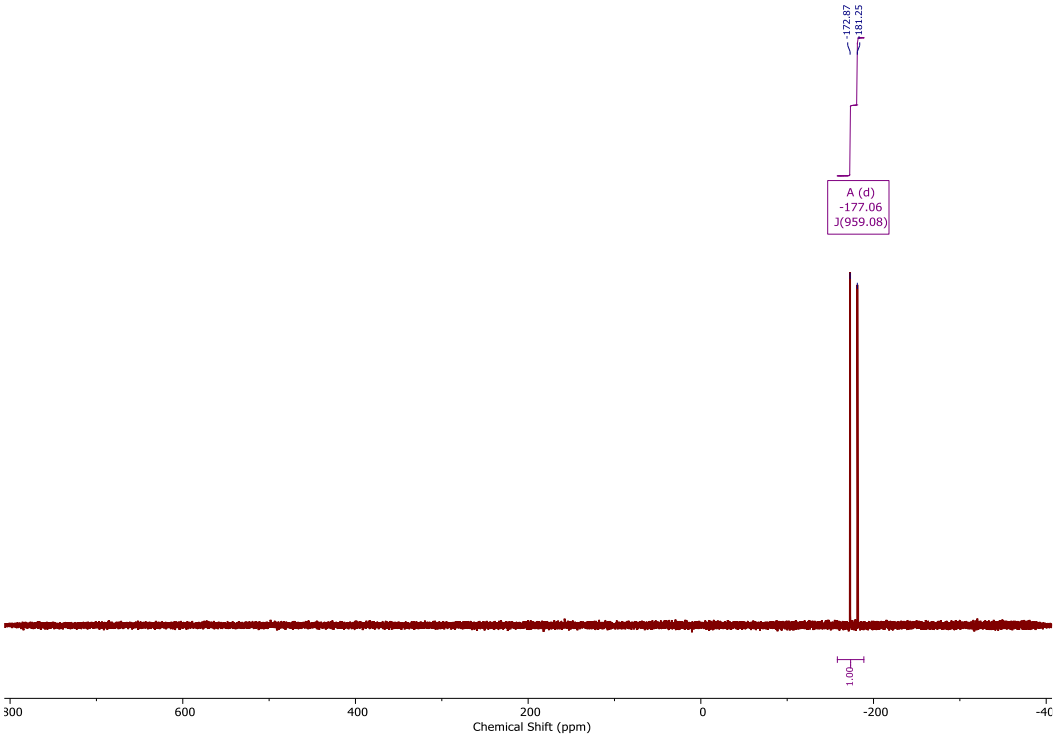

Figure B4. ^{77}Se NMR (115 MHz, $CDCl_3$) spectrum of Cat-PSe.

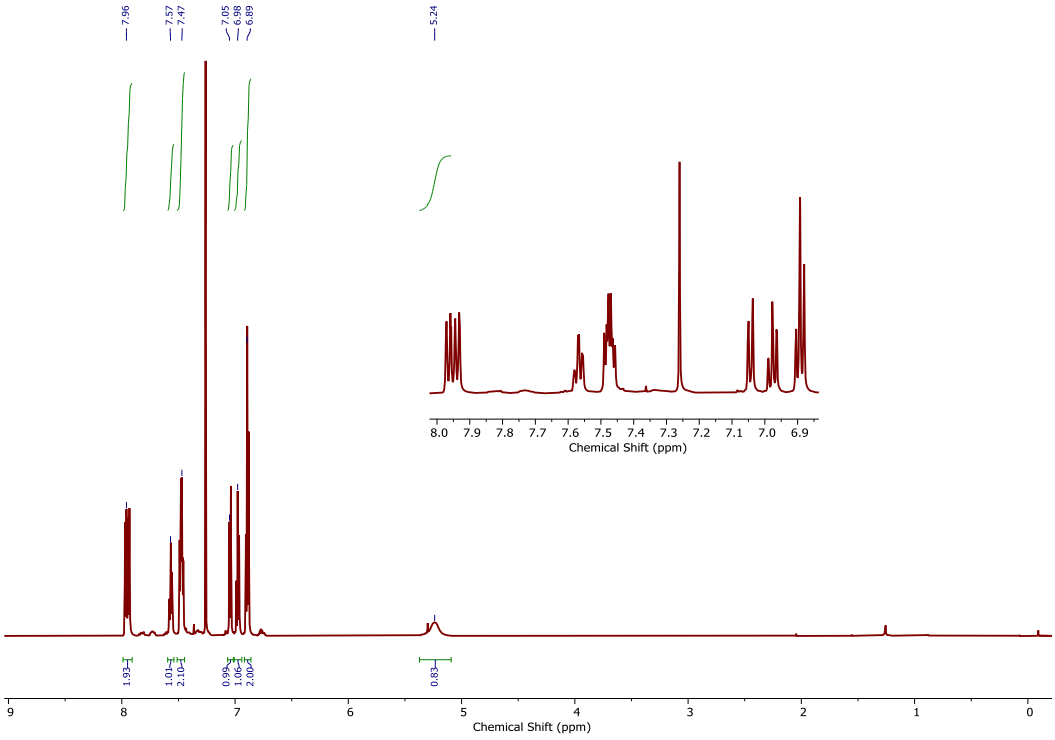

Figure B5. ^{1}H NMR (600 MHz, $CDCl_3$) spectrum of 2AP-PSe.

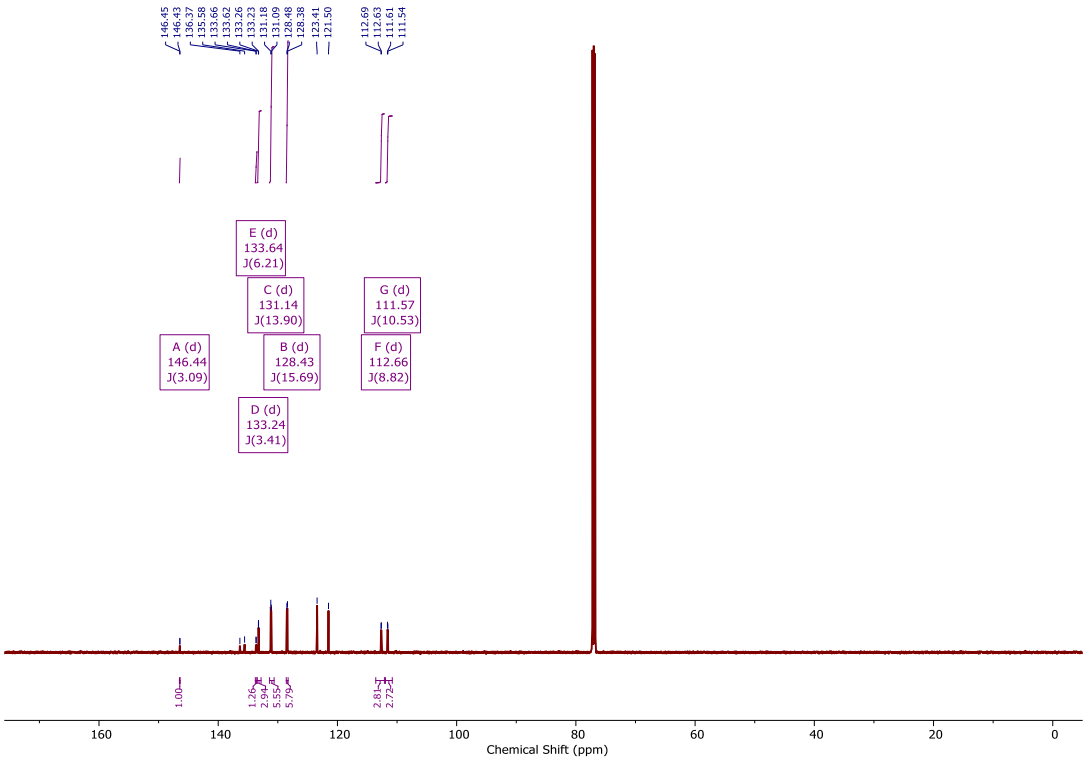

Figure B6. $^{13}C\{^{1}H\}$ NMR (151 MHz, $CDCl_3$) spectrum of 2AP-PSe.

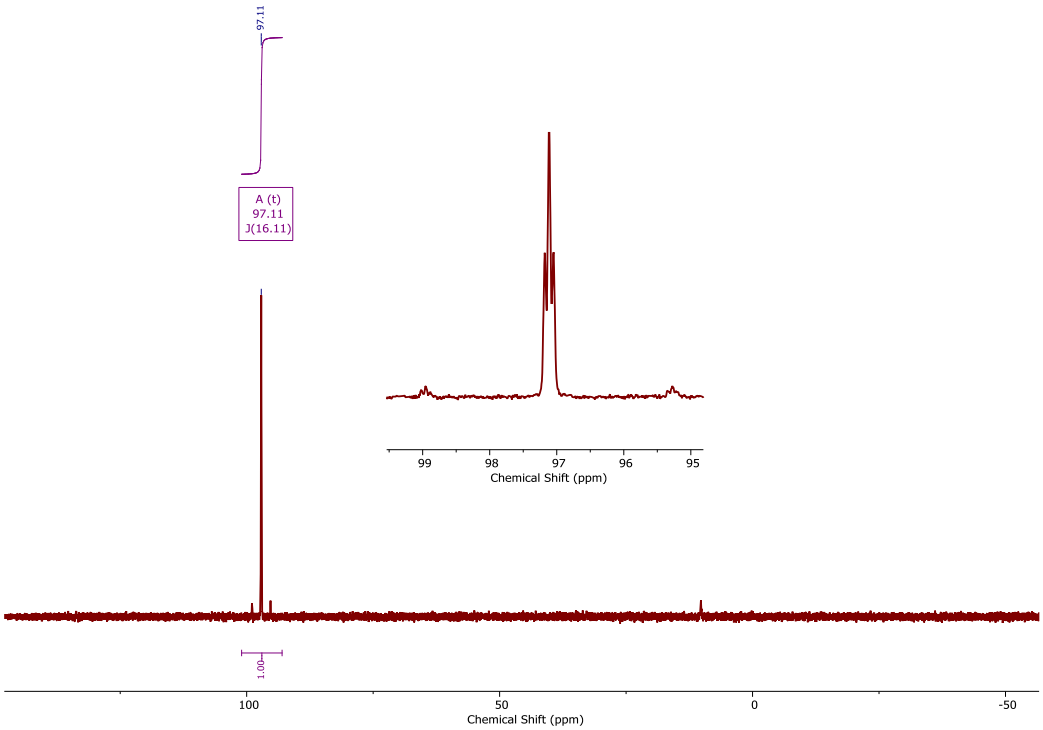

Figure B7. ^{31}P NMR (241 MHz, $CDCl_3$) spectrum of 2AP-PSe.

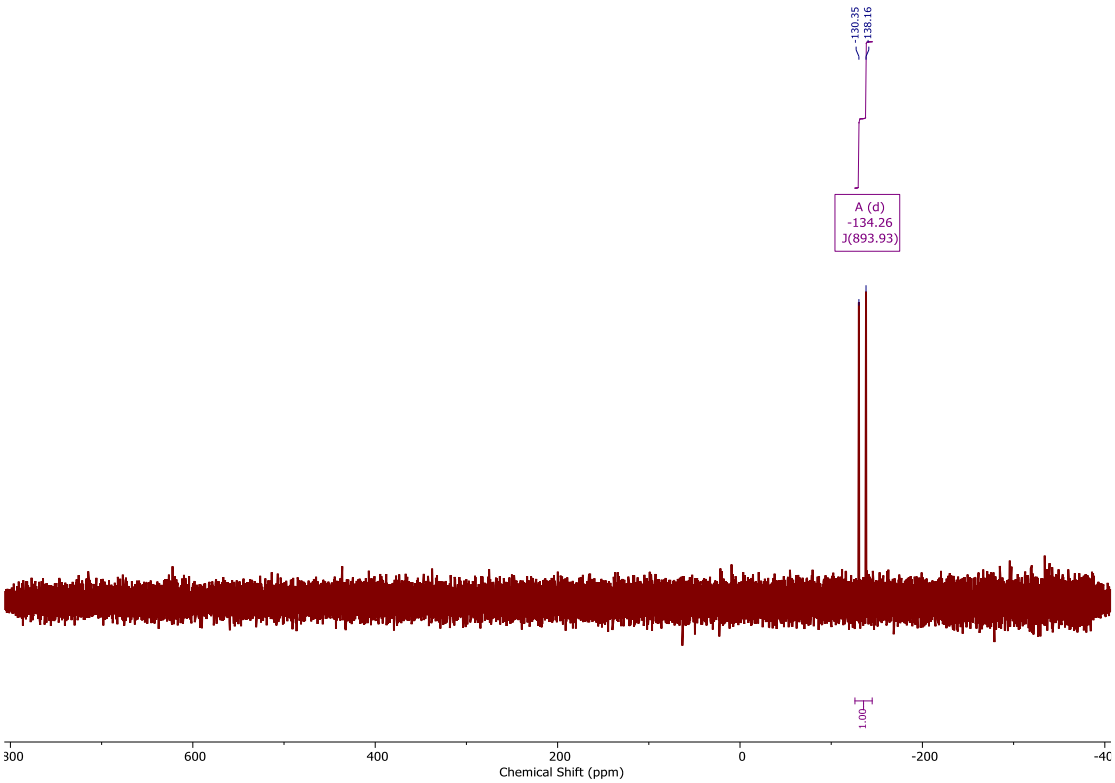

Figure B8. ^{77}Se NMR (115 MHz, $CDCl_3$) spectrum of 2AP-PSe.

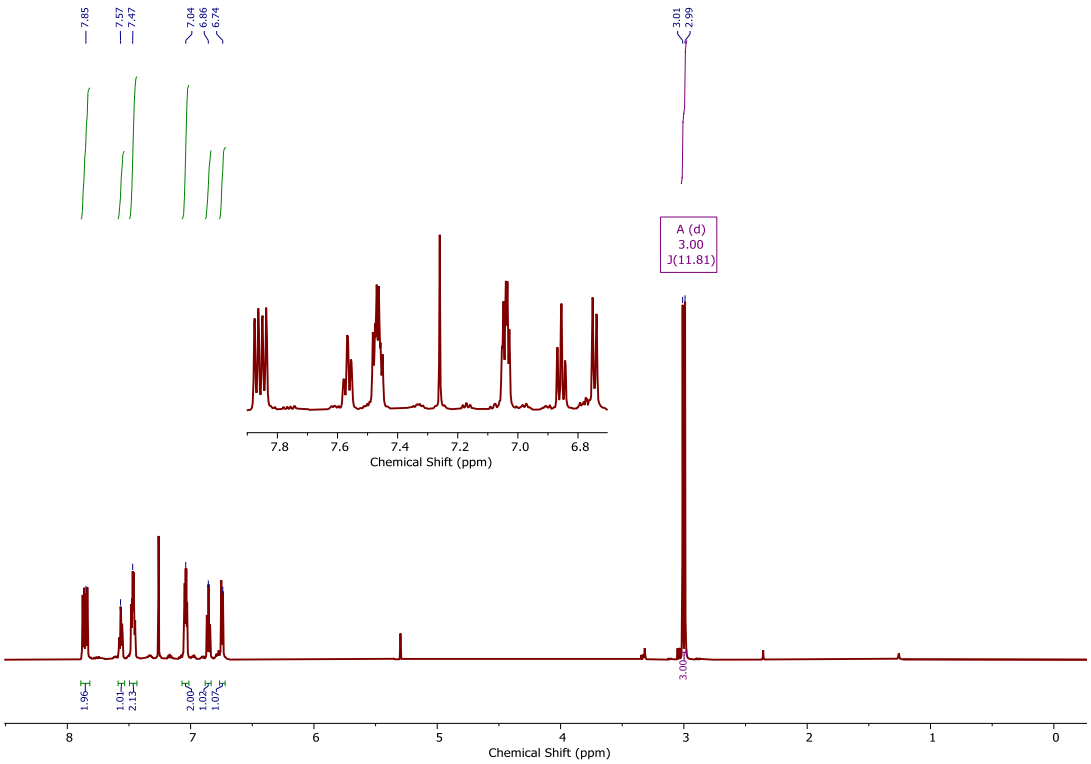

Figure B9. ^{1}H NMR (600 MHz, $CDCl_3$) spectrum of NMe2AP-PSe.

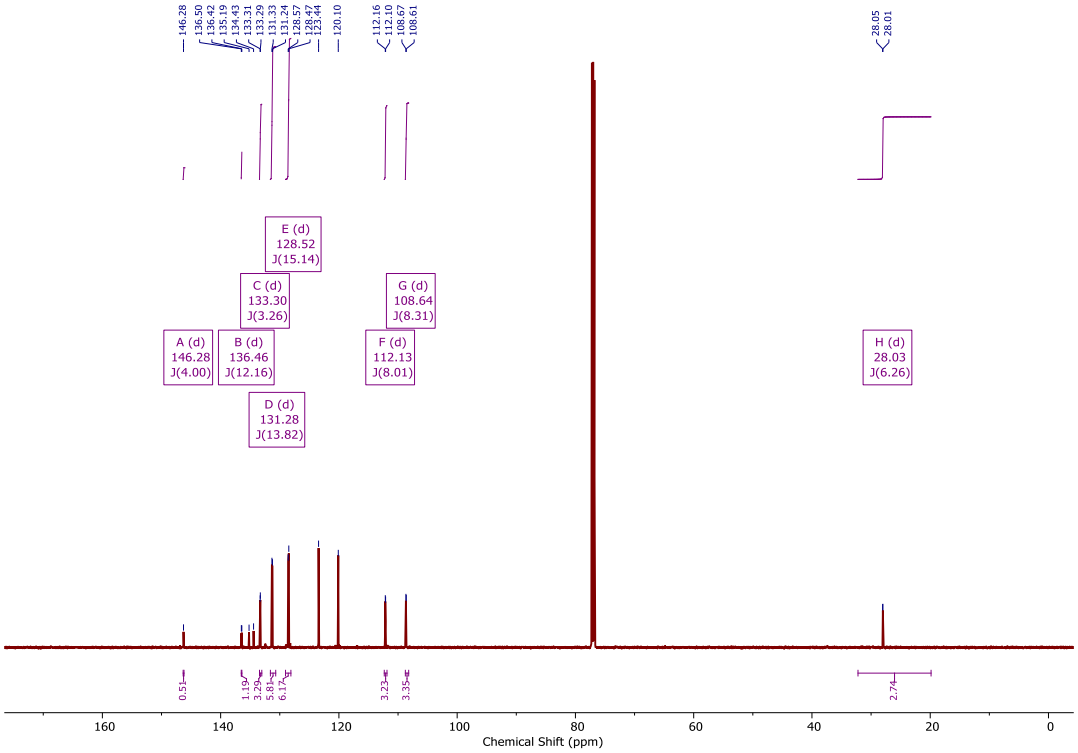

Figure B10. $^{13}C\{^{1}H\}$ NMR (151 MHz, $CDCl_3$) spectrum of NMe2AP-PSe.

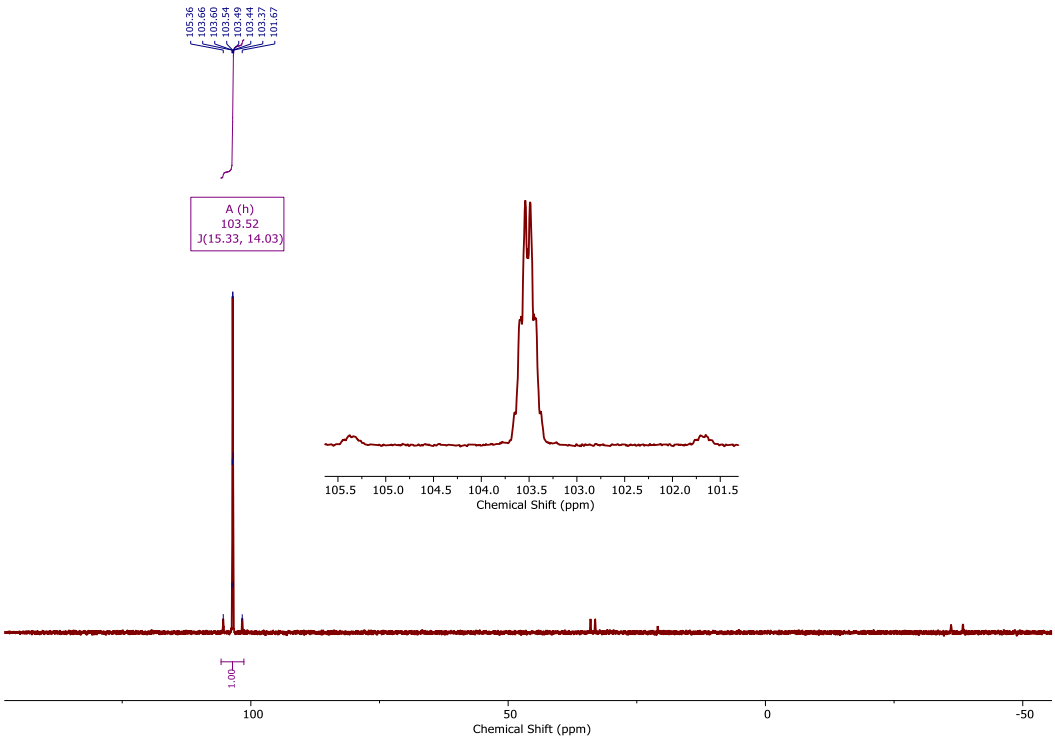

Figure B11. ^{31}P NMR (241 MHz, $CDCl_3$) spectrum of NMe2AP-PSe.

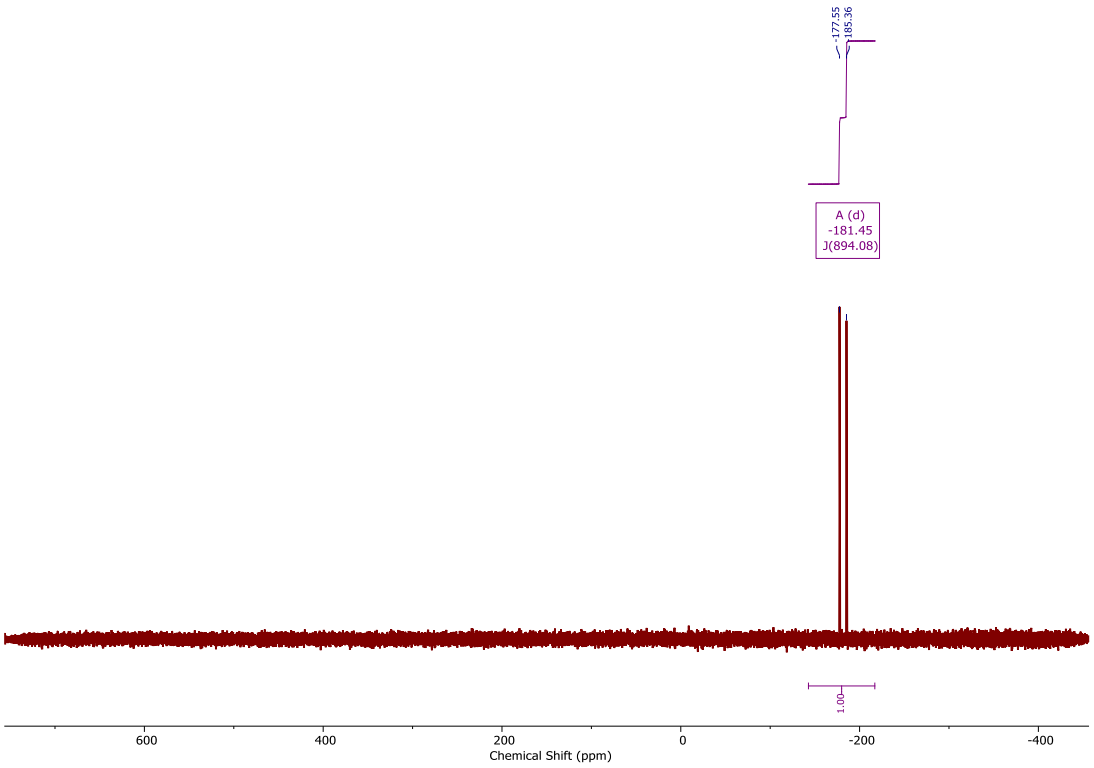

Figure B12. ^{77}Se NMR (115 MHz, $CDCl_3$) spectrum of NMe2AP-PSe.

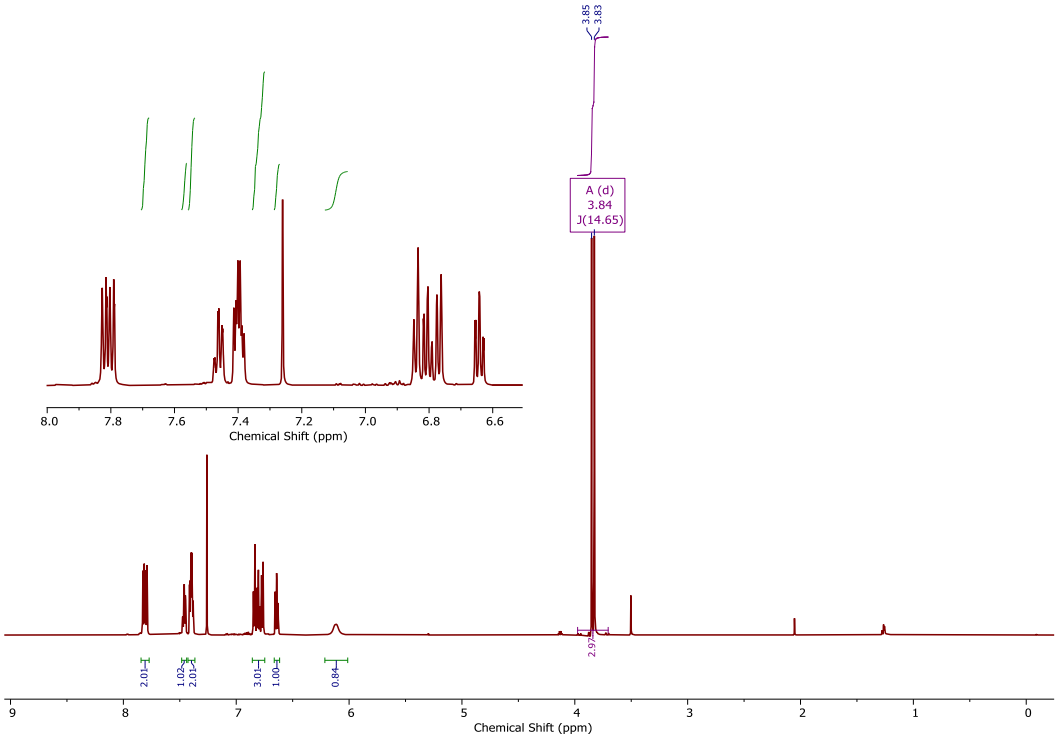

Figure B13. ^{1}H NMR (600 MHz, $CDCl_3$) spectrum of 2AP-PSe-OMe.

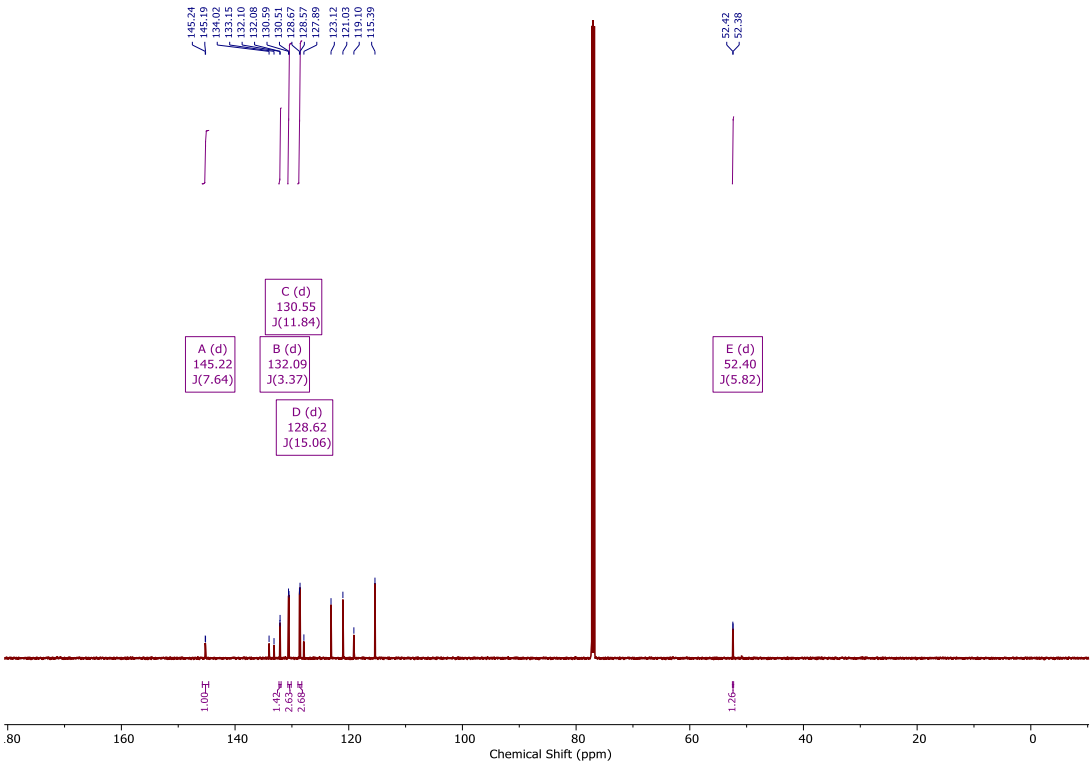

Figure B14. $^{13}C\{^{1}H\}$ NMR (151 MHz, $CDCl_3$) spectrum of 2AP-PSe-OMe.

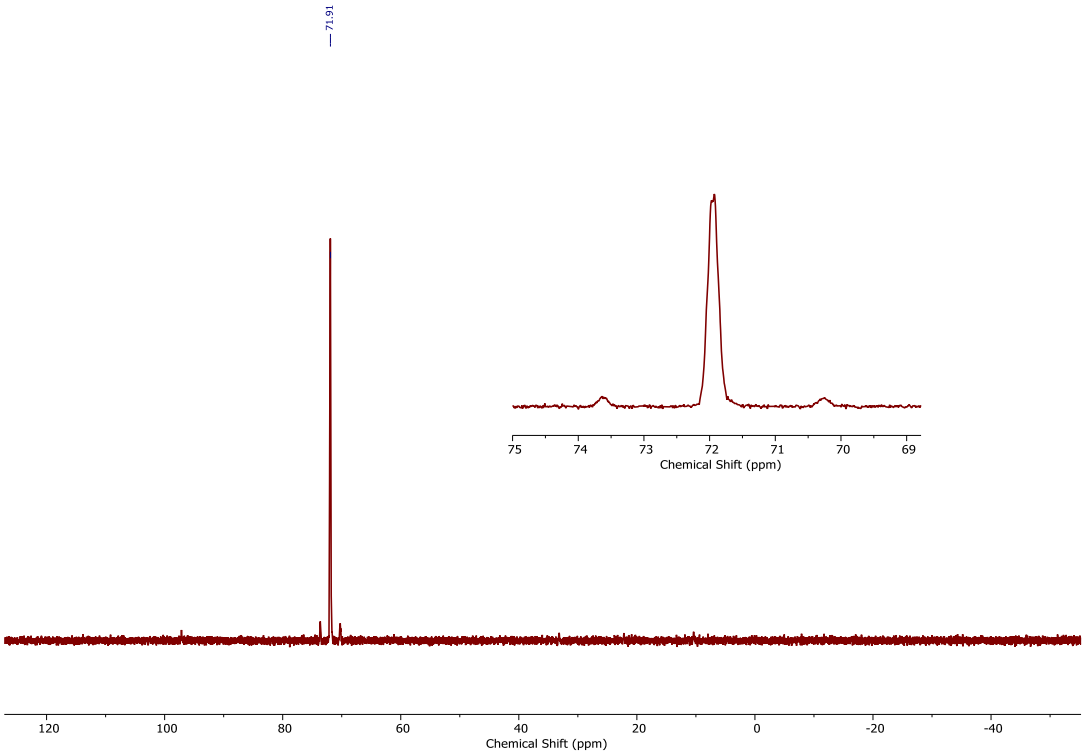

Figure B15. ^{31}P NMR (241 MHz, $CDCl_3$) spectrum of 2AP-PSe-OMe.

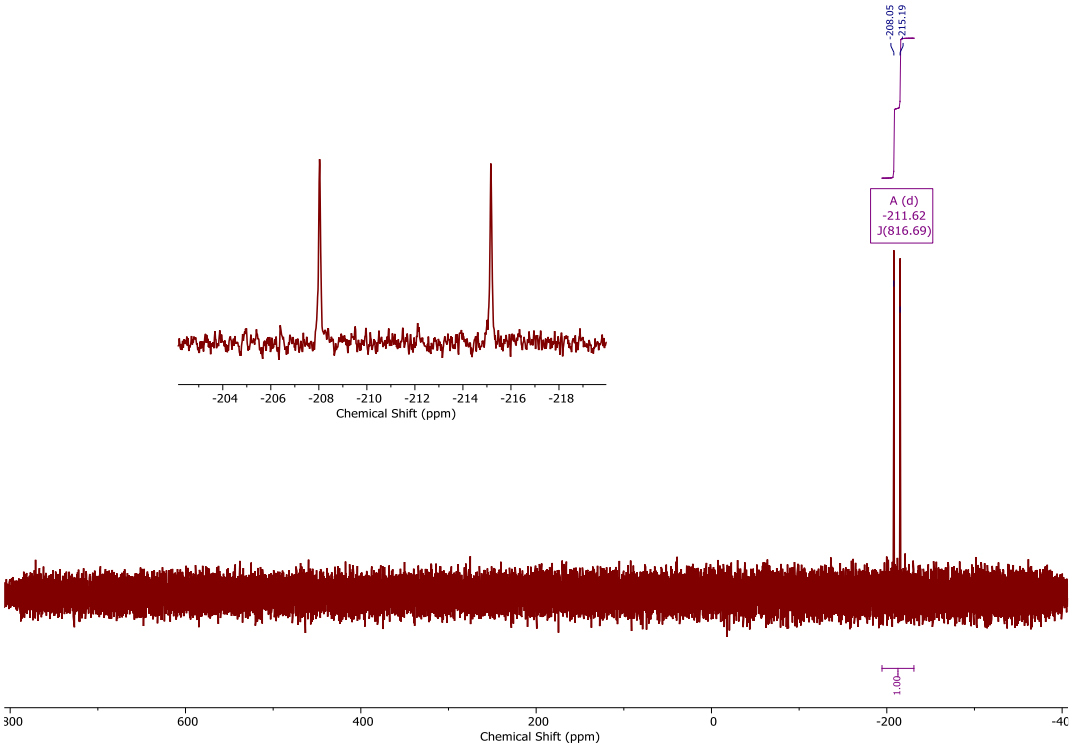

Figure B16. ^{77}Se NMR (115 MHz, $CDCl_3$) spectrum of 2AP-PSe-OMe.

Crystallographic Data

Table B1. Tabulated crystallographic data from structural analysis.

	NMe2AP-PSe	**2AP-PSe-OMe**
formula	$C_{13}H_{12}NOPSe$	$C_{13}H_{14}NO_2PSe$
fw	308.17	326.18
temperature (K)	173 (2)	173 (2)
crystal syst	monoclinic	monoclinic
space group	*P* $2_1/c$	*P* 2_1/c
a (Å)	8.3447(7)	10.368(2)
b (Å)	9.6454(8)	13.157(3)
c (Å)	16.0701(13)	11.153(2)
α (deg)	90	90
β (deg)	103.323(1)	117.417(3)
γ (deg)	90	90
V (Å^3)	1258.64(18)	1350.6(4)
Z	4	4
ρ (mm^{-1})	1.626	1.604
F(000)	616.0	656.0
cryst size (mm^3)	0.18 × 0.16 × 0.11	0.17 × 0.14 × 0.11
θ range (deg)	2.51 – 30.31	2.21 – 27.85
completeness to θ (%)	97.0	99.7
total reflns	11912	12129
indep reflns	3702	3332
Data / restraints / param	3702 / 0 / 202	3332 / 0 / 219
max, min transmn	0.746, 0.640	0.746, 0.662
R1 (wR2) [I > 2σ(*I*)]	0.0254 (0.0641)	0.0319 (0.0651)
R1 (wR2)	0.0303 (0.0664)	0.0517 (0.0705)
GOF (F^2)	1.049	1.051
max, min peaks (e Å^{-3})	0.643, -0.349	0.380, -0.387

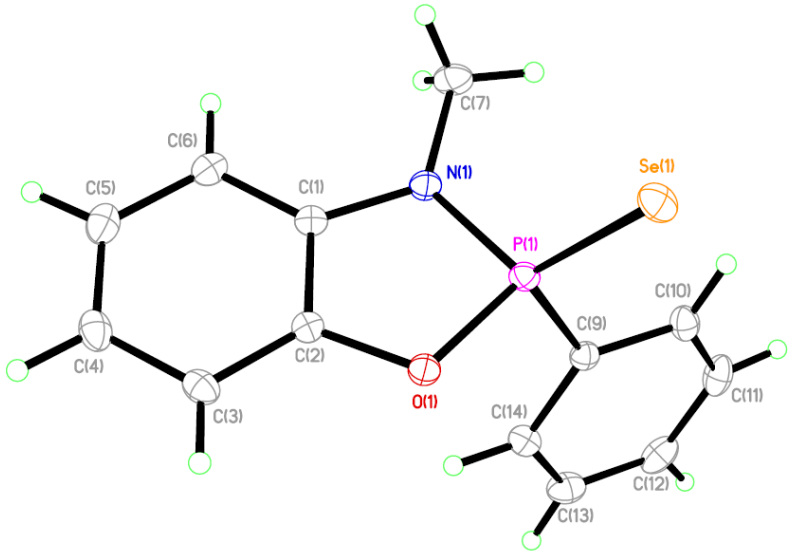

Figure B17. Crystal structure of NMe2AP-PSe (ORTEP ellipsoid, 50% probability)

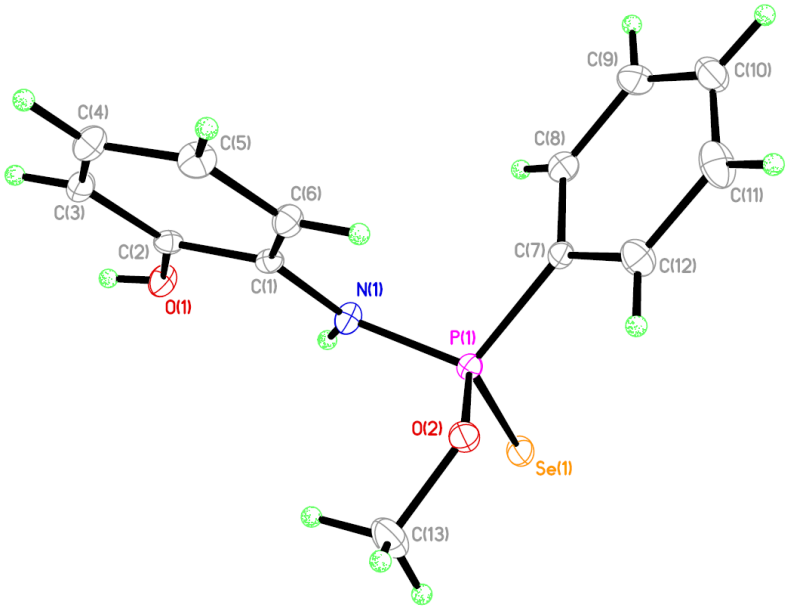

Figure B18. Crystal structure of 2AP-PSe-OMe (ORTEP ellipsoid, 50% probability)

Hydrolysis Studies

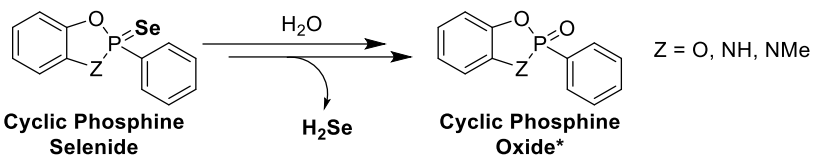

Scheme B2. Proposed general pathway of hydrolysis for Cyclic-PSe compounds

Recorded spectra:

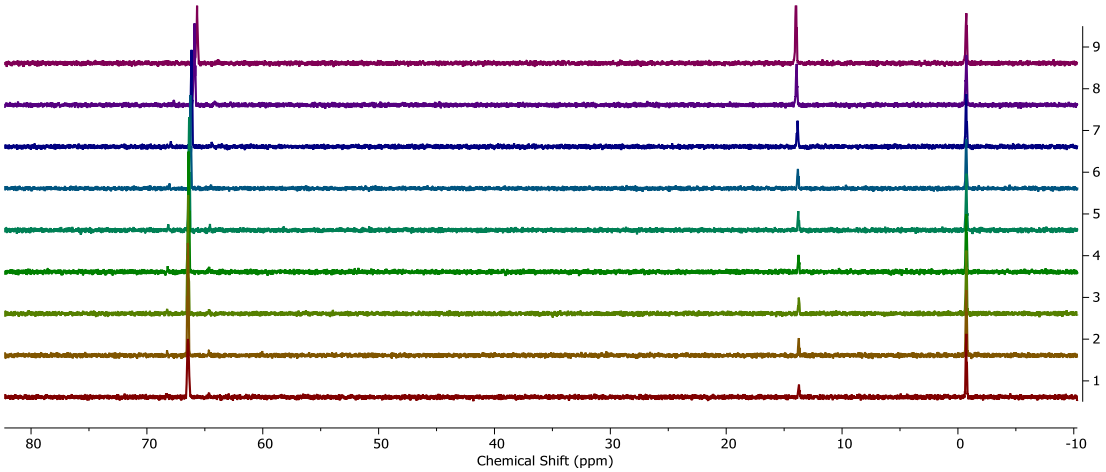

Figure B19. ^{31}P NMR (202 MHz, THF) spectra of Cat-PSe hydrolysis at pH 7.4.

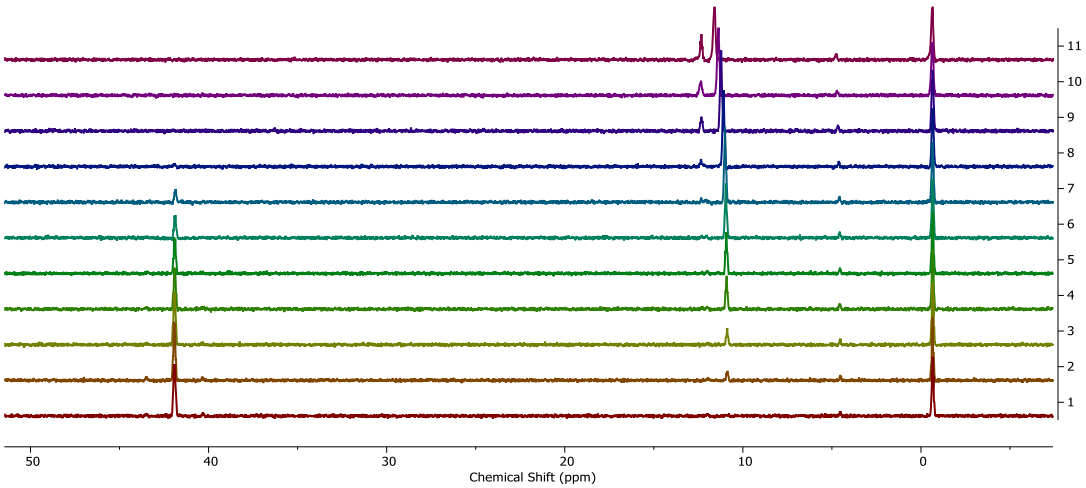

Figure B20. ^{31}P NMR (202 MHz, THF) spectra of 2AP-PSe hydrolysis at pH 7.4.

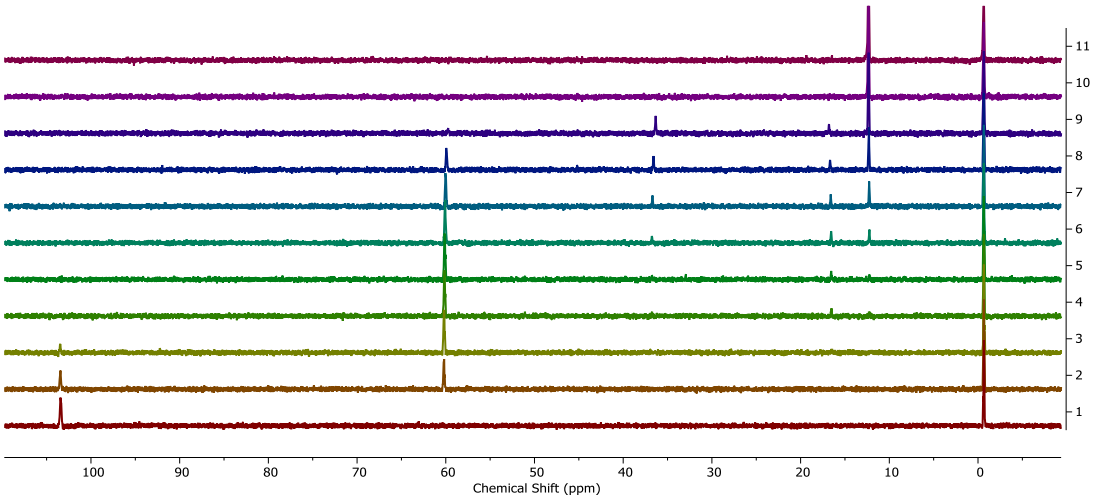

Figure B21. ^{31}P NMR (202 MHz, THF) spectra of NMe2AP-PSe hydrolysis at pH 7.4.

H_2Se Trapping Experiments with BnBr

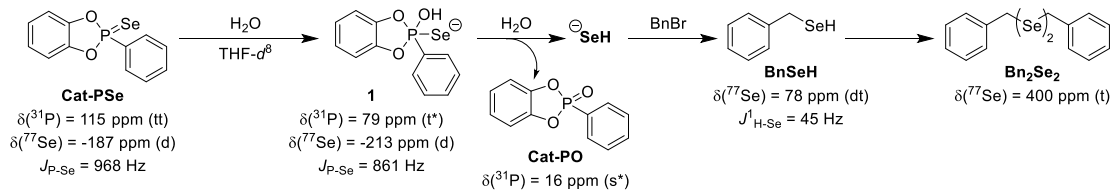

Scheme B3. Proposed pathway for the hydrolysis of Cat-PSe in the presence of BnBr, leading to an anionic intermediate (1) with further hydrolysis affording a trapped selenide product Bn_2Se_2 via auto-oxidation of generated BnSeH.

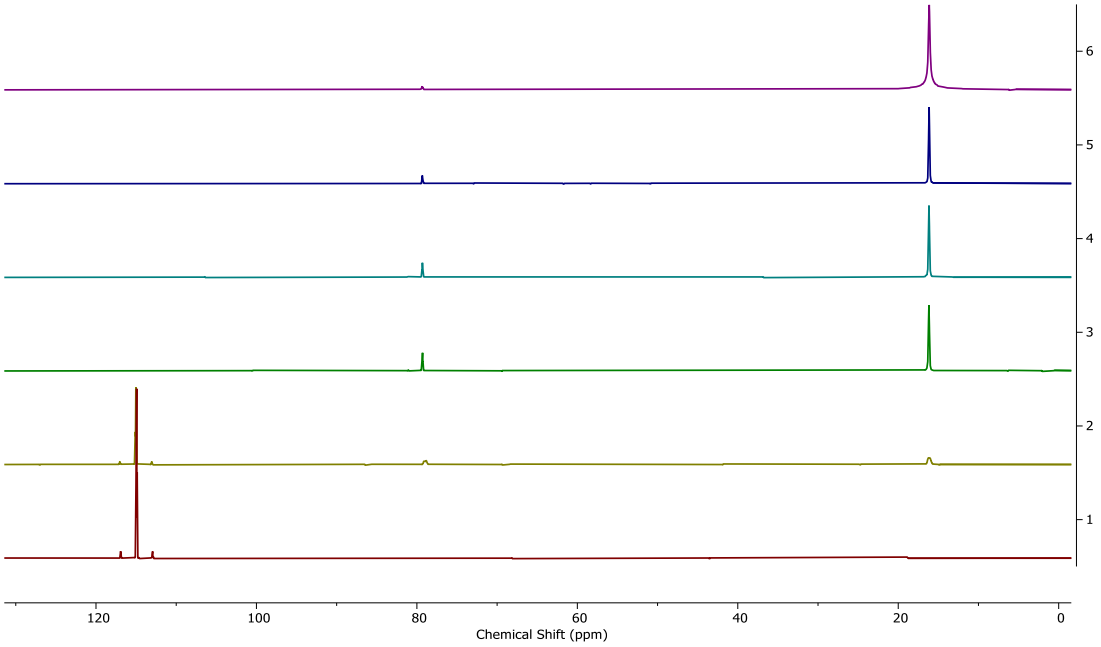

Figure B22. ^{31}P NMR (242 MHz, THF-d^{8}) stacked spectra of Cat-PSe hydrolysis in the presence of BnBr.

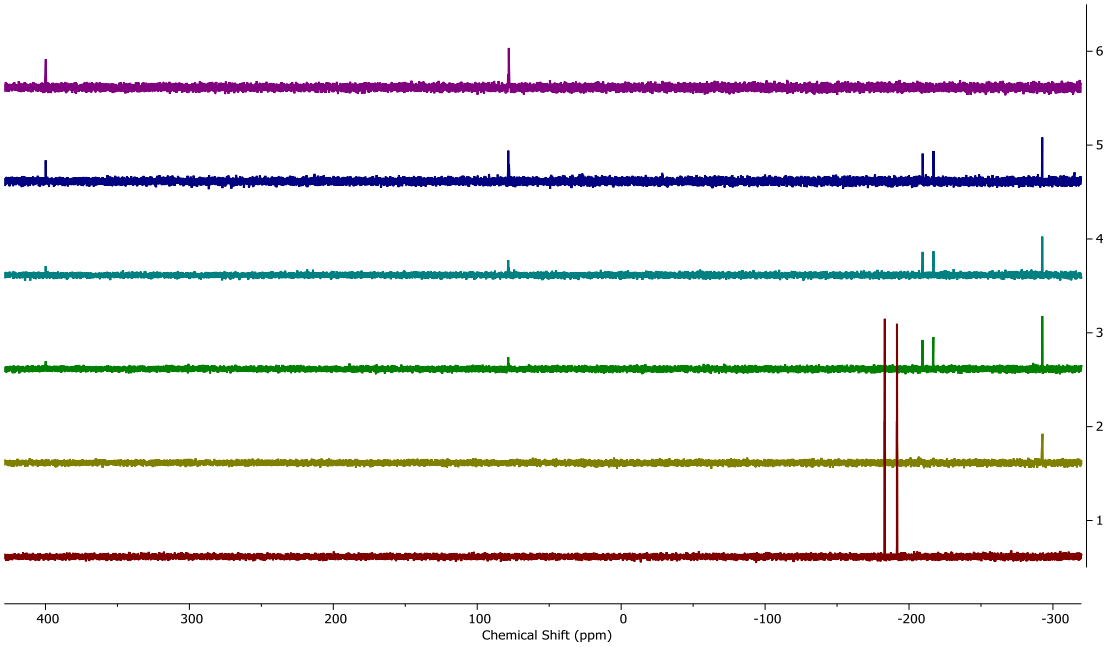

Figure B23. ^{77}Se NMR (115 MHz, THF-d^{8}) stacked spectra of Cat-PSe hydrolysis in the presence of BnBr.

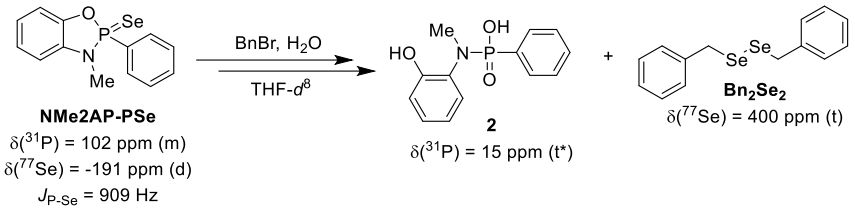

Scheme B4. Proposed pathway for the hydrolysis of NMe2AP-PSe in the presence of BnBr, leading to the trapped selenide product Bn_2Se_2 via generation of BnSeH with rapid auto-oxidation.

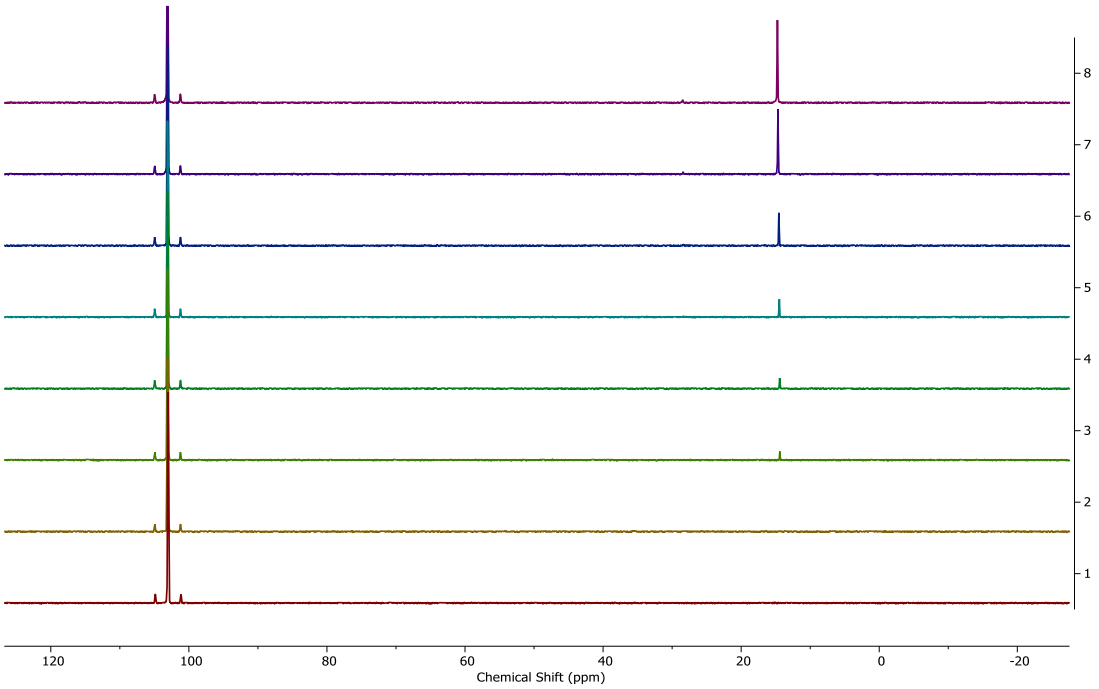

Figure B24. ^{31}P NMR (242 MHz, THF-d^8) stacked spectra of NMe2AP-PSe hydrolysis in the presence of BnBr.

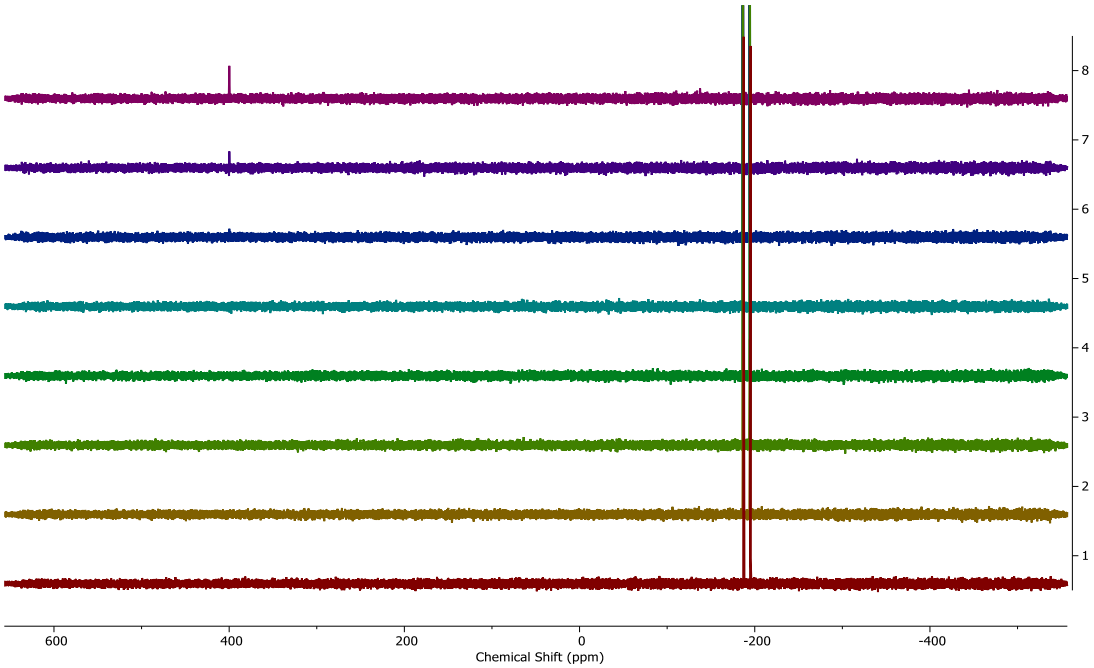

Figure B25. ^{77}Se NMR (115 MHz, THF-d^{8}) stacked spectra of NMe2AP-PSe hydrolysis in the presence of BnBr.

Cellular Proliferation and Antioxidant Activity Assays

Cell viability assay: CCK8 with 2AP-PSe in HeLa cells

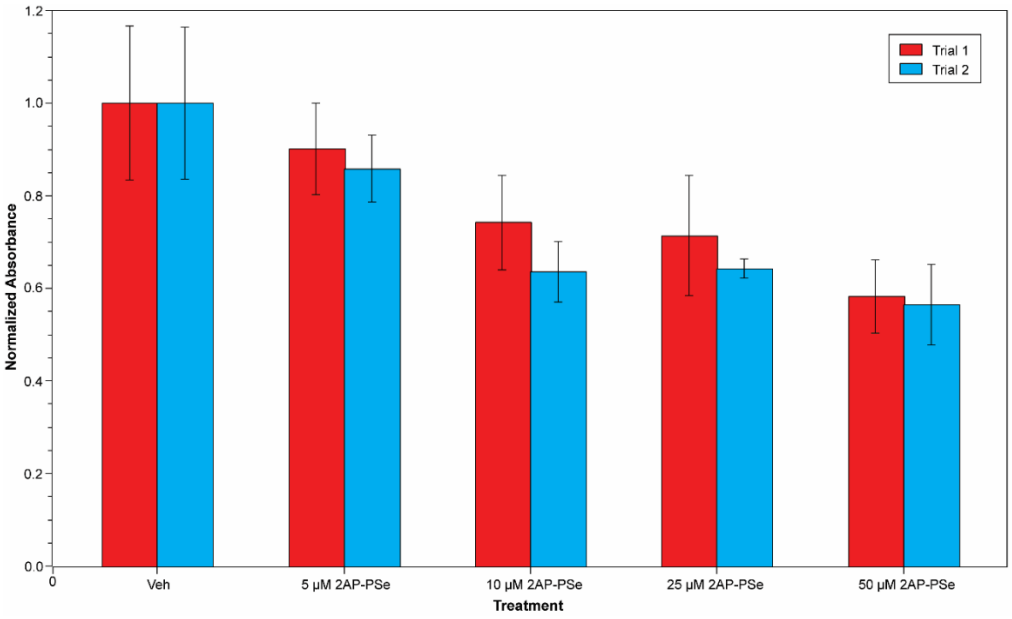

Figure B26. CCK8 assay results of incubating 2AP-PSe with HeLa cells for 20 h.

APPENDIX C

SUPPLEMENTARY INFORMATION FOR CHAPTER IV

Appendix C is the supplementary information for Chapter 4 of this dissertation. It includes experimental procedures, spectra, and data relevant to the content of Chapter 4.

Materials and methods

Reagents were purchased from Sigma-Aldrich, Alfa Aesar, and TCI Chemicals and were and used directly as received. Deuterated solvents were purchased from Cambridge Isotope Laboratories and used directly as received. ^{1}H, $^{13}C\{^{1}H\}$, ^{19}F, and ^{77}Se NMR spectra were recorded on Bruker 500 and 600 MHz instruments. Chemical shifts are reported relative to residual protic solvent resonances for ^{1}H and $^{13}C\{^{1}H\}$ spectra. All air-free manipulations were performed in an inert atmosphere using standard Schlenk techniques or an Innovative Atmospheres N_2-filled glove box.

Synthesis of isoselenocyanates

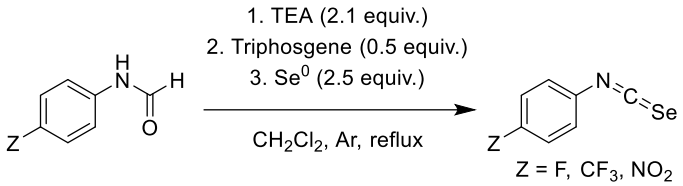

Scheme C1. General synthesis of isoselenocyanates from formanilides.

4-nitrophenyl isoselenocyanate. To an oven-dried flask was added CH_2Cl_2 (25.0 mL), 3 Å molecular sieves, and 4-nitroformanilide (600 mg, 3.60 mmol). The flask was capped with a septum and placed on a stir plate, where it received triethylamine (1.15 mL, 7.60 mmol); the flask was then connected to a condenser, the atmosphere was purged with argon from a balloon, and the apparatus was lowered into an oil bath at 45 °C. Once refluxing, a solution of triphosgene (650 mg, 1.80 mmol) in CH_2Cl_2 (5.00 mL) was added dropwise over 30 minutes. After full addition, the mixture was allowed to reflux for 3 hours

before selenium powder (710 mg, 9.00 mmol) was added. TLC analysis (3:1 hexanes/EtOAc) was conducted, and the reaction was allowed to reflux overnight, with subsequent TLC analysis revealing the completion of the reaction (R_f = 0.55). The mixture was then removed from the oil bath, allowed to cool to room temperature, filtered through a celite pad, and concentrated to dryness. The resulting crude product was purified via SiO_2 column chromatography (gradient hexanes to 1:1 EtOAc/hexanes) to afford a yellow solid (0.571 g, 70%). ^{1}H NMR (600 MHz, $CDCl_3$) δ: 8.27 (m, 2H), 7.43 (m, 2H). $^{13}C\{^1H\}$ NMR (151 MHz, $CDCl_3$) δ: 146.21, 135.85, 135.72, 126.90, 125.32. ^{77}Se NMR (115 MHz, $CDCl_3$) δ: -255.85 (s).

4-fluorophenyl isoselenocyanate. This compound was obtained from an identical procedure on 7.40 mmol scale as a red-orange solid (1.16 g, 78%). ^{1}H NMR (600 MHz, $CDCl_3$) δ: 7.28 (m, 2H), 7.39 (m, 2H). $^{13}C\{^1H\}$ NMR (151 MHz, $CDCl_3$) δ: 161.58 (d, $J_{1C\text{-}F}$ = 250.75 Hz), 129.98, 127.92 (d, $J_{3C\text{-}F}$ = 9 Hz), 125.94, 116.82 (d, $J_{2C\text{-}F}$ = 23 Hz). ^{19}F NMR (564 MHz, $CDCl_3$) δ: -110.21 (m). ^{77}Se NMR (115 MHz, $CDCl_3$) δ: -298.68 (s).

4-(trifluoromethyl)phenyl isoselenocyanate. This compound was obtained from an identical procedure on 3.70 mmol scale as a red-orange solid (1.16 g, 78%). ^{1}H NMR (600 MHz, $CDCl_3$) δ: 7.64 (d, 2H), 7.39 (d, 2H). $^{13}C\{^1H\}$ NMR (151 MHz, $CDCl_3$) δ: 133.16, 129.81 (q, $J_{1C\text{-}F}$ = 33 Hz), 126.91 (q, $J_{2C\text{-}F}$ = 4 Hz), 126.49, 124.37, 122.56. ^{19}F NMR (564 MHz, $CDCl_3$) δ: -62.73 (s). ^{77}Se NMR (115 MHz, $CDCl_3$) δ: -278.65 (s).

Phenyl isoselenocyanate. This compound was obtained from an identical procedure on 1.50 mmol scale as a clear-yellow liquid (264 mg, 95%). ^{1}H NMR (600 MHz, $CDCl_3$) δ: 7.39-7.31 (m, 3H), 7.29 (m, 2H). $^{13}C\{^1H\}$ NMR (151 MHz, $CDCl_3$) δ: 129.75, 129.62, 129.21, 128.15, 126.15. ^{77}Se NMR (115 MHz, $CDCl_3$) δ: -297.58 (s).

Synthesis of selenocarbamates

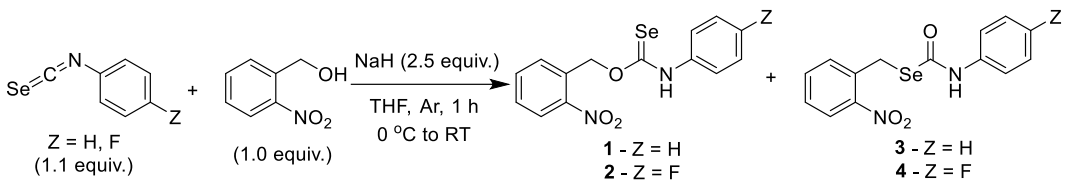

Scheme C2. General synthesis of PhotoSeCMs from isoselenocyanates.

PFA-PhotoSeCM (2). To an oven-dried flask was added THF (12.0 mL) and 2-nitrobenzyl alcohol (153 mg, 1.00 mmol), then the flask was septum-sealed, wrapped in foil, purged with argon from a balloon, and placed in an ice bath to cool for 20 min. After this time, NaH (60% on paraffin, 120 mg, 3.00 mmol) was added under a positive pressure of argon, then the flask was removed from the ice bath and allowed to acclimate to room temperature, the atmosphere being repurged with argon. After 30 min, 4-fluorophenyl isoselenocyanate (240 mg, 1.20 mmol) in THF (3.00 mL) was added dropwise to the flask, turning the reaction mixture a deep red color. TLC analysis (1:1 EtOAc/hexanes) was conducted periodically over the course of an hour to monitor formation of the product **2** (R_f = 0.50) and the undesired isomer **4** (R_f = 0.30); when formation of **4** was observed, the reaction was quenched in brine. The resulting mixture was extracted in EtOAc (3x15 mL), dried over $MgSO_4$, filtered, and concentrated to dryness. The resulting orange solid (181 mg, 51%) was shown to be acceptably pure for future studies without further purification. ^{1}H NMR (600 MHz, d^6-DMSO) δ: 11.91 (s, 1H), 8.15 (d, 1H), 7.87-7.53 (m, 4H), 7.40 (m, 1H), 7.28-7.16 (m, 2H), 6.01 (s, 2H). ^{13}C{^{1}H} NMR (151 MHz, d^6-DMSO) δ: 189.38, 147.81, 134.72, 134.19, 131.42, 129.93, 126.78, 125.42, 125.24, 116.13, 72.59. ^{19}F NMR (564 MHz, $CDCl_3$) δ: -116.05 (m). ^{77}Se NMR (115 MHz, d^6-DMSO) δ: 278.34 (s).

PhotoSeCM (1). An identical procedure was followed on a 1.25 mmol scale to afford this product as an orange solid (80 mg, 19%). ^{1}H NMR (600 MHz, d^6-DMSO) δ: 11.78 (s, 1H), 8.14 (s, 1H), 8.21 (d, 2H), 7.72 (m, 3H), 7.35 (m, 6H), 7.19 (brs, 2H), 6.82 (brs, 1H), 5.72 (s, 2H). ^{13}C{^{1}H} NMR (151 MHz, d^6-DMSO) δ: 189.41, 153.42, 147.79,

134.67, 134.55, 132.76, 129.71, 129.29, 125.44, 123.00, 121.93, 118.69, 72.61, 62.92. ^{77}Se NMR (115 MHz, d^6-DMSO) δ: 281.16 (s).

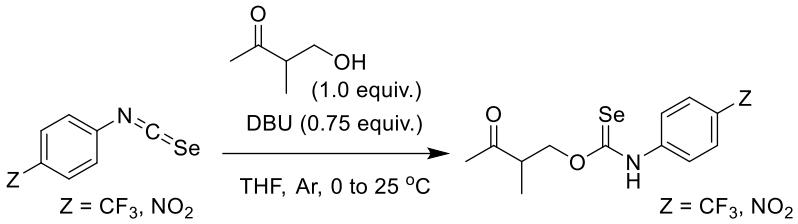

Scheme C3. General synthesis of GKSeCMs from isoselenocyanates.

*PNA-MeGKSeCM (**6**)*. To an oven-dried flask was added THF (20.0 mL) and PNA-NCSe (0.300 g, 1.32 mmol) before the flask was capped with a septum and placed on a stir plate, then 4-hydroxy-3-methyl-2-butanone (148 µL, 1.44 mmol) was added dropwise over 5 minutes. The flask was then wrapped in foil and placed in an ice bath for 20 minutes before DBU (148 µL, 1.00 mmol) was added, turning the yellow mixture red-brown; the atmosphere was then purged with argon from a balloon. TLC analysis was conducted (1:1 hexanes/EtOAc) periodically to monitor product formation, and after 6 hours, the reaction was quenched with brine (25 mL). The resulting mixture was extracted with EtOAc (3 x 20 mL), the organic layers were combined and dried over $MgSO_4$ before filtration and concentration to dryness *in vacuo*. The resulting crude material was purified via SiO_2 column chromatography (gradient of hexanes to 1:1 hexanes/EtOAc) to afford a yellow-orange solid (37.9 mg, 9%). The identity of the product was verified by ^{1}H, ^{13}C{^{1}H}, and ^{77}Se-NMR spectroscopy. ^{1}H NMR (600 MHz, d^6-DMSO) δ: 12.17 (s, 1H), 8.21 (d, 2H), 7.61 (brs, 2H), 4.70 (m, 2H), 3.17 (q, 1H), 2.18 (s, 3H), 1.13 (d, 3H). ^{13}C{^{1}H} NMR (151 MHz, d^6-DMSO) δ: 209.68, 192.10, 144.05, 125.74, 125.21, 122.28, 76.51, 45.48, 28.87, 13.46. ^{77}Se NMR (115 MHz, d^6-DMSO) δ: 350.94 (brs).

*PNA-Me$_2$GKSeCM (**7**)*. An identical procedure was followed on a 0.25 mmol scale to afford this product as a yellow solid (9.1 mg, 11%). ^{1}H NMR (600 MHz, d^6-DMSO) δ: 12.17 (s, 1H), 8.22 (d, 2H), 7.54 (brs, 2H), 4.65 (s, 2H), 2.17 (s, 3H), 1.18 (S, 6H). ^{13}C{^{1}H} NMR (151 MHz, d^6-DMSO) δ: 211.36, 191.04, 144.62, 125.16, 122.51, 81.11, 47.87, 25.78, 21.79. ^{77}Se NMR (115 MHz, d^6-DMSO) δ: 352.81 (brs).

NMR spectra of synthesized compounds

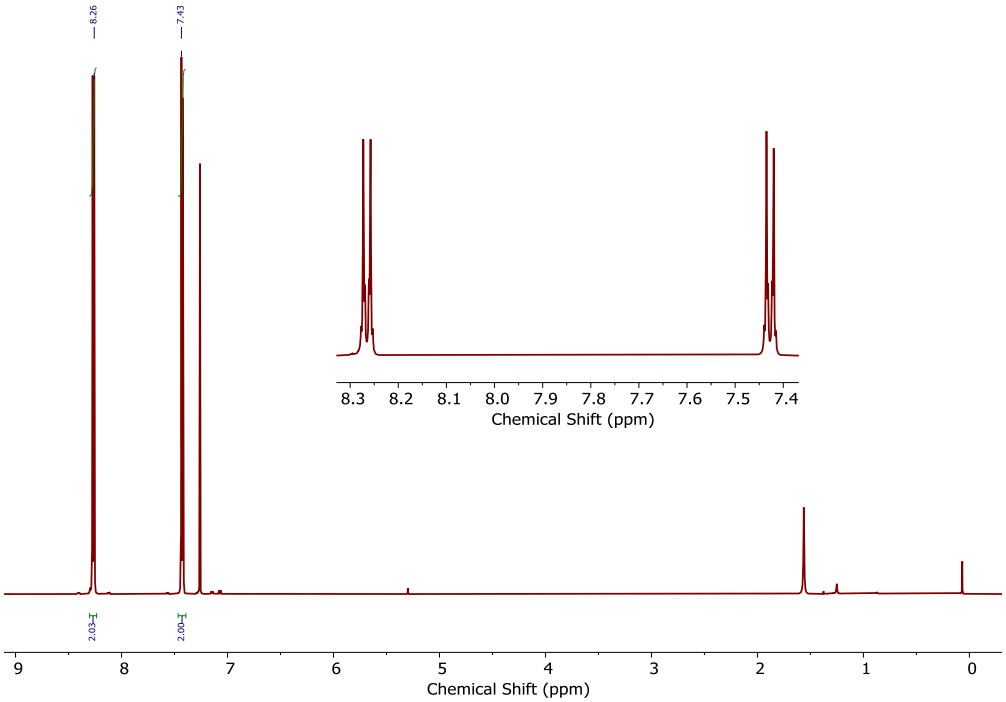

Figure C1. ^{1}H NMR (600 MHz, $CDCl_3$) spectrum of 4-nitrophenyl isoselenocyanate.

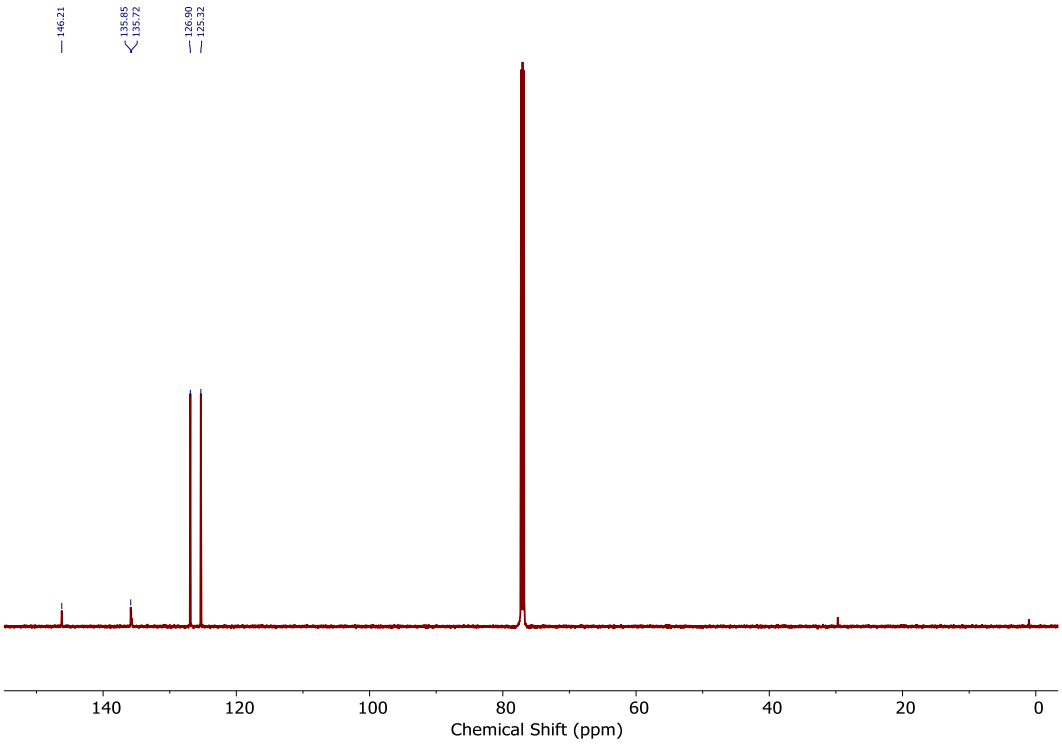

Figure C2. $^{13}C\{^{1}H\}$ NMR (151 MHz, $CDCl_3$) spectrum of 4-nitrophenyl isoselenocyanate.

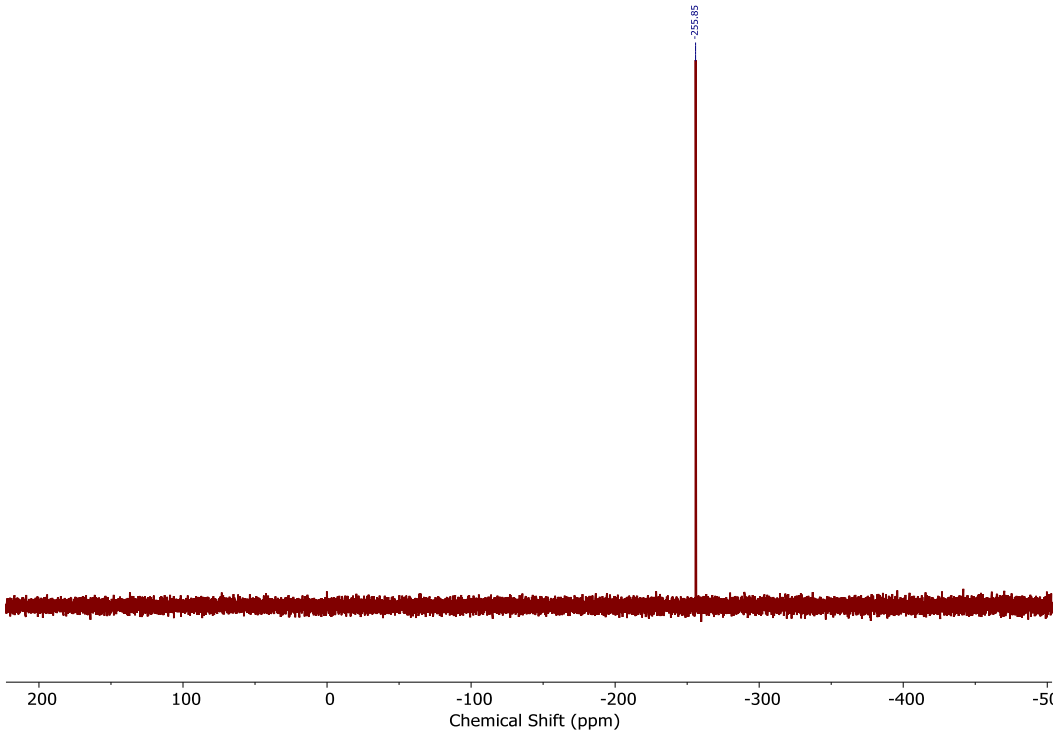

Figure C3. ^{77}Se NMR (115 MHz, $CDCl_3$) spectrum of 4-nitrophenyl isoselenocyanate.

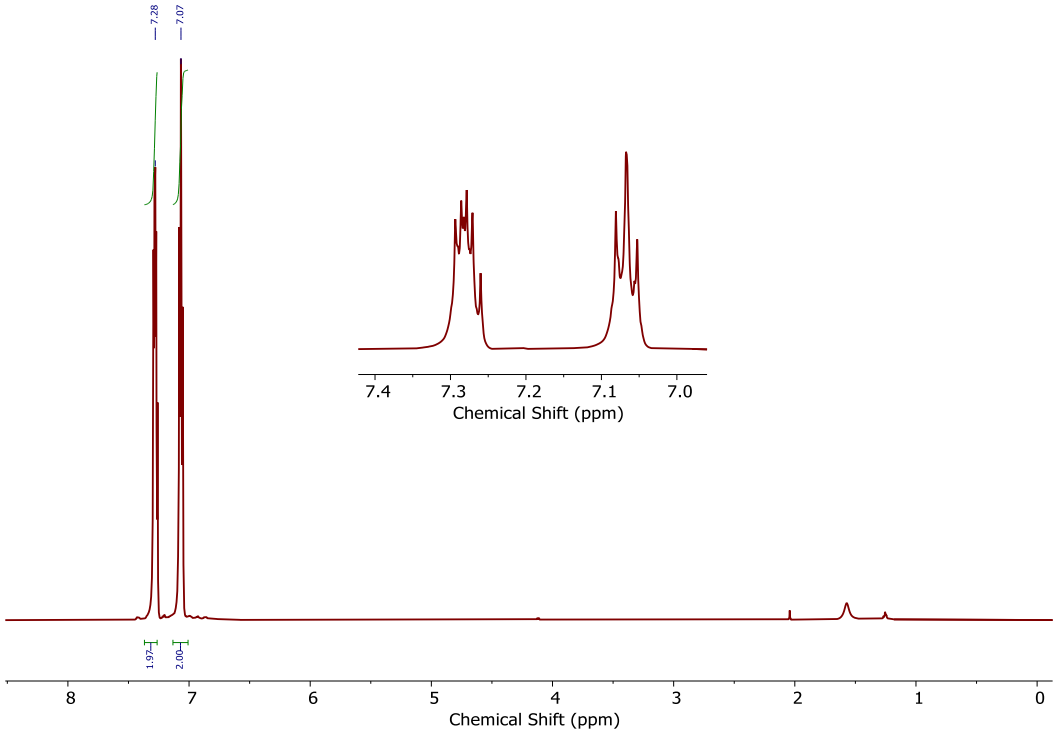

Figure C4. ^{1}H NMR (600 MHz, $CDCl_3$) spectrum of 4-fluorophenyl isoselenocyanate.

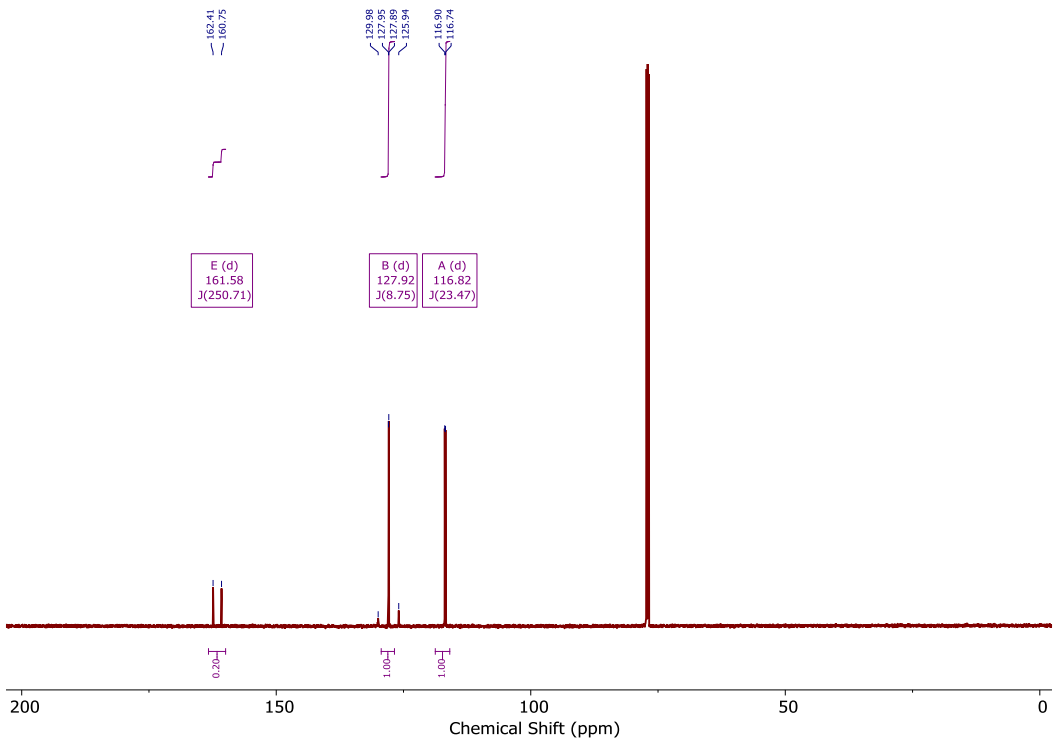

Figure C5. $^{13}C\{^{1}H\}$ NMR (151 MHz, $CDCl_3$) spectrum of 4-fluorophenyl isoselenocyanate.

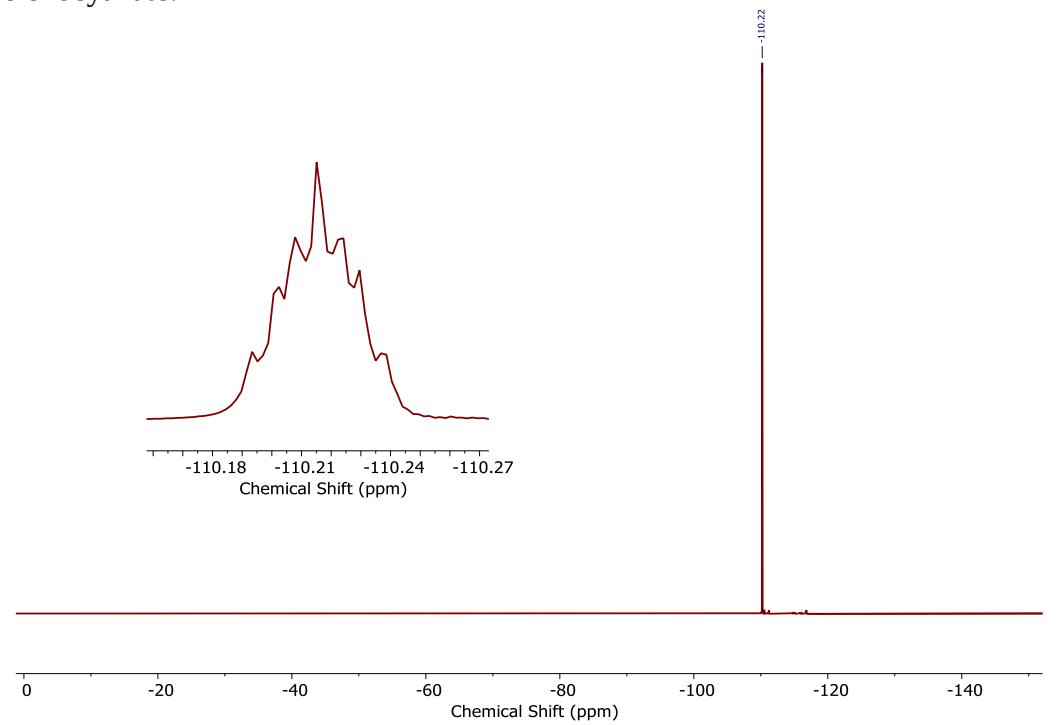

Figure C6. ^{19}F NMR (564 MHz, $CDCl_3$) spectrum of 4-fluorophenyl isoselenocyanate.

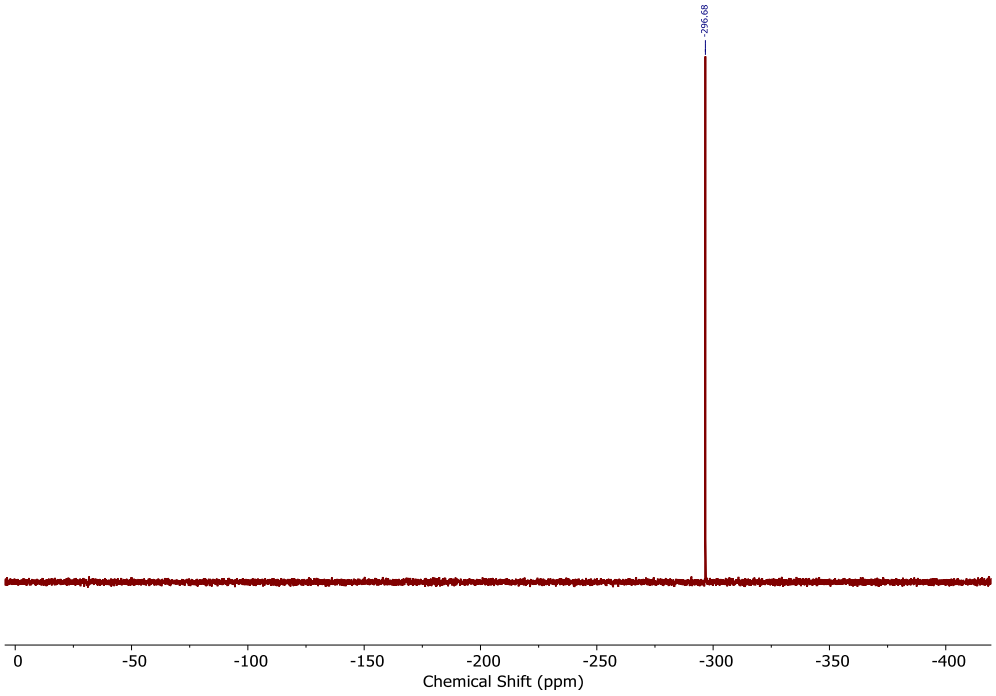

Figure C7. ^{77}Se NMR (115 MHz, $CDCl_3$) spectrum of 4-fluorophenyl isoselenocyanate.

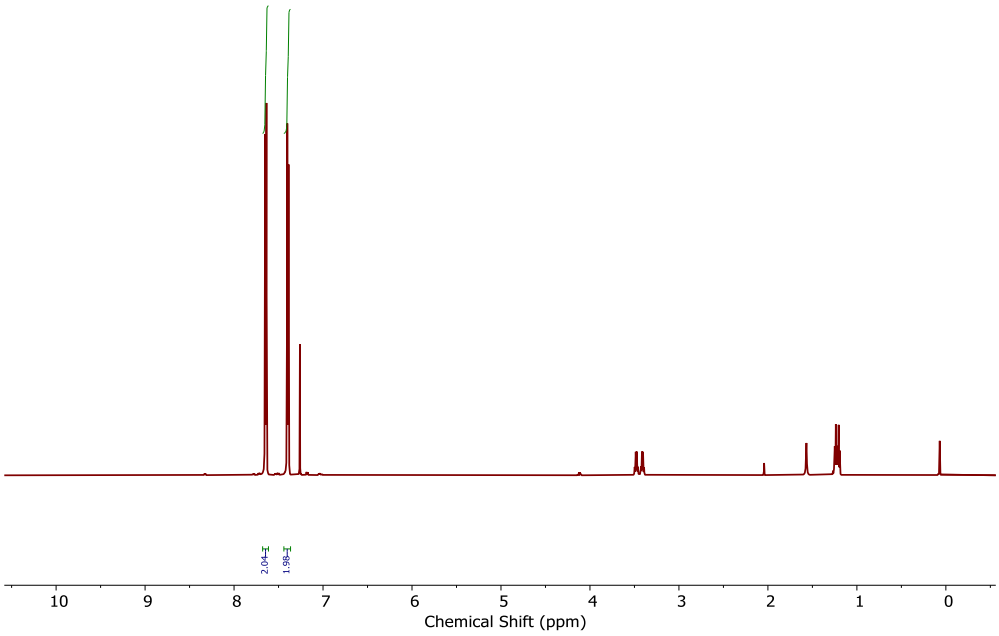

Figure C8. ^{1}H NMR (600 MHz, $CDCl_3$) spectrum of 4-(trifluoromethyl)phenyl isoselenocyanate.

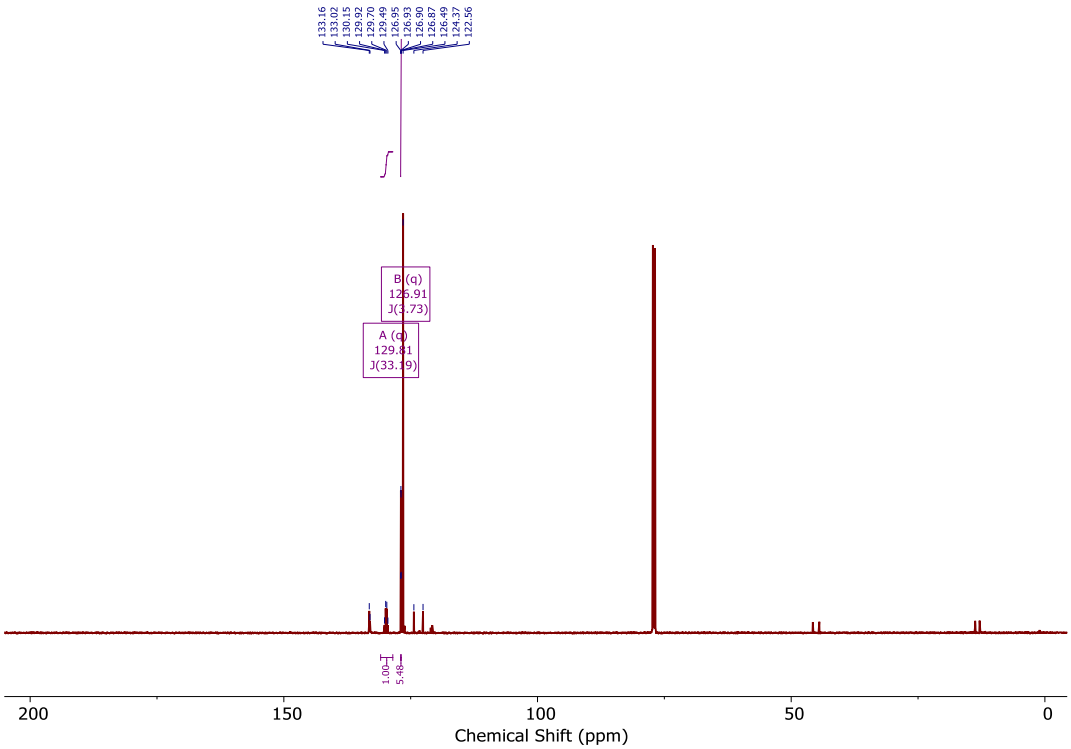

Figure C9. $^{13}C\{^{1}H\}$ NMR (151 MHz, $CDCl_3$) spectrum of 4-(trifluoromethyl)phenyl isoselenocyanate.

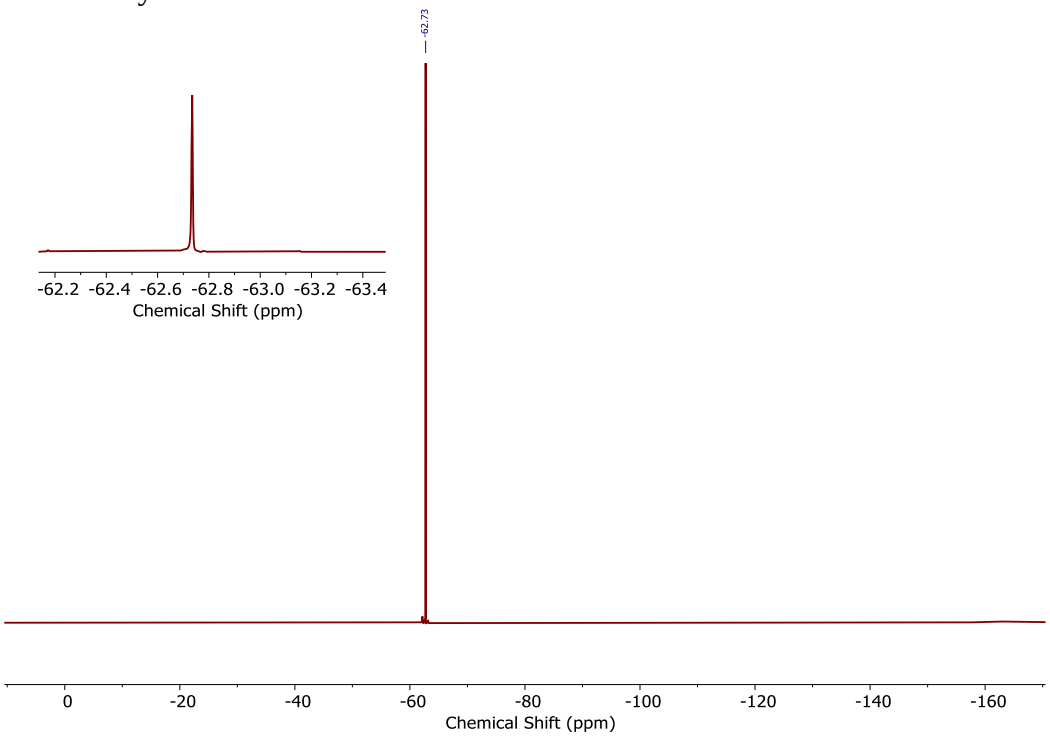

Figure C10. ^{19}F NMR (564 MHz, $CDCl_3$) spectrum of 4-(trifluoromethyl)phenyl isoselenocyanate.

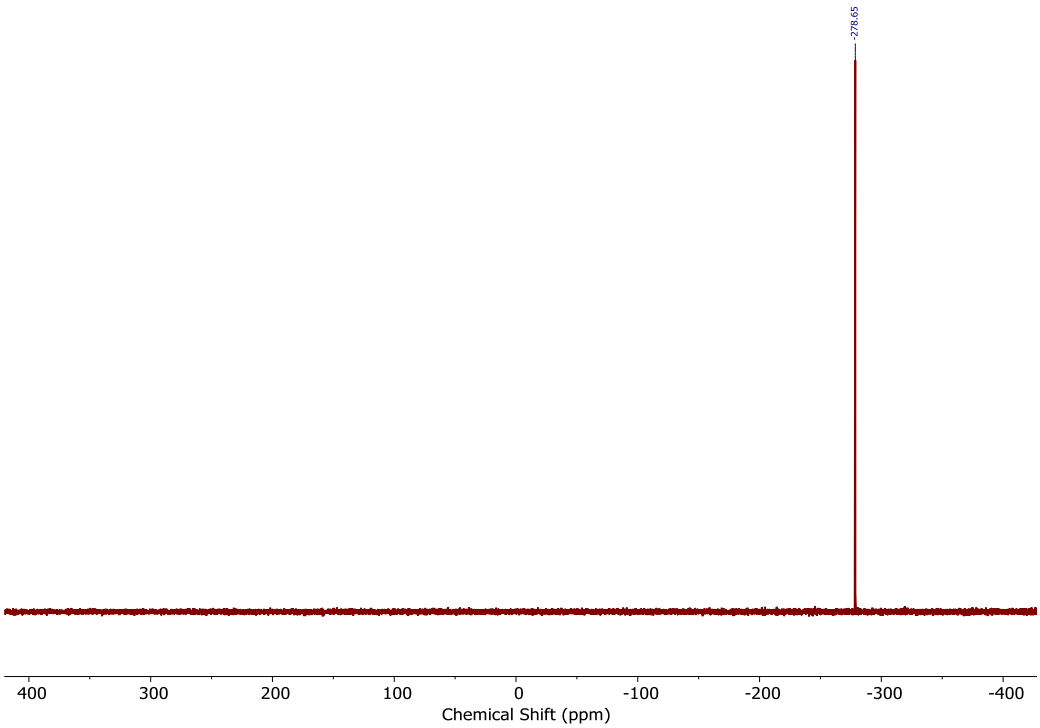

Figure C11. ^{77}Se NMR (115 MHz, $CDCl_3$) spectrum of 4-(trifluoromethyl)phenyl isoselenocyanate.

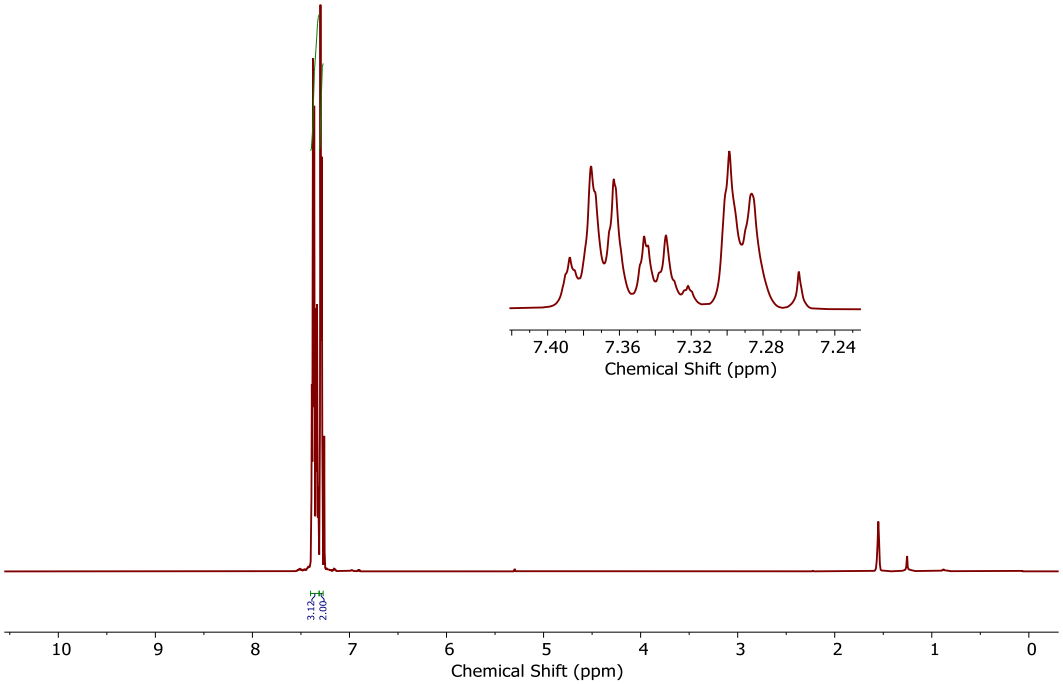

Figure C12. ^{1}H NMR (600 MHz, $CDCl_3$) spectrum of phenyl isoselenocyanate.

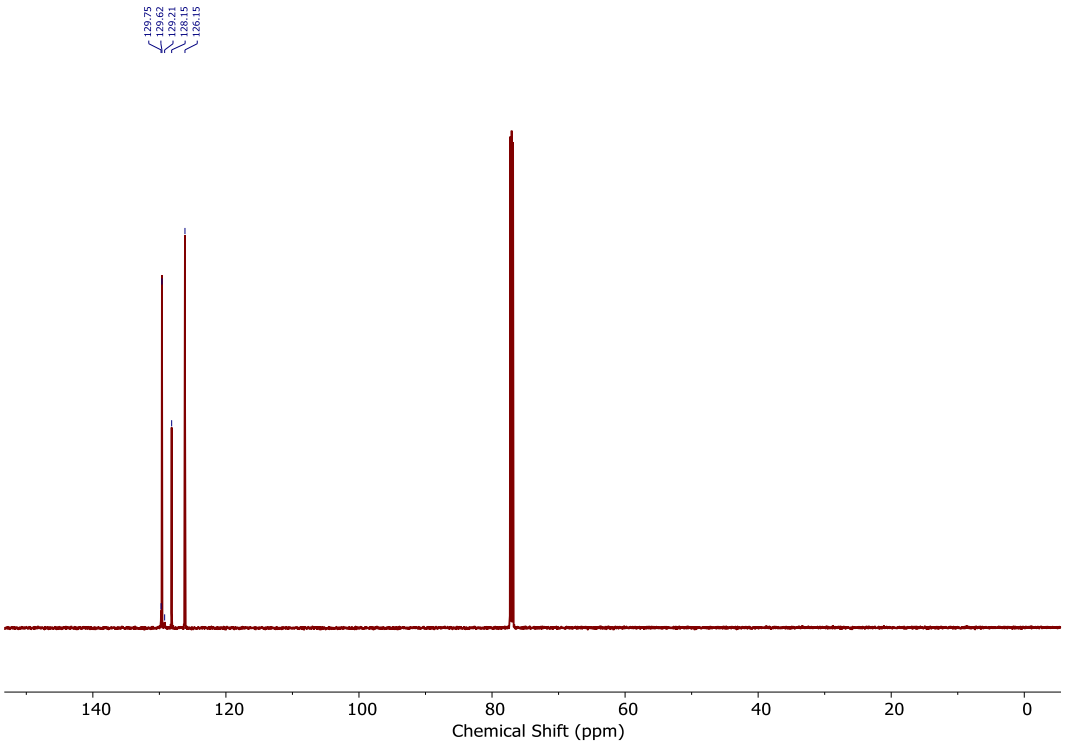

Figure C13. $^{13}C\{^{1}H\}$ NMR (151 MHz, $CDCl_3$) spectrum of phenyl isoselenocyanate.

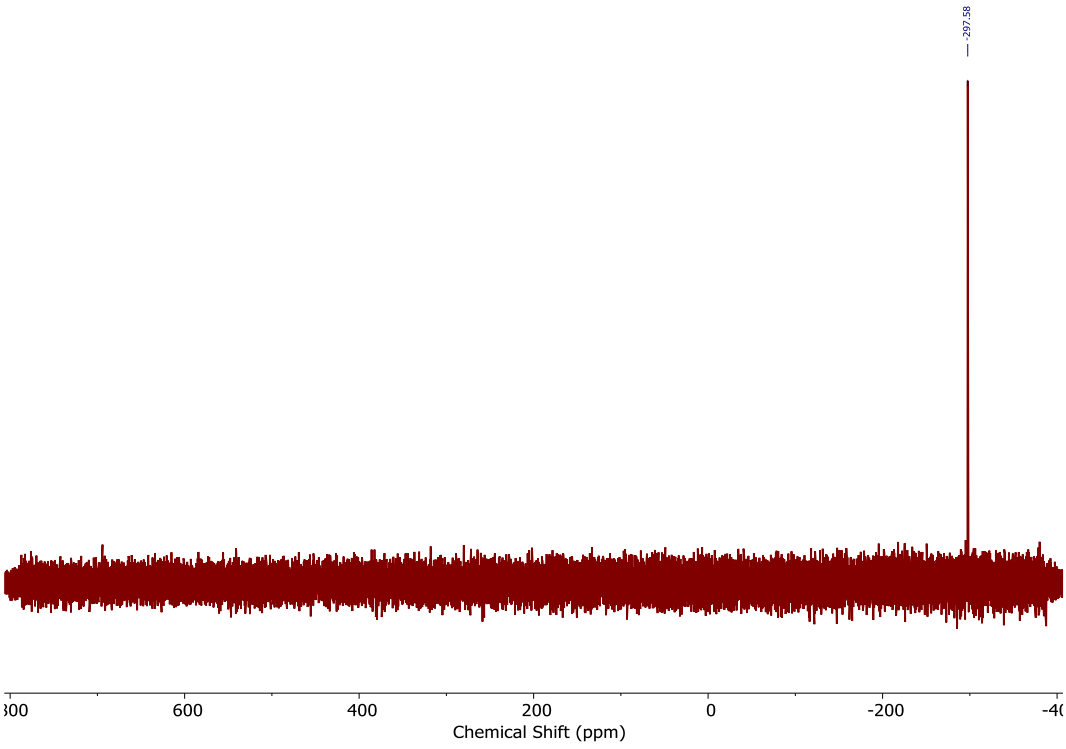

Figure C14. ^{77}Se NMR (115 MHz, $CDCl_3$) spectrum of phenyl isoselenocyanate.

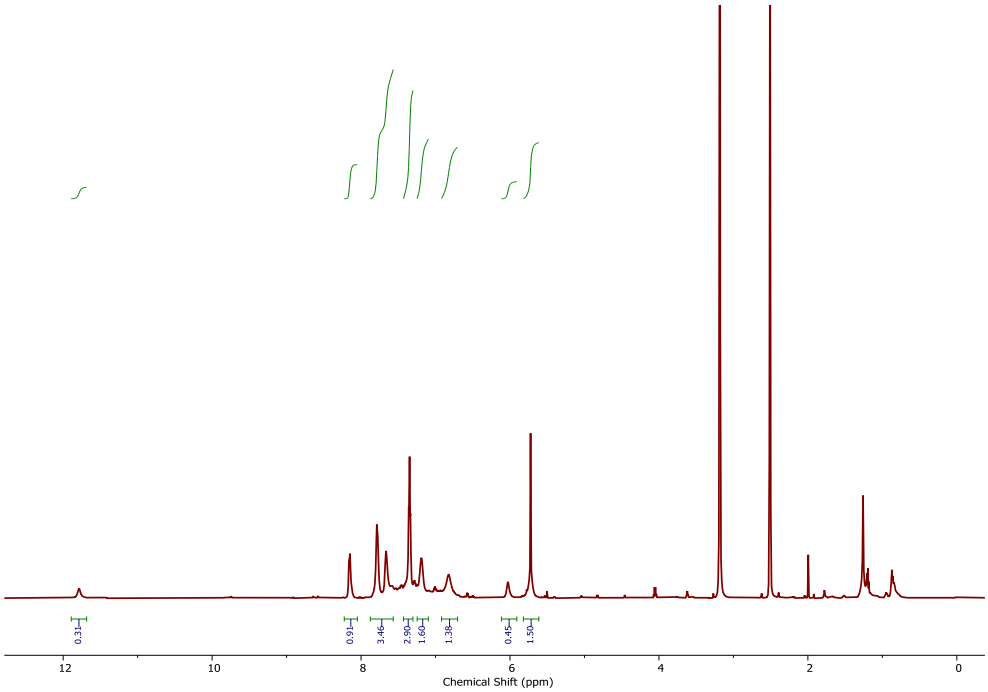

Figure C15. ^{1}H NMR (600 MHz, DMSO-d^{6}) spectrum of PhotoSeCM.

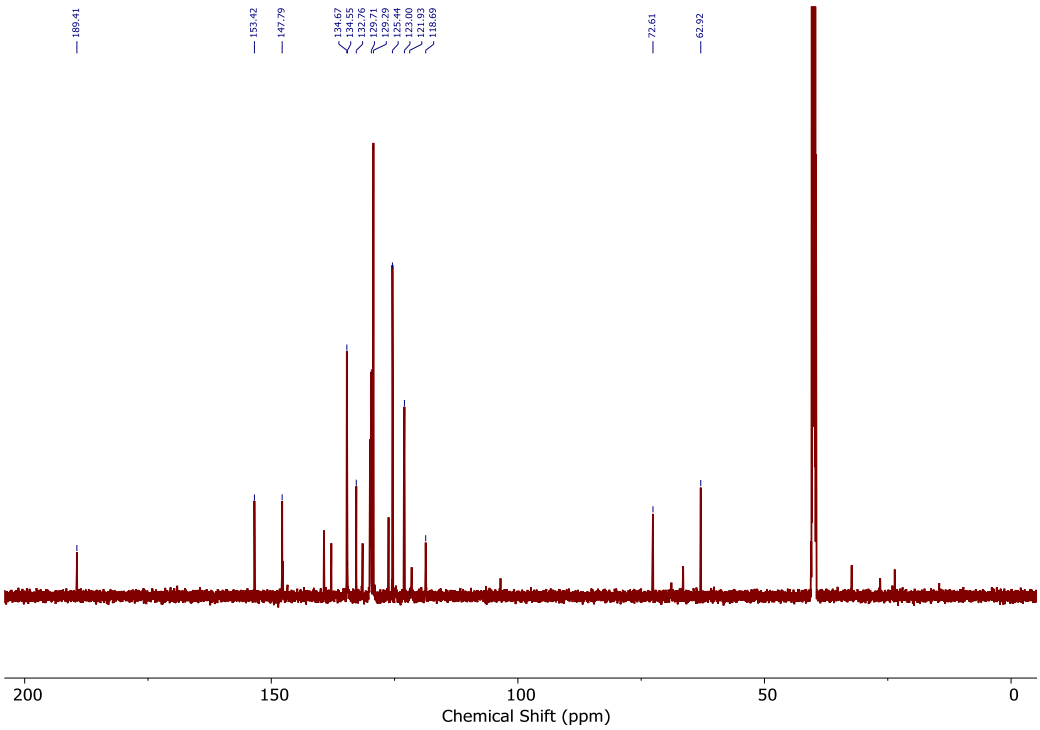

Figure C16. ^{13}C{^{1}H} NMR (151 MHz, DMSO-d^{6}) spectrum of PhotoSeCM.

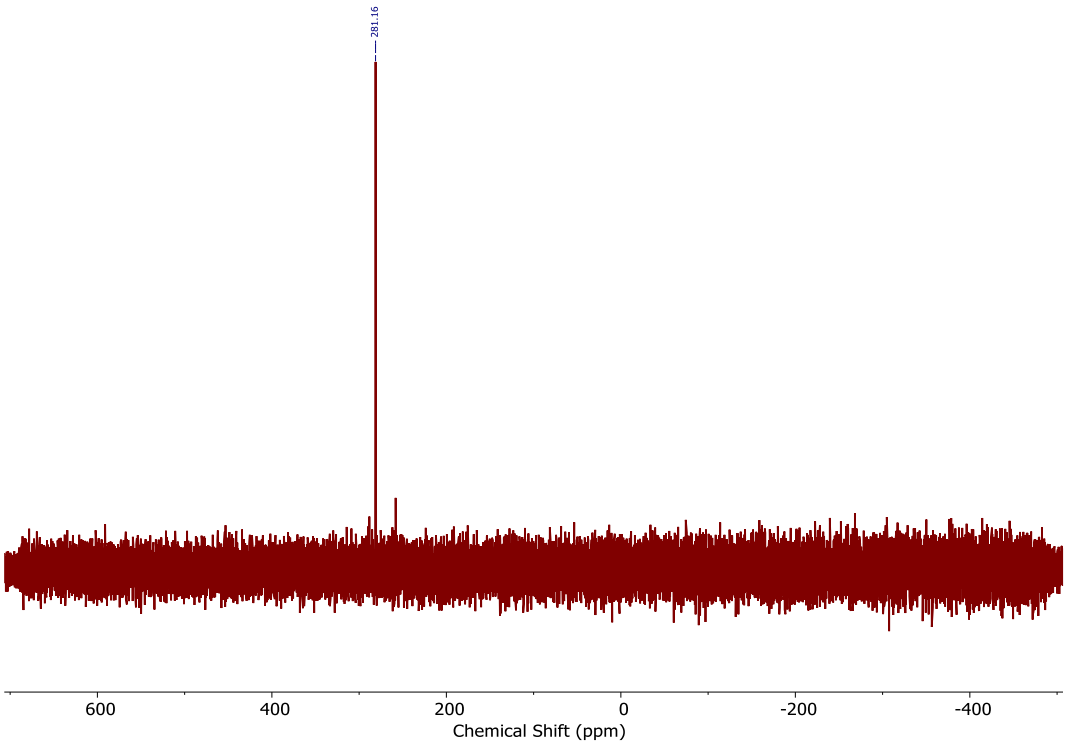

Figure C17. ^{77}Se NMR (115 MHz, DMSO-d^6) spectrum of PhotoSeCM.

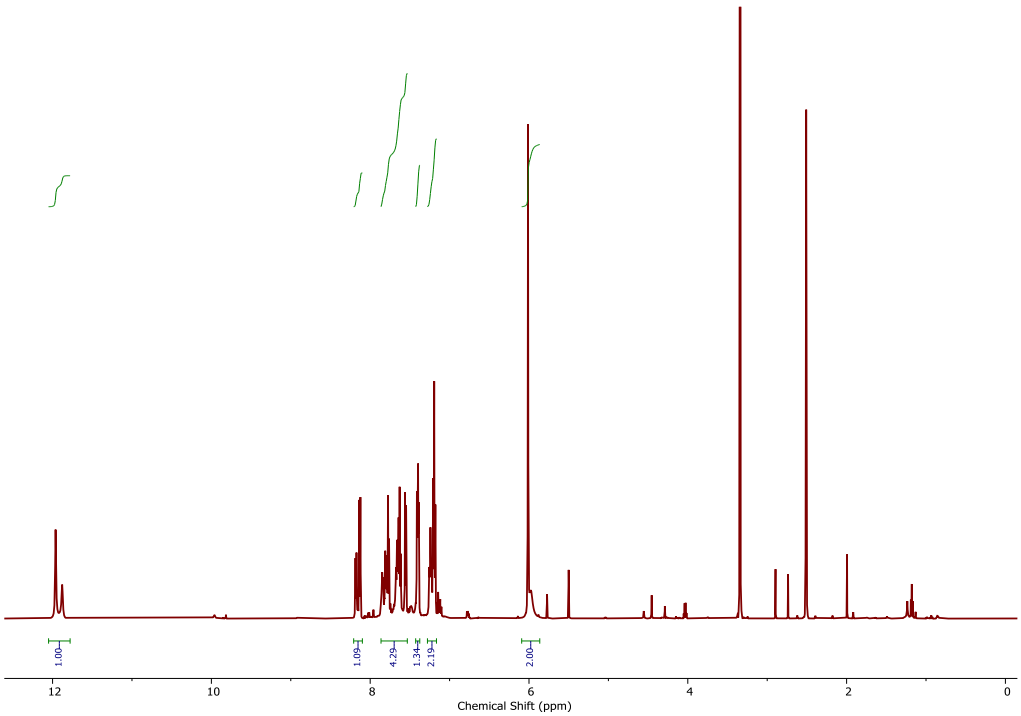

Figure C18. ^{1}H NMR (600 MHz, DMSO-d^6) spectrum of pF-PhotoSeCM.

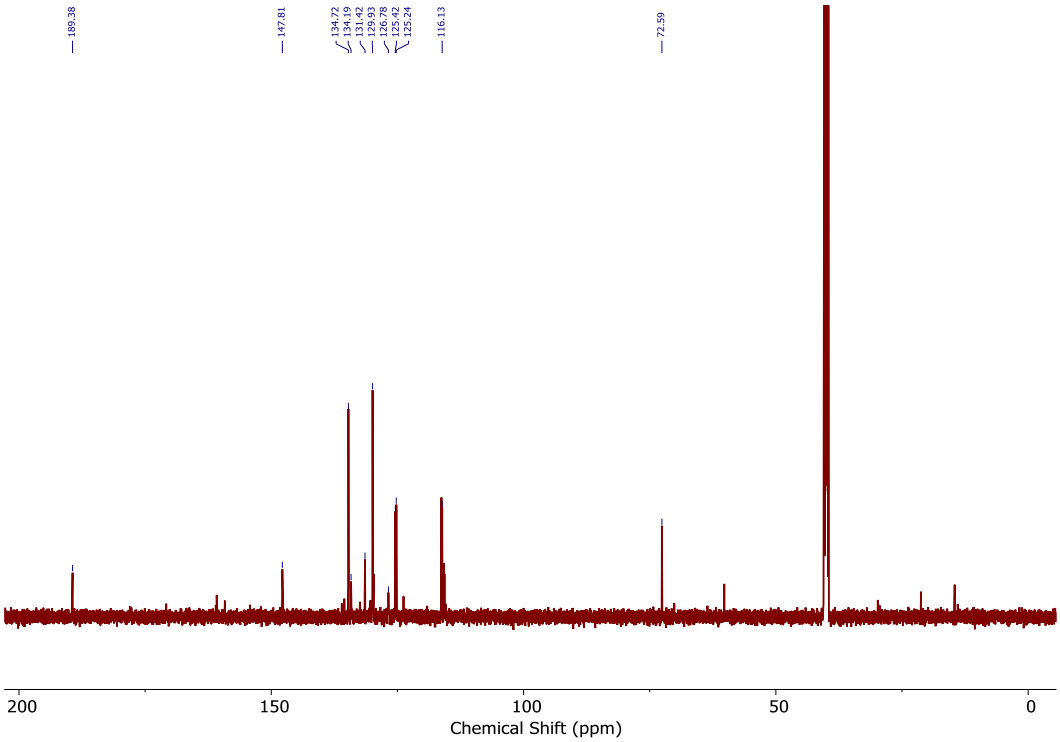

Figure C19. $^{13}C\{^{1}H\}$ NMR (151 MHz, DMSO-d^6) spectrum of pF-PhotoSeCM.

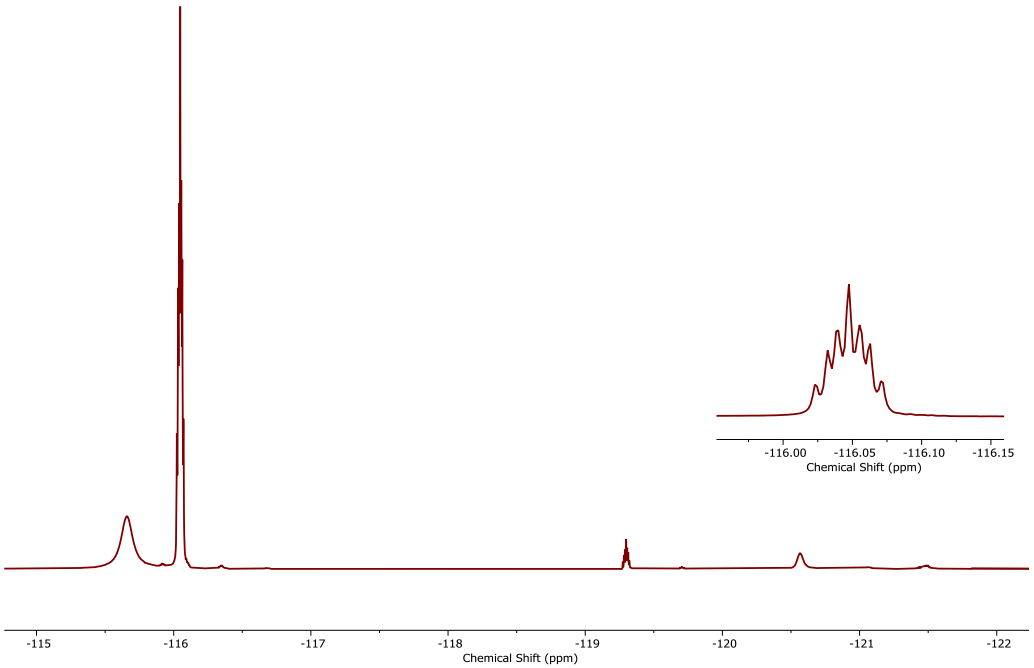

Figure C20. ^{19}F NMR (564 MHz, DMSO-d^6) spectrum of pF-PhotoSeCM.

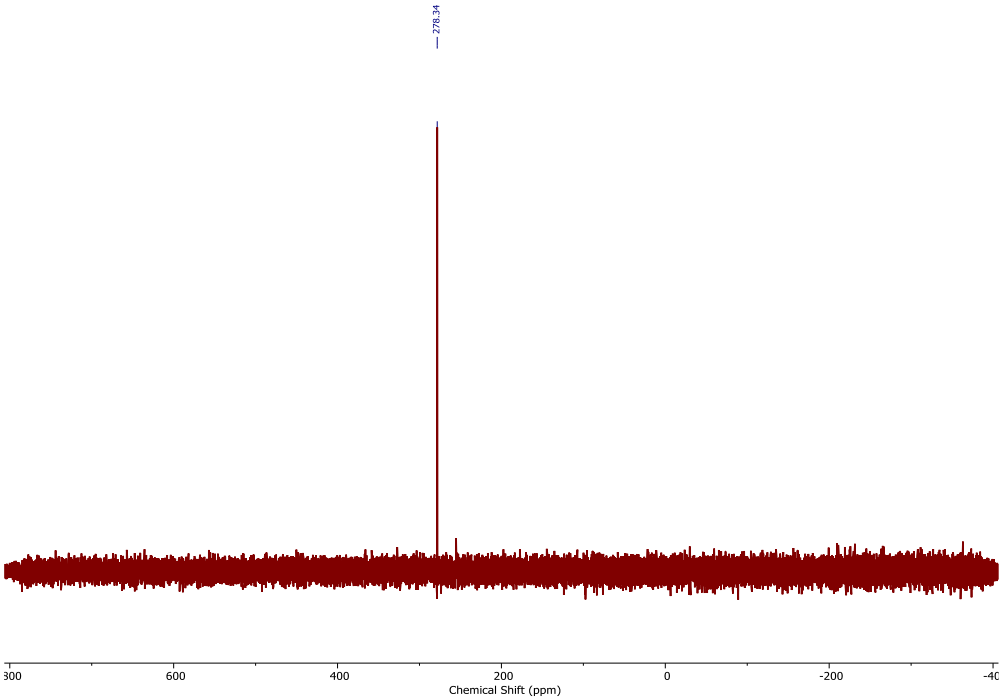

Figure C21. ^{77}Se NMR (115 MHz, DMSO-d^6) spectrum of pF-PhotoSeCM.

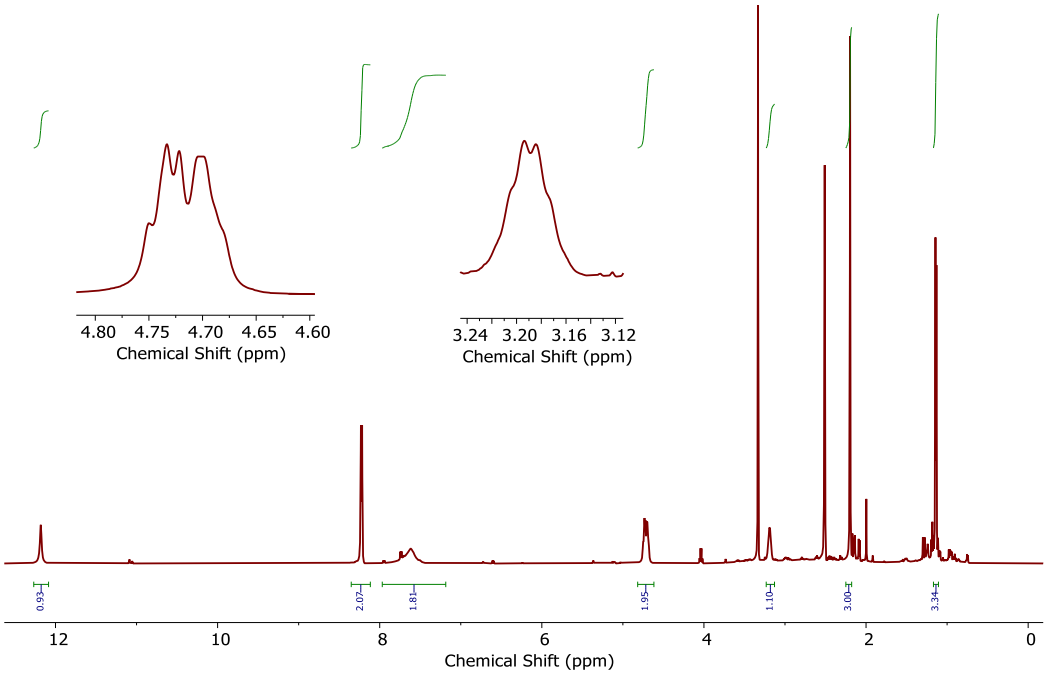

Figure C22. ^{1}H NMR (600 MHz, DMSO-d^6) spectrum of PNA-MeGKetoSeCM.

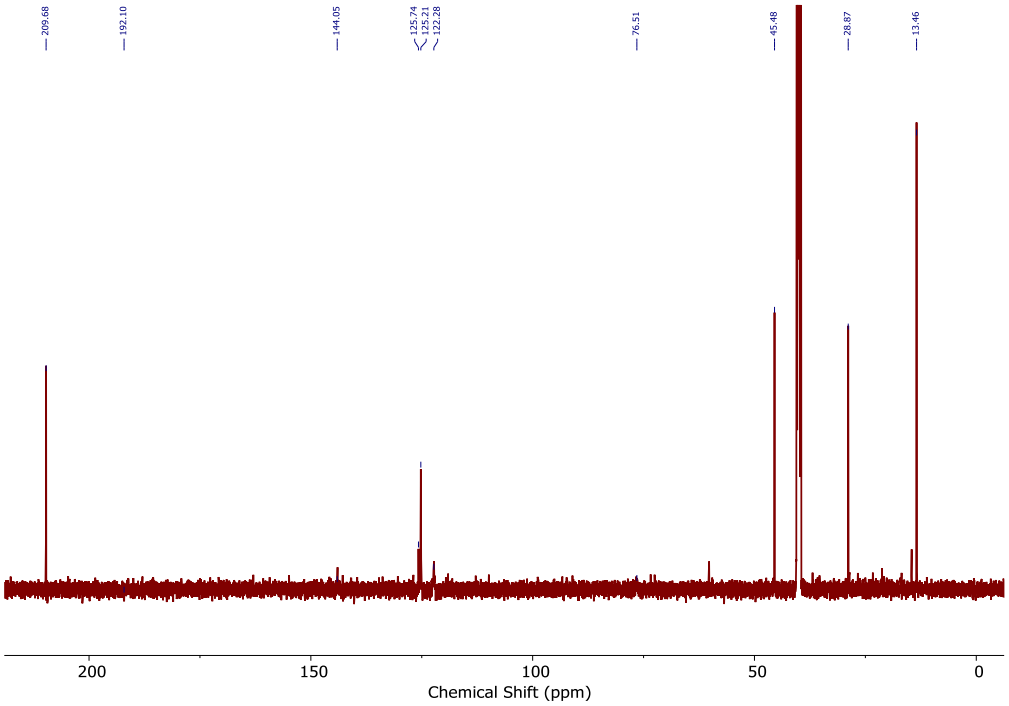

Figure C23. $^{13}C\{^{1}H\}$ NMR (151 MHz, DMSO-d^6) spectrum of PNA-MeGKetoSeCM.

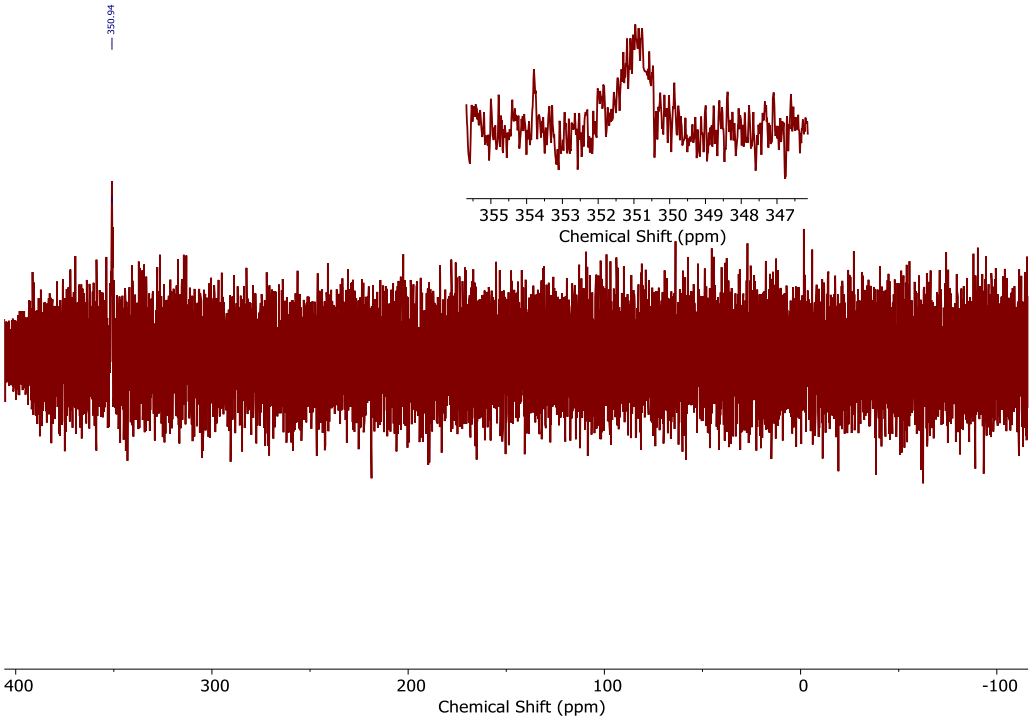

Figure C24. ^{77}Se NMR (115 MHz, DMSO-d^6) spectrum of PNA-MeGKetoSeCM.

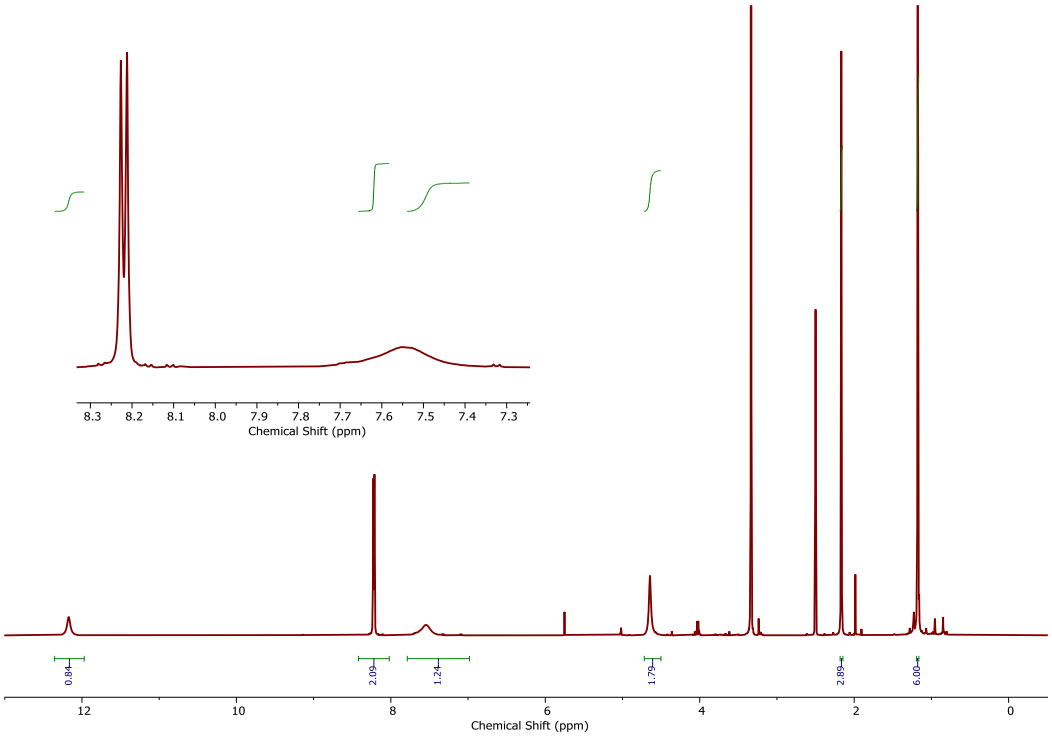

Figure C25. ^{1}H NMR (600 MHz, DMSO-d^{6}) spectrum of PNA-Me$_2$GKetoSeCM.

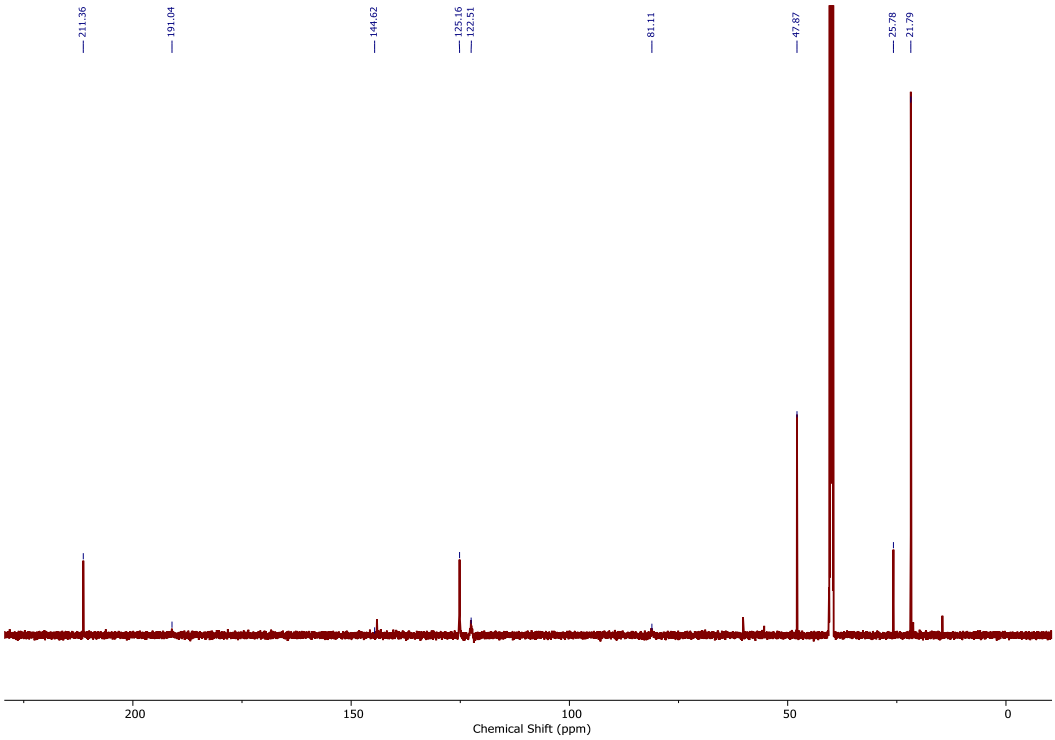

Figure C26. ^{13}C{^{1}H} NMR (151 MHz, DMSO-d^{6}) spectrum of PNA-Me$_2$GKetoSeCM.

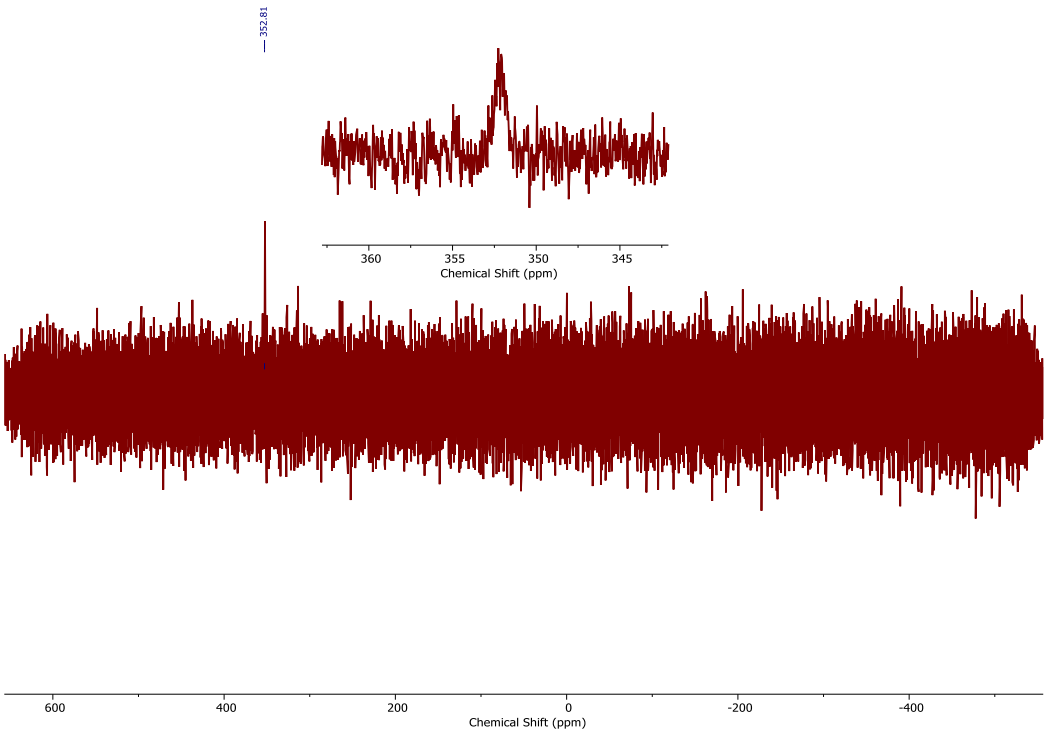

Figure C27. ^{77}Se NMR (115 MHz, DMSO-d^6) spectrum of PNA-Me$_2$GKetoSeCM.

Hydrolysis Studies

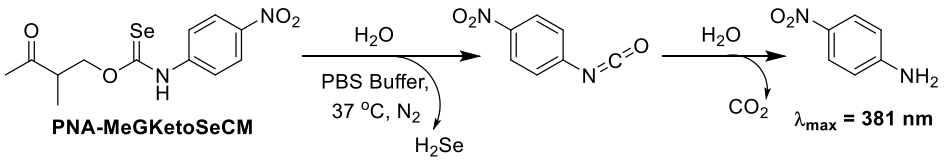

Scheme C4. Proposed general pathway of hydrolysis for GKSeCM compounds to produce H_2Se and 4-nitroaniline (PNA).

General hydrolysis procedure: A stock solution of the GKSeCM (10 mM in DMSO) was prepared in a glovebox in a GC vial along with a quartz cuvette (1 cm, septum cap, stir flea) containing PBS buffer (3.0 mL, pH 7.4, 10 mM). After removal from the glovebox, the cuvette was placed in the Cary 60 UV-vis spectrometer to warm to 37 °C while the experimental software was prepared: 650-250 nm scan window, 2 nm resolution, scan every 30 min. Once prepared, the baseline scan was taken, the GKSeCM was injected (20 µL, making 66 µM solution in cuvette), and the experiment was started. Over time, a decrease in absorbance at 335 nm (A_D) was observed along with an increase in absorbance

at 381 nm (A_P), signifying consumption of GKSeCM and production of PNA. When completed, this data was worked up so that A_P/A_D could be plotted against time to obtain observed rate constants (k_{obs}).

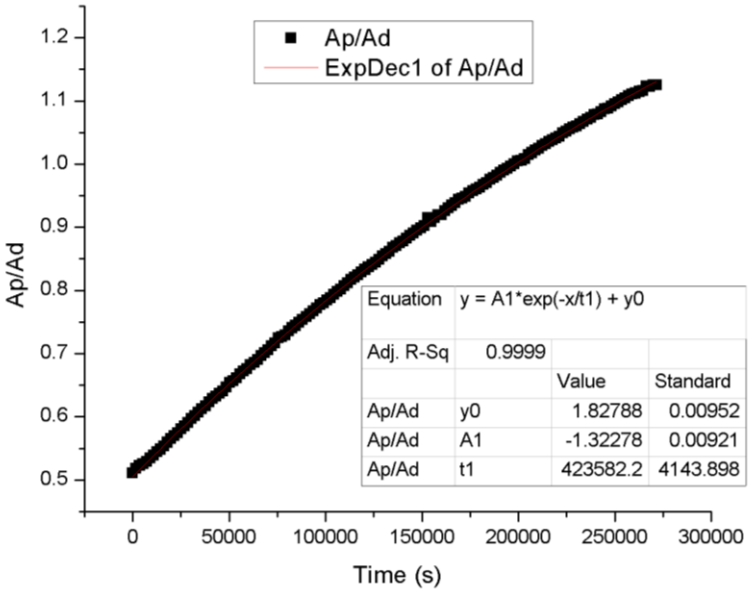

Figure C28. Representative hydrolysis curve from pH 6.0 sample with inset values from fitting an exponential decay function.

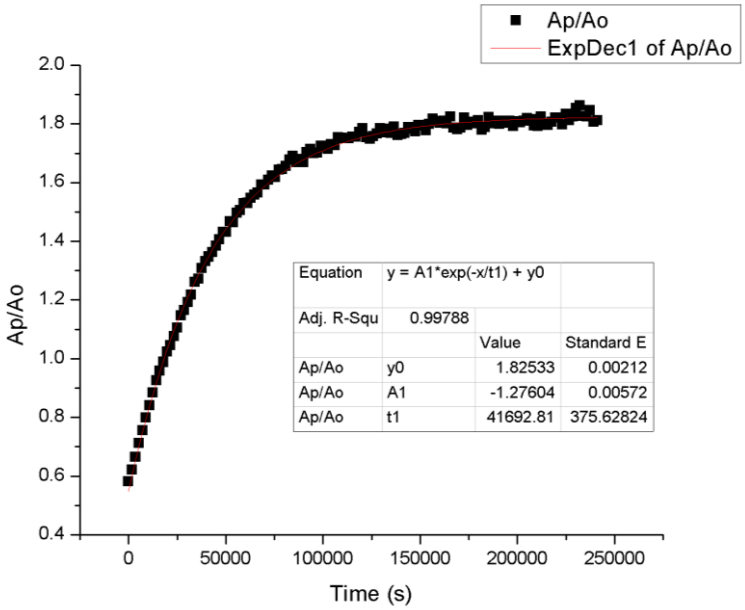

Figure C29. Representative hydrolysis curve from pH 7.4 sample with inset values from fitting an exponential decay function.

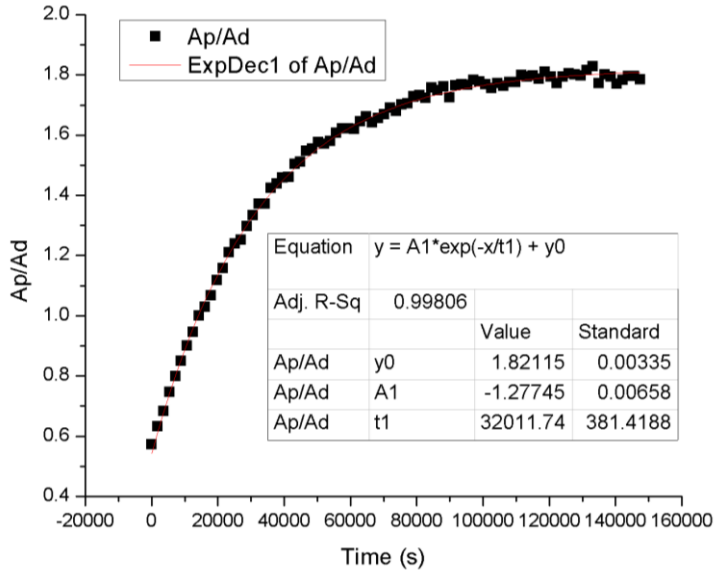

Figure C30. Representative hydrolysis curve from pH 8.0 sample with inset values from fitting an exponential decay function.

Table C1. Tabulated kinetic data from triplicate hydrolysis experiments at different pH.

pH 6.0	1	2	3	Avg	StDev	Err
t-value	423582.3	408372.9	416013.7	415989.6	6209.2	1%
kobs	2.361E-06	2.449E-06	2.404E-06	2.404E-06	3.59E-08	1%

pH 7.4	1	2	3	Avg	StDev	Err
t-value	41692.8	38275.3	39208.8	39725.6	1442.3	4%
kobs	2.398E-05	2.613E-05	2.550E-05	2.521E-05	9.00E-07	4%

pH 8.0	1	2	3	Avg	StDev	Err
t-value	28587.2	32011.8	32951.1	30299.5	1875.4	6%
kobs	3.498E-05	3.124E-05	3.035E-05	3.311E-05	2.01E-06	6%

Mechanistic Investigations via Alkylative Trapping

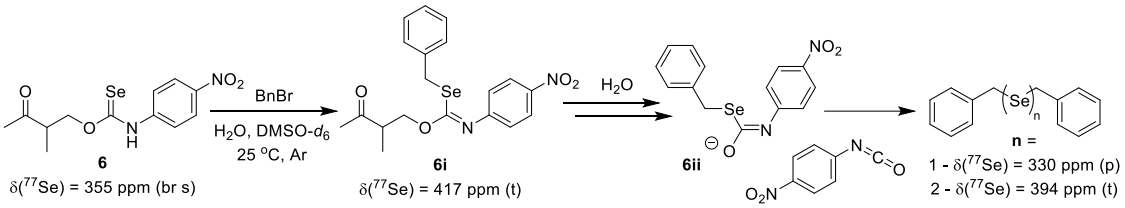

Scheme C5. Proposed mechanism of PNA-MeGKSeCM hydrolysis in the presence of alkylating agent benzyl bromide (BnBr).

Alkylative trapping procedure: In a glovebox, a stock solution (50 mM) of **6** was prepared in a GC vial in DMSO-d[6]; an NMR tube was then charged with an aliquot of this stock solution (0.50 mL), and the tube was septum-capped and tape-sealed before being removed from the box. Baseline scans were taken on the NMR spectrometer (^{1}H, ^{77}Se), then the tube was removed and received an injection of BnBr (2.5 equiv.) and then water (25 µL) that had been basified to pH 10 using NaOH. The tube was shaken and taped over the septum before being returned to the spectrometer for further scans; this reaction was monitored via the same nuclei over the next two days to show production of the alkylated selenide products.

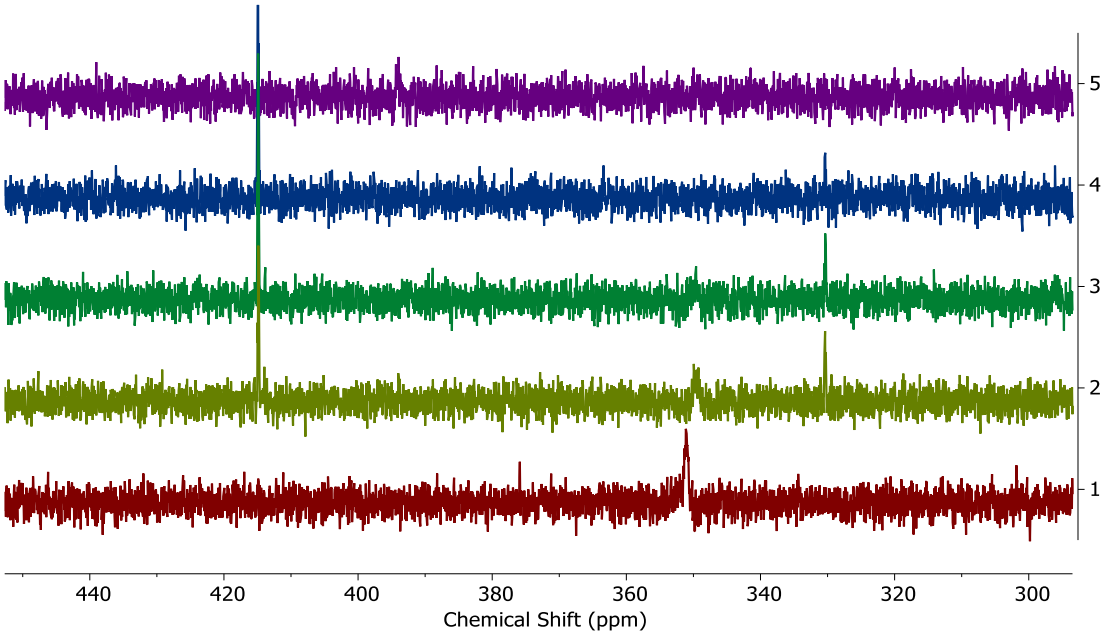

Figure C31. Recorded ^{77}Se NMR spectra of PNA-MeGKSeCM hydrolysis and alkylation over 48 h.

APPENDIX D

SUPPLEMENTARY MANUSCRIPT

Appendix D is a supplementary project on H_2S donors that was pursued before the investigations on H_2Se donor technology. This work played a part in inspiring my curiosity about other biologically important chalcogenide species and attracted me to this body of research. This appendix includes previously published and co-authored material from Cerda, M.M.; Newton, T.D.; Bolton, Zhao, Y.; Collins, B.K.; Hendon, C.H; Pluth, M.D. Dithioesters: simple, tunable, cysteine-selective H_2S donors. *Chem. Sci.* **2019**, *10*, 1773-1779. This manuscript was written by Dr. Matthew M. Cerda with editorial assistance from Professor Michael D. Pluth. The project in this chapter was conceived of by Dr. Matthew M. Cerda, Dr. Yu Zhao, and Professor Michael D. Pluth. The experimental work was performed by Dr. Matthew M. Cerda and Turner D. Newton. Computational work was performed by Brylee K. Collins and Dr. Christopher H. Hendon.

Introduction

Prevalent in the field of polymer chemistry, dithioesters are utilized as chain transfer agents in reversible addition-fragmentation chain transfer (RAFT) polymerizations.[100] Arising from the ability to readily react with propagating radical monomers, the design of thiocarbonyl-containing motifs such as dithioesters, trithiocarbonates, and dithiocarbamates has been well studied to enhance the RAFT polymerization of various monomers.[101-102] We recently demonstrated that related thionoesters, which are structural isomers of thioesters bearing a thiocarbonyl motif, undergo a chemoselective reaction with cysteine to generate a dihydrothiazole and hydrogen sulfide (H_2S).[103] Despite recent advancements in the synthesis of thionoesters,[104] the ability to prepare a diverse library of thionoester-based H_2S donors is limited by the availability of stable, readily-accessible starting materials. However, based on structural similarities between thionoesters and dithioesters, we hypothesized that dithioesters could provide similar reactivity in the presence of cysteine and allow for the

development of tunable H_2S donors with precise control over H_2S release rates and efficiencies.

Complementing carbon monoxide and nitric oxide, hydrogen sulfide (H_2S) is now classified as an important biological signaling molecule.[105] Commonly referred to as gasotransmitters, these small, gaseous molecules are produced endogenously, readily permeate cell membranes, and exert physiological responses upon binding to cellular and/or molecular targets.[106] The involvement of H_2S-mediated signaling has been observed in a variety of physiological processes such as vasodilation,[107] angiogenesis,[108] and scavenging of reactive oxygen species.[109] In recent years, researchers have become increasingly interested in utilizing H_2S donors for the development of both important research tools and novel therapeutics.[110-111] Towards this goal, researchers have relied heavily on the use of sodium hydrosulfide (NaSH), which is a water-soluble source of H_2S, for preliminary studies. However, a comparison between H_2S production from native enzymes including cystathionine-β-synthase and cystathionine-γ-lyase against exogenous administration of H_2S (via NaSH) has revealed stark differences which should be taken into consideration.[112] The dissolution of NaSH in buffered solutions leads to a rapid, almost spontaneous increase in local H_2S concentration,[113] whereas endogenous H_2S production occurs at a slower, yet gradual rate. To address this issue, researchers have developed synthetic H_2S donors, which release H_2S either passively via hydrolysis or in the presence of a specific analyte at rates comparable to enzymatic H_2S production (Figure D1).[114-117]

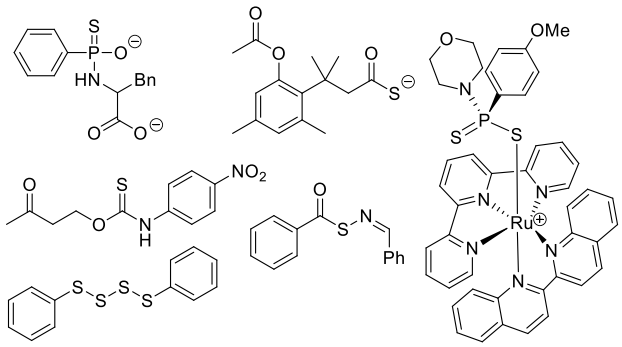

Figure D1. Selected examples of synthetic H_2S donors.

Drawing parallels to the dissolution of NaSH, small molecules derived from dithiole-3-thione[118] and phosphorodithioate[119-120] motifs respectively have been synthesized as hydrolysis-activated H_2S donors, although we note the overall low H_2S-releasing efficiencies from these donors. Towards improving releasing yields and tuning rates of H_2S release, analyte-responsive small molecules have been prepared to release H_2S as a function of pH,[121] in the presence of native enzymes,[122] and upon irradiation with light.[123-125] Initially reported by our group,[126] the conversion of carbonyl sulfide (COS) to H_2S by carbonic anhydrase has been used to access a library of COS/H_2S donors.[127-129] Inspired by the endogenous production of H_2S via enzymatic conversion of cysteine, a number of thiol-triggered H_2S donors have been reported. Abundant in nature, organic polysulfides[130] have been shown to release H_2S in the presence of biological thiols including cysteine[131] and reduced glutathione (GSH).[132] The generation of persulfides, an important class of biologically-relevant reactive sulfur species,[133] via thiol-mediated reduction has been used to prepare a series of synthetic H_2S donors with potent protective effects against myocardial-ischemia reperfusion injury.[124] Similarly, the generation of *N*-mercaptan species in the presence of thiols has been demonstrated as a viable platform for H_2S delivery with tunable releasing kinetics.[134-136] Under physiological conditions, thionoesters react rapidly with cysteine via a native chemical ligation-like mechanism to afford an equivalent of phenol, H_2S, and a cysteine-derived dihydrothiazole (Figure D2a). Although dithioesters have been used to prepare polymeric H_2S donors,[137-138] direct use of this motif as an H_2S donor scaffold has not been reported. Herein, we present our findings on the development of dithioesters as novel, cysteine-triggered H_2S donors (Figure D2b). We demonstrate the release of H_2S in the presence of cysteine from a representative (*bis*)phenyl dithioester with a comprehensive kinetic analysis. Additionally, we demonstrate the ability to tune the rate of H_2S release from dithioesters via simple alkyl functionalization.

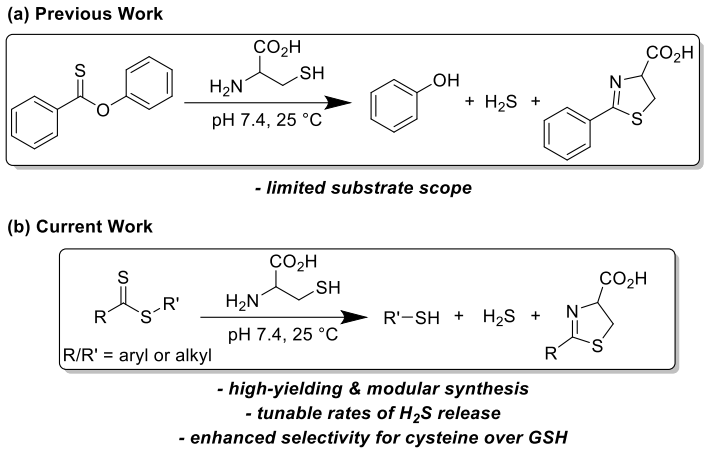

Figure D2. a) Mechanism of cysteine-triggered H_2S release from thionoesters. b) Cysteine-triggered H_2S release from dithioesters.

Results and Discussion

Building upon our previous work, we hypothesized that the intermediate dithioester formed during the chemoselective reaction of cysteine with thionoesters could provide a platform for future investigations leading to the development of novel, cysteine-triggered H_2S donors. Unfortunately, the functionalization of thionoester-based H_2S donors is hindered by a limited number of stable, isolable alkyl chlorothionoformates. By contrast, the enhanced reactivity of Lawesson's reagent toward thioesters over esters allows for convenient functionalization and synthetic accessibility of various dithioesters.[139] To prepare different dithioesters, we treated the desired thiol with the desired acid chloride in the presence of triethylamine followed by thionation with Lawesson's reagent to access to a library of dithioesters with good to excellent yields (Scheme D1). The modularity of this synthetic route readily allows for the introduction of various functional groups and can be expanded upon to include payloads of interest including fluorophores and known therapeutics for the development of H_2S-releasing prodrugs. In the interest of accessing tunable H_2S donors, we hypothesized modulation of thiocarbonyl electrophilicity and thiolate leaving group ability would directly alter the rates of cysteine-triggered H_2S release from dithioesters.

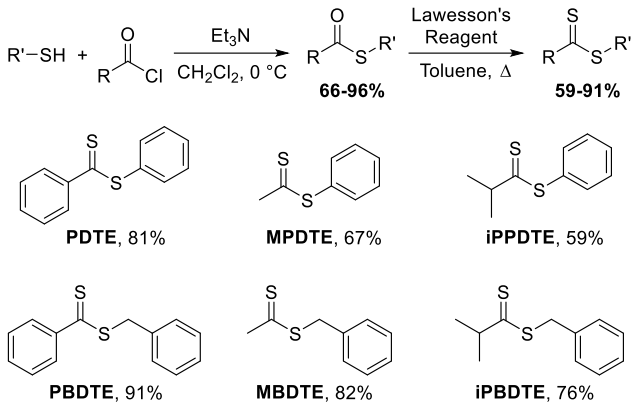

Scheme D1. General synthesis of dithioesters.

With synthesized dithioesters in hand, we began our studies by examining the reactivity of **PDTE** (25 μM) as a representative dithioester towards various concentrations of cysteine (250, 500, 1000, and 1250 μM) and monitoring the release of H_2S via the spectrophotometric methylene blue assay, which allows for H_2S quantification (Figure D3a).[140] Consistent with our hypothesis, we observed increasing amounts of H_2S released with increasing cysteine concentrations from **PDTE**. To quantify the H_2S-releasing efficiency, we used a methylene blue calibration curve generated with NaSH (see Supporting Information) and we found 25 μM **PDTE** released approximately 17 μM H_2S after 1 h, which corresponds to a releasing efficiency of ~68%. Under identical conditions, we note a slight decrease in H_2S-releasing efficiency between dithioesters and thionoesters (80%), although both of these constructs are efficient H_2S-releasing motifs. To quantify the rate of H_2S release, we were able to fit these releasing curves and obtain pseudo-first order rate constants (k_{obs}). A plot of log[Cys] versus log(k_{obs}) provided a linear plot with slope near one, which suggests the overall reaction is first order in cysteine and proceeds via a mechanism similar to the reaction of thionoesters with cysteine (Figure D3b). A plot of [Cys] versus k_{obs} yielded a second-order rate constant (k_2) of 1.8 ± 0.1 M^{-1} s^{-1} (Figure D3c), which is approximately five times slower relative to cysteine-triggered H2S from thionoesters (9.1 ± 0.3 M^{-1} s^{-1}). This difference in H_2S-releasing kinetics prompted us to further investigate the kinetics of cysteine-triggered H_2S release from dithioesters and elucidate potential mechanistic differences between both classes of H_2S donors.

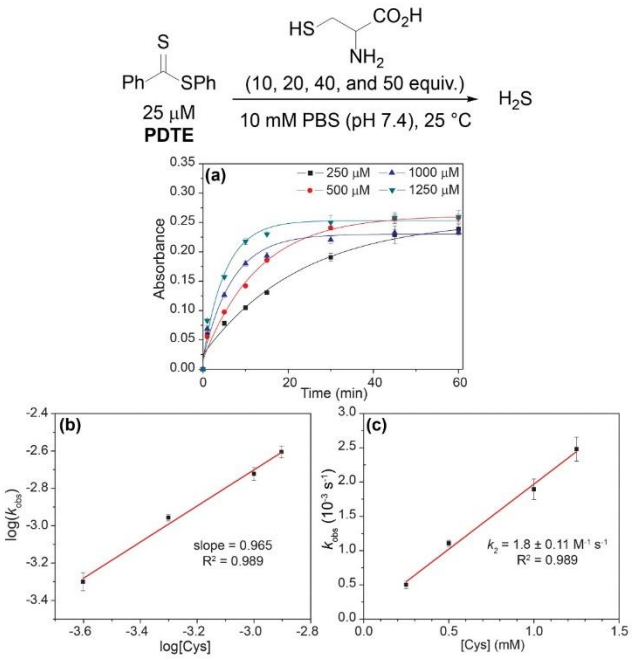

Figure D3. (a) Release of H_2S from **PDTE** (25 μM) in the presence of increasing cysteine concentrations (250, 500, 1000, and 1250 μM). (b) Plot of log(k_{obs}) vs. log([Cys]). (c) Plot of k_{obs} vs. [Cys].

To further probe the reactivity of dithioesters with respect to H_2S release, we next investigated the effect of cysteine derivatives and related thiol-based nucleophiles on H_2S release from **PDTE** (Figure D4). In the absence of nucleophiles, we did not observe H_2S release under hydrolytic conditions. Although the conversion of a thiocarbonyl to the corresponding carbonyl is thermodynamically favorable with an enthalpic gain of ~43 kcal/mol when comparing C=S versus C=O bond strengths, the hydrolysis of dithioesters is a slow process and can be considered neglible when considering the rate of cysteine-triggered H_2S release.[141-142] Further supporting a similar mechanism of cysteine-triggered H_2S release between thionoesters and dithioesters, masking of either the thiol or amine moieties in cysteine completely abolished H_2S release from **PDTE**. Additionally, the use of cysteine methyl ester did not affect H_2S release when compared to H_2S release in the presence of cysteine. To assess the effect of cysteine analogues on H_2S release, we measured H_2S release in the presence of homocysteine and penicillamine. Interestingly, we observed a significant reduction in the H_2S release rate in the presence of homocysteine relative to cysteine-triggered H_2S release. In the presence of penicillamine,

we failed to observe significant H_2S release, which we attribute to a reduction in nucleophilicity due to the presence of geminal methyl groups

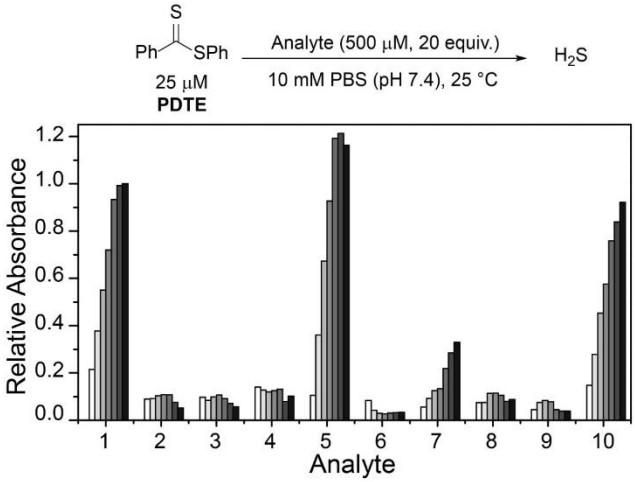

Figure D4. Selectivity of H_2S release from **PDTE** in the presence of different analytes. Data were acquired at 1, 5, 10, 15, 30, 45, and 60 min. Methylene blue absorbance values are relative to the maximum absorbance value obtained from H_2S release in the presence of cysteine (1). Analytes: H_2O (2), *N*-acetyl-L-cysteine (3), *S*-methyl-L-cysteine (4), L-cysteine methyl ester hydrochloride (5), *N*-acetyl-L-cysteine methyl ester (6), DL-homocysteine (7), DL-penicillamine (8), GSH (9), cysteine + 1 mM GSH (10).

We next examined the release of H_2S from **PDTE** in the presence of reduced glutathione (GSH), the most abundant biological thiol to determine the effect of competitive thiols on H_2S release. In the presence of 500 μM GSH, we did not observe significant H_2S release, but also could not rule out that transthioesterification by GSH, which would result in consumption of the dithioester moiety with a lack of H_2S release. Considering the nucleophilicity of the departing thiophenol, we hypothesized that the reversibility of transthioesterification is likely to be more efficient for dithioesters than for thionoesters, which should result in enhanced selectivity for cysteine over GSH. To test this hypothesis, we measured H_2S release from **PDTE** in the presence of 500 μM cysteine and 1 mM GSH. In support of the expected enhanced reversibility, we observed minimal change on the cysteine-triggered H_2S release from **PDTE** even in the presence of excess GSH. This presents a considerable advancement over the thionoester scaffold, which yielded a decreased level of H_2S-releasing efficiency in the presence of GSH and cysteine. Taken together, these results demonstrate the selectivity of the dithioester

scaffold for cysteine over other thiol-based nucleophiles including GSH and we proposed the following mechanism of H_2S release (Scheme D2).

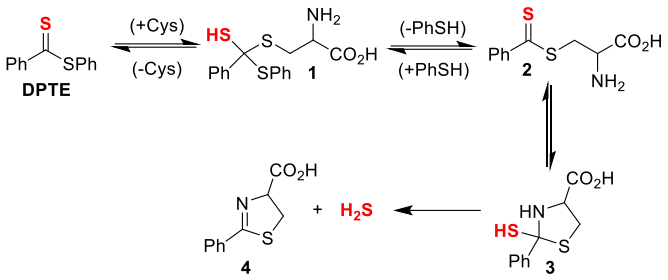

Scheme D2. Proposed mechanism of release of H_2S from **PDTE** in the presence of cysteine

Initial nucleophilic attack by cysteine on **PDTE** generates tetrahedral intermediate **1**, which collapses upon thiocarbonyl formation and extrusion of thiophenol to yield intermediate **2**. Nucleophilic attack by the pendant amine generates intermediate **3**, which extrudes H_2S upon formation of dihydrothiazole **4**. Based on the neglible loss in H_2S-releasing efficiency in the presence of excess GSH, the generation of **1** and **2** is likely highly reversible and could provide enhanced selectivity of the dithioester moiety for cysteine. In the mechanism of cysteine-triggered release of H_2S from thionoesters, the poor nucleophilicity of the departing alcohol likely impedes formation of the initial thionoester. In our proposed mechanism of H_2S release from dithioesters, the departing thiolate bears enhanced nucleophilicity and likely reacts with the intermediate dithioester to regenerate the initial dithioester effectively reversing cysteine addition. Additionally, the enhanced reversibility of transdithioesterifcation supports the considerably slower kinetics between dithioesters and thionoesters. Taken together, we hypothesized this enhanced reversibility would result in the initial nucleophilic attack by cysteine being the rate-determining step of cysteine-triggered H_2S release from dithioesters.

To confirm the formation of a cysteine-based dihydrothiazole, **PDTE** (100 μM) was treated with L-cysteine methyl ester (2 mM, 20 equiv.) and a reaction aliquot after 1 h was subjected to HPLC analysis (see Supporting Information). In agreement with our proposed mechanism, the HPLC analysis revealed the formation of the expected dihydrothiazole in ~61% yield, which is consistent with the H_2S-releasing efficiency of

PDTE as measured via the methylene blue assay. To gain insights on the rate-determining step, we measured the effect of temperature on the rate of H_2S release from **PDTE** (25 μM) in the presence of cysteine (500 μM, 20 equiv.) (Figure D5). If nucleophilic attack by cysteine on **PDTE** is the rate-determining step of the reaction, we would expect to observe an entropy of activation $\Delta S^{\ddagger}$) of approximately -20 eu, which would be characteristic of a bimolecular reaction.[143-144]

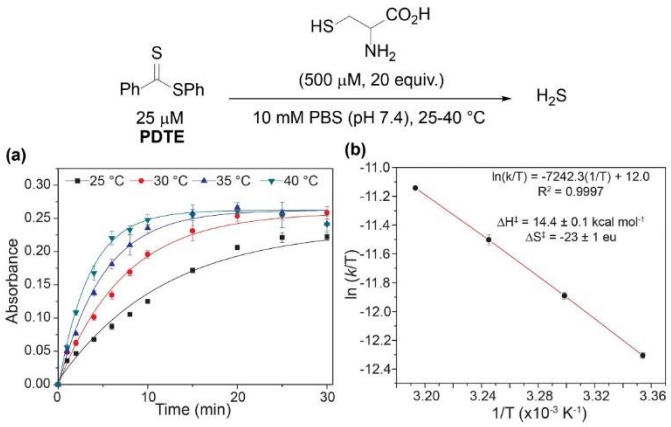

Figure D5. (a) Effect of temperature on rate of H_2S release from **PDTE** (25 μM) in the presence of cysteine (500 μM, 20 equiv). (b) Eyring analysis of cysteine-triggered H_2S release from **PDTE**.

Upon measuring the rates of H_2S release at different temperatures, we constructed an Eyring plot using the obtained k_{obs} values, which afforded $\Delta S^{\ddagger}$ = -23 ± 1 eu. The observed $\Delta S^{\ddagger}$ supports our mechanistic hypothesis and is consistent with the initial addition of cysteine to the dithioester to generate **1** being the rate-determining step of cysteine-triggered H_2S release from dithioesters. In the reaction of thionoesters with cysteine, we interpreted an experimentally-determined $\Delta S^{\ddagger}$ = -38 ± 3 eu to suggest the intramolecular cyclization as the rate determining step. In comparison between both mechanisms, by simply altering the nucleophilicity of the leaving group (i.e. alcohol vs. thiol) we have shunted the rate-determining step. Additionally, our results suggest cysteine-triggered H_2S release from dithioesters and native chemical ligation share a similar rate-determining step.

To complement our experimental results, we used density functional theory (DFT) to examine the potential energy surface for H_2S release from dithioesters. Because

PDTE was used for our experimental mechanistic investigations, we chose to investigate the reaction of **PDTE** with cysteine thiolate using Gaussian 09 at the B3LYP/6-311++G(d,p) level of theory applying the IEF-PCM water solvation model. We found that the initial nucleophilic attack by cysteine thiolate on **PDTE** resulted in an activation barrier of 19.1 kcal/mol, which was the highest barrier on the reaction coordinate and qualitatively agrees with the experimentally-observed $\Delta H^{\ddagger}$ of 14.4 kcal/mol. The resultant transthioesterified cysteine adduct is 3.7 kcal/mol more stable than the **PDTE** starting material, and subsequently undergoes an intramolecular S to N thioacyl transfer reaction with an associated barrier of 8.9 kcal/mol, resulting in the final and more thermodynamically-favorable dihydrothiazole product.

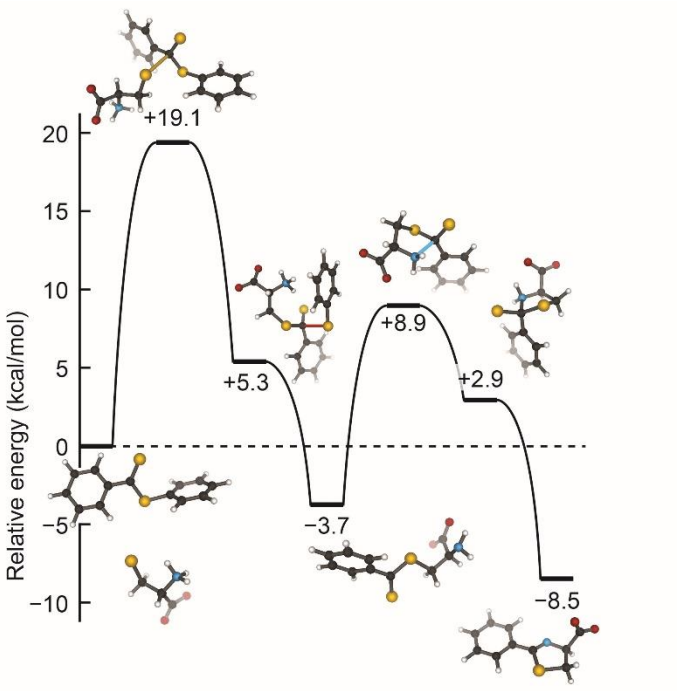

Figure D6. Potential energy surface for the attack of cysteine thiolate on **PDTE**. Calculations were performed in Gaussian 09 at the B3LYP/6-311++G(d,p) level of theory applying the IEF-PCM water solvation model.

The ease of synthesis of dithioester compounds also enabled further investigation into the effect of alkyl functionalization on H_2S release. We hypothesized that the electrophilicity at the thiocarbonyl position could be modified directly by introducing various alkyl, and thus alter the rate of H_2S release. Additionally, we hypothesized that

modification of the departing thiolate nucleophilicity would also alter the rate of H_2S release from dithioesters. We anticipated the introduction of inductively donating alkyl groups, such as methyl and isopropyl, would decrease the thiocarbonyl electrophilicity and resulting in decreased rates of H_2S release. Additionally, we anticipated that replacement of thiophenol with benzyl mercaptan would result in decreased rates of H_2S release due to the enhanced nucleophilicity of benzyl mercaptan over thiophenol. To test our hypotheses, we measured H_2S release from our library of alkyl functionalized dithioesters (25 μM) in the presence of cysteine (500 μM, 20 equiv.) (Figure D7).

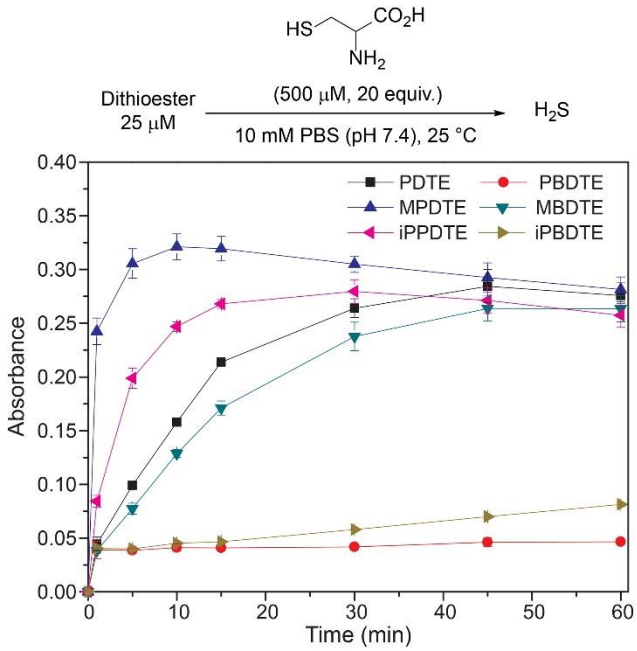

Figure D7. Effect of alkyl functionalization on the rate of H_2S release from dithioesters.

Contrary to our initial hypothesis, the incorporation of inductively-donating alkyl groups led to enhanced rates of H_2S release relative to **PDTE**. To better understand the apparent releasing trends, we considered the stability of the charge-separated thiocarbonyl motif and the effect of different alkyl groups (Figure D8). In the case of **PDTE**, a charge-separated thiocarbonyl yields a benzylic carbocation which can readily delocalize via resonance effectively altering the electrophilicity of the thiocarbonyl via delocalization of the carbocation. In the presence of inductively donating groups such as methyl and isopropyl in **MPDTE** and **iPPDTE** respectively, the resulting carbocation is

localized to the thiocarbonyl position, which would result in enhanced rates of H_2S release in comparison to **PDTE**. Incorporation of an isopropyl group in **iPPDTE**, however, also introduces the potential for an intermediate 1,2-methyl shift which would partially delocalize the carbocation and hinder H_2S release relative to **MPDTE**. Considering these contributions, we interpret the enhanced release of H_2S from alkyl-functionalized dithioesters as a reflection of altered thiocarbonyl electrophilicity via carbocation delocalization. Although this outcome was contrary to our initial hypothesis, these findings demonstrate the ability to tune the rate of H_2S release from dithioesters by simple alkyl substitutions.

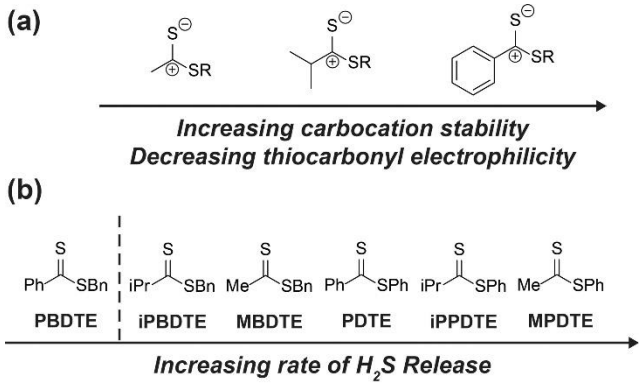

Figure D8. a) Effect of pendant groups on thiocarbonyl electrophilicity and carbocation stability. b) Scale of increasing H_2S releasing rates for reported dithioesters.

Furthering our studies, we also examined the effect of benzyl mercaptan as a leaving group on H_2S release from **MBDTE**, **PBDTE**, and **iPBDTE** respectively. In comparison to thiophenol, benzyl mercaptan is a considerably better nucleophile and likely perturbs the equilibrium of transthioesterification to disfavor the addition of cysteine. In concert with the effect of alkyl groups on thiocarbonyl electrophilicity, we anticipated H_2S release from dithioesters bearing benzyl mercaptan to be dramatically altered relatively to their thiophenol analogue. In agreement with our hypothesis, H_2S release was observed exclusively from **MBDTE**. Considering the lack of carbocation delocalization by the pendant methyl group, this result suggests the thiocarbonyl moiety in **MBDTE** is sufficiently electrophilic to promote H_2S release in the presence of cysteine. Alternatively, we observed effectively no H_2S release from **PBDTE** and relatively slow H_2S release from **iPBDTE**. Considering the effect of alkyl groups on

thiocarbonyl electrophilicity via carbocation delocalization in concert with the enhanced nucleophilicity of benzyl mercaptan, a significantly hindered rate of release from **iPBDTE** and complete shutdown of H_2S release from **PBDTE** is also in agreement with our hypothesis. Overall, we found the use of benzyl mercaptan decreased overall H_2S-releasing efficiency and yielded hindered rates of release in comparison to thiophenol-based dithioesters. Taken together, these findings demonstrate the rate of H_2S release from dithioesters can be enhanced or decreased as a function of alkyl substitution. In the future, this can be used to provide dithioesters with predictable rates of H_2S release for use *in cellulo* or *in vivo*.

Conclusions

Advancing our previous work on synthetic H_2S donors via the chemoselective condensation of thionoesters and cysteine, we have identified that dithioesters are a viable and tunable platform for developing cysteine-triggered H_2S donors. Using **PDTE** as a representative dithioester, we have demonstrated H_2S release in the presence of cysteine proceeds with good efficiency, and that dithioesters provide significant advancements over thionoesters, including ease of functionalization and enhanced selectivity for cysteine over other thiol-based nucleophiles including GSH. Mechanistic investigations, including rate-order analysis and activation parameters support a mechanism in which the initial nucleophilic attack by cysteine on the dithioesters is the rate-determining step of the reaction, which is also supported by computation. Furthermore, we demonstrated that the rate of H_2S release from a small library of dithioesters can be controlled by alkyl substitution. The findings presented herein provide several advancements over thionoesters as cysteine-triggered H_2S donors and provides a foundation for further development of dithioesters for expanding upon the chemical biology of H_2S.

Supporting Information

Materials and Methods.

Reagents were purchased from Tokyo Chemical Industry and/or Oakwood Chemicals and used directly as received. Deuterated solvents were purchased from Cambridge Isotope Laboratories and used as received. ^{1}H and $^{13}C\{^{1}H\}$ NMR were recorded on Bruker 500 and 600 MHz instruments. Chemical shifts are reported relative to residual protic solvent resonances. Silica gel (SiliaFlash F60, Silicycle, 230-400 mesh) was used for column chromatography. All air-free manipulations were performed under an inert atmosphere using standard Schlenk technique or an Innovative Atmospheres N_2-filled glove box. UV-Vis spectra were acquired on an Agilent Cary 60 UV-Vis spectrophotometer equipped with a Quantum Northwest TC-1 temperature controller at 25 °C ± 0.05 °C.

Synthesis

General Procedure for the Synthesis of Thioesters

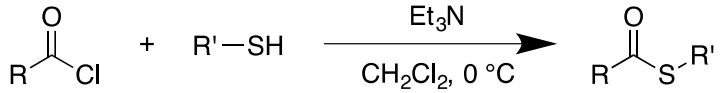

Thiol (1.1 equiv.) and triethylamine (1.1 equiv.) were added to anhydrous CH_2Cl_2 (20 mL) and cooled to 0 °C. Once cooled, acid chloride (1.0 equiv.) was added dropwise and the reaction was stirred at 0 °C for 1 h. Reaction was quenched with deionized H_2O (30 mL) and organic layer was separated. Aqueous layer was extracted with CH_2Cl_2 (2 x 20 mL). Collected organic extractions were washed with brine (1 x 20 mL), dried over $MgSO_4$, and concentrated under reduced pressured. Desired product was obtained via column chromatography.

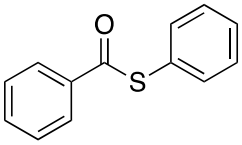

S-phenyl benzothioate

White powder, 852 mg (**96%**)

25% DCM in Hexanes, R_f = 0.23

^{1}H NMR (600 MHz, $CDCl_3$) δ 8.04 (d, 2H), 7.61 (t, 1H), 7.55 – 7.44 (m, 7H).

$^{13}C\{^1H\}$ NMR (151 MHz, $CDCl_3$) δ 190.14, 136.63, 135.09, 133.65, 129.52, 129.24, 128.74, 127.48, 127.34.

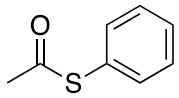

S-phenyl ethanethioate

Clear oil, 538 mg (**86%**)

50% CH_2Cl_2 in Hexanes, R_f = 0.42

^{1}H NMR (500 MHz, $CDCl_3$) δ 7.42 (s, 5H), 2.43 (s, 3H).

$^{13}C\{^1H\}$ NMR (151 MHz, $CDCl_3$) δ 194.06, 134.44, 129.43, 129.19, 127.91, 30.19.

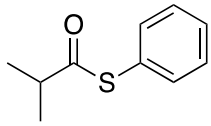

S-phenyl 2-methylpropanethioate

Clear oil, 492 mg (**66%**)

50% CH_2Cl_2 in Hexanes, R_f = 0.56

^{1}H NMR (500 MHz, $CDCl_3$) δ 7.41 (s, 5H), 2.87 (hept, J = 6.9, 1.9 Hz, 1H), 1.27 (d, J = 7.0, 1.8 Hz, 6H).

^{13}C NMR (126 MHz, $CDCl_3$) δ 201.85, 134.56, 129.17, 129.09, 127.87, 42.99, 19.37.

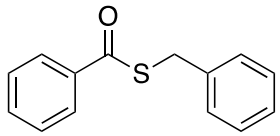

S-benzyl benzothioate

Clear oil, 779 mg (**93%**)

33% CH_2Cl_2 in Hexanes, R_f = 0.40

^{1}H NMR (500 MHz, $CDCl_3$) δ 7.98 (d, J = 7.6 Hz, 2H), 7.57 (t, J = 7.4 Hz, 1H), 7.45 (t, J = 8.0 Hz, 2H), 7.39 (d, J = 8.1 Hz, 2H), 7.33 (t, J = 7.5 Hz, 2H), 7.29 – 7.24 (m, 1H), 4.33 (s, 2H).

^{13}C NMR (126 MHz, $CDCl_3$) δ 191.27, 137.45, 136.78, 133.42, 128.96, 128.61, 127.31, 127.28, 33.32.

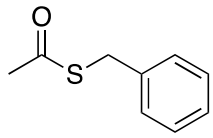

S-benzyl ethanethioate

Clear oil, 405 mg (**67%**)

25% CH_2Cl_2 in Hexanes, R_f = 0.24

^{1}H NMR (600 MHz, $CDCl_3$) δ 7.31 – 7.27 (m, 4H), 7.27 – 7.23 (m, 1H), 4.13 (s, 2H), 2.35 (s, 3H).

^{13}C NMR (151 MHz, $CDCl_3$) δ 195.09, 137.56, 128.77, 128.60, 127.24, 33.42, 30.29.

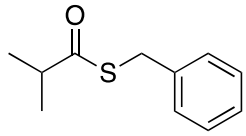

S-benzyl 2-methylpropanethioate

Clear oil, 577 mg (**66%**)

33% CH_2Cl_2 in Hexanes, R_f = 0.48

^{1}H NMR (600 MHz, $CDCl_3$) δ 7.31 – 7.28 (m, 4H), 7.25 – 7.22 (m, 1H), 4.11 (s, 2H), 2.76 (hept, J = 6.9 Hz, 1H), 1.21 (d, J = 6.9 Hz, 6H).

^{13}C NMR (151 MHz, $CDCl_3$) δ 203.44, 137.73, 128.79, 128.59, 127.17, 42.88, 32.89, 19.35.

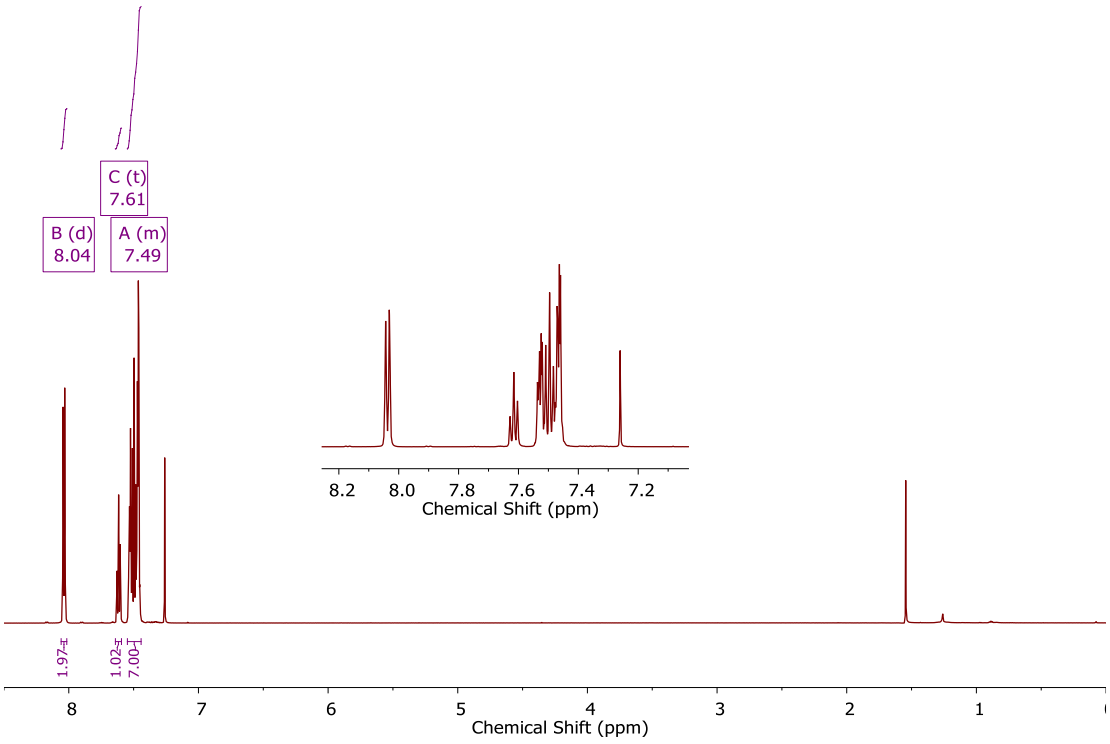

Figure D9. ^{1}H NMR (600 MHz, $CDCl_3$) spectrum of *S*-phenyl benzothioate

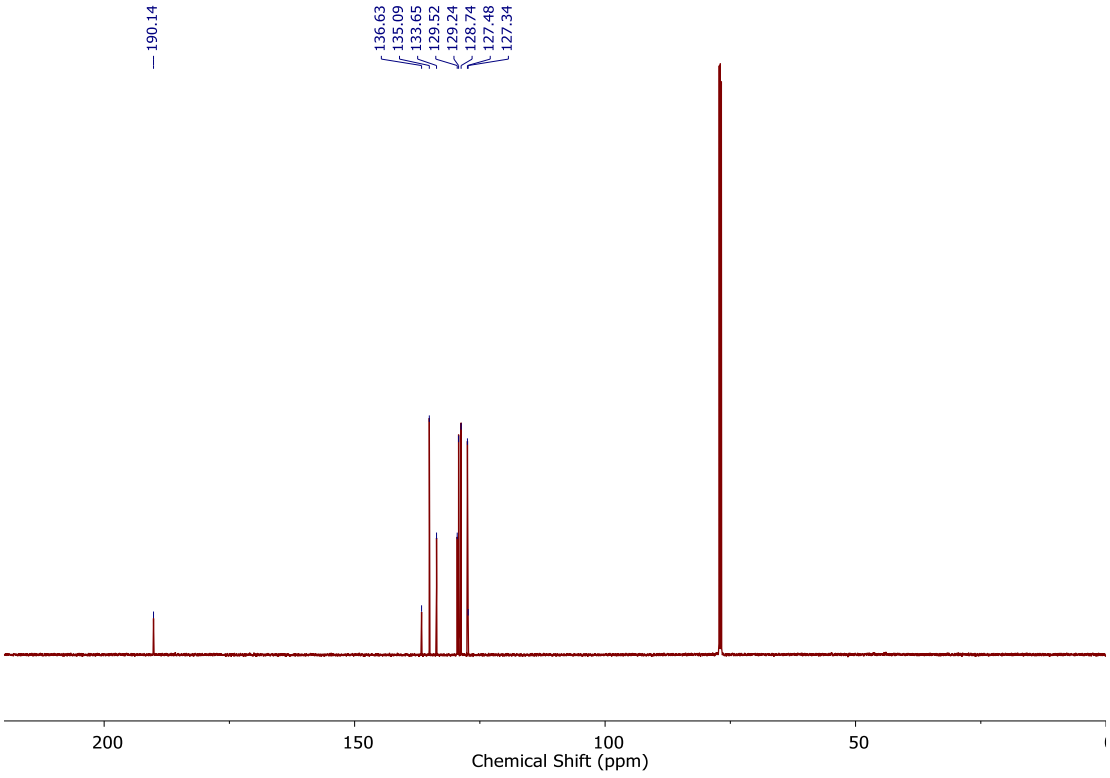

Figure D10. $^{13}C\{^{1}H\}$ NMR (151 MHz, $CDCl_3$) spectrum of *S*-phenyl benzothioate

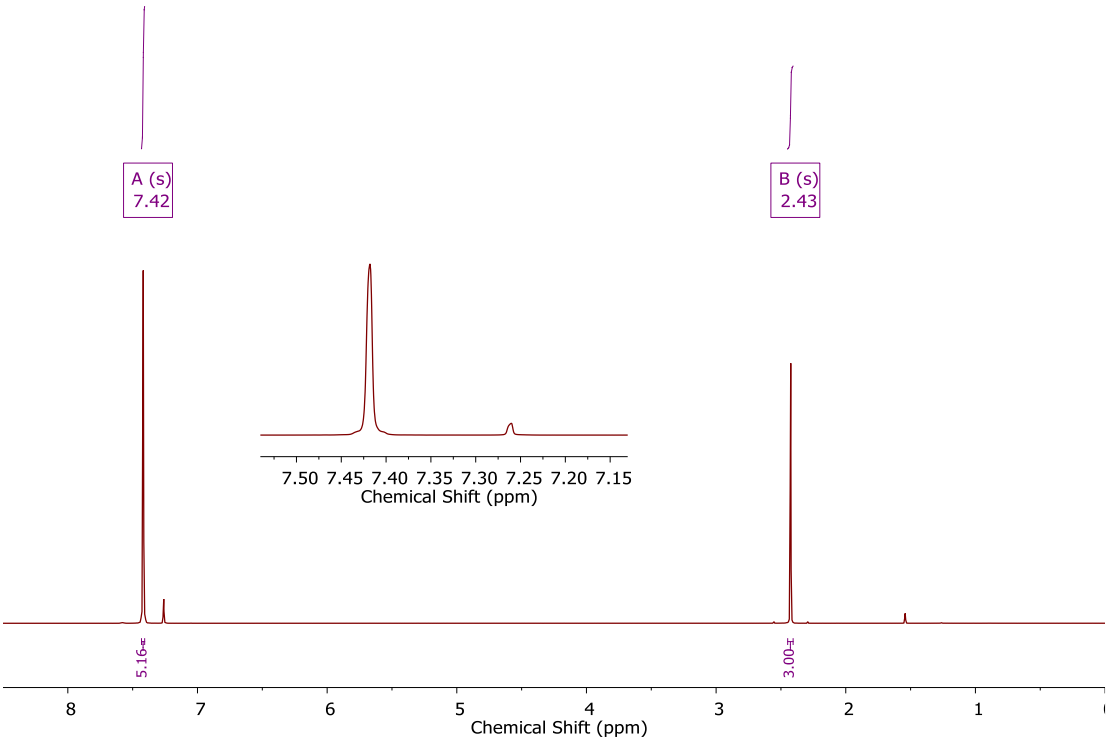

Figure D11. ^{1}H NMR (500 MHz, $CDCl_3$) spectrum of *S*-phenyl ethanethioate

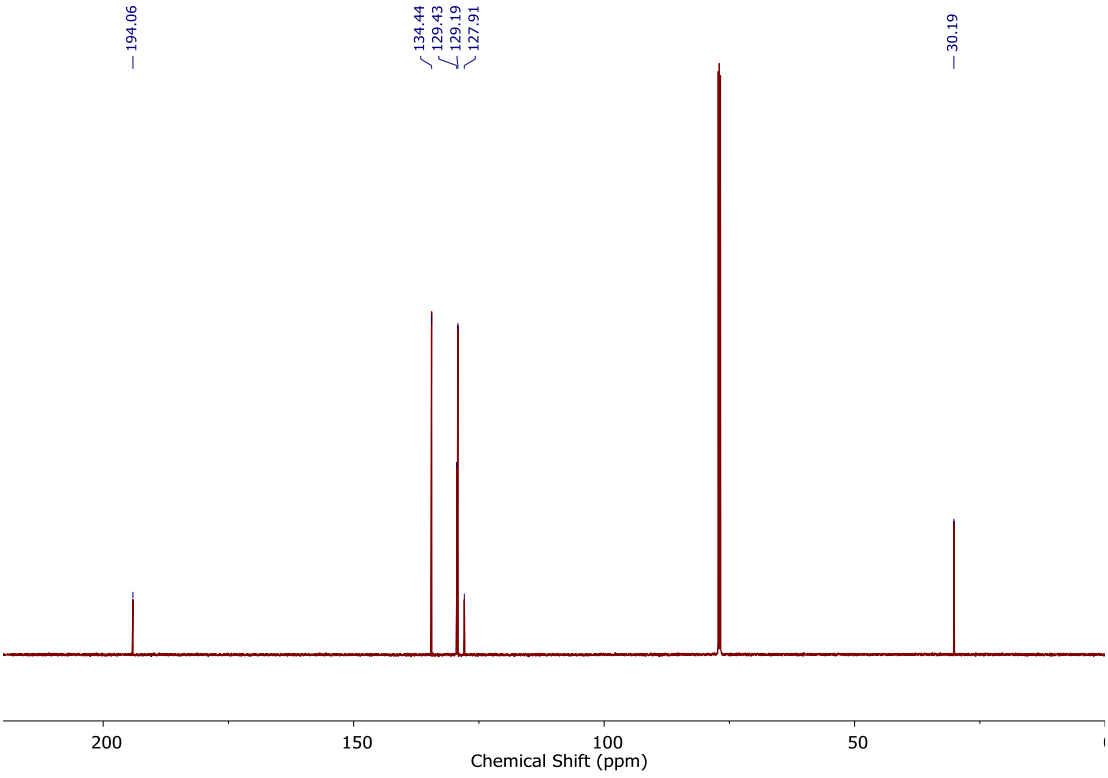

Figure D12. $^{13}C\{^{1}H\}$ NMR (151 MHz, $CDCl_3$) spectrum of *S*-phenyl ethanethioate

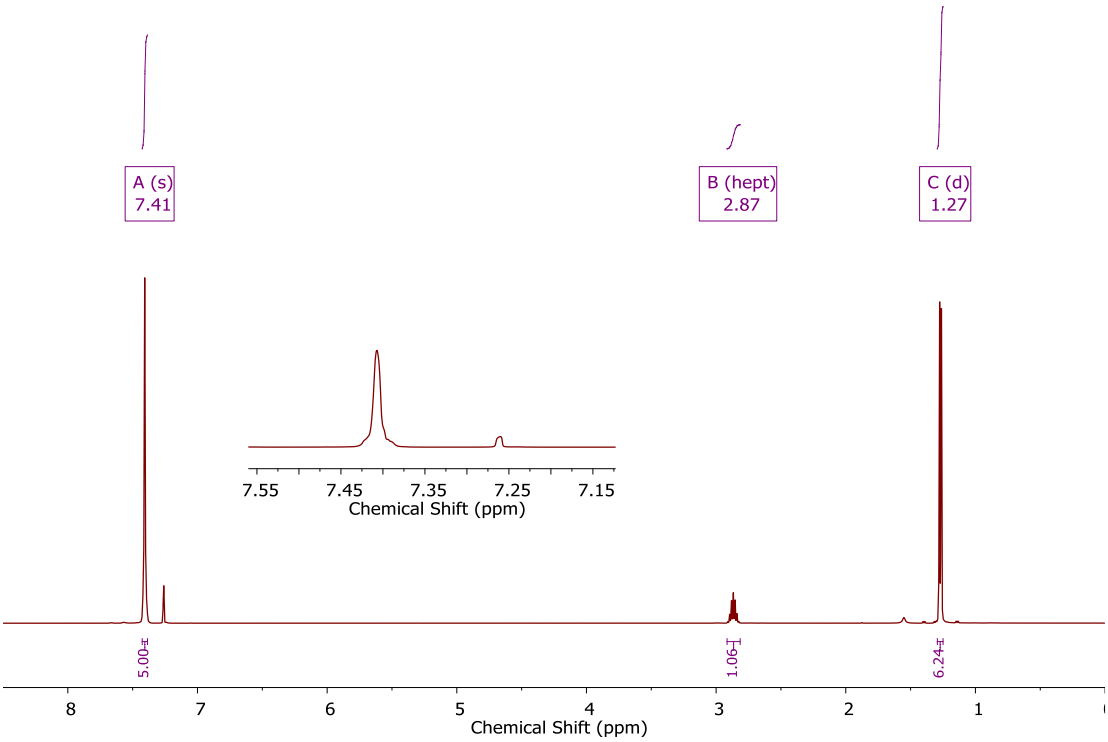

Figure D13. ^{1}H NMR (500 MHz, $CDCl_3$) spectrum of *S*-phenyl 2-methylpropanethioate

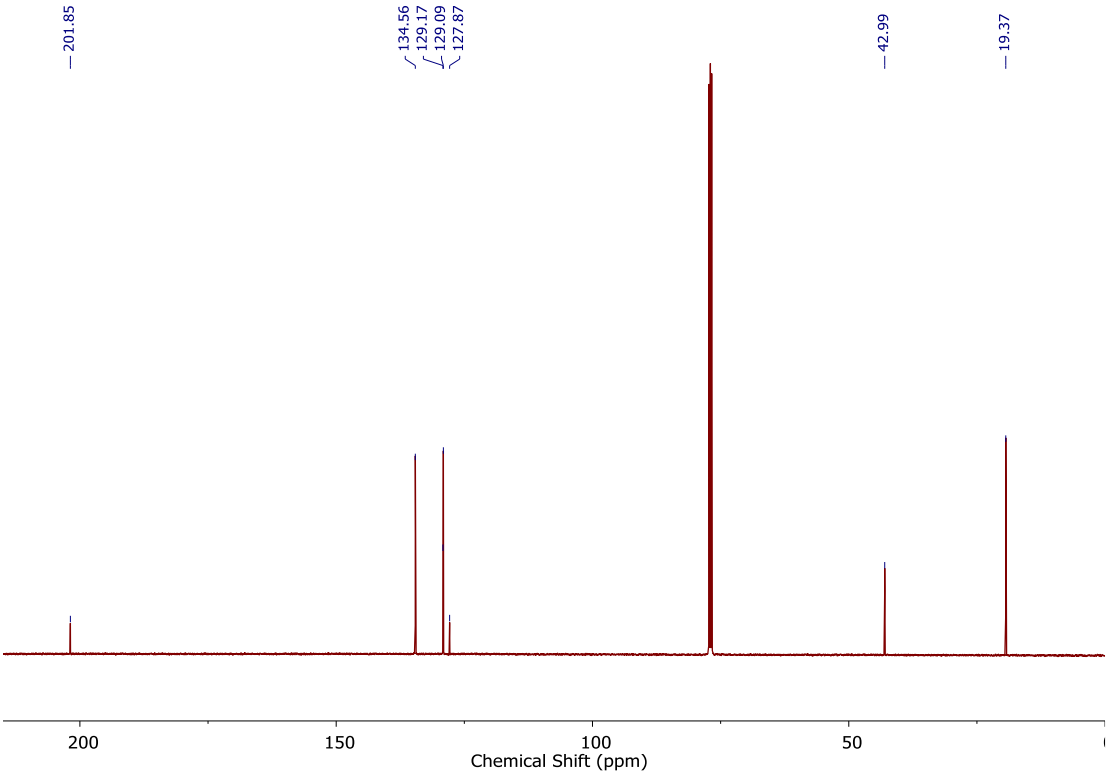

Figure D14. $^{13}C\{^{1}H\}$ NMR (126 MHz, $CDCl_3$) spectrum of *S*-phenyl 2-methylpropanethioate

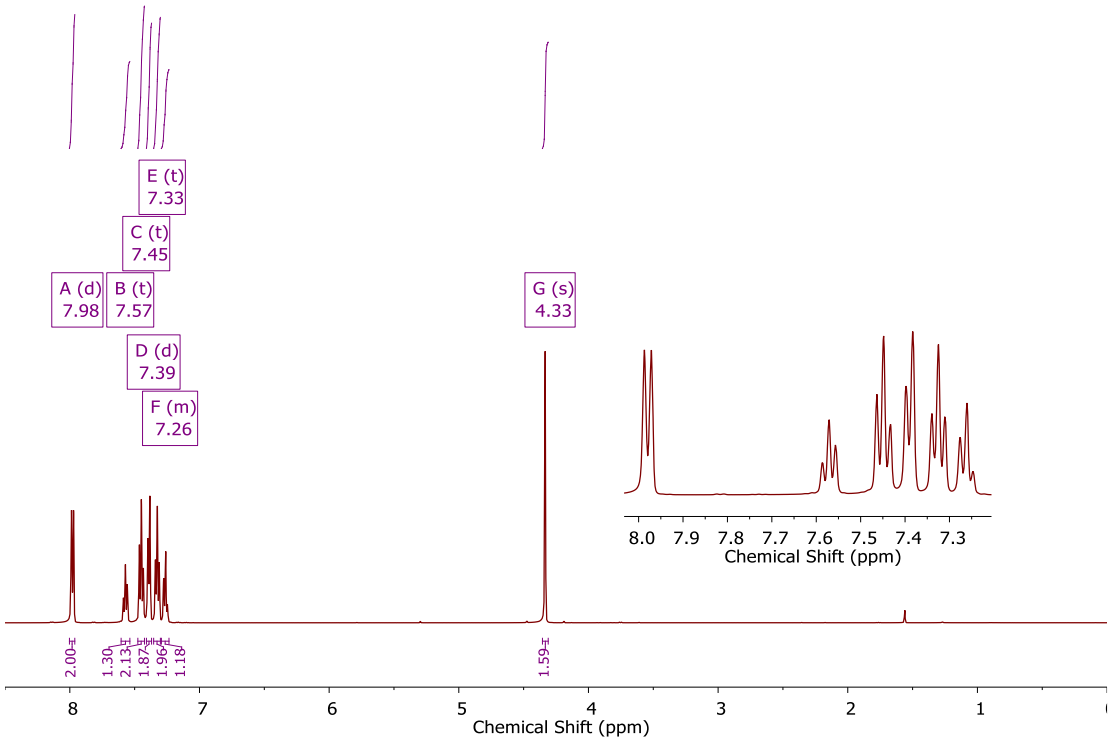

Figure D15. ^{1}H NMR (500 MHz, $CDCl_3$) spectrum of *S*-benzyl benzothioate

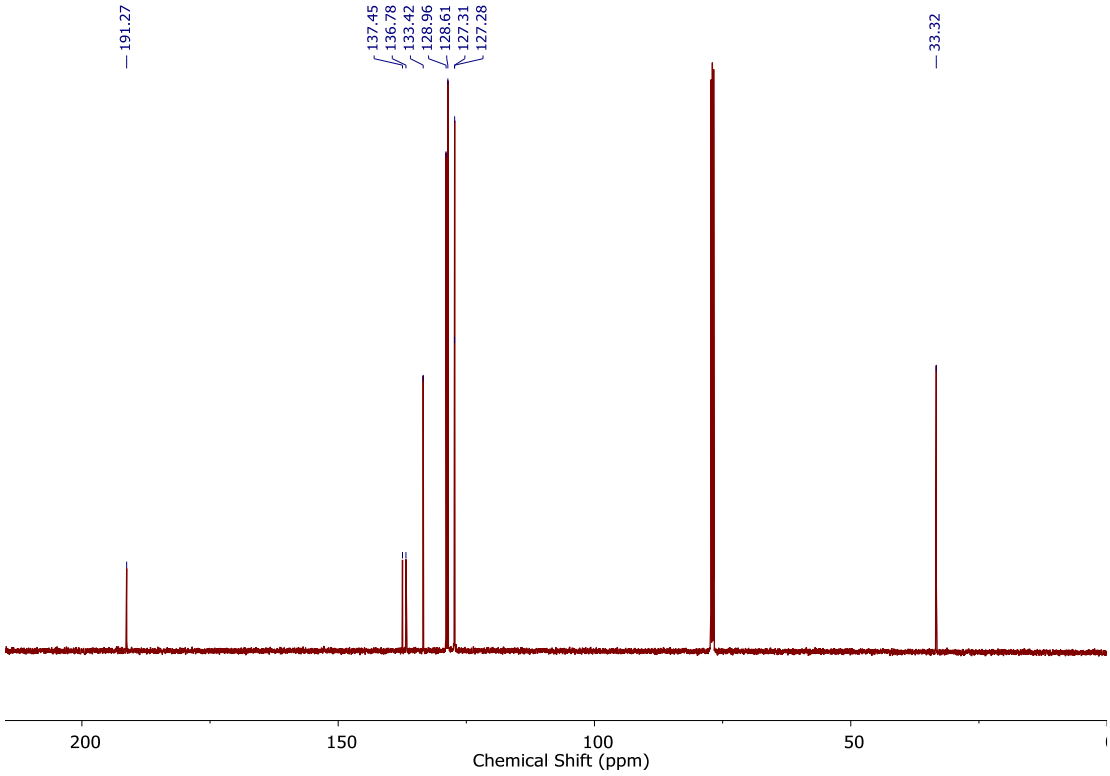

Figure D16. $^{13}C\{^{1}H\}$ NMR (126 MHz, $CDCl_3$) spectrum of *S*-benzyl benzothioate

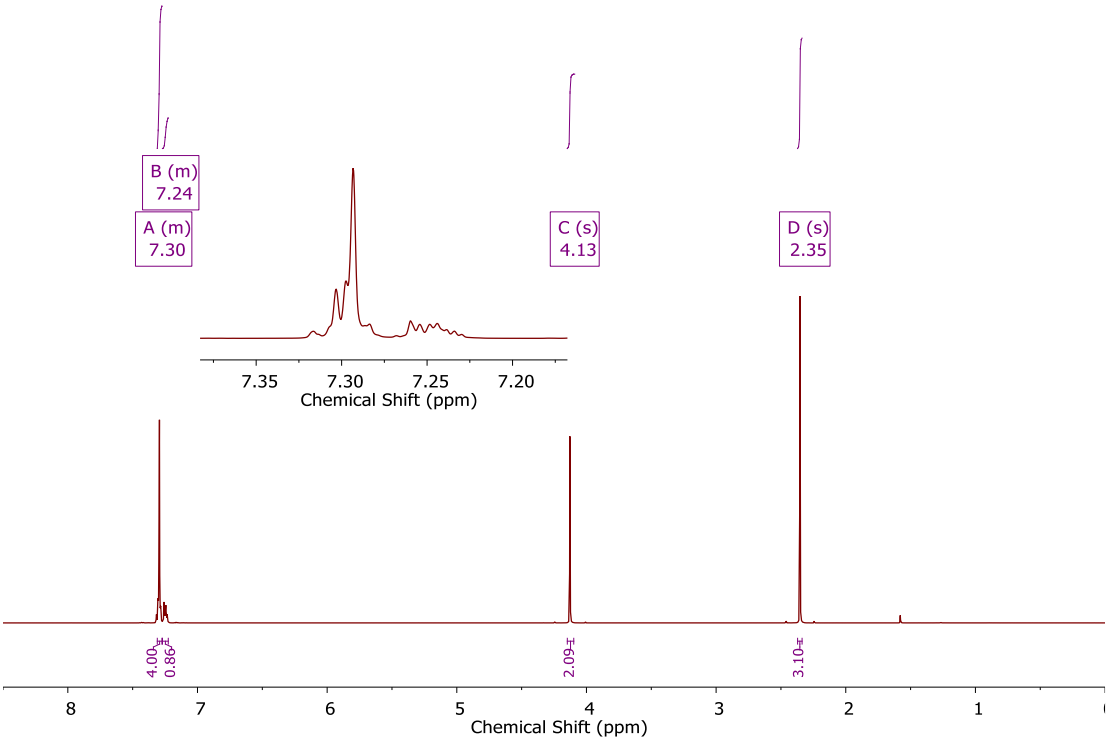

Figure D17. ^{1}H NMR (600 MHz, $CDCl_3$) spectrum of *S*-benzyl ethanethioate

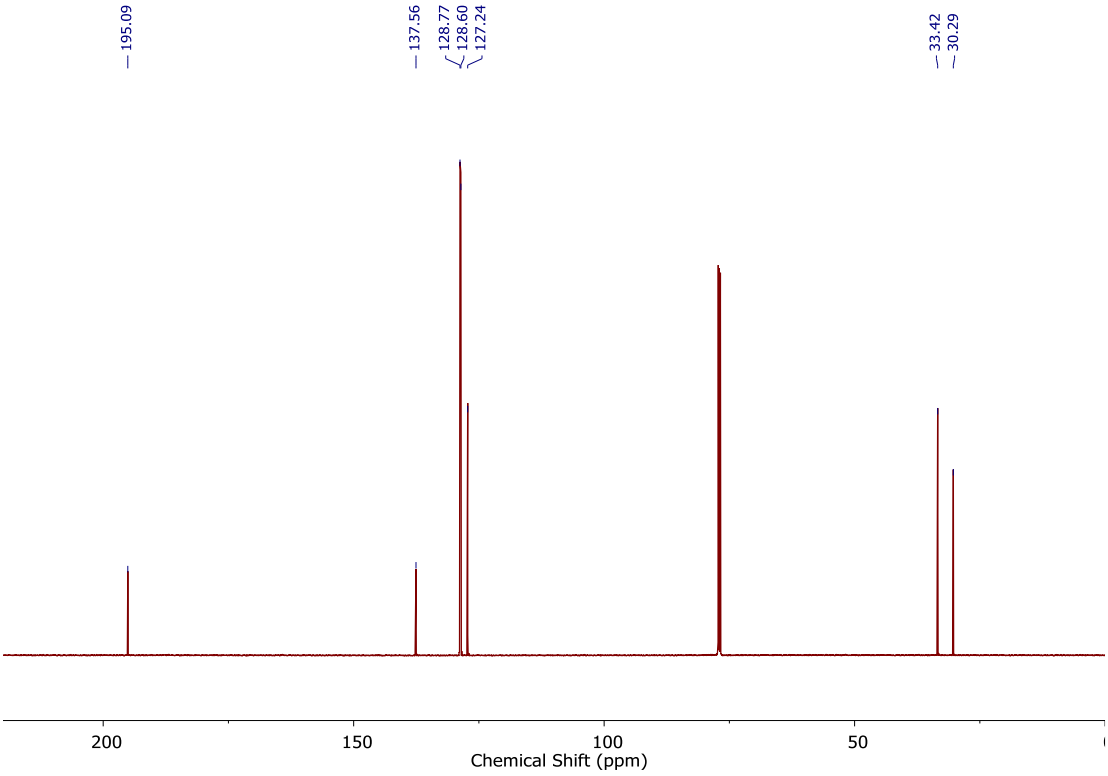

Figure D18. $^{13}C\{^{1}H\}$ NMR (151 MHz, $CDCl_3$) spectrum of *S*-benzyl ethanethioate

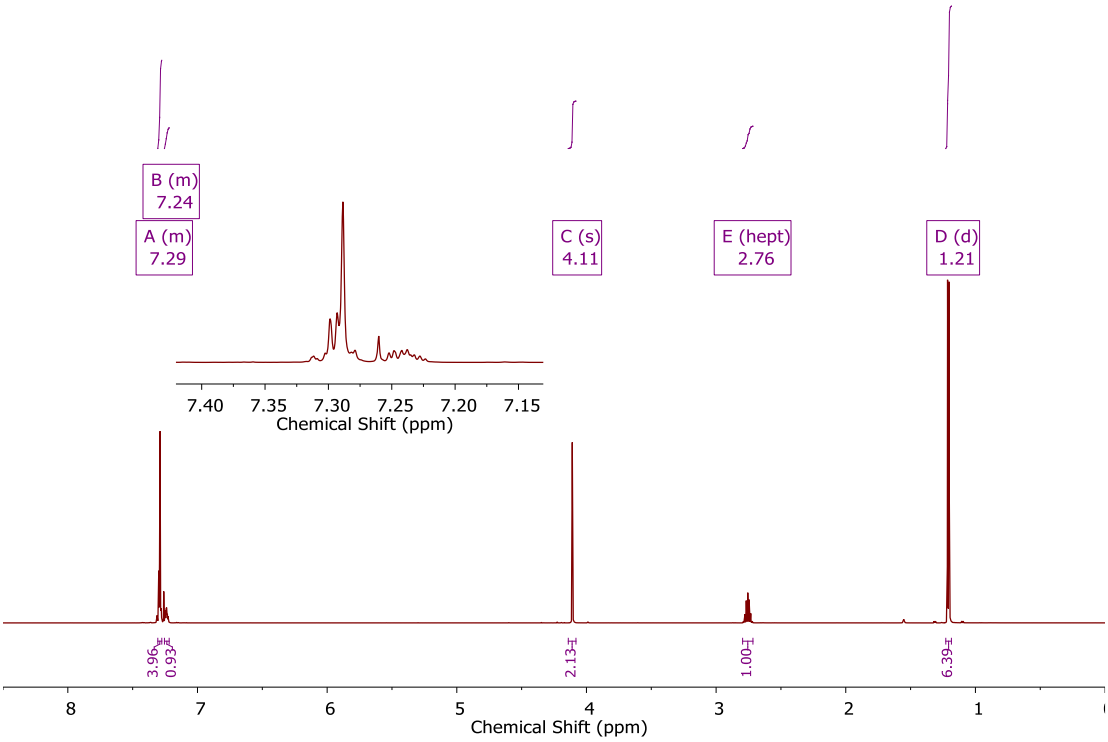

Figure D19. ^{1}H NMR (600 MHz, $CDCl_3$) spectrum of *S*-benzyl 2-methylpropanethioate

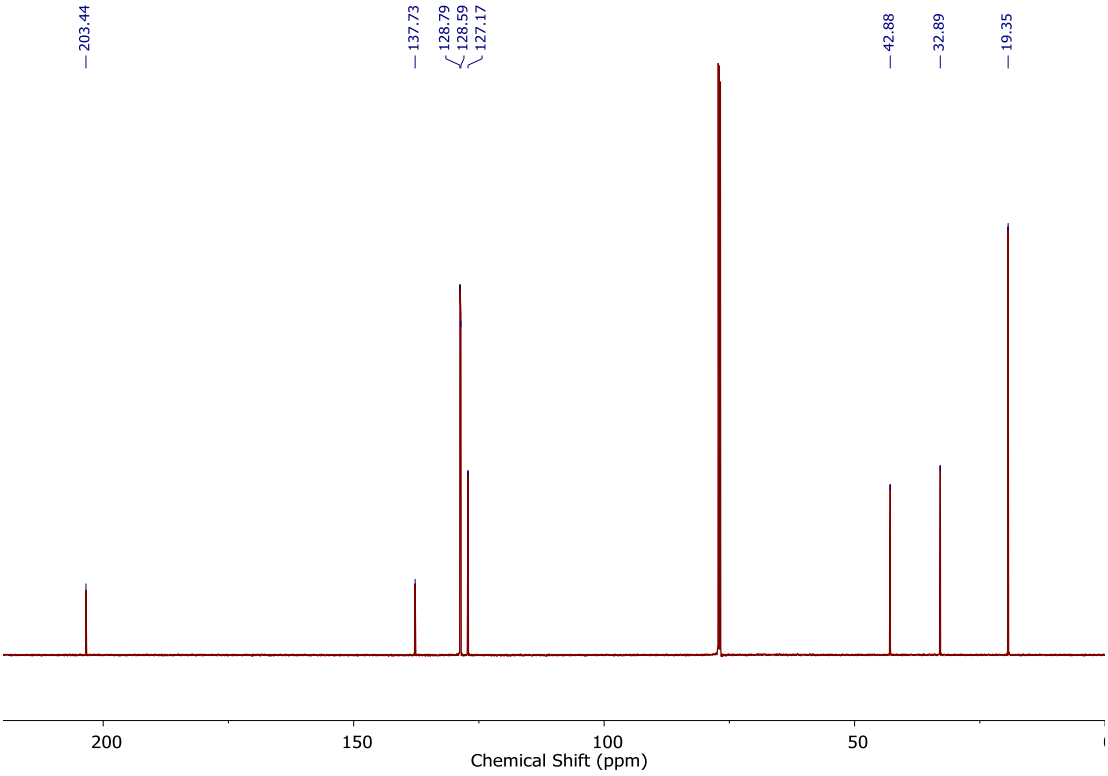

Figure D20. $^{13}C\{^{1}H\}$ NMR (151 MHz, $CDCl_3$) spectrum of *S*-benzyl 2-methylpropanethioate

General Procedure for the Synthesis of Dithioesters

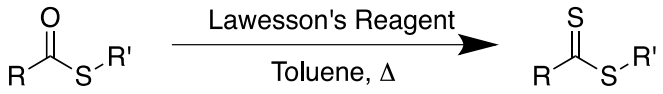

Added thioester (1.0 equiv.) and Lawesson's Reagent (0.75 equiv.) to anhydrous toluene (20 mL) and heated to 120 °C under reflux. After 5.5 h, cooled reaction mixture to room temperature and filtered. Concentrated filtrate under reduced pressure and isolated desired product via column chromatography.

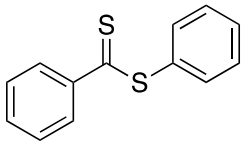

Phenyl benzodithioate (**PDTE**)

Red-violet solid, 217 mg (**81%**)

20% CH_2Cl_2 in Hexanes, R_f = 0.42

^{1}H NMR (600 MHz, $CDCl_3$) δ 8.10 (d, J = 7.1 Hz, 1H), 7.57 (t, 1H), 7.54 – 7.47 (m, 6H), 7.45 – 7.40 (m, 2H).

^{13}C NMR (151 MHz, $CDCl_3$) δ 228.49, 144.59, 135.38, 132.60, 131.38, 130.36, 129.66, 128.40, 126.99.

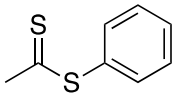

Phenyl ethanedithioate (**MPDTE**)

Burnt orange oil, 185 mg (**67%**)

20% CH_2Cl_2 in Hexanes, R_f = 0.40

^{1}H NMR (500 MHz, $CDCl_3$) δ 7.52 – 7.46 (m, 3H), 7.45 – 7.40 (m, 2H), 2.87 (s, 3H).

^{13}C NMR (151 MHz, $CDCl_3$) δ 234.30, 134.74, 131.77, 130.36, 129.60, 38.95.

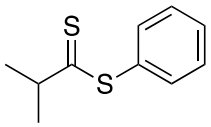

Phenyl 2-methylpropanedithioate (**iPPDTE**)

Yellow oil, 129 mg (**59%**)

25% CH_2Cl_2 in Hexanes, R_f = 0.58

^{1}H NMR (600 MHz, $CDCl_3$) δ 7.50 – 7.47 (m, 3H), 7.42 – 7.39 (m, 2H), 3.54 (hept, J = 6.7 Hz, 1H), 1.38 (d, J = 6.6 Hz, 6H).

^{13}C NMR (151 MHz, $CDCl_3$) δ 246.77, 134.97, 130.83, 130.18, 129.51, 48.70, 24.24.

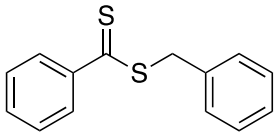

Benzyl benzodithioate (**PBDTE**)

Red oil, 243 mg (**91%**)

20% CH_2Cl_2 in Hexanes, R_f = 0.41

^{1}H NMR (500 MHz, $CDCl_3$) δ 8.00 (d, J = 7.7 Hz, 2H), 7.53 (t, J = 7.5 Hz, 1H), 7.42 – 7.27 (m, 8H), 4.61 (s, 2H).

^{13}C{^{1}H} NMR (126 MHz, $CDCl_3$) δ 227.69, 144.75, 134.97, 132.40, 129.29, 128.72, 128.34, 127.75, 126.90, 42.28.

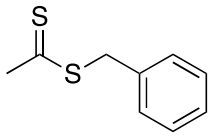

Benzyl ethanedithioate (**MBDTE**)

Yellow-brown oil, 181 mg, (**82%**)

25% CH_2Cl_2 in Hexanes, R_f = 0.54

^{1}H NMR (600 MHz, $CDCl_3$) δ 7.34 – 7.26 (m, 5H), 4.46 (s, 2H), 2.85 (s, 3H).

^{13}C{^{1}H} NMR (151 MHz, $CDCl_3$) δ 232.29, 135.13, 129.09, 128.67, 127.66, 41.98, 38.85.

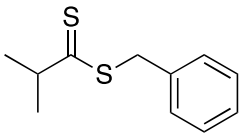

Benzyl 2-methylpropanedithioate (**iPBDTE**)

Orange-brown oil, 164 mg (**76%**)

25% CH_2Cl_2 in Hexanes, R_f = 0.58

^{1}H NMR (600 MHz, $CDCl_3$) δ 7.34 – 7.26 (m, 5H), 4.45 (s, 2H), 3.42 (hept, J = 6.7 Hz, 1H), 1.34 (d, J = 6.7 Hz, 7H).

^{13}C{^{1}H} NMR (151 MHz, $CDCl_3$) δ 245.91, 135.22, 129.13, 128.67, 127.58, 49.35, 40.52, 24.19.

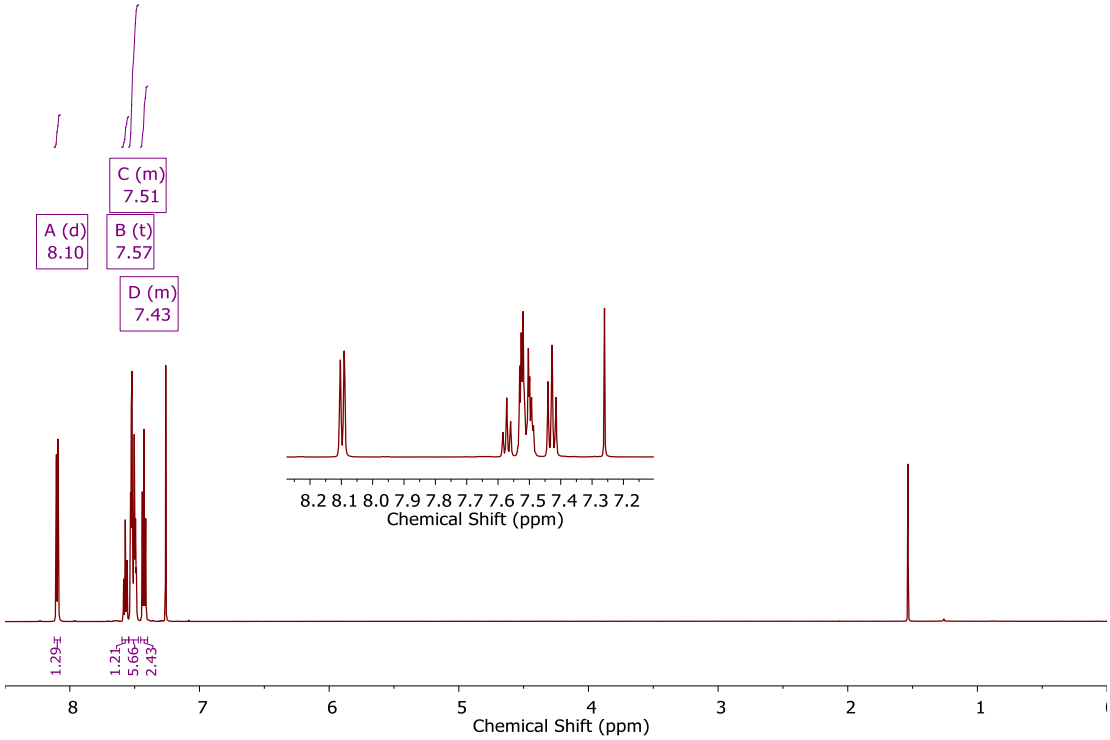

Figure D21. ^{1}H NMR (600 MHz, $CDCl_3$) spectrum of **PDTE**

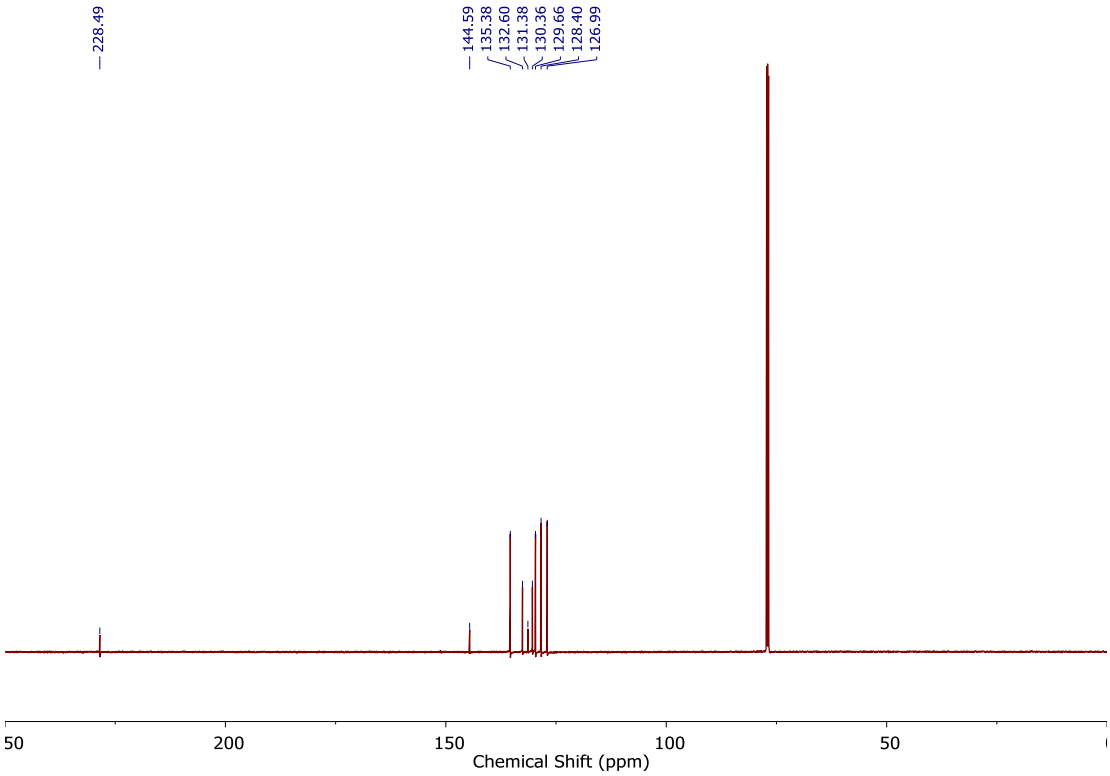

Figure D22. $^{13}C\{^{1}H\}$ NMR (151 MHz, $CDCl_3$) spectrum of **PDTE**

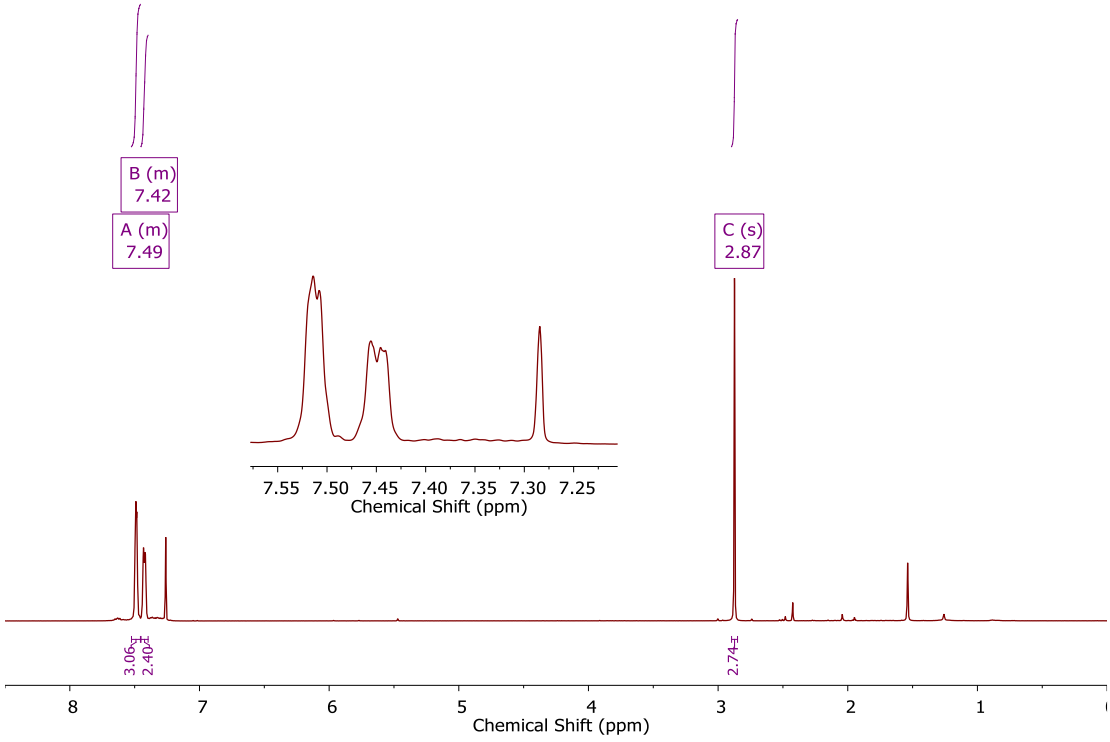

Figure D23. ^{1}H NMR (500 MHz, $CDCl_3$) spectrum of **MPDTE**

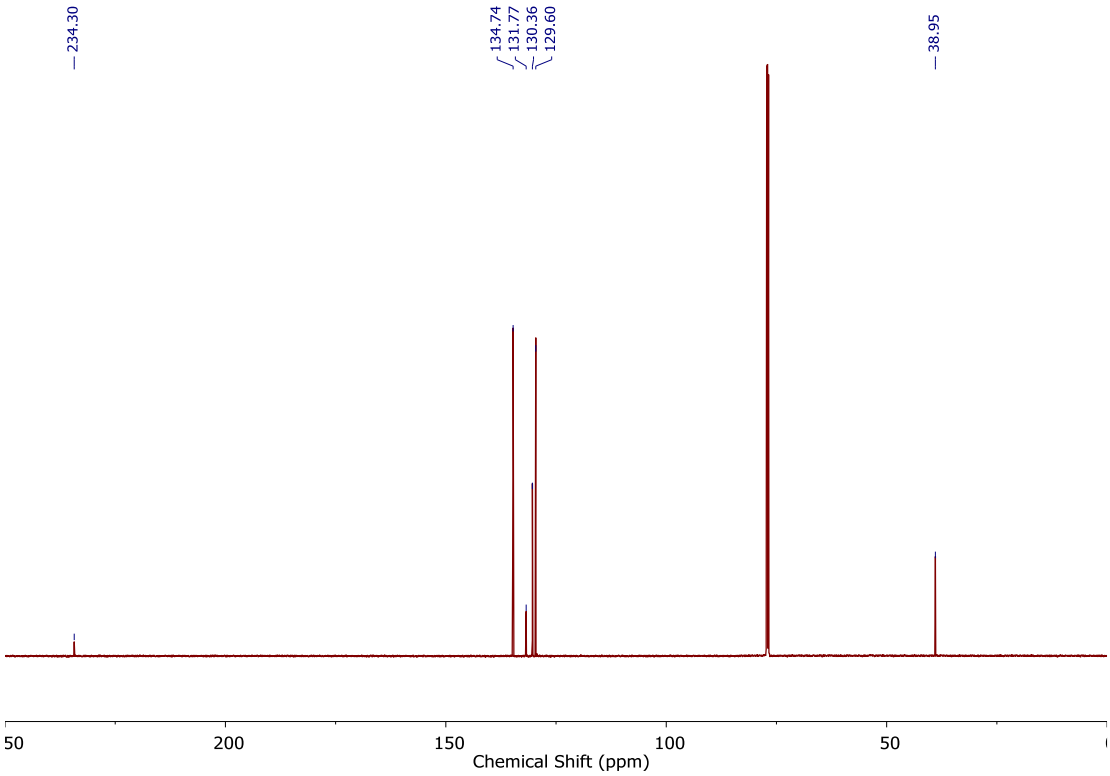

Figure D24. $^{13}C\{^{1}H\}$ NMR (151 MHz, $CDCl_3$) spectrum of **MPDTE**

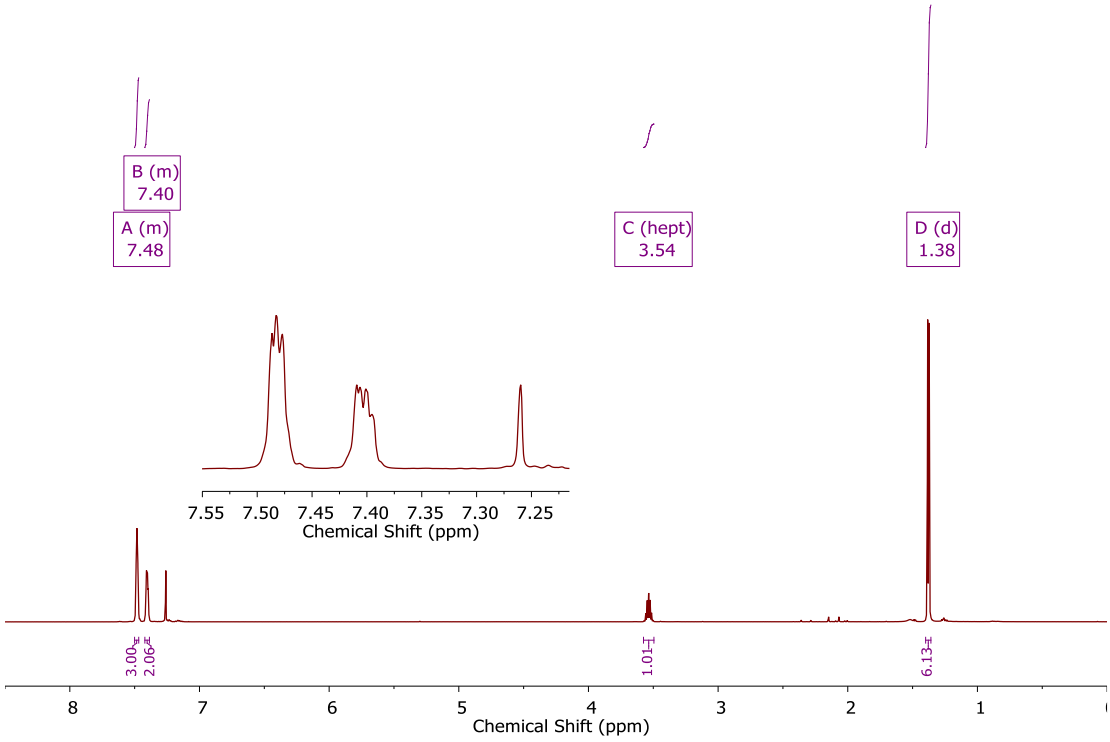

Figure D25. ^{1}H NMR (600 MHz, $CDCl_3$) spectrum of **iPPDTE**

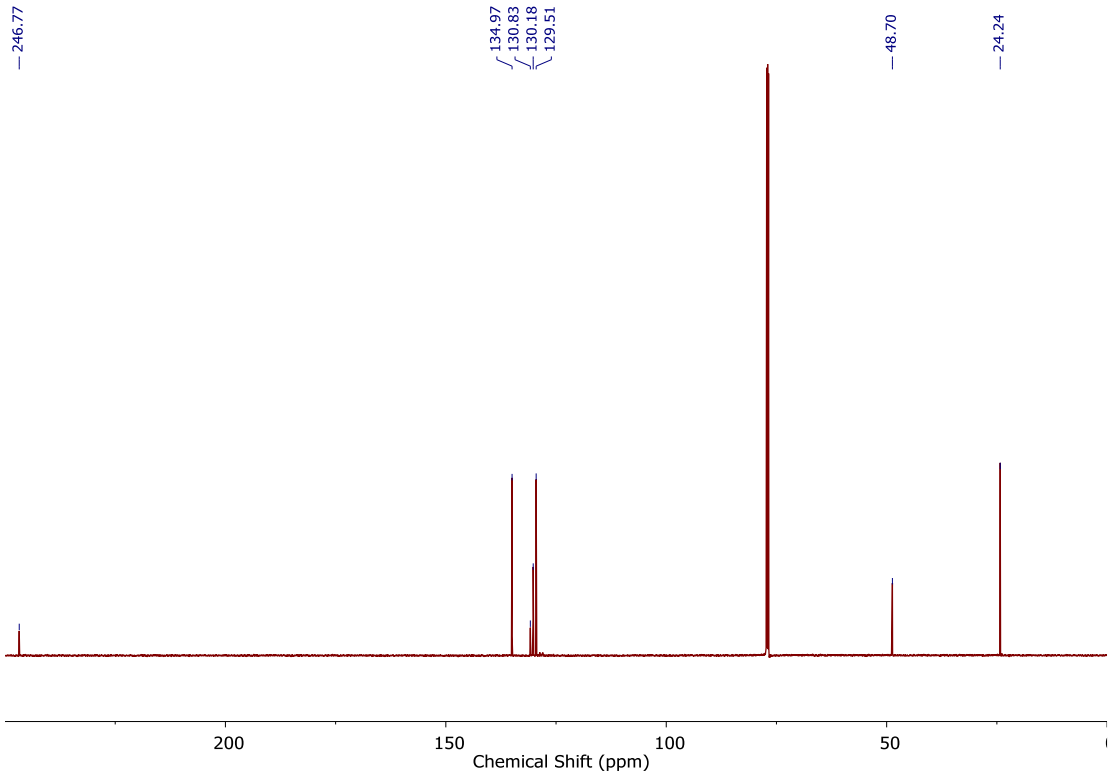

Figure D26. $^{13}C\{^{1}H\}$ NMR (151 MHz, $CDCl_3$) spectrum of **iPPDTE**

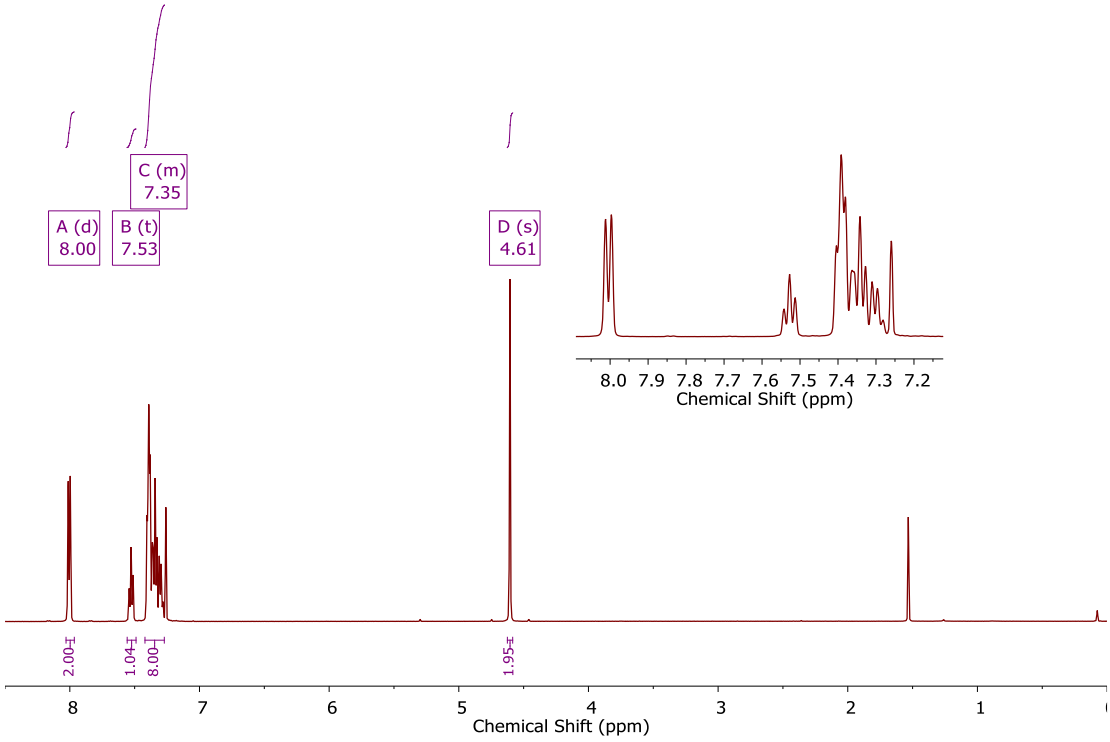

Figure D27. ^{1}H NMR (500 MHz, $CDCl_3$) spectrum of **PBDTE**

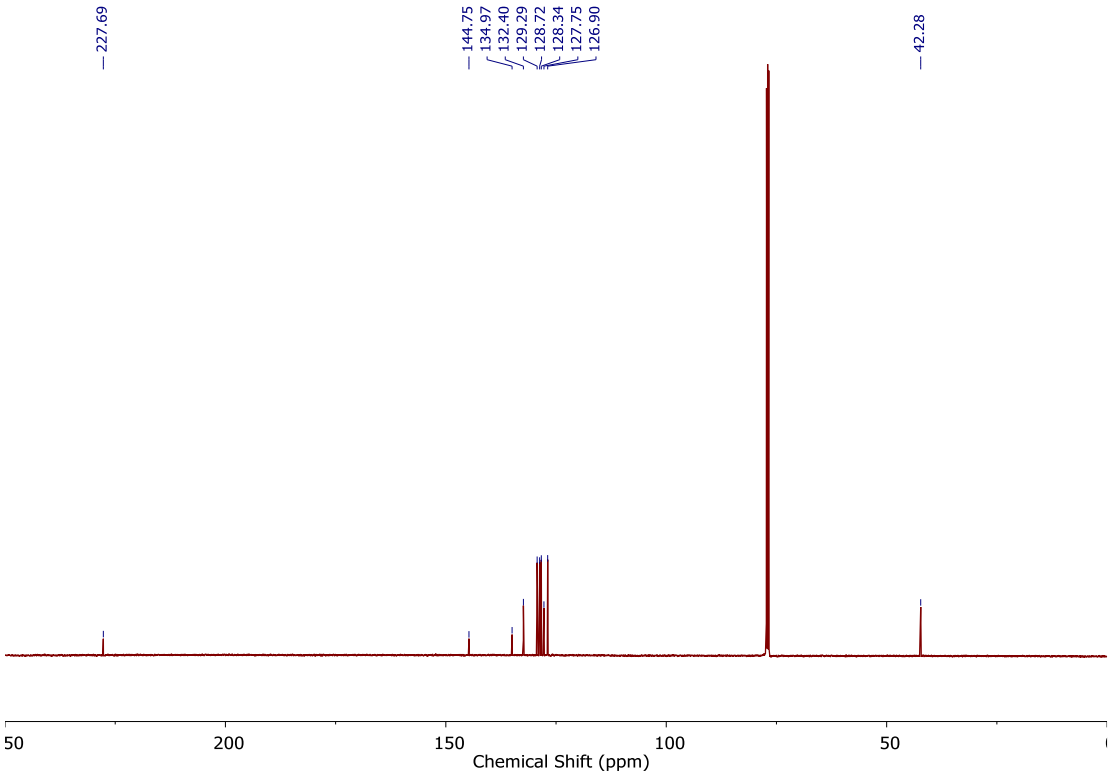

Figure D28. $^{13}C\{^{1}H\}$ NMR (126 MHz, $CDCl_3$) spectrum of **PBDTE**

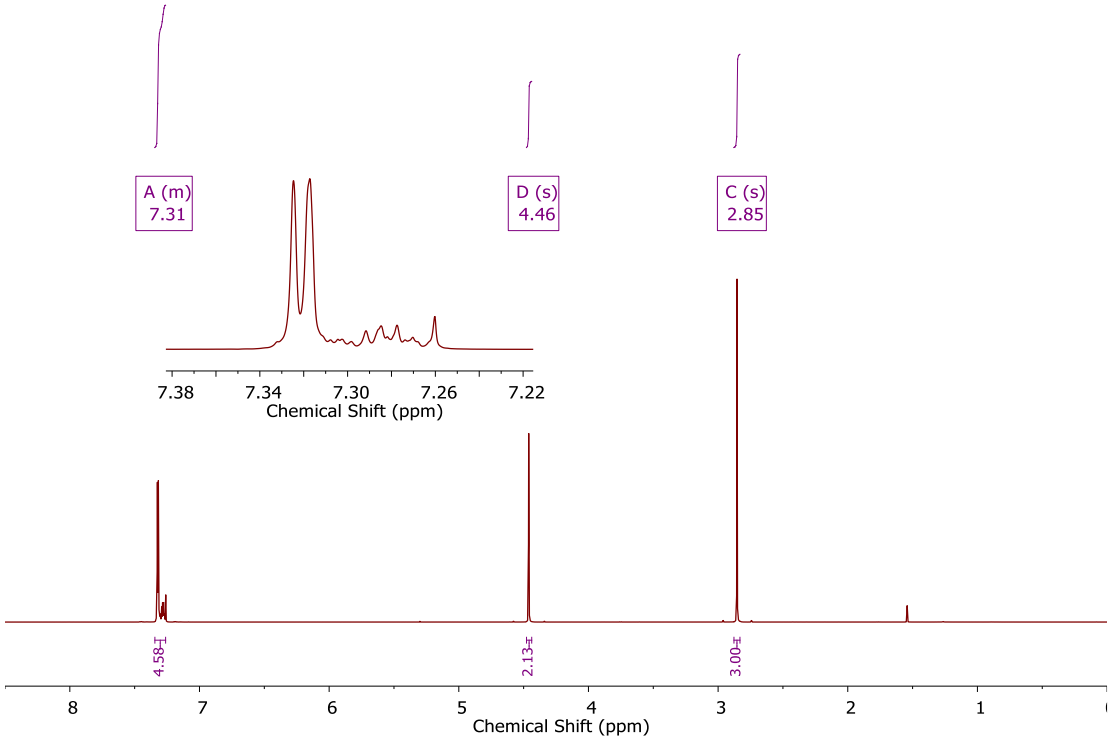

Figure D29. ^{1}H NMR (600 MHz, $CDCl_3$) spectrum of **MBDTE**

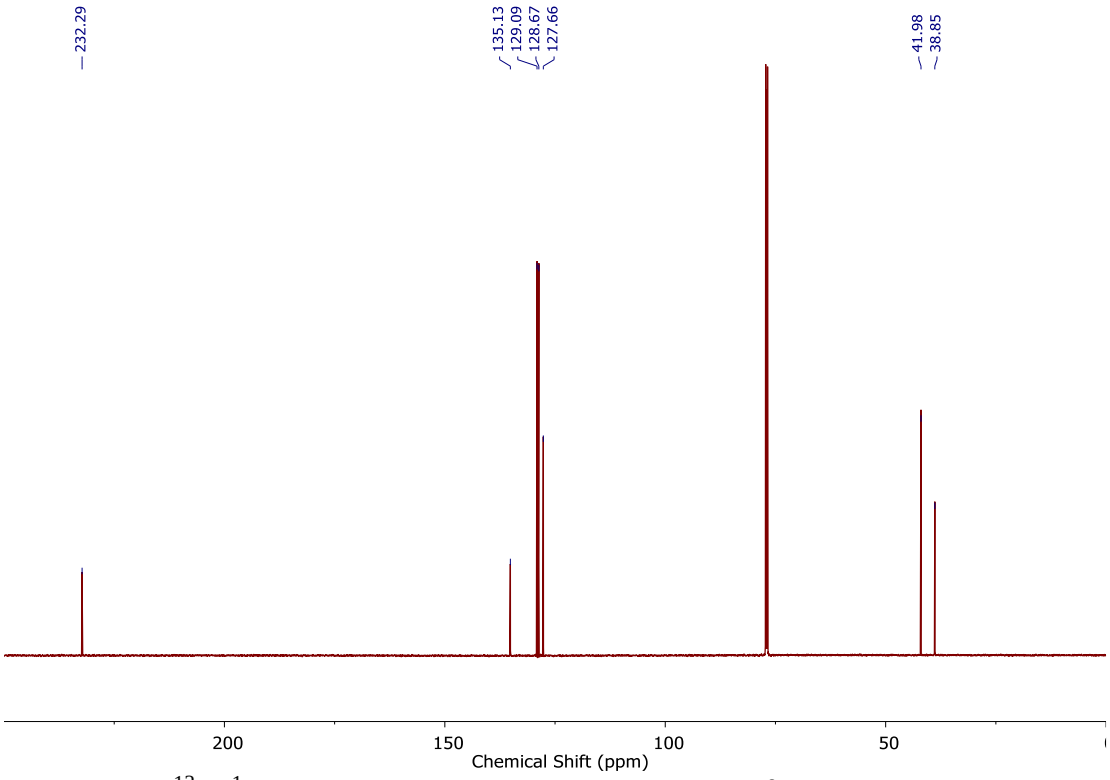

Figure D30. $^{13}C\{^{1}H\}$ NMR (151 MHz, $CDCl_3$) spectrum of **MBDTE**

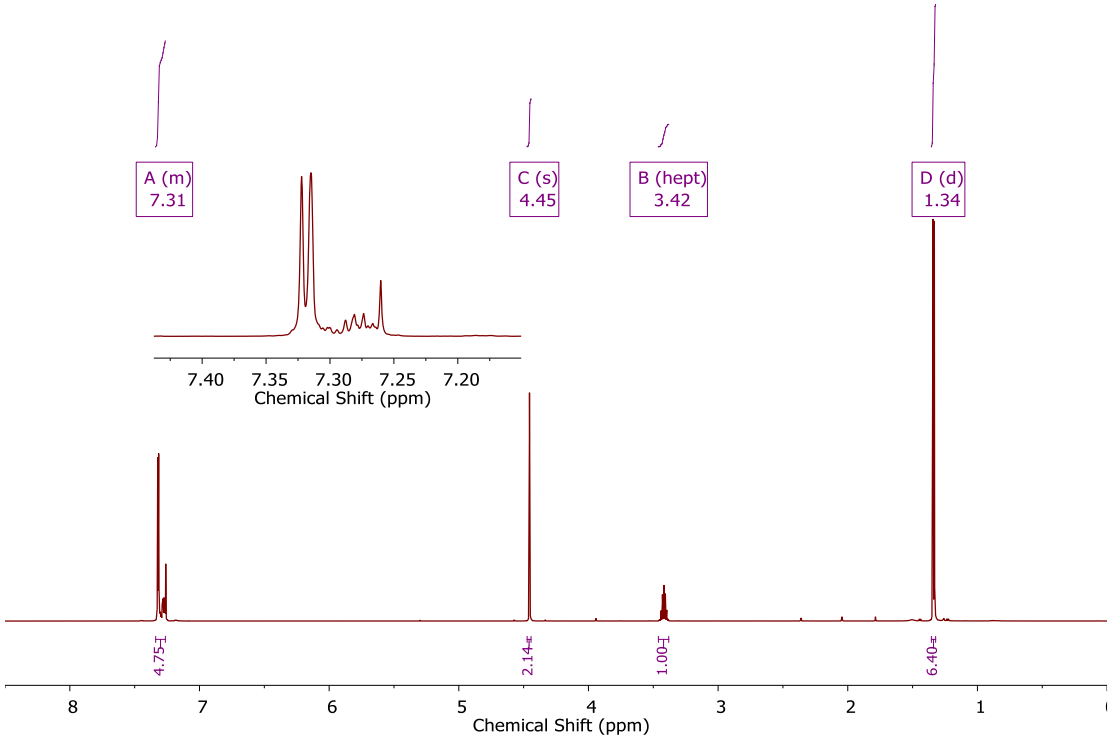

Figure D31. ^{1}H NMR (600 MHz, $CDCl_3$) spectrum of **iPBDTE**

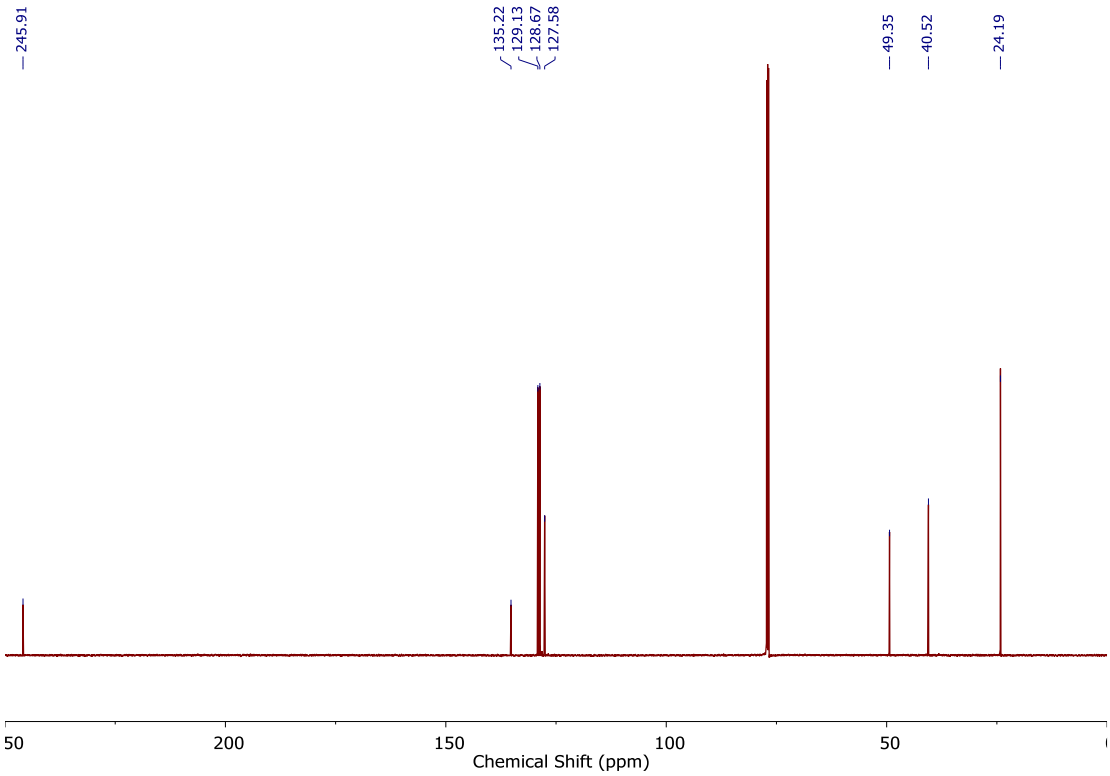

Figure D32. $^{13}C\{^{1}H\}$ NMR (151 MHz, $CDCl_3$) spectrum of **iPBDTE**

H_2S Detection Materials and Methods Phosphate buffered saline (PBS) tablets (1X, CalBioChem) were used to prepare buffered solutions (140 mM NaCl, 3 mM KCl, 10 mM phosphate, pH 7.4) in deionized water. Buffer solutions were sparged with N_2 to remove dissolved oxygen and stored in an N_2-filled glovebox. Donor stock solutions (in DMSO) were prepared inside an N_2-filled glovebox and stored at -25 °C until immediately before use. Trigger stock solutions (in PBS) were freshly prepared in an N_2-filled glovebox immediately before use.

General Procedure for Measuring H_2S Release via Methylene Blue Assay (MBA). Scintillation vials containing 20 mL of PBS were prepared in an N_2-filled glovebox. To these solutions, 20 μL of 500 mM analyte stock solution (in PBS) was added for a final concentration of 500 μM. While stirring, the solutions were allowed to thermally equilibrate in heating block at the desired temperature for approximately 20-30 min. Immediately prior to donor addition, 0.5 mL solutions of methylene blue cocktail were prepared in disposable 1.5 mL cuvettes. The methylene blue cocktail solution contains:

200 µL of 30 mM $FeCl_3$ in 1.2 M HCl, 200 µL of 20 mM *N*,*N*-dimethyl-*p*-phenylene diamine in 7.2 M HCl, and 100 µL of 1% (w/v) $Zn(OAc)_2$. To begin an experiment, 20 µL of 25 mM donor stock solution (in DMSO) was added for a final concentration of 25 µM. At set time points after the addition of donor, 500 µL reaction aliquots were added to the methylene blue cocktail solutions and incubated for 1 h at room temperature shielded from light. Absorbance values at 670 nm were measured 1 h after addition of reaction aliquot. Each experiment was performed in quadruplicate unless stated otherwise.

MBA Calibration Curve. Solutions containing 0.5 mL of the methylene blue cocktail and 0.5 mL PBS containing 500 µM cysteine were freshly prepared in disposable cuvettes (1.5 mL). Under inert conditions, a 10 mM stock solution of NaSH (Strem Chemicals) in PBS was prepared and diluted to 1 mM. Immediately after dilution, 1 mM NaSH was added to 1.0 mL solutions for final concentrations of 10, 20, 30, 40, and 50 µM. Solutions were mixed thoroughly, incubated at room temperature for 1 h, and shielded from light. Absorbance values at 670 nm were measured after 1 h.

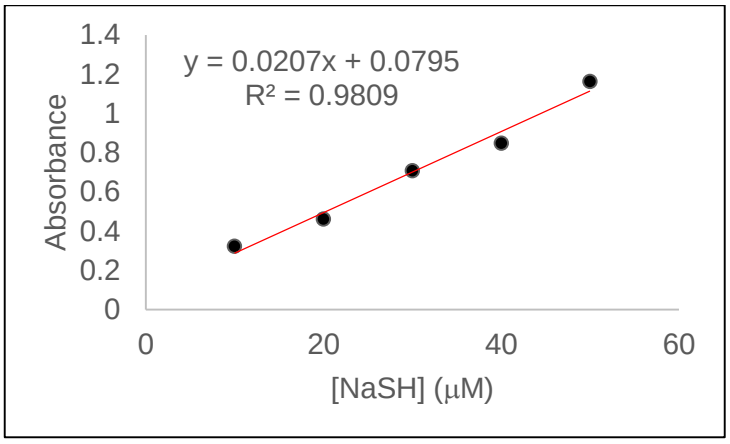

Figure D33. MBA calibration curve generated using known concentrations of NaSH.

Reaction Product Analysis via HPLC

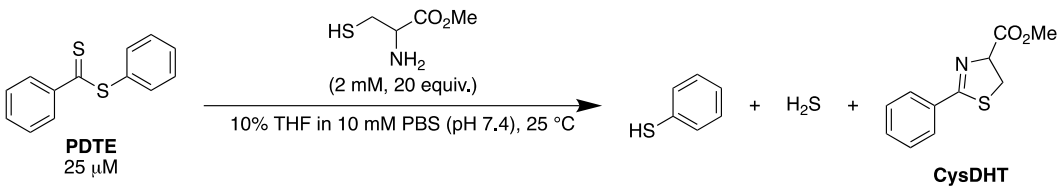

To a 20 mL solution of 10% THF in PBS (10 mM, pH 7.4) containing 2 mM L-cysteine methyl ester (20 equiv.), 20 mL of 100 mM **PDTE** in THF was added for 100 mM **PDTE** and stirred at room temperature. After 1 h, a 1 mL reaction aliquot was analyzed by HPLC. HPLC analysis was performed on an Agilent 1260 HPLC instrument with a Poroshell 120 EC-C18 4.6x100 mm column and monitored at 280 nm. Solvent A: 95% H_2O, 5% MeOH, Solvent B: 100% MeCN. Gradient: 35% Solvent A/65% Solvent B for 2 min. Change to 100% Solvent B over 4 min and hold for 6.5 min. Change to 35% Solvent A/65% Solvent B over 0.5 min and hold for 4.5 min. Flow Rate: 0.5 mL/min, 2 □L injection. The concentration of **CysDHT** present at the end of the reaction was determined by measurement against calibration curves for each compound.

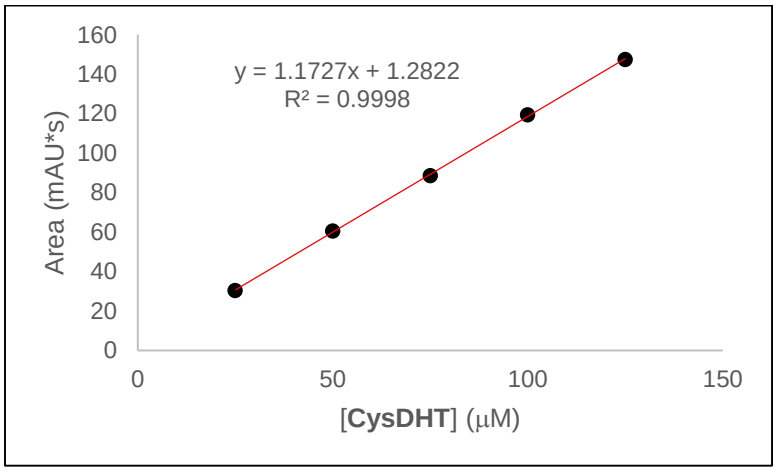

Figure D34. HPLC Calibration Curve of **CysDHT**

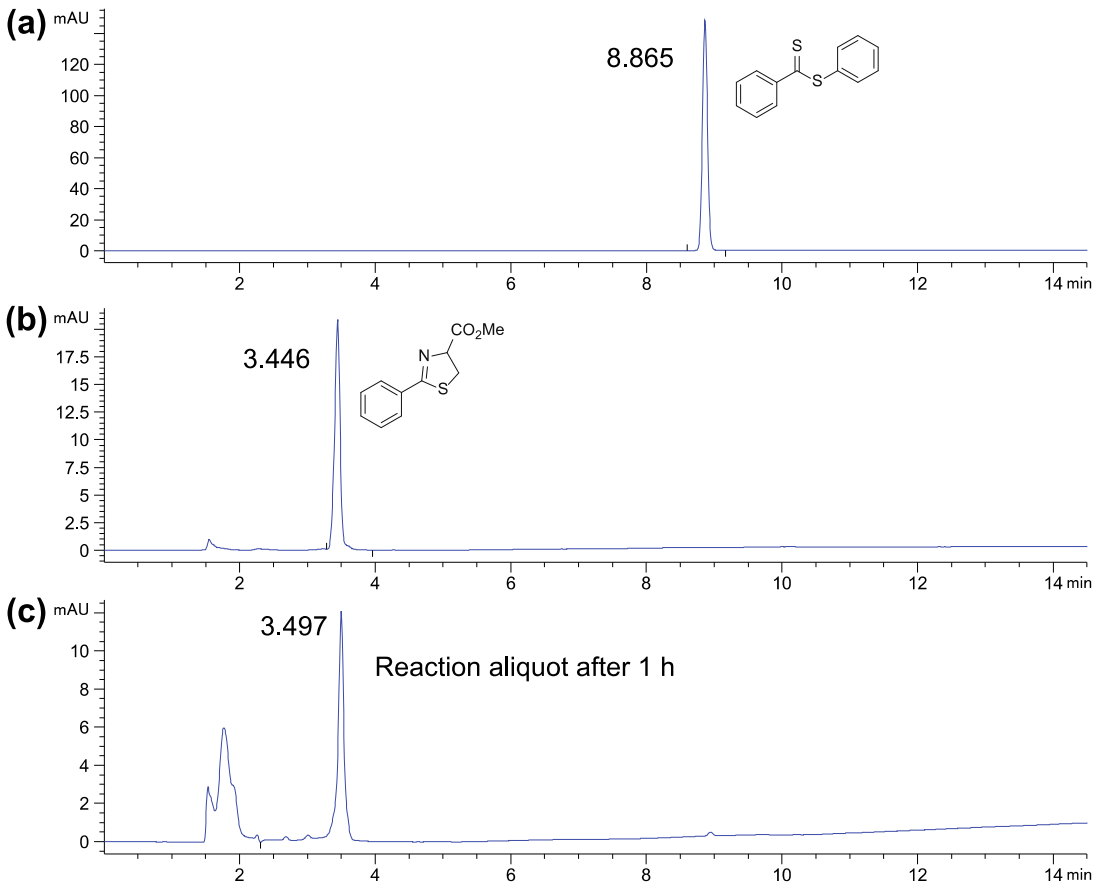

Figure D35. a) 100 ppm **PDTE** in Hexanes b) 100 μM **CysDHT** in 10 mM PBS (pH 7.4) with 10% THF c) Reaction aliquot after 1 h.

REFERENCES CITED

1. Hatfield, D. L.; Tsuji, P. A.; Carlson, B. A.; Gladyshev, V. N., Selenium and selenocysteine: roles in cancer, health, and development. *Trends in Biochemical Sciences* **2014,** *39* (3), 112-120.

2. Fairweather-Tait, S. J.; Bao, Y.; Broadley, M. R.; Collings, R.; Ford, D.; Hesketh, J. E.; Hurst, R., Selenium in Human Health and Disease. *Antioxid Redox Signal* **2011,** *14* (7), 1337-1383.

3. Rayman, M. P., Selenium and human health. *Lancet* **2012,** *379* (9822), 1256-1268.

4. Yao, Y.; Pei, F.; Kang, P., Selenium, iodine, and the relation with Kashin-Beck disease. *Nutrition* **2011,** *27* (11-12), 1095-100.

5. Chen, J. S., An original discovery: selenium deficiency and Keshan disease (an endemic heart disease). *Asia Pacific Journal of Clinical Nutrition* **2012,** *21* (3), 320-326.

6. Rayman, M. P., Food-chain selenium and human health: emphasis on intake. *Br J Nutr* **2008,** *100* (2), 254-268.

7. Kang, D.; Lee, J.; Wu, C.; Guo, X.; Lee, B. J.; Chun, J.-S.; Kim, J.-H., The role of selenium metabolism and selenoproteins in cartilage homeostasis and arthropathies. *Exp Mol Med* **2020,** *52*, 1198-1208.

8. Burk, R. F.; Hill, K. E., Regulation of selenium metabolism and transport. *Annual Review of Nutrition* **2015,** *35*, 109-134.

9. Minich, W. B., Selenium Metabolism and Biosynthesis of Selenoproteins in the Human Body. *Biochem. (Mosc.)* **2022,** *87*, S168-S177.

10. Muller, D.; Desel, H., Acute selenium poisoning by paradise nuts (Lecythis ollaria). *Human & Experimental Toxicology* **2010,** *29* (5), 431-434.

11. Senthilkumaran, S.; Balamurugan, N.; Vohra, R.; Thirumalaikolundusubramanian, P., Paradise Nut Paradox: Alopecia Due to Selenosis from a Nutritional Therapy. *Int J Trichology* **2012,** *4* (4), 283-284.

12. Battin, E. E.; Brumaghim, J. L., Antioxidant activity of sulfur and selenium: a review of reactive oxygen species scavenging, glutathione peroxidase, and metal-binding antioxidant mechanisms. *Cell Biochem Biophys* **2009,** *55* (1), 1-23.

13. Wessjohann, L. A.; Schneider, A.; Abbas, M.; Brandt, W., Selenium in chemistry and biochemistry in comparison to sulfur. *Biol Chem* **2007,** *388* (10), 997-1006.

14. Baker, L. M.; Raudonikiene, A.; Hoffman, P. S.; Poole, L. B., Essential thioredoxin-dependent peroxiredoxin system from Helicobacter pylori: genetic and kinetic characterization. *J Bacteriol* **2001,** *183* (6), 1961-73.

15. St. Germain, D. L.; Galton, V. A.; Hernandez, A., Defining the Roles of the Iodothyronine Deiodinases: Current Concepts and Challenges. *Endocrinology* **2009,** *150* (3), 1097-1107.

16. Larsen, P. R.; Zavacki, A. M., Role of the Iodothyronine Deiodinases in the Physiology and Pathophysiology of Thyroid Hormone Action. *Eur Thyroid J* **2012,** *1*, 232-242.

17. Schweizer, U.; Schomburg, L.; Kohrle, J., Selenoprotein P and Selenium Distribution in Mammals. In *Selenium: Its Molecular Biology and Role in Human Health*, 4 ed.; Springer: 2016; pp 261-274.

18. Burk, R. F.; Hill, K. E., Selenoprotein P - Expression, Functions, and Roles in Mammals. *Biochim Biophys Acta* **2009,** *1790* (11), 1441-1447.

19. Pietschmann, N.; Rijntjes, E.; Hoeg, A.; Stoedter, M.; Schweizer, U.; Seemann, P.; Schomburg, L., Selenoprotein P is the essential selenium transporter for bones. *Metallomics* **2014,** *6* (5), 1043-1049.

20. Barbosa, N. V.; Noguiera, C. W.; Nogara, P. A.; de Bem, A. F.; Aschner, M.; Rocha, J. B. T., Organoselenium compounds as mimics of selenoproteins and thiol modifier agents. *Metallomics* **2017,** *9* (12), 1703-1734.

21. Santi, C.; Scimmi, C.; Sancineto, L., Ebselen and Analogues: Pharmacological Properties and Synthetic Strategies for Their Preparation. *Molecules* **2021,** *26* (14), 4230-4254.

22. Schewe, T., Molecular actions of Ebselen-an antiinflammatory antioxidant. *General Pharmacology* **1995,** *26* (6), 1153-1169.

23. Wang, J.; Wang, P.; Dong, C.; Zhao, Y.; Zhou, J.; Yuan, C.; Zou, L., Mechanisms of ebselen as a therapeutic and its pharmacology applications. *Future Med. Chem.* **2020,** *12* (23), 2141-2160.

24. Wehrle, R. J.; Ste. Marie, E. J.; Hondal, R. J.; Masterson, D. J., Synthesis of alpha-methyl selenocysteine and its utilizatino as a glutathione peroxidase mimic. *J. Pept. Sci.* **2019,** *25* (6).

25. Manna, D.; Mugesh, G., Regioselective Deiodination of Thyroxine by Iodothyronine Deiodinase Mimics: An Unusual Mechanistic Pathway Involving Cooperative Chalcogen and Halogen Bonding. *J. Am. Chem. Soc.* **2012,** *134* (9), 4269-4279.

26. Wang, Y.; Ma, J.; Zhou, L.; Chen, J.; Liu, Y.; Qiu, Z.; Zhang, S., Dual functional selenium-substituted hydroxyapatite. *Interface Focus* **2012,** *2* (3).

27. Lipinski, B., Rationale for the treatment of cancer with sodium selenite. *Medical Hypotheses* **2005,** *64*, 806-810.

28. Khan, S.; Ullah, M. W.; Siddique, R.; Liu, Y.; Ullah, I.; Xue, M.; Yang, G.; Hou, H., Catechins-Modified Selenium-Doped Hydroxyapatite Nanomaterials for Improved Osteosarcoma Therapy Through Generation of Reactive Oxygen Species. *Front Oncol* **2019,** *9*, 499.

29. Cupp-Sutton, K. A.; Ashby, M. T., Biological Chemistry of Hydrogen Selenide. *Antioxidants* **2016,** *5* (4), 42-59.

30. Halpin, K. M.; Baker, D. H., Selenium Deficiency and Transsulfuration in the Chick. *Journal of Nutrition* **1984,** *114* (3), 606-612.

31. Schrauzer, G. N., Selenium yeast: Composition, quality, analysis, and safety. *Pure Appl. Chem.* **2006,** *78* (1), 105-109.

32. Kong, F. P.; Ge, L. H.; Pan, X. H.; Xu, K. H.; Liu, X. J.; Tang, B., A highly selective near-infrared fluorescent probe for imaging H2Se in living cells and in vivo. *Chemical Science* **2016,** *7* (2), 1051-1056.

33. Kong, F. P.; Zhao, Y. H.; Liang, Z. Y.; Liu, X. J.; Pan, X. H.; Luan, D. R.; Xu, K. H.; Tang, B., Highly Selective Fluorescent Probe for Imaging H2Se in Living Cells and in Vivo Based on the Disulfide Bond. *Analytical Chemistry* **2017,** *89* (1), 688-693.

34. Tian, Y.; Xin, F.; Jing, J.; Zhang, X., Fluorescence imaging of lysosomal hydrogen selenide under oxygen-controlled conditions. *J Mater Chem B* **2019,** *7* (17), 2829-2834.

35. Xin, F.; Tian, Y.; Zhang, X., Ratiometric fluorescent probe for highly selective detection of gaseous H_2Se. *Dyes Pigm* **2020,** *177*, 108274-108278.

36. Xiong, J.; Xu, K.; Hou, X.; Wu, P., AuNCs-Catalyzed Hydrogen Selenide Oxidation: Mechanism and Application for Headspace Fluorescent Detection of Se (IV). *Anal. Chem.* **2019,** *91* (9), 6141-6148.

37. Bagheri, N.; Saraji, M., Combining gold nanoparticle-based headspace single-drop microextraction and a paper-based colorimetric assay for selenium determination. *Anal. Bioanal. Chem.* **2019,** *411*, 7441-7449.

38. Iwata, A.; Morrison, M. L.; Blackwood, J. E.; Roth, M. B., Selenide Targets to Reperfusing Tissue and Protects It From Injury. *Critical Care Medicine* **2015,** *43* (7), 1361-1367.

39. Samra, K.; Kuganesan, M.; Smith, W.; Kleyman, A.; Tidswell, R.; Arulkumaran, N.; Singer, M.; Dyson, A., The Pharmacology and Therapeutic Utility of Sodium Hydroselenide. *Int J Mol Sci* **2021,** *22* (6), 3258-3277.

40. Newton, T. D.; Pluth, M. D., Development of a hydrolysis-based small-molecule hydrogen selenide (H2Se) donor. *Chem Sci* **2019,** *10* (46), 10723-10727.

41. Newton, T. D.; Bolton, S. G.; Garcia, A. C.; Chouinard, J. E.; Golledge, S. L.; Zakharov, L. N.; Pluth, M. D., Hydrolysis-Based Small-Molecule Hydrogen Selenide (H2Se) Donors for Intracellular H2Se Delivery. *J Am Chem Soc* **2021,** *143* (46), 19542-19550.

42. Kang, X.; Huang, H.; Jiang, C.; Cheng, L.; Sang, Y.; Cai, X.; Dong, Y.; Sun, L.; Wen, X.; Xi, Z.; Yi, L., Cysteine-Activated Small-Molecule H2Se Donors Inspired by Synthetic H2S Donors. *J Am Chem Soc* **2022,** *144* (9), 3957-3967.

43. Kharma, A.; Misak, A.; Grman, M.; Brezova, V.; Kurakova, L.; Baráth, P.; Jacob, C.; Chovanec, M.; Ondrias, K.; Domínguez-Álvarez, E., Release of reactive selenium species from phthalic selenoanhydride in the presence of hydrogen sulfide and glutathione with implications for cancer research. *New Journal of Chemistry* **2019,** *43* (29), 11771-11783.

44. McKenzie, R. C.; Rafferty, T. S.; Beckett, G. J., Selenium: An essential element for immune function. *Immunology Today* **1998,** *19* (8), 342-345.

45. Schomburg, L.; Schweizer, U.; Kohrle, J., Selenium and selenoproteins in mammals: extraordinary, essential, enigmatic. *Cellular and Molecular Life Sciences* **2004,** *61* (16), 1988-1995.

46. Reich, H. J.; Hondal, R. J., Why Nature Chose Selenium. *Acs Chemical Biology* **2016,** *11* (4), 821-841.

47. Sudre, P.; Mathieu, F., Kashin-Beck disease: from etiology to prevention or from prevention to etiology? *International Orthopaedics* **2001,** *25* (3), 175-179.

48. Papp, L. V.; Lu, J.; Holmgren, A.; Khanna, K. K., From selenium to selenoproteins: Synthesis, identity, and their role in human health. *Antioxidants & Redox Signaling* **2007,** *9* (7), 775-806.

49. Schewe, T., MOLECULAR ACTIONS OF EBSELEN - AN ANTIINFLAMMATORY ANTIOXIDANT. *Gen. Pharmacol. Vasc. S.* **1995,** *26* (6), 1153-1169.

50. Wedding, J. L.; Lai, B.; Vogt, S.; Harris, H. H., Investigation into the intracellular fates, speciation and mode of action of selenium-containing neuroprotective agents using XAS and XFM. *Biochimica Et Biophysica Acta-General Subjects* **2018,** *1862* (11), 2393-2404.

51. Hsieh, H. S.; Ganther, H. E., ACID-VOLATILE SELENIUM FORMATION CATALYZED BY GLUTATHIONE REDUCTASE. *Biochemistry* **1975,** *14* (8), 1632-1636.

52. Kessi, J.; Hanselmann, K. W., Similarities between the abiotic reduction of selenite with glutathione and the dissimilatory reaction mediated by Rhodospirillum rubrum and Escherichia coli. *Journal of Biological Chemistry* **2004,** *279* (49), 50662-50669.

53. Kharma, A.; Misak, A.; Grman, M.; Brezova, V.; Kurakova, L.; Barath, P.; Jacob, C.; Chovanec, M.; Ondrias, K.; Domínguez-Álvarez, E., Release of Reactive Selenium Species from phthalic selenoanhydride in the presence of hydrogen sulfide and glutathione with implications for cancer research. *New Journal of Chemistry* **2019**.

54. Fargher, H. A.; Lau, N.; Zakharov, L. N.; Haley, M. M.; Johnson, D. W.; Pluth, M. D., Expanding reversible chalcogenide binding: supramolecular receptors for the hydroselenide (HSe-) anion. *Chemical Science* **2019,** *10* (1), 67-72.

55. Sun, H. J.; Rathinasabapathi, B.; Wu, B.; Luo, J.; Pu, L. P.; Ma, L. Q., Arsenic and selenium toxicity and their interactive effects in humans. *Environment International* **2014,** *69*, 148-158.

56. Zwolak, I., The Role of Selenium in Arsenic and Cadmium Toxicity: an Updated Review of Scientific Literature. *Biological trace element research* **2019**, 1-20.

57. Pan, X. H.; Song, X. X.; Wang, C.; Cheng, T. T.; Luan, D. R.; Xu, K. H.; Tang, B., H2Se Induces Reductive Stress in HepG(2) Cells and Activates Cell Autophagy by Regulating the Redox of HMGB1 Protein under Hypoxia. *Theranostics* **2019,** *9* (6), 1794-1808.

58. Schroeder, H. A.; Frost, D. V.; Balassa, J. J., ESSENTIAL TRACE METALS IN MAN - SELENIUM. *Journal of Chronic Diseases* **1970,** *23* (4), 227-+.

59. Wang, R., Two's company, three's a crowd: can H2S be the third endogenous gaseous transmitter? *Faseb Journal* **2002,** *16* (13), 1792-1798.

60. Zanatta, S. D.; Jarrott, B.; Williams, S. J., Synthesis and Preliminary Pharmacological Evaluation of Aryl Dithiolethiones with Cyclooxygenase-2-Selective Inhibitory Activity and Hydrogen Sulfide-Releasing Properties. *Australian Journal of Chemistry* **2010,** *63* (6), 946-957.

61. Cerda, M. M.; Newton, T. D.; Zhao, Y.; Collins, B. K.; Hendon, C. H.; Pluth, M. D., Dithioesters: simple, tunable, cysteine-selective H2S donors. *Chemical Science* **2019,** *10* (6), 1773-1779.

62. Levinn, C. M.; Steiger, A. K.; Pluth, M. D., Esterase-Triggered Self-Immolative Thiocarbamates Provide Insights into COS Cytotoxicity. *Acs Chemical Biology* **2019,** *14* (2), 170-175.

63. Li, L.; Whiteman, M.; Guan, Y. Y.; Neo, K. L.; Cheng, Y.; Lee, S. W.; Zhao, Y.; Baskar, R.; Tan, C. H.; Moore, P. K., Characterization of a novel, water-soluble hydrogen sulfide - Releasing molecule (GYY4137): New insights into the biology of hydrogen sulfide. *Circulation* **2008,** *117* (18), 2351-2360.

64. Li, L.; Salto-Tellez, M.; Tan, C. H.; Whiteman, M.; Moore, P. K., GYY4137, a novel hydrogen sulfide-releasing molecule, protects against endotoxic shock in the rat. *Free Radical Biology and Medicine* **2009,** *47* (1), 103-113.

65. Lee, Z. W.; Teo, X. Y.; Tay, E. Y. W.; Tan, C. H.; Hagen, T.; Moore, P. K.; Deng, L. W., Utilizing hydrogen sulfide as a novel anti-cancer agent by targeting cancer glycolysis and pH imbalance. *British Journal of Pharmacology* **2014,** *171* (18), 4322-4336.

66. Meng, G. L.; Wang, J.; Xiao, Y. J.; Bai, W. L.; Xie, L. P.; Shan, L. Y.; Moore, P. K.; Ji, Y., GYY4137 protects against myocardial ischemia and reperfusion injury by attenuating oxidative stress and apoptosis in rats. *Journal of Biomedical Research* **2015,** *29* (3), 203-213.

67. Carter, J. M.; Brown, E. M.; Grace, J. P.; Salem, A. K.; Irish, E. E.; Bowden, N. B., Improved growth of pea, lettuce, and radish plants using the slow release of hydrogen sulfide from GYY-4137. *Plos One* **2018,** *13* (12).

68. de Oliveira, A. R. M.; Piovan, L.; Simonelli, F.; Barison, A.; Santos, M. D. C.; de Mello, M. B. M., A Se-77 NMR study of elemental selenium reduction using NaBH4. *Journal of Organometallic Chemistry* **2016,** *806*, 54-59.

69. Ganther, H. E.; Kraus, R. J., IDENTIFICATION OF HYDROGEN SELENIDE AND OTHER VOLATILE SELENOLS BY DERIVATIZATION WITH 1-FLUORO-2,4-DINITROBENZENE. *Analytical Biochemistry* **1984,** *138* (2), 396-403.

70. Ganther, H. E.; Kraus, R. J., HYDROGEN SELENIDE AND METHYLSELENOL. *Methods in Enzymology* **1987,** *143*, 32-38.

71. Twiss, D. F., The action of nitro-substituted aryl haloids on alkali thiosulphates and selenosulphates. *Journal of the Chemical Society, Transactions* **1914,** *105*, 1672-1678.

72. Navarro-Alarcon, M.; Cabrera-Vique, C., Selenium in food and the human body: A review. *Science of the Total Environment* **2008,** *400* (1-3), 115-141.

73. Letavayova, L.; Vlckova, V.; Brozmanova, J., Selenium: From cancer prevention to DNA damage. *Toxicology* **2006,** *227* (1-2), 1-14.

74. Paton, N. D.; Cantor, A. H.; Pescatore, A. F.; Ford, M. J.; Smith, C. A., The effect of dietary selenium source and level on the uptake of selenium by developing chick embryos. *Poultry Science* **2002,** *81* (10), 1548-1554.

75. Subburayan, K.; Thayyullathil, F.; Pallichankandy, S.; Cheratta, A. R.; Galadari, S., Superoxide-mediated ferroptosis in human cancer cells induced by sodium selenite. *Translational Oncology* **2020,** *13* (11).

76. Chen, H. J.; Zhou, J., Effects of Sodium Selenite on Oxidative Damage in the Liver, Kidney and Brain in a Selenite Cataract Rat Model. *Biological Trace Element Research* **2020,** *197* (2), 533-543.

77. Tarze, A.; Dauplais, M.; Grigoras, I.; Lazard, M.; Ha-Duong, N. T.; Barbier, F.; Blanquet, S.; Plateau, P., Extracellular production of hydrogen selenide accounts for thiol-assisted toxicity of selenite against Saccharomyces cerevisiae. *Journal of Biological Chemistry* **2007,** *282* (12), 8759-8767.

78. Szabo, C.; Papapetropoulos, A., Hydrogen sulphide and angiogenesis: mechanisms and applications. *British Journal of Pharmacology* **2011,** *164* (3), 853-865.

79. Kuganesan, M.; Samra, K.; Evans, E.; Singer, M.; Dyson, A., Selenium and hydrogen selenide: essential micronutrient and the fourth gasotransmitter? *Intensive Care Medicine Experimental* **2019,** *7* (1).

80. Newton, T. D.; Pluth, M. D., Development of a hydrolysis-based small-molecule hydrogen selenide (H2Se) donor. *Chemical Science* **2019,** *10* (46), 10723-10727.

81. Feng, W.; Teo, X. Y.; Novera, W.; Ramanujulu, P. M.; Liang, D.; Huang, D. J.; Moore, P. K.; Deng, L. W.; Dymock, B. W., Discovery of New H2S Releasing Phosphordithioates and 2,3-Dihydro-2-phenyl-2-sulfanylenebenzo d 1,3,2 oxazaphospholes with Improved Antiproliferative Activity. *Journal of Medicinal Chemistry* **2015,** *58* (16), 6456-6480.

82. Bhattacharyya, P.; Slawin, A. M. Z.; Woollins, J. D., {PhP(Se)(mu-Se)}(2) by 1,2-C6H4(EH)(E ' H) (E, E ' = O or NH). X-ray crystal structure of PhP(Se)(NHC6H4NH-1,2). *Journal of Organometallic Chemistry* **2001,** *623* (1-2), 116-119.

83. Hua, G. X.; Fuller, A. L.; Slawin, A. M. Z.; Woollins, J. D., Novel Five- to Ten-Membered Organoselenium Heterocycles from the Selenation of Aromatic Diols. *European Journal of Organic Chemistry* **2010,** *2010* (13), 2607-2615.

84. Montoya, L. A.; Pearce, T. F.; Hansen, R. J.; Zakharov, L. N.; Pluth, M. D., Development of Selective Colorimetric Probes for Hydrogen Sulfide Based on Nucleophilic Aromatic Substitution. *Journal of Organic Chemistry* **2013,** *78* (13), 6550-6557.

85. Yi, L.; Xi, Z., Thiolysis of NBD-based dyes for colorimetric and fluorescence detection of H2S and biothiols: design and biological applications. *Organic & Biomolecular Chemistry* **2017,** *15* (18), 3828-3839.

86. Jiang, C. Y.; Huang, H. J.; Kang, X. Y.; Yang, L.; Xi, Z.; Sun, H. Y.; Pluth, M. D.; Yi, L., NBD-based synthetic probes for sensing small molecules and proteins: design, sensing mechanisms and biological applications. *Chemical Society Reviews* **2021,** *50* (13), 7436-+.

87. Levinn, C.; Pluth, M., Learning from Our Mistakes: We Have a Scientific and Fiscal Obligation to Publish Failed Results. *ChemRxiv* **2020**.

88. Myhre, O.; Andersen, J. M.; Aarnes, H.; Fonnum, F., Evaluation of the probes 2 ',7 '-dichlorofluorescin diacetate, luminol, and lucigenin as indicators of reactive species formation. *Biochemical Pharmacology* **2003,** *65* (10), 1575-1582.

89. Fargher, H. A.; Lau, N.; Zakharov, L. N.; Haley, M. M.; Johnson, D. W.; Pluth, M. D., Expanding reversible chalcogenide binding: supramolecular receptors for the hydroselenide (HSe^-) anion. *Chemical Science* **2019,** *10* (1), 67-72.

90. Levinn, C. M.; Cerda, M. M.; Pluth, M. D., Development and Application of Carbonyl Sulfide-Based Donors for H_2S Delivery. *Acc. Chem. Res.* **2019,** *52* (9), 2723-2731.

91. Gilbert, A. K.; Zhao, Y.; Otteson, C. E.; Pluth, M. D., Development of Acid-Mediated H_2S/COS Donors that Respond to a Specific pH Window. *J. Org. Chem.* **2019,** *84* (22), 14469-14475.

92. Zhao, Y.; Bolton, S. G.; Pluth, M. D., Light-Activated COS/H_2S Donation from Photocaged Thiocarbamates. *Org. Lett.* **2017,** *19* (9), 2278-2281.

93. Zhao, Y.; Steiger, A. K.; Pluth, M. D., Cysteine-Activated Hydrogen Sulfide (H_2S) Delivery through Caged Carbonyl Sulfide (COS) Donor Motifs. *Chem. Commun.* **2018,** *54*, 4951-4954.

94. Zhao, Y.; Henthorn, H. A.; Pluth, M. D., Kinetic Insights into Hydrogen Sulfide Delivery from Caged Carbonyl Sulfide Isomeric Donor Platforms. *J. Am. Chem. Soc.* **2017,** *139* (45), 16365-16376.

95. Levinn, C. M.; Steiger, A. K.; Pluth, M. D., Esterase-Triggered Self-Immolative thiocarbamates Provide Insights into COS Cytotoxicity. *ACS Chem. Biol.* **2019,** *14* (2), 170-175.

96. Lopez, O.; Maza, S.; Ulgar, V.; Maya, I.; Fernandez-Bolanos, J. G., Synthesis of sugar-derived isoselenocyanates, selenoureas, and selenazoles. *Tetrahedron* **2009,** *65* (12), 2556-2566.

97. Eriksen, K.; Ulfkjaer, A.; Solling, T. I.; Pittelkow, M., Benzylic Thio and Seleno Newman-Kwart Rearrangements. *J. Org. Chem.* **2018,** *83* (18), 10786-10797.

98. Zhao, Y.; Steiger, A. K.; Pluth, M. D., Colorimetric Carbonyl Sulfide (COS)/Hydrogen Sulfide (H_2S) Donation from g-Ketothiocarbamate Donor Motifs. *Angew. Chem. Int. Ed. Engl.* **2018,** *57* (40), 13101-13105.

99. Hammett, L. P., The Effect of Structure upon the Reactions of Organic Compounds: Benzene Derivatives. *J. Am. Chem. Soc.* **1937,** *59* (1), 96-103.

100. Chiefari, J.; Chong, Y. K.; Ercole, F.; Krstina, J.; Jeffery, J.; Le, T. P. T.; Mayadunne, R. T. A.; Meijs, G. F.; Moad, C. L.; Moad, G.; Rizzardo, E.; Thang, S. H., Living Free-Radical Polymerization by Reversible Addition−Fragmentation Chain Transfer: The RAFT Process. *Macromolecules* **1998,** *31* (16), 5559-5562.

101. Chiefari, J.; Mayadunne, R. T. A.; Moad, C. L.; Moad, G.; Rizzardo, E.; Postma, A.; Skidmore, M. A.; Thang, S. H., Thiocarbonylthio compounds (S=C(Z)S-R) in free radical polymerization with reversible addition-fragmentation chain transfer (RAFT polymerization). Effect of the activating group Z. *Macromolecules* **2003,** *36* (7), 2273-2283.

102. Chong, Y. K.; Krstina, J.; Le, T. P. T.; Moad, G.; Postma, A.; Rizzardo, E.; Thang, S. H., Thiocarbonylthio Compounds [SC(Ph)S−R] in Free Radical Polymerization with Reversible Addition-Fragmentation Chain Transfer (RAFT Polymerization). Role of the Free-Radical Leaving Group (R). *Macromolecules* **2003,** *36* (7), 2256-2272.

103. Cerda, M. M.; Zhao, Y.; Pluth, M. D., Thionoesters: A Native Chemical Ligation-Inspired Approach to Cysteine-Triggered H2S Donors. *J Am Chem Soc* **2018,** *140* (39), 12574-12579.

104. Newton, J. J.; Britton, R.; Friesen, C. M., Base-Catalyzed Transesterification of Thionoesters. *J Org Chem* **2018,** *83* (20), 12784-12792.

105. Mustafa, A. K.; Gadalla, M. M.; Snyder, S. H., Signaling by gasotransmitters. *Sci Signal* **2009,** *2* (68), re2.

106. Wang, R., Two's company, three's a crowd: can H2S be the third endogenous gaseous transmitter? *FASEB J* **2002,** *16* (13), 1792-8.

107. Zhao, W.; Zhang, J.; Lu, Y.; Wang, R., The vasorelaxant effect of H(2)S as a novel endogenous gaseous K(ATP) channel opener. *EMBO J* **2001,** *20* (21), 6008-16.

108. Altaany, Z.; Yang, G.; Wang, R., Crosstalk between hydrogen sulfide and nitric oxide in endothelial cells. *J Cell Mol Med* **2013,** *17* (7), 879-88.

109. Yang, G.; Zhao, K.; Ju, Y.; Mani, S.; Cao, Q.; Puukila, S.; Khaper, N.; Wu, L.; Wang, R., Hydrogen sulfide protects against cellular senescence via S-sulfhydration of Keap1 and activation of Nrf2. *Antioxid Redox Signal* **2013,** *18* (15), 1906-19.

110. Wallace, J. L.; Wang, R., Hydrogen sulfide-based therapeutics: exploiting a unique but ubiquitous gasotransmitter. *Nat Rev Drug Discov* **2015,** *14* (5), 329-45.

111. Zheng, Y.; Yu, B.; De La Cruz, L. K.; Roy Choudhury, M.; Anifowose, A.; Wang, B., Toward Hydrogen Sulfide Based Therapeutics: Critical Drug Delivery and Developability Issues. *Med Res Rev* **2018,** *38* (1), 57-100.

112. Whiteman, M.; Li, L.; Rose, P.; Tan, C. H.; Parkinson, D. B.; Moore, P. K., The effect of hydrogen sulfide donors on lipopolysaccharide-induced formation of inflammatory mediators in macrophages. *Antioxid Redox Signal* **2010,** *12* (10), 1147-54.

113. DeLeon, E. R.; Stoy, G. F.; Olson, K. R., Passive loss of hydrogen sulfide in biological experiments. *Anal Biochem* **2012,** *421* (1), 203-7.

114. Powell, C. R.; Dillon, K. M.; Matson, J. B., A review of hydrogen sulfide (H2S) donors: Chemistry and potential therapeutic applications. *Biochem Pharmacol* **2018,** *149*, 110-123.

115. Szabo, C.; Papapetropoulos, A., International Union of Basic and Clinical Pharmacology. CII: Pharmacological Modulation of H2S Levels: H2S Donors and H2S Biosynthesis Inhibitors. *Pharmacol Rev* **2017,** *69* (4), 497-564.

116. Bora, P.; Chauhan, P.; Pardeshi, K. A.; Chakrapani, H., Small molecule generators of biologically reactive sulfur species. *RSC Advances* **2018,** *8* (48), 27359-27374.

117. Zhao, Y.; Biggs, T. D.; Xian, M., Hydrogen sulfide (H2S) releasing agents: chemistry and biological applications. *Chem Commun (Camb)* **2014,** *50* (80), 11788-805.

118. Li, L.; Rossoni, G.; Sparatore, A.; Lee, L. C.; Del Soldato, P.; Moore, P. K., Anti-inflammatory and gastrointestinal effects of a novel diclofenac derivative. *Free Radic Biol Med* **2007,** *42* (5), 706-19.

119. Li, L.; Whiteman, M.; Guan, Y. Y.; Neo, K. L.; Cheng, Y.; Lee, S. W.; Zhao, Y.; Baskar, R.; Tan, C. H.; Moore, P. K., Characterization of a novel, water-soluble hydrogen sulfide-releasing molecule (GYY4137): new insights into the biology of hydrogen sulfide. *Circulation* **2008,** *117* (18), 2351-60.

120. Park, C. M.; Zhao, Y.; Zhu, Z.; Pacheco, A.; Peng, B.; Devarie-Baez, N. O.; Bagdon, P.; Zhang, H.; Xian, M., Synthesis and evaluation of phosphorodithioate-based hydrogen sulfide donors. *Mol Biosyst* **2013,** *9* (10), 2430-4.

121. Kang, J.; Li, Z.; Organ, C. L.; Park, C. M.; Yang, C. T.; Pacheco, A.; Wang, D.; Lefer, D. J.; Xian, M., pH-Controlled Hydrogen Sulfide Release for Myocardial Ischemia-Reperfusion Injury. *J Am Chem Soc* **2016,** *138* (20), 6336-9.

122. Zheng, Y.; Yu, B.; Ji, K.; Pan, Z.; Chittavong, V.; Wang, B., Esterase-Sensitive Prodrugs with Tunable Release Rates and Direct Generation of Hydrogen Sulfide. *Angew Chem Int Ed Engl* **2016,** *55* (14), 4514-8.

123. Xiao, Z.; Bonnard, T.; Shakouri-Motlagh, A.; Wylie, R. A. L.; Collins, J.; White, J.; Heath, D. E.; Hagemeyer, C. E.; Connal, L. A., Triggered and Tunable Hydrogen Sulfide Release from Photogenerated Thiobenzaldehydes. *Chemistry* **2017,** *23* (47), 11294-11300.

124. Devarie-Baez, N. O.; Bagdon, P. E.; Peng, B.; Zhao, Y.; Park, C. M.; Xian, M., Light-induced hydrogen sulfide release from "caged" gem-dithiols. *Org Lett* **2013,** *15* (11), 2786-9.

125. Woods, J. J.; Cao, J.; Lippert, A. R.; Wilson, J. J., Characterization and Biological Activity of a Hydrogen Sulfide-Releasing Red Light-Activated Ruthenium(II) Complex. *J Am Chem Soc* **2018,** *140* (39), 12383-12387.

126. Steiger, A. K.; Pardue, S.; Kevil, C. G.; Pluth, M. D., Self-Immolative Thiocarbamates Provide Access to Triggered H2S Donors and Analyte Replacement Fluorescent Probes. *J Am Chem Soc* **2016,** *138* (23), 7256-9.

127. Zhao, Y.; Steiger, A. K.; Pluth, M. D., Colorimetric Carbonyl Sulfide (COS)/Hydrogen Sulfide (H2 S) Donation from gamma-Ketothiocarbamate Donor Motifs. *Angew Chem Int Ed Engl* **2018,** *57* (40), 13101-13105.

128. Sharma, A. K.; Nair, M.; Chauhan, P.; Gupta, K.; Saini, D. K.; Chakrapani, H., Visible-Light-Triggered Uncaging of Carbonyl Sulfide for Hydrogen Sulfide (H2S) Release. *Org Lett* **2017,** *19* (18), 4822-4825.

129. Powell, C. R.; Foster, J. C.; Okyere, B.; Theus, M. H.; Matson, J. B., Therapeutic Delivery of H2S via COS: Small Molecule and Polymeric Donors with Benign Byproducts. *J Am Chem Soc* **2016,** *138* (41), 13477-13480.

130. Pluth, M.; Bailey, T.; Hammers, M.; Hartle, M.; Henthorn, H.; Steiger, A., Natural Products Containing Hydrogen Sulfide Releasing Moieties. *Synlett* **2015,** *26* (19), 2633-2643.

131. Ercole, F.; Whittaker, M. R.; Halls, M. L.; Boyd, B. J.; Davis, T. P.; Quinn, J. F., Garlic-inspired trisulfide linkers for thiol-stimulated H2S release. *Chem Commun (Camb)* **2017,** *53* (57), 8030-8033.

132. Cerda, M. M.; Hammers, M. D.; Earp, M. S.; Zakharov, L. N.; Pluth, M. D., Applications of Synthetic Organic Tetrasulfides as H2S Donors. *Org Lett* **2017,** *19* (9), 2314-2317.

133. Filipovic, M. R.; Zivanovic, J.; Alvarez, B.; Banerjee, R., Chemical Biology of H2S Signaling through Persulfidation. *Chem Rev* **2018,** *118* (3), 1253-1337.

134. Zhao, Y.; Wang, H.; Xian, M., Cysteine-activated hydrogen sulfide (H2S) donors. *J Am Chem Soc* **2011,** *133* (1), 15-7.

135. Zhao, Y.; Yang, C.; Organ, C.; Li, Z.; Bhushan, S.; Otsuka, H.; Pacheco, A.; Kang, J.; Aguilar, H. C.; Lefer, D. J.; Xian, M., Design, Synthesis, and Cardioprotective Effects of N-Mercapto-Based Hydrogen Sulfide Donors. *J Med Chem* **2015,** *58* (18), 7501-11.

136. Foster, J. C.; Powell, C. R.; Radzinski, S. C.; Matson, J. B., S-aroylthiooximes: a facile route to hydrogen sulfide releasing compounds with structure-dependent release kinetics. *Org Lett* **2014,** *16* (6), 1558-61.

137. Foster, J. C.; Radzinski, S. C.; Zou, X.; Finkielstein, C. V.; Matson, J. B., H2S-Releasing Polymer Micelles for Studying Selective Cell Toxicity. *Mol Pharm* **2017,** *14* (4), 1300-1306.

138. Ercole, F.; Mansfeld, F. M.; Kavallaris, M.; Whittaker, M. R.; Quinn, J. F.; Halls, M. L.; Davis, T. P., Macromolecular Hydrogen Sulfide Donors Trigger Spatiotemporally Confined Changes in Cell Signaling. *Biomacromolecules* **2016,** *17* (1), 371-83.

139. Ozturk, T.; Ertas, E.; Mert, O., Use of Lawesson's reagent in organic syntheses. *Chem Rev* **2007,** *107* (11), 5210-78.

140. Siegel, L. M., A direct microdetermination for sulfide. *Analytical Biochemistry* **1965,** *11* (1), 126-132.

141. Levesque, G.; Arsène, P.; Fanneau-Bellenger, V.; Pham, T.-N., Protein Thioacylation: 2. Reagent Stability in Aqueous Media and Thioacylation Kinetics. *Biomacromolecules* **2000,** *1* (3), 400-406.

142. Thomas, D. B.; Convertine, A. J.; Hester, R. D.; Lowe, A. B.; McCormick, C. L., Hydrolytic Susceptibility of Dithioester Chain Transfer Agents and Implications in Aqueous RAFT Polymerizations†. *Macromolecules* **2004,** *37* (5), 1735-1741
.
143. In *Organic Reaction Mechanisms 1967*, Capon, B.; Perkins, M. J.; Rees, C. W., Eds. Wiley-Interscience: London, 1967.

144. Anslyn, E. V.; Dougherty, D. A., In *Modern Physical Organic Chemistry*, University Science: Sausalito, CA, 2006.